Technische Universität München
Fakultät für Elektrotechnik und Informationstechnik
Lehrstuhl für Kommunikationsnetze

Operation and Control of Device-to-Device Communication in Cellular Networks

Dipl.-Ing. (Univ.) Markus Klügel

Vollständiger Abdruck der von der Fakultät für Elektrotechnik und Informationstechnik der Technischen Universität München zur Erlangung des akademischen Grades eines

Doktor-Ingenieurs (Dr.-Ing.)

genehmigten Dissertation.

Vorsitzender:		Prof. Dr. Holger Boche
Prüfer der Dissertation:	1.	Prof. Dr.-Ing. Wolfgang Kellerer
	2.	Prof. Dr.-Ing. Wolfgang Utschick

Die Dissertation wurde am 11.01.2018 bei der Technischen Universität München eingereicht und durch die Fakultät für Elektrotechnik und Informationstechnik am 22.11.2018 angenommen.

Abstract

Future cellular networks are designed not only to offer Internet access with high data rate but to be adaptable to a variety of demands and situations. One situation that is explicitly challenging is that of high device density, for which a direct, low distance communication between mobile user equipments (UEs), called Device-to-Device (D2D) communication, is envisioned by companies and standardization bodies.

The introduction of direct links into cellular networks creates a paradigm shift: It turns their star-like communication structure into a managed mesh that can be used to realize any wireless network topology. Infrastructure nodes such as the base station (BS), formerly the only communication endpoints, reduce to management entities with gateway functionality. Managing D2D links is arguably more complex than managing traditional cellular communication. On the one hand, when allowing direct links, the total number of links can be expected to increase, as mesh topologies allow more links than star structures. On the other hand, information about link properties, such as channel qualities, need to be explicitly gathered for direct links, while they can be assumed available from ongoing communication for cellular networks. This creates a communication overhead and reporting delay for direct links that has to be kept low. As a result, parts of cellular communication need to be redesigned to fully leverage and support the new, direct communication type.

In this thesis the impact of D2D communication on cellular networks is investigated and ways to correctly manage a D2D enabled cellular network are explored:

Assuming an action flow as axiomatic basis, that leads from a service level communication demand to a medium access level D2D flow, scalability laws for the spatial density of D2D links are established. The impact of service penetration among UEs, service-layer device pairing strategies and network-layer mode selection strategies on scaling behavior is evaluated. The results are general requirements under which direct links are, at all, a use-case of impact.

The ability of D2D communication to lead to desirable network states is discussed, with the outcome that traditional network management for utility maximization can only partly leverage direct links in a good fashion. A resource efficiency metric is proposed that consistently captures all intuitive aspects of the three D2D-gains with respect to cellular communication, i.e., the proximity-, hop- and reuse-gain, which have been postulated in literature. Fundamental aspects of resource efficiency as a metric are established, creating a basic understanding of its properties and impact. The outcome are conditions under which utility

maximization serves to leverage the D2D option, as well as an understanding of what alternatives should be considered.

Based on the resulting insights, two strategies for offloading links to D2D communication are proposed. The first is based on traditional utility maximization and can be claimed to result in a utility-optimal network state, provided that the utility can be optimized on a convex space in a sub-step. The second is based on resource efficiency, targeting the situations in which utility-maximization is not applicable.

Finally, ways to manage interference among direct links with dynamic power control are explored. Two D2D related problems are solved, reuse feasibility estimation and reuse maximization. The resulting communication structure enables semi-distributed interference management, where power control is done in a decentralized fashion, while an outer-loop optimization is solved with centralized knowledge. The structure is shown to be generalizable to solve arbitrary network utility maximization problems with interference coupling.

The entirety of presented insights serves to identify potential applications for D2D links, recognize situations in which the direct link is the better option and proposes ways to control ongoing communications. It thus helps to correctly operate and control Device-to-Device communication.

Kurzfassung

Künftige Mobilfunknetze sollen nicht nur den Internet-Zugriff mit hoher Datenrate ermöglichen, sondern sollen auf eine Vielzahl von Szenario und Randbedingungen anpassbar sein. Eine Randbedingung die besonders herausfordernd ist, ist eine hohe örtlicher Nutzerdichte. Für solche sehen Unternehmen und Standardisierungsgremien eine Direktkommunikation zwischen Endgeräten, genannt Device-to-Device (D2D)-Kommunikation, vor.

Die Einführung von Direktkommunikation in Mobilfunknetzen erzeugt einen Paradigmenwechsel: Sie verwandelt die traditionelle Stern-Struktur in ein koordiniertes Mesh-Netz, mit welchem beliebige Netz-Topologien realisiert werden können. Desweiteren reduziert sich die Rolle der Infrastruktur-Knoten, welche vorher die einzigen Kommunikations-Endpunkte waren, zu Verwaltungseinheiten mit Gateway-Funktionalität. Direktkommunikation zu steuern ist intuitiv komplexer als das Steuern traditioneller Mobilfunkkommunikation. Zum einen ist anzunehmen, dass Gesamtzahl der Verbindungen in D2D-Netzen vergleichsweise höher ist, da Mesh-Netze mehr Verbindungsmöglichkeiten erlauben als Stern-Netze. Außerdem ist Information über Kommunikationseigenschaften, wie z.B. Kanalgüte, für Direktkommunikation nicht mehr automatisch an der Basisstation vorhanden, sondern muss explizit geschätzt werden. Dies erzeugt einen erhöhten Signalisierungsaufwand und erhöhte Latenz. Um diese gering zu halten und dennoch eine definierte Kommunikationsgüte garantieren zu können, müssen Teile des aktuellen Mobilfunk-Systems neu gestaltet werden.

Diese Dissertation widmet sich dem Einfluss von Direktkommunikation auf Mobilfunknetze, sowie den Möglichkeiten, solche korrekt zu steuern:

Es werden Skalierungs-Gesetze für die mittlere Ortsdichte von Direktverbindungen hergeleitet. Diese gelten unter axiomatischer Annahme eines grundlegenden Ablaufs, welcher von Kommunikationswünschen auf Dienst-Schicht zur Entstehung von Direktkommunikation auf Medienzugriffs-Schicht führt. Der Einfluss von Dienstverfügbarkeit auf Endgeräten, Geräte-Paarung in der Dienst-Schicht und Modus-Wahl in der Netz-Schicht auf die Skalierung wird untersucht. Das Ergebnis sind grundlegende Anforderungen, unter denen Direktverbindungen überhaupt eine erhöhte Bedeutung zukommt.

Die Fähigkeit von Direktkommunikation, zu erhöhter Netzgüte zu führen, wird diskutiert, mit dem Ergebnis, dass traditionelle Utility-Maximierung Direktverbindungen nur teilweise erfolgreich nutzen kann. Eine neue Ressourcen-Effizienz Metrik wird vorgeschlagen, welche die intuitiv in der Literatur definierten D2D-Gains zu fassen vermag. Grundlegen-

de Eigenschaften dieser Metrik werden untersucht. Auf Direktkommunikation angewandt führt diese zu Bedingungen, unter denen Utility-Maximierung Direktverbindungen gut in Szene setzen kann, sowie zu einem Verständnis, was für Alternativen in Betracht kommen.

Basierend auf den gewonnenen Erkenntnissen werden zwei Entscheidungsstrategien vorgeschlagen, welche Kommunikation als Direktkommunikation zu realisieren ist. Die erste basiert auf traditioneller Utility-Maximierung und ist Utility-optimal, vorausgesetzt, dass die Gütefunktion in einem Zwischenschritt optimiert werden kann. Die zweite basiert auf Ressourceneffizienz und zielt auf Situationen, in welchen Utility-Maximierung nicht anwendbar ist.

Schlussendlich werden Wege untersucht, die Wiederverwendung von Kanälen trotz Interferenz im Mobilfunknetz mit Direktkommunikation und Sendeleistungssteuerung dynamisch zu verwalten. Zwei Probleme werden untersucht: Schnelle Erkennung der Erreichbarkeit einer Dienstgüte trotz Interferenz und die Maximierung der Kanalverwendung auf einem einzelnen Kanal. Das Ergebnis ist eine semi-dezentrale Verwaltungsstruktur, in welcher Leistungssteuerung dezentral geschieht, aber Ressourcen-Management zentral. Es wird gezeigt, dass dieselbe Struktur auf eine Vielzahl von Utility-Maximierungs-Problemen mit Interferenz anwendbar ist.

Die präsentierten Erkenntnisse helfen, mögliche Anwendungsfälle für Direktkommunikation zu erkennen, sowie konkret Situationen auszumachen in denen direkte Kommunikation die bessere Wahl ist und laufende Direktverbindungen gut zu verwalten. Sie ermöglicht, Direktkommunikation korrekt zu handhaben und zu steuern.

Preface

At this point, a short comment on the organization and contributions of this thesis shall be given.

Thesis Organization

This work presents results on the impact of D2D communication in cellular networks, proposes ways how to successfully leverage the direct link option and control ongoing communication. In general, the thesis has been optimized in several steps for both, linear reading and cross-reading among different chapters. Each chapter is consistent in itself, targeting a different, closed aspect of D2D-communication. The chapters start with a short introduction and recapitulation of the considered aspect and problem statement, as well as a review on state of the art and cross-reference to introduced and used models. After producing the key results, a summary of the gained insights is given and their impact is discussed. Apart from being consistent in themselves, the different chapters are organized in a top-down approach on the network layers. That is, the contributions start with service level arguments and end with interference management.

As the investigations touch aspects of several network layers, a variety of models are used, depending on the considered system aspect. In fact, a core part of the research phase consisted of collecting existing models, evaluating their applicability to the D2D set-up and, if possible, adapting them to the given requirements. While most researchers are acquainted with some of the models, most, including the author, will not have full overview over all aspects of all used models. Putting at least the key points of all used models into one document in a clean and consistent fashion is a concern that the author has taken the freedom to follow. While this strictly speaking is no own contribution, it serves to show that the different models hook into one another, forming a holistic network description.

As for mathematical notations, this thesis follows the common standards for nomenclature, i.e., sets are upper case calligraphic letters, vectors are lower case and bold, matrices are upper case and bold, etc. For resolution of any questions, details on the nomenclature are given in Appendix A. All variables in this thesis are defined with as little overlap as possible. In networking community, many different abbreviations are used, which are explicitly written out in the Glossary at the end of the document. For convenience of the reader, in the .pdf version of this document, all abbreviations and references are linked with their glossary descriptions and counterparts, respectively.

Overview and Contribution of this Thesis

This thesis is roughly grouped into three parts, an introductory part of Chapters 1 - 2, a property part of Chapters 3 - 4 and an operational part in Chapters 5 - 6.

In Chapter 1, an overview over the intentions behind cellular networks, their current design and expected future of cellular networks is given. Further, nomenclature and motivation for D2D communication are presented, together with borders of the scenario, typically used classifications and research questions. The classification can be considered a minor contribution, as it does not exist in this style to the best knowledge of the author. Chapter 2 gives an overview over all used network models, together with their key intuitions and main used properties. All models are consistently applied to the D2D-scenario, giving an overview over all considered system aspects. This chapter mainly serves as reference for the reader and contains little to no own contribution, except for gathering all knowledge into a single place and applying it to a new scenario. An exception is Section 2.1.4, which presents a model that has been developed by the author.

The remaining Chapters 3 - 6 contain the main contributions of the author. In Chapter 3, scaling laws of D2D communication are investigated, using the stochastic geometry framework and an axiomatic setup-flow for direct links. The chapter mainly relies on publication [1], with a slight extension that is novel. Chapter 4 discusses the gains of D2D links with respect to cellular communication and relates it to traditional network utility maximization. A resource efficiency metric is defined and analyzed, resulting in conclusions on correct management tasks for direct links. The contributions of this chapter have partly been published in [4], [5], however, all aspects are for the first time put together into a holistic fashion in this thesis. Also, the notion of resource efficiency, its' impact and properties, are significantly enhanced compared to [4], [5], and thus must be considered novel. Ways for D2D Mode selection are investigated in Chapter 5. The first proposed algorithm has been published in [5], while the second is novel and for the first time developed and produced here. Finally, Chapter 6 targets interference management in cellular D2D communication and bases on the publications [2], [6], [7]. The extension of interference management towards arbitrary utility maximization is novel in this thesis, but has been submitted to [8]. In Chapter 7, the gained insights are summarized and open research directions are pointed out.

Publications by the author

Journal publications

[1] M. Klügel and W. Kellerer, "Dominant factors for device-to-device occurrence probabilities in cellular networks," *Wireless Networks*, 2017, ISSN: 1572-8196. DOI: 10.1007/s11276-017-1503-4. [Online]. Available: https://doi.org/10.1007/s11276-017-1503-4.

[2] M. Klügel and W. Kellerer, "The device-to-device reuse maximization problem with power control," *IEEE Transactions on Wireless Communications*, 2017. DOI: 10.1109/TWC.2017.2785818.

[3] T. Şahin, M. Klügel, C. Zhou, and W. Kellerer, "Virtual cells for 5g v2x communications," *IEEE Communication Standards Magazine*, 2018.

Conference publications

[4] M. Klügel and W. Kellerer, "Introduction of an efficiency metric for device-to-device communication in cellular networks," in *Vehicular Technology Conference (VTC Fall) 2014*, 2014, pp. 1–6. DOI: 10.1109/VTCFall.2014.6966021.

[5] M. Klugel and W. Kellerer, "Leveraging the d2d-gain: Resource efficiency based mode selection for device-to-device communication," in *2016 IEEE Global Communications Conference (GLOBECOM)*, 2016, pp. 1–7. DOI: 10.1109/GLOCOM.2016.7841953.

[6] M. Klügel and W. Kellerer, "Determining frequency reuse feasibility in device-to-device cellular networks," in *2015 IEEE 26th Annual International Symposium on Personal, Indoor, and Mobile Radio Communications (PIMRC)*, 2015, pp. 1503–1508. DOI: 10.1109/PIMRC.2015.7343536.

[7] M. Klügel, M. He, and W. Kellerer, "Investigation of decision metrics for reuse link selection in device-to-device communication," in *2016 IEEE 27th Annual International Symposium on Personal, Indoor, and Mobile Radio Communications (PIMRC)*, 2016, pp. 1–6. DOI: 10.1109/PIMRC.2016.7794861.

[8] M. Klügel and W. Kellerer, "Poster abstract: Semi-decentralized interference management in d2d-enabled cellular networks," pp. 1–2, 2018. DOI: 10.1109/INFCOMW.2018.8406902.

[9] M. Klügel and W. Kellerer, "On the feasibility of frequency reuse and spatial occupation in wireless device-to-device networks," in *2014 IEEE International Black Sea Conference on Communications and Networking (BlackSeaCom)*, 2014, pp. 154–159. DOI: 10.1109/BlackSeaCom.2014.6849029.

[10] M. Botsov, M. Klügel, W. Kellerer, and P. Fertl, "Location dependent resource allocation for mobile device-to-device communications," in *2014 IEEE Wireless Communications and Networking Conference (WCNC)*, 2014, pp. 1679–1684. DOI: 10.1109/WCNC.2014.6952482.

[11] M. Botsov, M. Klügel, W. Kellerer, and P. Fertl, "Location-based resource allocation for mobile d2d communications in multicell deployments," in *2015 IEEE International Conference on Communication Workshop (ICCW)*, 2015, pp. 2444–2450. DOI: 10.1109/ICCW.2015.7247545.

[12] M. Klügel, M. Newinger, W. Utschick, and W. Kellerer, "The relaxed power control algorithm," in *2017 European Conference on Networks and Communications (EuCNC)*, 2017, pp. 1–6. DOI: 10.1109/EuCNC.2017.7980715.

[13] T. Şahin, M. Klügel, C. Zhou, and W. Kellerer, "Multi-user-centric virtual cell operation for v2x communications in 5g networks," in *2017 IEEE Conference on Standards for Communications and Networking (CSCN)*, 2017, pp. 84–90. DOI: 10.1109/CSCN.2017.8088603.

Contents

Chapter 1

Introduction

Cellular, wireless communication systems have seen a fast evolution within the last years. Designed to transport human speech at first, they have developed to transport arbitrary data in digital form. The main use-case of cellular networks has changed from speech towards Internet access, including video and audio streaming, messaging and gaming. Internet providers extrapolate the current usage trends and foresee an exponentially increasing demand for high data rates that needs to be served.

However, this is not the only foreseen trend. As the amount of devices with wireless communication abilities is increasing and their functionalities are becoming more sophisticated, new application scenarios for cellular networks become viable and profitable. Examples are Machine-Type Communication (MTC), which includes sensor-actuator communication or vehicular communication, but also community applications like ad-hoc gaming, or peer-to-peer applications such as opportunistic content sharing. While some of these applications indeed require high data rates, others rather produce low-rate traffic but appear with high device densities, or need guarantees for the end-to-end latency and packet error rates. The combined trends, together with the visions of future networking concepts lead to the conclusion cellular networks should incorporate more than the "mere" delivery of data at high rates.

Standardization bodies currently are in the process of defining the next generation cellular networks – which is the 5th generation, 5G – to be capable of serving (1) high device density situations, (2) low delay requirements, (3) low outage requirements and (4) high data rates. The notion here is not to meet all requirements at the same time. Instead, the cellular network should be able to realize all types of requirements and coordinate them when they conflict each other.

One solution approach that can be used to implement core aspects of the desired future networks is D2D communication. Compared to current cellular communication, where a data stream is transmitted from a mobile UE to the BS, which forwards it into the core network of the operator and via another BS back to the receiving UE, D2D communication allows establishing a direct sidelink between two UEs. This breaks the star-like structure of cellular networks and allows the formation of arbitrary network topologies. At the same time it re-defines the role of the infrastructure, which is then reduced from an active participant

in ongoing communication to a set of management entities with gateway functionality.

The expected advantages of allowing sidelinks becomes evident in high density situations. Assuming an appropriate application such as distributed caching, communicating devices have a high probability of connection possibilities with nearby nodes. For sufficient spatial confinement, traffic among nearby nodes can use less energy and still achieve higher data rates and lower outage probabilities on the sidelink than towards the base station, due to the better channel conditions. Further, the use of a sidelink prevents data from being routed into the core network of the service provider, enabling low latency communications, and takes communication load off the base station.

The advantages of D2D communication are countered by the high complexity introduced into the system with sidelinks. In D2D capable networks, the infrastructure is not necessarily active part of the communication anymore. It thus does not automatically have access to information required for appropriate management, such as channel gains and buffer states. Further, the number of potential links in D2D networks is much larger than in cellular networks, because the former are mesh networks while the latter have a star structure. In overall, the infrastructure remotely needs to coordinate an increasing number of links, with less information available for this task. The combined complexity of managing sidelinks has achieved major attention in wireless research over the last years.

This thesis aims at analyzing the impact of direct links on cellular communication systems in a fundamental and generalizable way. While later chapters consider specific aspects of D2D communication, this chapter provides an overview over the targeted system and presents the general D2D set-up. Further, possible classification of D2D sub-cases, expectations of benefits from using direct links and open research questions are discussed.

1.1 Cellular Communication Systems

Cellular communication systems refer to a special type of infrastructure based, wireless communication systems that are designed to create wide-spread connectivity for mobile users. The core principle behind such systems is that of communication cells, which have a single access point with fixed location, the base station (BS), that serves as gateway to a fixed network. The counterpart of the base stations, the mobile stations (MSs), often also referred to as user equipments (UEs), establish connections with the BSs to access the fixed network and, via this, communicate with each other or with servers in the Internet. By placing base stations appropriately close, network coverage can be provided over a wide area, granting connectivity to the UEs irrespective of their current location. The placement creates a cell-like structure, shown as example in Figure 1.1.

Cellular networks have been originally developed as telephone networks and thus are operated by mobile network operators. Interoperability among them is an important practical aspect, which is why cellular communication systems are highly standardized. However, different standards for cellular communication exist and are roughly grouped in “generations”, which consider sets of standards that match certain criteria:

The first generation (1G) denotes analogue telephone cellular networks, whereas the first

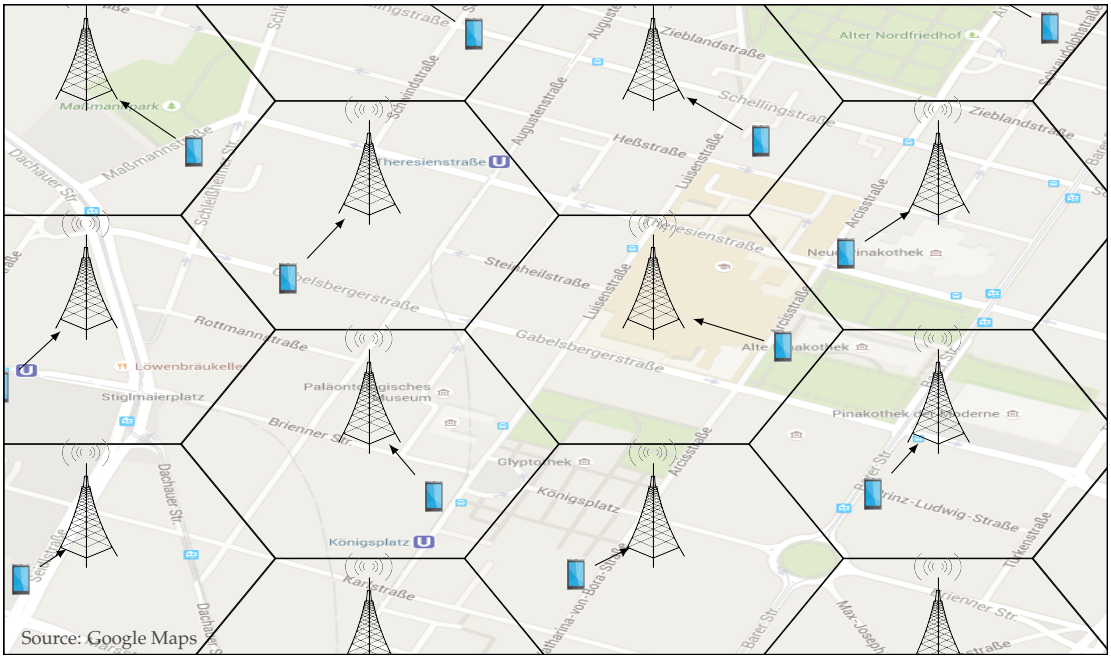

Figure 1.1: Example cellular network.

digital telephone networks, such as the Global System for Mobile Communications (GSM), are referred to as the second generation (2G). Although 2G networks allow digital data connections, for example Short Message Service (SMS), their main purpose is voice connectivity. Third generation cellular networks (3G) , e.g., Universal Mobile Telecommunications System (UMTS), are the first to explicitly target high data rate transmissions and Internet access. The fourth generation (4G) , which is the currently latest deployed with the LTE Advanced (LTE-A) standard, already allows peak data rates of up to 1 Gbps and is the first to be fully packetized, meaning that voice calls are treated just as one of many different, possible applications.

The next generation of cellular network standards, the fifth generation (5G), is currently undergoing standardization process [14], [15] with the aim of having first base stations deployed by around 2020. The aim of 5G networks is to enable new application scenarios and provide a more ubiquitous connectivity that goes beyond Internet access with high rates. In particular, massive connectivity scenarios, such as those required by sensor networks or vehicular communication, and ultra low latency communication, as necessary for MTC, shall be enabled along with a further improved high data rate Internet access. Standardization of 5G has initiated a series of research projects [16]–[20], as well as company efforts [21]–[28], that target at exploring the design space and propose example system designs.

To enable the different requirements, the focus of 5G is twofold [21], [24], [26], [28]. First, 5G networks are targeted to be *reconfigurable*. The different communication types might require the application of different networking structures with differences not only in the used prioritization mechanisms but even different medium access schemes. The current vision is that for each of the communication scenarios, a networking mode will be standardized and the overall network then is targeted to dynamically adapt to requirements by choosing

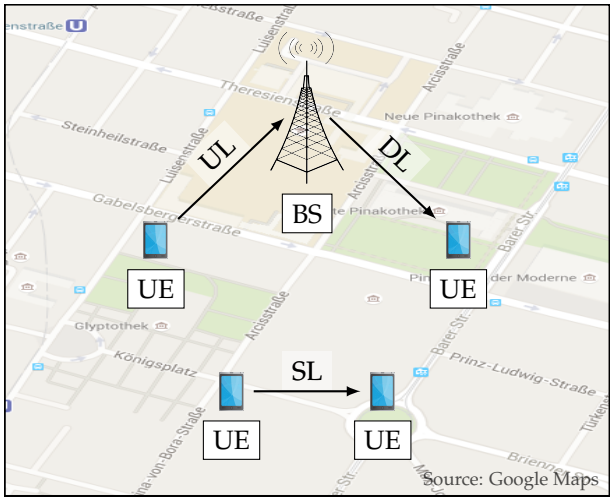

Figure 1.2: D2D-enabled cellular network

the appropriate mode. Second, 5G networks will be *virtualized*. This means that in both, fixed and wireless networking part, virtual, non-interfering network slices can be created and dedicated to a certain communication type. On wireless part, this requires an appropriate, interference free partitioning of resources such that all demands can be fulfilled. In the fixed network, virtualization techniques aim at providing interference free partitioning of communication resources, such as link data rates and node computational power, and are a current field of research. Both concepts, reconfiguration and virtualization, are expected to enable core aspects of 5G cellular networks.

1.2 Device-to-Device (D2D) Communication

One possibility to realize communication in high density scenarios is that of direct wireless transmission among UEs, also referred to as D2D communication [29]–[35]. In a D2D-enabled cellular network, devices are allowed to establish direct, low-distance sidelinks (SLs), effectively by-passing the fixed network infrastructure. This is depicted as an example in Figure 1.2. When allowed, these low-distance links are assumed to be useful and highly probable in ultra dense networks. Compared to cellular transmission, in high density scenarios D2D links have the advantage that communication flows do not have to travel into the core network of the provider, only to be routed back to their originating BS and to the recipient over the wireless link [29], [30]. Especially for cell-edge users, the uplink to the BS is often the bottleneck and higher transmission rates with lower energy and delay might be achievable on the sidelink. As the SLs are assumed to be low-distance and low-power, dynamic frequency reuse can be targeted within a single cell, which allows to increase the frequency reuse factor and hence the system spectral efficiency.

1.2.1 Properties of D2D Communication

The introduction of D2D sidelinks has been proposed specifically for cellular networks in licensed spectrum, which are highly standardized and operated by companies. However, ideas also exist to leverage different technologies for D2D links, such as WiFi or Bluetooth, with the advantage that they use a non-licensed, free spectrum. In this section, it will be shown that the D2D concept can in fact be transferred also to pure WiFi networks and further be abstracted towards a generalized D2D scenario. Main properties that create a D2D-enabled communication system are discussed and finally, the borders towards other related concepts, such as cognitive radio, are defined.

General Idea of D2D

Other network technologies such as WiFi [36], [37] or Bluetooth [38], [39] consider network structures that are also cellular, such that the D2D principle is applicable. In WiFi networks, there is an access point (AP) that serves as logical coordinator for a local area network (LAN) and as gateway to the fixed back-haul, with the possibility of providing Internet access. Smaller networks consist of a single AP only, whereas larger networks in companies have many APs that are connected by the same back-haul. Mobile devices are associated with a single AP that needs to be switched when they move too far. Similar to commercial cellular networks, Wireless-LANs (WLANs) have a star structure in the wireless part. A communication flow among devices is realized as two-hop communication towards and from the APs, eventually passing through the back-haul network as well. As both hops share the transmission channel, when devices are mutually within communication range, a two-hop communication will mostly achieve a lower throughput than a direct link between two devices. The introduction of direct links into such a network can thus be similarly motivated as for cellular networks. Ways for direct communication in WLANs have been proposed and are standardized, e.g., with WiFi-Direct [40]. In practice, however, WiFi-Direct has mostly been adopted as successor for the previously known ad-hoc mode of WLANs, in which direct connections are not automatically established but need to be set-up manually.

The WiFi-Direct example differs from the cellular network in the used MAC scheme, the used standards and level of centralization in network management. The core idea of direct communication for bypassing infrastructure, however, remains the same. D2D communication can thus be abstracted for arbitrary networks: In an abstract sense, D2D communication refers to the establishment of direct links in an infrastructure-based wireless network with star topology. An infrastructure thereby can contain any number of management entities and have different scale and back-haul topology. Further, the back-haul need not consist of wired connections but can also be wireless or heterogeneous. In the extreme forms, the infrastructure can consist of a single AP on the one hand, as often observed in a small WiFi or Bluetooth network, or a large infrastructure that provides full-area coverage on the other hand, as in commercial cellular networks. The direct communication is managed by the infrastructure entities, which however can decide to offload the management task to the direct links.

Link Type	Sensor	Broadcast	Ad-Hoc	Infrastructure	D2D-S	D2D-B	D2D-C
UL	✓			✓	✓		✓
DL		✓		✓		✓	✓
SL			✓		✓	✓	✓

Table 1.1: Wireless networks, classified according to their support for UL, DL and SL.

Uplink, Downlink and Sidelink

The introduction of D2D communication leads to a definition issue concerning traffic types. Per definition, traffic from a UE targeted to an AP is called *uplink (UL)*, whereas traffic from an AP towards a UE is called *downlink (DL)*. For D2D links, however, neither of both is appropriate because the AP is not involved in communication. For this reason, the term *sidelink (SL)* for D2D links is becoming increasingly popular [32]–[35].

Networks can be grouped by considering which types of links they allow. Uplink and downlink in this case correspond to communication to and from infrastructure nodes, using an arbitrary technology. The result of this classification is shown in Table 1.1. A network that allows downlink only would be a broadcast network. While a network that allows uplink only is not commonly deployed, it would resemble a sensor network, which is used, e.g., for monitoring an area. When a network contains only sidelinks, this means that no infrastructure is involved at all, hence the scenario is that of an ad-hoc network. When up- and downlink are allowed but no sidelinks, this corresponds to an infrastructure based network such as cellular networks or WLANs. The case that only uplink or downlink are allowed together with sidelinks corresponds to multi-hop sensor/broadcast networks (D2D-S/B). These cases have been considered in literature, however unrelated to D2D networks. They can be interpreted as a D2D enhanced broadcast/sensor network. When all three link types exist, the scenario is that of a D2D enabled infrastructure network (D2D-C).

The conclusion is that in general, a D2D network is any infrastructure based network that allows either uplink or downlink or both and is enhanced by sidelinks. As result, a network can comply with the D2D scenario irrespective of the used technology on it's communication layers. D2D networks can thus exist in licensed or unlicensed spectrum, with scheduled or random access based MAC layer, on terrestrial ground, on the sea, in airspace and even in space. In particular, it shall be noted that many of the results presented in this thesis are in fact not bound to the cellular network scenario, although they are derived from this perspective.

From Star to Mesh Topology

D2D communication is mostly motivated from a data rate perspective but in fact introduces a paradigm shift in infrastructure based networks. When direct links are allowed, the MAC layer communication topology is transformed from a star into a mesh structure. As this is done on MAC layer, several D2D links can be concatenated to realize a logical link via multi-

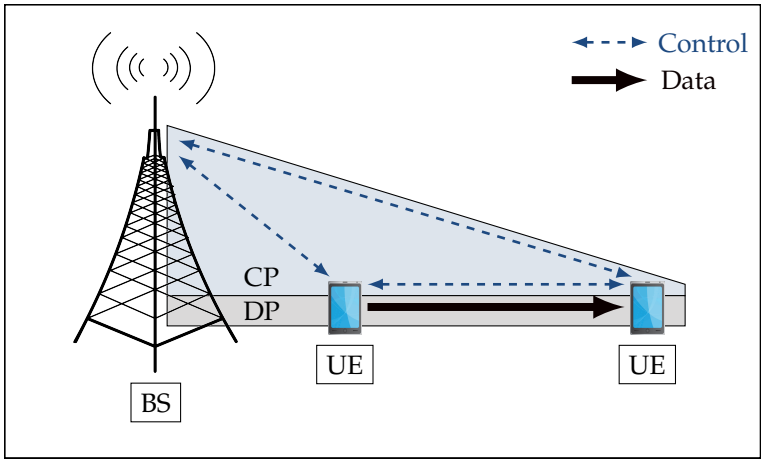

Figure 1.3: Control-Plane / Data-Plane Split of a D2D enabled cellular network. TheControl-Plane (CP) comprises of all possible management links, which can be included in UL, DL or SL as shown with the dashed arrows. The Data-Plane (DP) comprises of data links, shown with thick arrows.

hop communication, or to form any other desired, local topology. From this perspective, concepts such as wireless relays for range extension, phantom cells [41] or femto-cells [42] can be realized with D2D links.

Infrastructure Re-Defined

With the introduction of D2D sidelinks, the role of APs and the common assumptions change. In contrast to infrastructure based networks, where the access point is active participant in all communication links, it does not participate in sidelinks per definition. This falsifies the core assumption that communication parameters are known at the AP, which can use these parameters for network management tasks. This lack of information has an impact on the communication structure, e.g., for reporting and signaling structures [30], [43].

Further, the role of the AP is changed from an active participant in communication, as in traditional networks, to a network management entity with gateway functionality. The level of coordination offered by APs nodes is however a design choice [30], [43]. In an extreme case, the AP can enforce a centralized management on all nodes. This approach is often favored in cellular D2D and has the potential of high efficiency, as the whole network can be optimized jointly, but also has the danger of large management overhead. In the other extreme, D2D communication links could manage themselves in a decentralized fashion. This would be the natural choice in WiFi D2D, which has a decentralized nature in first place. The exact amount of centralization depends on the considered networking scenario and in general is subject to research.

Control-Plane / Data-Plane Split

To realize D2D links, it must be possible to separate the Data-Plane (DP), consisting of transport data traffic, from the Control-Plane (CP), comprising of management traffic [43]. In traditional cellular networks, CP traffic is often piggy-backed on transport channels for in-

D2D-Related Topics	Mesh Networks; Relay Networks; Tiered Cellular Networks; Multi-Hop Cellular Networks; Vehicular Networks
Non-D2D Topics	Ad-Hoc Networks; Cognitive Radio Networks

Table 1.2: Wireless research areas, classified according to their relation to the D2D scenario.

creased efficiency. However, this is often not possible in D2D links. In an extreme case, two links that are exchanging data do not actually exchange any control messages but are entirely coordinated by infrastructure nodes, with whom the control traffic is exchanged. In this case, control traffic is separated from data traffic. Of course, there are also cases where it makes sense to exchange control messages directly among communicating links, or where only part of control is done directly. However, combining CP and DP traffic is possible only when the SLs manage themselves decentrally. As this is only expected to happen partly, it motivates the need for a CP/DP split, which is shown in Figure 1.3.

Borders of the D2D Scenario

It is important to differentiate the D2D scenario from other, related topics. Many tasks required to realize direct sidelinks appear just as well in other scenarios, such as wireless mesh networks, mobile ad-hoc networks, relay-enhanced and tiered cellular networks or cognitive radio networks. The classification defines, which types of work need to be considered and compared against. After the preceding discussion, the core differences towards several related topics can be identified. The resulting classification is summarized in Table 1.2.

Related cases **that are not D2D** mainly include ad-hoc networks and cognitive radio networks. Ad-hoc networks inherently assume an entirely decentral architecture, from MAC layer up to the management layer. This requires decentralized solutions, which need to be accepted even if they are sub-optimal, as any centralized solution would require explicit cooperation of the nodes. For D2D networks, the existence of a centralized architecture is assumed, that may allow for decentral management but can just as well take control of the management. That is, decentralized solutions would be explicitly allowed but not a priori assumed. Similar arguments hold for cognitive radio, which assumes that nodes act opportunistically and inherently without central coordination.

Many other scenarios **can be realized with D2D**, although they are not thought as D2D communication in first place. These cases include cellular mesh networks, multi-hop cellular communication, cellular relay networks and vehicular networks. All of these use-cases inherently assume that there is an existing infrastructure that is in principle centrally coordinated and in some ways enhanced with direct links among UEs.

1.2.2 D2D Classification

Several types of D2D communication have been identified in literature and are grouped according to a nomenclature [44], which is presented in this section. The grouping is done from

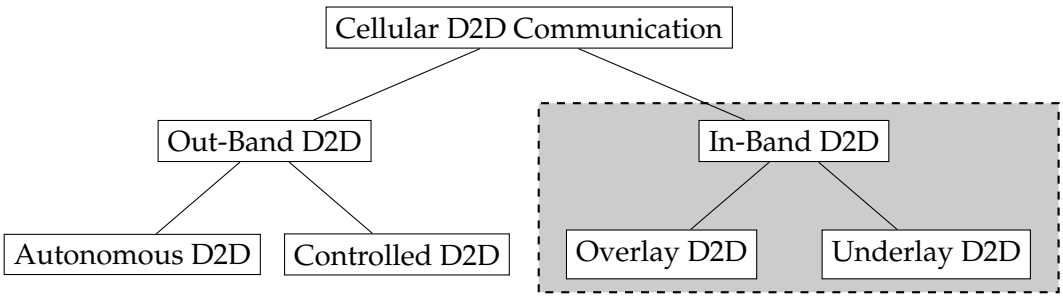

Figure 1.4: Nomenclature and classification of D2D works according to spectrum use. The cases considered in this thesis are highlighted with a gray box.

a cellular networking point of view and assumes that all communication is occurring in a cellular network, which manages the traffic in a standardized way. This grouping thus has to be seen independent of the property discussion of section 1.2.1. It distinguishes between the dimensions of **in-band**/**out-band**, **autonomous**/**controlled** and **overlay**/**underlay** D2D, as shown in Figure 1.4.

In-Band D2D communication considers D2D links that transmit on spectrum resources licensed by the Mobile Network Operator (MNO). In this case, the MNO has the legal right and technical possibility of strong influence on the communication, up to the extreme case where all parameters such as used transmission powers and modulation and coding schemes are tuned centrally. In the **out-band** D2D case, D2D links are offloaded to unlicensed spectrum, in which they communicate using random-access technology

Different levels of coordination in unlicensed band motivate the notion of autonomous and controlled D2D. In **autonomous** D2D, the direct links are established using a different MAC technology, such as WiFi. In this case, the BS is mainly a high-level management entity that chooses which links should be offloaded and assists with the device pairing to establish a WiFi link. With **controlled** D2D, on the other hand, the cellular network enforces some degree of control over the outband MAC technology. An example for this is LTE Unlicensed (LTE-U), where an Long Term Evolution (LTE) frame structure is imposed onto an unlicensed band.

The distinction among overlay and underlay communication assumes in-band D2D links. **Overlay** D2D therein refers to sidelinks that are scheduled on the same spectrum as uplink and downlink under exclusive resource usage. In the simplest case, this means that all links use orthogonal resources. However, it can also refer to the case where D2D links are assigned a resource pool which they can sub-divide among themselves in an orthogonal or non-orthogonal way. **Underlay** D2D communication assumes that D2D links are allowed to reuse transmission resources of uplink or downlink, as long as the created interference is within certain bounds. Often a one-fold reuse is targeted, however, in principle an arbitrary number of links may reuse a transmission resource subject to the bound constraints. This scenario resembles that of cognitive radio, where links try to opportunistically occupy licensed, but unused spectrum under the constraint that the actual licensees, the primary users, are not disturbed too much. The main difference between cognitive radio and underlay D2D is in the management structure, which is decentralized for cognitive radio but central for D2D.

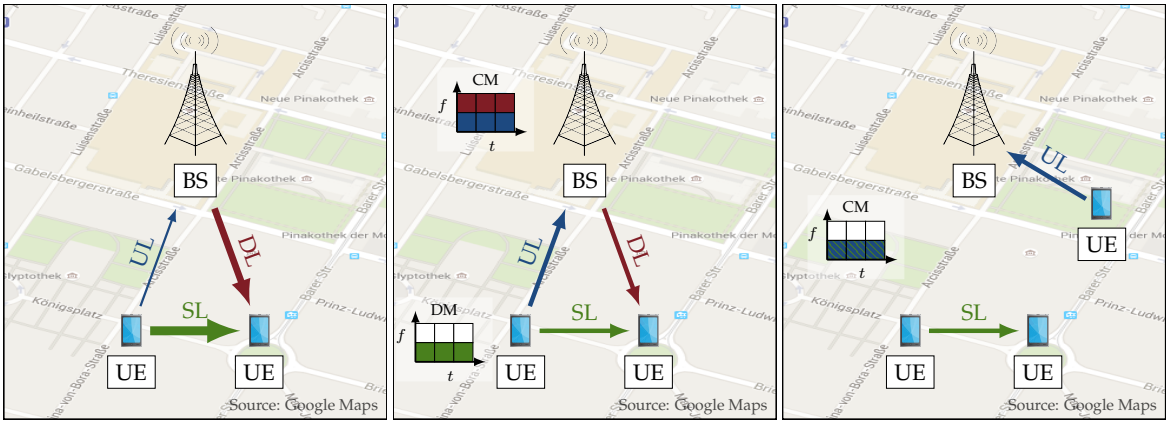

(a) Proximity-Gain **(b)** Hop-Gain **(c)** Reuse-Gain

Figure 1.5: Visualization of the three D2D gains postulated in [30]. The strength of arrows indicates relative channel quality, colors in the time-frequency grids indicate which links uses the resource. Resource reuse is indicated by the stripe-pattern in Figure 1.5c.

Underlay D2D has the potential to enable a highly efficient use of transmission resources but also is one of the most challenging scenarios due to the nonlinearity if wireless interference management problems.

1.2.3 Expected Gains from D2D in Cellular Networks

The idea of establishing direct links in a cellular network has been stated as early as 1998, long before the term "device-to-device" was established. Main works that introduce direct communication into cellular networks include "cellular ad-hoc united communication system" [45], "multihop cellular communication" [46], "hybrid wireless networks" [47] and "Unified Cellular and Ad-Hoc Network" (UCAN) [48], among others. However, these ideas did not attract much interest due to the high management complexity and low applicability, as direct connection possibilities were deemed very improbable. Only the recent estimation change, that future cellular networks will see a device densification by several orders of magnitude, has changed the attitude towards direct links.

The main expectations of introducing D2D, illustrated in Figure 1.5, have been well formalized by G. Fodor et al. [30], who postulated three gain types originating from direct communication: The **Proximity-Gain**, shown in Figure 1.5a, originates from the spatial proximity of direct sidelinks. As these are assumed to be low-distance, the direct channels are in general strong compared to the uplink channels, which often form the bottle-neck of cellular networks. The use of sidelinks thus allows high data rates at lower transmission power and with low delay, due to device proximity. This is illustrated in Figure 1.5a, where the strength of a channel is indicated by the strength of the arrows. The **Hop-Gain** denotes the fact that inherently, sidelinks require less transmission resources than an uplink-downlink communication because resources for two hops need to be used to transport an amount of data when relaying via the infrastructure, whereas only one hop needs resources for the sidelink. Further, bypassing the infrastructure drastically reduces latency, as the data does

not enter the core network and one transmission delay is omitted. The hop-gain is shown in Figure 1.5b. Resource use is therein indicated by the time-frequency grids, which are colored according to the links that use it. The resource benefit originates from omitting one network hop and is topology inherent rather than channel dependent. Finally, the **Reuse-Gain** comes from the fact that sidelinks can reuse transmission resources from uplink and downlink, or among themselves. As they are low-distance and require little transmission power for good transmission quality, they are robust against interference from other links and produce little interference in return. The proximity-gain is shown in Figure 1.5c, where resource use is indicated by the stripe-pattern of the resource grid.

The gain types Proximity-, Hop- and Reuse-Gain have been used as motivational argument for introducing D2D links and as qualitative intuition on where the benefits of certain offloading strategies originate from.

1.3 Research Questions

Several challenges arise in D2D enabled cellular networks, that are often targeted in research [29], [30], [44], [49] and will be given as a short motivation here. The challenges investigated in this thesis mainly refer to device pairing (Chapter 3), mode selection (Chapters 4 and 5) and interference aware resource allocation (Chapter 6).

Neighbor Discovery

Neighbor discovery targets the basic set-up mechanisms of D2D links. It refers to creating awareness of potential sidelink connectivities and is typically tackled by appropriate signaling methods. In general, it is assumed that there exist a set of paging resources, on which the devices may advertise their applications, to create awareness. However, interference and self-interference limit the amount of advertisements that can be received simultaneously. The target thus is to receive as many advertisements within as short time as possible.

Device Pairing

Device pairing refers to choosing the correct D2D pairs among a set of possible to create a well-defined networking situation. Whereas there are situations without a choice for pairing, e.g., if there is only one possible partner UE, other scenarios allow to form a variety of device pairs for D2D links. Examples here are distributed caching or gaming, where different choices for using a cache, or grouping of gaming partners, exist. The task then is to find appropriate pairs to optimize the network state, with respect to mutual interference or achievable rates. Pairing is mainly considered as cache selection for the distributed caching use-case, while other research branches simply assume direct links to exist. However, it will be shown to have a key impact on the number of D2D links in this work.

Mode Selection

Mode selection considers the question when a certain network flow should be served via a sidelink, called direct mode (DM), and when via uplink/downlink communication, which is the cellular mode (CM). The direct mode is sometimes further sub-classed into an overlay mode and underlay mode. Correct mode selection is crucial for network management, as offloading the wrong links can lead to severe performance degradation.

Resource Allocation and Interference Management

Resource allocation and interference management tasks need to be solved for D2D links, as in any other cellular wireless scenario. Apart from being complex to solve in general, the main difficulty in a D2D set-up is the lack of information at the central controller, the BS. Both, resource allocation and interference management need to be performed as decentralized as possible, to create as little management overhead as possible. The combination of resource allocation and interference management is one of the core research areas for D2D enabled cellular networks.

Chapter 2

System Description

In this chapter, the considered cellular system and D2D communication are introduced and used system models are formalized. D2D communication touches aspects of several networking layers reaching from device pairing to interference management, for each of which different aspects of the network need to be modeled. As a result, different models are available and used when appropriate.

As was stated in the Preface already, the main contribution of this chapter is to present the key points of all used models in a clean and consistent fashion and apply them to the D2D use case. The chapter mainly serves as reference for modeling aspects that the reader is not acquainted with. An exception is Section 2.1.4, which presents a model that has been developed by the author and thus is an own, novel contribution.

All used models are introduced in Section 2.1. For each model, the basic notations, relations and the main intuition are re-produced. The introductions are, in fact, brief compared to the possible depth of each direction. However, they serve to give a general notion and hint to sources for more background, if required. In Section 2.2, the introduced models are merged into an overall description of a D2D-enabled cellular network. The assumed action flows within the network are presented together with system assumptions and finally, the used simulation frameworks are introduced.

2.1 System Layer Models

D2D communication touches aspects of several networking layers, for each of which different aspects are modeled. On MAC level, the interest is in interference management, admission control and resource allocation for D2D networks, whereas mode selection and device pairing are considered to reside on network layer and above.

The different models will be introduced in a bottom-up approach: First, distributions of devices will be considered and the used channel models are presented. Then, the model for power control and interference management will be introduced. Afterwards a multi-hop commodity flow perspective is presented for scheduling problems and finally, the basis of a formal method to measure wireless transmission resources will be developed, which is required for subsequent analysis. For each of the models, main properties, known problems

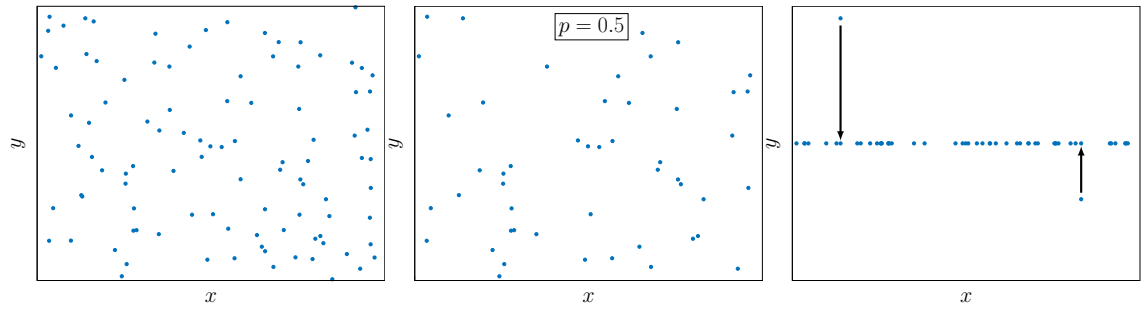

(a) Poisson Point Process **(b)** Thinning **(c)** Point Translation

Figure 2.1: An example p.p.p. in a 2-D plane and two related, possible transformations. Figure 2.1a shows the original, homogeneous p.p.p., whereas 2.1b shows a thinned version with constant retention probability $p = 0.5$. Figure 2.1c shows a translation that maps the thinned p.p.p. onto a single line, which results in a one-dimensional p.p.p..

and their solutions will be reviewed. Afterwards, in Section 2.2, the considered cellular network with D2D links will be fully modeled and the considered problem statements will be formally introduced.

2.1.1 Device Positions

The number and positions of devices are modeled as Poisson Point Process (p.p.p.) Φ, according to the Stochastic Geometry framework presented in [50]. Such p.p.p.'s are d-dimensional, typically 2D, point processes and are considered appropriate to model devices with independent, uncorrelated positions.

A point process can be interpreted as a collection of random points that appear in space according to a stochastic process. A realization of such random points is shown in Figure 2.1a. Formally, let there be a spatial observation area $\mathcal{V} \subseteq \mathbb{R}^d$ of size $|\mathcal{V}|$. Then for each point $\boldsymbol{x} \in \mathbb{R}^d$ define an indicator function $\delta_{\boldsymbol{x}} : 2^{\mathbb{R}^d} \mapsto \{0, 1\}$. The function takes an area $\mathcal{V}$ as input and indicates whether point $\boldsymbol{x}$ is in $\mathcal{V}$, i.e., $\delta_{\boldsymbol{x}}$ takes values according to $\delta_{\boldsymbol{x}}(\mathcal{V}) = 1$ if $\boldsymbol{x} \in \mathcal{V}$ and $\delta_{\boldsymbol{x}}(\mathcal{V}) = 0$ if $\boldsymbol{x} \notin \mathcal{V}$. Based on $\delta_{\boldsymbol{x}}$ the number of points N appearing in an area $\mathcal{V}$ can be assessed by defining a counting measure $\phi(\mathcal{V}) = \sum_{\boldsymbol{x}_i \in \Phi} \delta_{\boldsymbol{x}_i}(\mathcal{V})$. Because the points follow a stochastic process, $N = \phi(\mathcal{V})$ is a random variable.

A point process is called p.p.p. if, and only if, it exhibits the Poisson property: Assume any number of mutually disjoint areas $\mathcal{V}_1, ..., \mathcal{V}_k$ and define $\Phi(\mathcal{V}_k)$ to contain only the points of Φ that are in $\mathcal{V}_k$. Then, Φ exhibits the Poisson property if, and only if, $\Phi(\mathcal{V}_1), ..., \Phi(\mathcal{V}_k)$ are independent point processes for all mutually disjoint $\mathcal{V}_1, ..., \mathcal{V}_k$. As all points of the point process used in this work are assumed statistically independent, the Poisson property readily follows [50]. For p.p.p.'s, the number of points in $\mathcal{V}$ is Poisson distributed with a parameter $\Lambda(\mathcal{V})$, i.e.,

$$N = \phi(\mathcal{V}) \sim \text{Pois}(\Lambda(\mathcal{V})), \quad E\{N\} = \Lambda(\mathcal{V}). \tag{2.1}$$

$\Lambda(\mathcal{V})$ is a locally finite, non-null measure on $\mathbb{R}^d$ that can depend on the spatial location and is called *intensity* of the process. The intensity can take any form as long as it is a mathematical, locally finite and non-null measure [50]. It can be imagined as total amount of point intensity

in $\mathcal{V}$, accumulated over all its sub-areas. A special case of p.p.p.'s are homogeneous p.p.p.'s, for which $\Lambda(\mathcal{V}) = \lambda\,|\mathcal{V}|$ holds, for a $\lambda \geq 0$ that is called point *density*.

Apart from statistical assessment of number of points, p.p.p.'s allow some sophisticated operations that are well summarized in [50]. A short summary of the main properties required in this thesis is given in the following.

Superposition and Thinning

Poisson point processes allow superposition and thinning operations, in which independent processes are added to form an overall p.p.p., or points are randomly taken out of a process to form a new one. A simple example for process thinning is shown in Figure 2.1b.

Formally, the superposition of different point processes Φ_k is denoted by $\Phi = \sum_k \Phi_k$ and leads to a new p.p.p. Φ containing the union of all points in all Φ_k. Φ has an intensity $\Lambda(\mathcal{V}) = \sum_k \Lambda_k(\mathcal{V})$ [50]. In the case of homogeneous p.p.p.'s, this leads to $\lambda = \sum_k \lambda_k$.

For thinning, consider a retention function $p : \mathcal{V} \to [0, 1]$ that assigns a probability to each location in $\mathcal{V}$. The *thinning* Φ_p of process Φ with retention function p is a point process that contains each point $\boldsymbol{x}_i \in \Phi$ with probability $p(\boldsymbol{x}_i)$. Φ_p contains a number of points according to $N_p = \phi_p(\mathcal{V}) = \sum_{\boldsymbol{x}_i \in \Phi} \alpha_{\boldsymbol{x}_i} \delta_{\boldsymbol{x}_i}$, where the $\alpha_{\boldsymbol{x}_i}$ are independent random variables that are one with probability $p(\boldsymbol{x}_i)$ and zero with probability $1 - p(\boldsymbol{x}_i)$ [50]. If Φ is a p.p.p. with intensity $\Lambda(\mathcal{V})$ then the thinning Φ_p is a p.p.p. with intensity $\Lambda_p(\mathcal{V}) = \int_{\mathcal{V}} p(\boldsymbol{x})\Lambda(d\boldsymbol{x})$ [50], where the integral refers to Lebesgue integration. For constant retention probability, i.e., if $p(\boldsymbol{x}_i) = p$ $\forall \boldsymbol{x}_i$, the intensities relate as $\Lambda_p(\mathcal{V}) = p\Lambda(\mathcal{V})$, which in particular leads to densities of form $\lambda_p = \lambda p$ for homogeneous p.p.p.'s [50], respectively.

Point Translation and Stationarity

Assume a probability kernel $p(\boldsymbol{x}, \mathcal{V}')$ for $\boldsymbol{x} \in \mathbb{R}^d$ and $\mathcal{V}' \subset \mathbb{R}^{d'}$, $d' \geq 1$, such that for any fixed $\boldsymbol{x}$, $p(\boldsymbol{x}, \cdot) : \mathcal{V}' \mapsto [0, 1]$ is a probability distribution on $\mathcal{V}'$. Consider that $p(\boldsymbol{x}, \mathcal{V}')$ contains the probability of a point at position $\boldsymbol{x}$ being shifted to a point in $\mathcal{V}'$. Then using this kernel, the points of a p.p.p. Φ can be shifted from $\boldsymbol{x}_i$ to $\boldsymbol{x}'_i \in \mathcal{V}'$ with random positions according to the probability kernel $p(\boldsymbol{x}, \mathcal{V}')$ [50]. The points $\boldsymbol{x}'_i$ create a new point process Φ' that is Poisson with intensity $\Lambda'(\mathcal{V}') = \int_{\mathbb{R}^d} p(\boldsymbol{x}, \mathcal{V}')\Lambda(d\boldsymbol{x})$.

An example for point translation is given in Figure 2.1c, where all points of 2.1b are shifted onto a line. By using point translation, movement of points according to random walk and random way-point can be modeled. Further, inhomogeneous processes can be transformed into homogeneous p.p.p.'s by using appropriate kernels [50].

Consider a probability kernel $p_{\boldsymbol{v}}(\boldsymbol{x}, \mathbb{R}^d) = \delta(\boldsymbol{x}' - (\boldsymbol{x} + \boldsymbol{v}))\ \forall \boldsymbol{x}' \in \mathbb{R}^d$, where $\delta(\boldsymbol{x})$ is the Dirac measure that is one for $\boldsymbol{x} = \boldsymbol{0}$ and zero otherwise. The kernel $p_{\boldsymbol{v}}(\boldsymbol{x}, \mathbb{R}^d)$ moves all points by a deterministic vector $\boldsymbol{v}$ and thus creates a shifted version $\Phi_{\boldsymbol{v}}$ of any p.p.p. Φ. A p.p.p. is called stationary if, for any $\boldsymbol{v}$, the kernel $p_{\boldsymbol{v}}(\boldsymbol{x}, \mathbb{R}^d)$ does not change its distribution, i.e., if the stochastic processes $\Phi_{\boldsymbol{v}} = \Phi\ \forall \boldsymbol{v}$. It is shown in [50] that any homogeneous p.p.p. is stationary.

Campbell Measure

The Campbell measure is a measure for the mean number of points of a Poisson point process Φ in an area $\mathcal{V}$, conditioned on the event that the points satisfy a certain property Π. Formally, Π is a set of process realizations that satisfy a desired relational property, such as minimum distance among points or a maximum number of points in a certain sub-set of $\mathcal{V}$. Then, the Campbell measure is defined as [50]

$$C(\mathcal{V} \times \Pi) = \mathrm{E}\left\{ \int_{\mathcal{V}} \mathbb{1}\{\Phi \in \Pi\} \phi(d\boldsymbol{x}) \right\}. \tag{2.2}$$

In words the Campbell measure considers the expected number of points in $\mathcal{V}$, where only realizations from Π contribute. By this, $C(\mathcal{V} \times \Pi)$ can be interpreted as expected number of points in $\mathcal{V}$ that satisfy Π. It can be shown [50] that $C(\mathcal{V} \times \Pi)$ satisfies the relation

$$C(\mathcal{V} \times \Pi) = \int_{\mathcal{V}} P(\Pi)\, M(d\boldsymbol{x}), \tag{2.3}$$

where $M(d\boldsymbol{x})$ is a measure for the expected number of points of the unconditioned process Φ in the area element $d\boldsymbol{x}$ and $P(\Pi)$ is the overall probability of Φ satisfying property Π. In a homogeneous p.p.p., as $M(d\boldsymbol{x})$ is constant, the expected number of points in an area, conditioned on a property Π, is given as:

$$C(\mathcal{V} \times \Pi) = \lambda\, |\mathcal{V}|\, P(\Pi). \tag{2.4}$$

Typical Points

Consider all realizations of a homogeneous p.p.p. Φ that have a point at $\boldsymbol{x}_i$. Without loss of generality, they can be interpreted as shifted version of realizations from another homogeneous p.p.p. $\Phi_{-\boldsymbol{x}_i}$ with point at the origin $\mathbf{0}$, where the shift from $\Phi_{-\boldsymbol{x}_i}$ to Φ has been done with probability kernel $p_{\boldsymbol{x}_i}(\boldsymbol{x}, \mathbb{R}^d)$, respectively. As homogeneous p.p.p.'s are stationary, the translational shift does not change the point distribution, i.e., $\Phi_{-\boldsymbol{x}_i} = \Phi$ [50]. Further, it can be shown that when creating a process $\Phi^{\setminus \boldsymbol{x}_i} = \Phi \setminus \{\boldsymbol{x}_i\}$ by removing the point $\boldsymbol{x}_i$ from Φ, both processes $\Phi^{\setminus \boldsymbol{x}_i}$ and Φ still share some statistical properties [50]. In particular, if Π is a set of possible realizations of Φ *without* a point at $\boldsymbol{x}_i$, then $\mathrm{P}\{\Phi^{\setminus \boldsymbol{x}_i} \in \Pi\} = \mathrm{P}\{\Phi \in \Pi\}$. Because of this, for a homogeneous process, its relative distribution as "seen" from a random point of its realization can be assessed by creating a related process $\Phi^{\setminus \mathbf{0}}_{-\boldsymbol{x}_i}$, which is a version of Φ shifted such that the point $\boldsymbol{x}_i$ is moved to the origin and afterwards removed. It then holds that $\mathrm{P}\{\Phi^{\setminus \mathbf{0}}_{-\boldsymbol{x}_i} \in \Pi\} = \mathrm{P}\{\Phi \in \Pi\}$. The intuitive interpretation is that when the statistical properties of Φ shall be analyzed as seen from a random point of the process, it is sufficient to analyze the statistical properties of Φ with respect to the origin [50]. This method is referred to as the analysis of a *typical point* $\boldsymbol{x}_0$ of Φ.

Concluding Remarks

The concept of p.p.p.'s has successfully been applied to describe the positions of BSs [51], [52] and is often used to model positions and movements of UEs. In general, it can be used

to capture the location dependent stochastic aspects of wireless communication [50] and has been applied to the D2D use-case in a number of scientific works. In this thesis, it will be mainly used in Chapter 3, where the number of expected D2D links are assessed.

2.1.2 MAC Power Control Model

In wireless communication, power control considers the question which transmission powers to use to create an appropriate transmission quality for all links. The main task for management of D2D sidelinks on the level of power control is that of interference management for frequency reuse. Main results from wireless communications exist [53]–[58] that can be transferred to the D2D use-case and are presented here.

The Wireless Channel

For wireless communication in a D2D enabled cellular network, a given, cellular transmitter-receiver structure is assumed. When a transmitter sends a signal to its receiver, it is subject to attenuation, reflection and other distorting effects. At the wireless receiver, the distortions can partly, but not fully, be canceled by a filter that re-freshes the signal before de-coding.

Assuming a sufficiently good transmit-receive structure and coding scheme, the achievable rate depends mainly on the average received power, interference and noise [59]. On this abstraction level, the main impact of the wireless channel is an effective signal attenuation that is due to spatial distance of transmitter and receiver, shadowing, scattering and multi-path effects. In this work, the channel is thus abstracted with a scalar attenuation factor $h_{ij} \leq 1$ from transmitter j to receiver i, which captures the combined effect of signal attenuation, fading and multi-path effects, transmit and receive filter matching, antenna gains, cable and filter losses. Because the channel effects are mostly unknown, h_{ij} is modeled as random variable with predefined distribution according to the known Rayleigh-Fading and Ricean-Fading models [59].

For realistic distributions, channel models exist that are created from real-world measurements [60], [61]. However, these are generated for cellular links to and from base stations. As there were no deployed D2D enabled networks during development of this thesis, no appropriate, validated channel models existed. During the METIS project [16], [62], measurement campaigns for new model parameters were run, which included models for D2D links [63]. Main results are that, except for some special cases, existing the WINNER+ models could be tuned to incorporate D2D links by adapting the BS height to that of a UE. This method has been adopted throughout this thesis.

Signal to Interference and Noise Ratio (SINR)

Due to the broadcast nature of the wireless channel, signals that are not orthogonalized, e.g., in time and frequency, superpose and hence interfere with each other. Assume a set of links $\mathcal{L}$ that all interfere during a transmission. For fixed transmit-receive structures and physical

parameters, the achievable rate for a wireless link i is [64]

$$R_i(\boldsymbol{p}) = \log_2\left(1 + \Gamma_i(\boldsymbol{p})\right); \;\; \Gamma_i(\boldsymbol{p}) = \frac{h_{ii}p_i}{\sum\limits_{\substack{j\in\mathcal{L}\\ j\neq i}} h_{ij}p_j + N_i}. \tag{2.5}$$

where p_i is the average power used by link i's transmitter and N_i is the intrinsic noise power of receiver i. The variable $\Gamma_i(\boldsymbol{p})$ is called Signal to Interference and Noise Ratio (SINR) and reflects how strong the received, desired signal is in relation to the present disturbance in terms of interference and noise. The SINR depends on the used transmission powers, gathered in the power vector $\boldsymbol{p}$. It has a fractional structure, which renders it highly non-linear. Interference thus couples the links in a network in a challenging fashion that has attracted much research attention. Transmission powers need to be non-negative to comply with physical properties of transmission, and are typically upper bounded by a value $p_{i,\text{max}}$ due to technical or regulatory restrictions. From these constraints, the allowed power set can be generated as

$$\mathcal{P} = \{\boldsymbol{p} : \boldsymbol{0} \leq \boldsymbol{p} \leq \boldsymbol{p}_{\text{max}}\}, \tag{2.6}$$

where $\boldsymbol{p}$ is a column vector of transmission powers and $\boldsymbol{p}_{\text{max}}$ is a vector of maximum allowed transmission powers.

General Link Quality Functions

The SINR is known to reflect the "signal quality" of a transmission, as it is directly related to the achievable data rate. However, it was motivated already that in future wireless networks, data rate is not the only measure of choice, but that there is a multitude of metrics such as packet error rates, energy efficiency and transmission delay, which become more important as soon as a minimum data rate has been achieved.

While these measures capture different aspects of communication, many of them are related to the SINR: To reduce packet error rates, bit error rates must be reduced, which implies that SINR needs to be increased. To reduce a transmission delay, data rate, and hence again SINR, must be increased. As for other metrics such as energy efficiency, they are mostly of interest as long as a minimum transmission rate, i.e., a minimum SINR, is achieved.

The conclusion is that optimization of several other measures leads to optimization of the SINR. From this perspective, other quality metrics are represented by the SINR, which in itself reflects a signal quality in an abstract sense [57]. However, the connections go even further. Consider equation (2.5), where $R_i(\boldsymbol{p})$ is seen to be strictly monotonically increasing with SINR $\Gamma_i(\boldsymbol{p})$. Maximizing $\Gamma_i(\boldsymbol{p})$ thus directly corresponds to maximizing $R_i(\boldsymbol{p})$ and posing a constraint of the form $\Gamma_i(\boldsymbol{p}) \geq \gamma_i$ corresponds to demanding $R_i(\boldsymbol{p}) \geq 2^{\gamma_i} - 1$. As both metrics have a bijective, strictly monotonic relation, not only the SINR can be interpreted as representative for the rate but the rate can also be interpreted as representative for the SINR. Thus, the achievable rate $R_i(\boldsymbol{p})$, too, can be considered as measure for signal quality.

A similar argumentation can be done for a series of relations, which is formalized by introducing two sets Ψ, Υ of link quality (LQ) functions, also known as Quality of Service

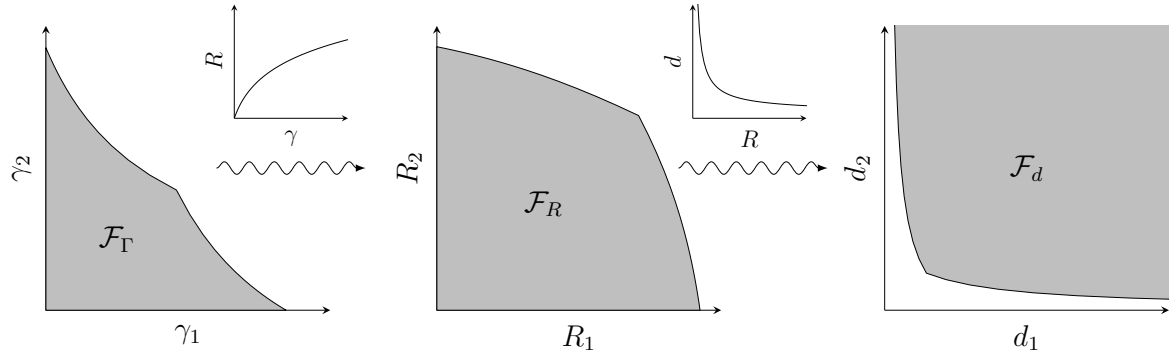

Figure 2.2: Transformation of feasible regions from feasible SINR, to feasible Rate and Delay.

(QoS) functions [57][1]. A function $\psi(\Gamma) \in \Psi$ is an LQ function when it can be written as a strictly monotonically increasing, bijective mapping of the SINR of each link. Similarly, a function $\phi(\Gamma) \in \Upsilon$ is an LQ function when it can be written as a strictly monotonically decreasing, bijective mapping of the SINR of each link. Any LQ function $\psi(\Gamma)$ or $\phi(\Gamma)$ can be interpreted to reflect the signal quality of an ongoing transmission, where the quality is considered better for increasing $\psi(\Gamma)$ or decreasing $\phi(\Gamma)$, respectively.

Examples of LQ functions are the achievable transmission rate $R(\Gamma) = \log_2(1 + \Gamma)$, SINR Γ itself and transmission delay $d(\Gamma) = c/R(\Gamma)$, further the bit error rate (BER) and decoding mean square error (MSE). Outage probabilities of the form $p_o(\Gamma) = P\{\Gamma \leq \gamma\}$ often define LQ functions, too, depending on the statistical properties of the channel.

Just as SINR, the value of any LQ function depends on the current transmission channels h_{ij}, noise values N_i and the used transmission powers $\boldsymbol{p}$. The LQ values of all links can be gathered in a vector representation $\boldsymbol{\psi}(\boldsymbol{p})$, where $\psi_i(\boldsymbol{p}) = \psi(\Gamma_i(\boldsymbol{p}))$, and $\boldsymbol{\phi}(\boldsymbol{p})$ analogously. For each LQ function, a set of feasible LQ-values can be defined as [57]

$$\mathcal{F}_\psi = \{\boldsymbol{x} \in \mathbb{R}_+^N : \exists \boldsymbol{p} \in \mathcal{P} : \boldsymbol{\psi}(\boldsymbol{p}) \geq \boldsymbol{x}\}; \text{ or } \mathcal{F}_\phi = \{\boldsymbol{x} \in \mathbb{R}_+^N : \exists \boldsymbol{p} \in \mathcal{P} : \boldsymbol{\phi}(\boldsymbol{p}) \leq \boldsymbol{x}\}, \tag{2.7}$$

where the first choice is for functions that increase with SINR and the second is for those that decrease with it. In words, $\mathcal{F}_\psi$ and $\mathcal{F}_\phi$ are the sets of multi-dimensional LQ-values that can be achieved by at least one power vector. For SINR, the set of feasible LQ-values is referred to as the feasible SINR region, for the rate as the feasible rate region, for delay as feasible delay region and so on.

An important property of the sets of LQ functions Ψ, Υ is that any quality constraint on an LQ function $\psi_1(\Gamma) \in \Psi$ can be transformed into a quality constraint of any other LQ function $\psi_2(\Gamma) \in \Psi$. This follows from their bijectivity, which makes the functions invertible, and strict monotonicity. Both together induce $\psi_1(\Gamma) \geq \psi_{1,\min} \Leftrightarrow \Gamma \geq \psi_1^{-1}(\psi_{1,\min}) \Leftrightarrow \psi_2(\Gamma) \geq \psi_2(\psi_1^{-1}(\psi_{1,\min}))$ for two increasing LQ functions, and analog for two decreasing functions, as well as a decreasing and an increasing function $\phi_1(\Gamma)$, $\psi_2(\Gamma)$, which yield $\phi_1(\Gamma) \leq \phi_{1,\min} \Leftrightarrow \Gamma \geq \phi_1^{-1}(\phi_{1,\min}) \Leftrightarrow \psi_2(\Gamma) \geq \psi_2(\phi_1^{-1}(\phi_{1,\min}))$. For example, $d(\Gamma) \leq d_{\min} \Leftrightarrow R(\Gamma) \geq R_{\min} \Leftrightarrow \Gamma \geq \gamma$.

[1] Note that the typical wording found in literature is QoS function. However, the term LQ function is used in this work to differentiate from higher layer QoS notions, which include the standardized integrated services (IntServ) and differentiated services (DiffServ) concept.

By this transformation, the feasible regions of all LQ functions are bijectively mappable and hence connected. This is depicted in Figure 2.2 for the three LQ functions SINR, rate and transmission delay. When different LQ functions are optimized, they will induce different optimal points, depending on their functional structures that favor different trade-offs. Constraints, on the other hand, are directly transferable among LQ functions. Further, if an optimization problem is infeasible for one LQ function, it is infeasible for any LQ function. It is thus often sufficient to consider aspects of one specific LQ function $\psi(\Gamma) \in \Psi$ or $\phi(\Gamma) \in \Upsilon$ while keeping in mind that it is representative for the whole class. In this work, the mainly investigated LQ function is the SINR.

Power Based Utility Maximization

Power control problems aim at maximizing a certain utility function $U(\boldsymbol{p})$ according to

$$\max_{\boldsymbol{p}} U(\boldsymbol{p}) \text{ s.t. } \boldsymbol{p} \in \mathcal{P}. \tag{2.8}$$

The utility reflects the quality of a certain power vector, in the sense of its capability of serving the current transmission demands. Typical utility functions are of the form $U(\boldsymbol{p}) = \sum_i U_i(\boldsymbol{p})$, [55], [57] where $U_i(\boldsymbol{p})$ can be:

- Weighted Sum-Rate: $U_i(\boldsymbol{p}) = w_i \log_2\left(1 + \Gamma_i(\boldsymbol{p})\right)$; for $w_i \geq 0$,
- α-Fairness: $U_i(\boldsymbol{p}) = \begin{cases} \log(R_i(\boldsymbol{p})) & \text{if } \alpha = 1, \\ (1-\alpha)^{-1} R_i(\boldsymbol{p})^{1-\alpha} & \text{if } \alpha \neq 1. \end{cases}$ for an $\alpha \geq 0$,
- Energy Efficiency: $U_i(\boldsymbol{p}) = \log_2\left(1 + \Gamma_i(\boldsymbol{p})\right)/p_i$,

among others. NUM problems can also be defined on higher layers, where they typically depend on the long-term average transmission rate and are only indirectly related to SINR values. In contrast to this, power control based NUM mostly refers to instantaneous SINR values and thus is only indirectly related to long-term transmission rates. Power control based utility maximization is a highly complex task, because the per-link utilities $U_i(\boldsymbol{p})$ are coupled through interference.

Inner and Outer Loop Problems

Most utility functions depend directly on the SINR and only via this with the transmission powers. This generates a problem structure which can be decomposed into easier to solve, functional sub-tasks of the form:

$$\max_{\boldsymbol{\gamma}} U(\boldsymbol{\gamma}) = \sum_i U_i(\gamma_i) \text{ s.t. } \boldsymbol{\gamma} \in \mathcal{F}_\Gamma \tag{NUM}$$

$$\min_{\boldsymbol{p}} 1 \text{ s.t. } \Gamma_i(\boldsymbol{p}) = \frac{h_{ii} p_i}{\sum\limits_{\substack{j \in \mathcal{L} \\ j \neq i}} h_{ij} p_j + N_i} \geq \gamma_i \ \ \forall i; \ \ \boldsymbol{p} \in \mathcal{P}. \tag{PC}$$

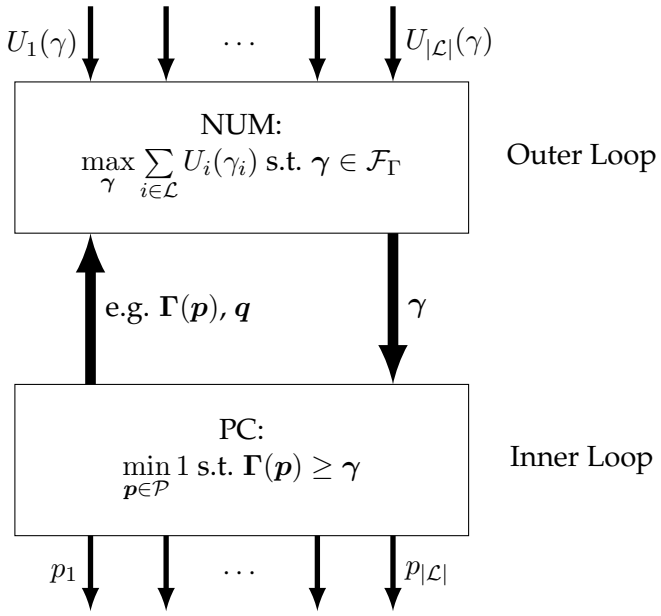

Figure 2.3: Inner/Outer loop structure of PC-NUM problems.

The first optimization problem, which is referred to as NUM problem, optimizes the utility function with respect to SINR. The chosen SINRs create constraints for the second problem, the power control (PC) problem. The optimizing function of the PC problem is constant, meaning that any point that satisfies the given constraints is in fact optimal. Hence, it aims at finding an arbitrary, feasible power vector. The core challenge of the two problems is the structure of $\mathcal{F}_\Gamma$, which depends on the current channel realizations and is often non-convex.

Both problems together create an implementable inner-outer loop structure that has been recognized in a series of works [55] and is shown exemplary in Figure 2.3, where $\boldsymbol{q}$ is a vector of interference plus noise temperatures $q_i = \sum_{j\neq i} h_{ij}p_j + N_i$. The exact feedback loop from the inner loop differs for different works, e.g., [65], [66], such that only examples are given in the figure. The PC problem is considered as inner loop and is steered by the outer loop NUM problem. The NUM problem regularly adapts SINR targets of the PC problem, which aims at achieving them, potentially reporting values back. An algorithm that solves the PC problem can thus be implemented in a module independently of the utility to be maximized. By doing so, the utility to be optimized can be switched arbitrarily, as the only coupling between both problems are the SINR and SINR target. It is typically assumed that the outer loop NUM problem is run by orders of magnitude slower than the inner loop PC problem [55]. Note that the split between NUM and PC problem as shown here is not mathematically concise but rather refers to functional blocks that can be used to solve interference aware networking problems.

The Power Control Problem

The focus is now on the inner loop, which considers the question how to achieve certain fixed SINR targets at all. As the SINR targets are fixed, the only remaining degree of freedom is that of transmission power and the resulting question is that of power control, i.e., how to adapt the transmission powers of all links to satisfy all SINR targets. The challenge here lies in the fact that all SINRs are globally coupled by interference, hence in general must be adapted together. One core question is that of decomposability, i.e., how to create an algorithm that allows all links to act independently, with little or no information exchange among them, and still be able to perform the PC in a satisfying manner.

PC problems have been intensively investigated in literature [53]–[55], [67]–[75], leading to a core representation that is introduced here. Consider a constraint on the SINR equation in (2.5), which can be re-written as

$$\frac{h_{ii}p_i}{\sum_{j\neq i} h_{ij}p_j + N_i} \geq \gamma_i \quad \Leftrightarrow \quad p_i \geq \sum_{j\neq i} \gamma_i \frac{h_{ij}}{h_{ii}} p_j + \gamma_i \frac{N_i}{h_{ii}} \quad \Leftrightarrow \quad p_i \geq \sum_{j=1}^{N} f_{ij}p_j + u_i, \tag{2.9}$$

where f_{ij} is a relative coupling coefficient, with $f_{ij} = \gamma_i \frac{h_{ij}}{h_{ii}}$ if $j \neq i$ and $f_{ij} = 0$ if $j = i$, and $u_i = \gamma_i \frac{N_i}{h_{ii}}$ is a relative noise value. The relative coefficients reflect the severity of interference and noise with respect to the link channel gain and the desired SINR target, respectively. A small channel gain or large γ_i will induce a large coupling coefficient, hence indicate severe interference, and vice versa. Inequation (2.9) can be stated for all links in a matrix-vector notation. For this, let $\boldsymbol{\Gamma}$ be a diagonal matrix with $\boldsymbol{\Gamma}_{ii} = \gamma_i$, let $\boldsymbol{D}$ be a diagonal matrix with $\boldsymbol{D}_{ii} = h_{ii}$ and $\boldsymbol{H}$ be the channel matrix with $\boldsymbol{H}_{ij} = h_{ij}$. Then (2.9) corresponds to

$$\begin{aligned} (\boldsymbol{I} - \boldsymbol{F})\,\boldsymbol{p} &\geq \boldsymbol{u}, \\ \text{where } \boldsymbol{F} &= \boldsymbol{\Gamma}\left(\boldsymbol{D}^{-1}\boldsymbol{H} - \boldsymbol{I}\right). \end{aligned} \tag{2.10}$$

$\boldsymbol{F}$ is called "relative gain matrix" or, sometimes, "Foschini's Matrix" and is a matrix with elements $\boldsymbol{F}_{ij} = f_{ij}$. Now define the feasible power set

$$\mathcal{F}_P(\boldsymbol{\gamma}) = \{\boldsymbol{p} : (\boldsymbol{I} - \boldsymbol{F})\,\boldsymbol{p} \geq \boldsymbol{u}\}, \tag{2.11}$$

respectively, which contains all power vectors that satisfy the given SINR constraints. Equation (2.10) gives an insight on the structure of $\mathcal{F}_P(\boldsymbol{\gamma})$: Each row of (2.10) defines a half-space of power vectors that are feasible for the corresponding link. Hence, $\mathcal{F}_P(\boldsymbol{\gamma})$ is known to be a cone defined by the intersection of such half-spaces [67], [76], as shown in Figure 2.4. Because of this structure, any $\boldsymbol{p} \in \mathcal{F}_P(\boldsymbol{\gamma})$ can be re-written as $\boldsymbol{p} = \boldsymbol{p}_p + \boldsymbol{p}_h$, where $(\boldsymbol{I} - \boldsymbol{F})\,\boldsymbol{p}_p = \boldsymbol{u}$ solves (2.10) with equality and $(\boldsymbol{I} - \boldsymbol{F})\,\boldsymbol{p}_h \geq \boldsymbol{0}$ is a vector that solves (2.10) for the noiseless case $\boldsymbol{u} = \boldsymbol{0}$. $\boldsymbol{p}_p$ points at the tip of the cone $\mathcal{F}_P(\boldsymbol{\gamma})$ and can be seen as the particular solution to (2.10). Accordingly, $\boldsymbol{p}_h$ is the homogeneous solution and points from the tip of $\mathcal{F}_P(\boldsymbol{\gamma})$ into $\mathcal{F}_P(\boldsymbol{\gamma})$. The structure of $\mathcal{F}_P(\boldsymbol{\gamma})$ and its relation to $\boldsymbol{p}_p$, $\boldsymbol{p}_h$ and $\boldsymbol{p}_{max}$ is depicted in Figure 2.4.

The matrix $\boldsymbol{F}$ has only positive or zero elements, i.e., is a non-negative matrix. According to the Perron-Frobenius Theorem for non-negative matrices [77], the maximum-norm eigen-

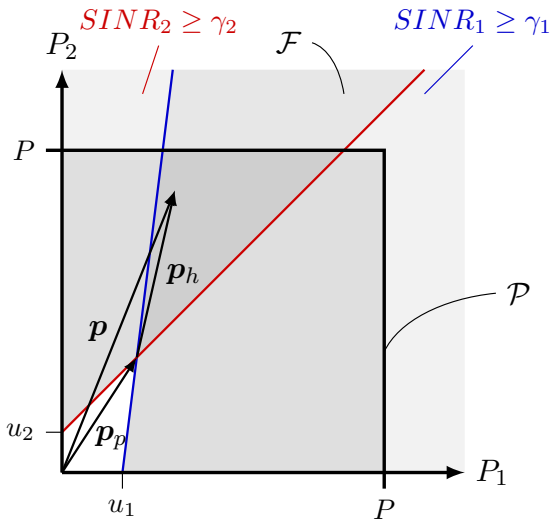

Figure 2.4: Structure of $\mathcal{F}_P(\boldsymbol{\gamma})$ and $\mathcal{P}$ with SINR-constraints for two links that both have P as maximum power.

value ρ of $\boldsymbol{F}$ is real and positive. This eigenvalue thus is equal to the matrix's spectral radius[2] $\rho(\boldsymbol{F})$. The eigenvector associated with ρ, which is denoted with $\boldsymbol{p}_\rho$, is known to have only positive elements [77], thus is a valid power vector [53], [67], [71]. $\boldsymbol{p}_\rho$ satisfies (2.10) for the noiseless case $\boldsymbol{u} = \boldsymbol{0}$ if and only if $\rho(\boldsymbol{F}) \leq 1$. Further, it can be shown that there is no solution to (2.10) if $\rho(\boldsymbol{F}) > 1$.

It can be concluded that there exists a valid solution to the PC problem if, and only if, $\boldsymbol{p}_p \leq \boldsymbol{p}_{\max}$ and $\rho(\boldsymbol{F}) \leq 1$. In the noise afflicted case $\boldsymbol{u} \neq \boldsymbol{0}$, this condition tightens to $\rho(\boldsymbol{F}) < 1$, because $\boldsymbol{p}_p \to \infty$ for $\rho(\boldsymbol{F}) \to 1$ [78].

The properties of the feasible power space and the notion of the eigenvector $\boldsymbol{p}_\rho$ as feasible solution in the noiseless case suggest that when noise is sufficiently low, finding $\boldsymbol{p}_\rho$ can help solving the PC problem.

The Power Control Algorithm

The structural properties of $\mathcal{F}_P(\boldsymbol{\gamma})$ shown in the previous section induce natural choices for power control algorithms (PCAs). Assume the interference limited case with $\boldsymbol{u} \approx 0$. In this case, a closed-form solution for the particular power vector can be given, which is $\boldsymbol{p}_p = \boldsymbol{0}$. Further, if $\rho \leq 1$, then

$$(\boldsymbol{I} - \boldsymbol{F})\boldsymbol{p}_\rho = (1 - \rho)\boldsymbol{p}_\rho \geq 0. \tag{2.12}$$

That is, if there are feasible power vectors, $\boldsymbol{p}_\rho$ will also be a feasible vector that satisfies all SINR constraints. The PC problem can thus be solved for arbitrary SINR targets by creating an algorithm that aims at finding $\boldsymbol{p}_\rho$. An algorithm that finds $\boldsymbol{p}_\rho$ would further be optimal in the sense that it finds a feasible power if, and only if, there is one.

One possibility to obtain $\boldsymbol{p}_\rho$ is the application of the mathematical power iteration [54], [79], which is a known method to find the dominant eigenvector, i.e., $\boldsymbol{p}_\rho$. The power iteration

[2] The spectral radius is the radius of the smallest ball, centered at the origin of the complex number space, that contains all eigenvalues.

update equation and its' convergence property are formally given as:

$$\boldsymbol{p}[k+1] = \boldsymbol{F}\boldsymbol{p}[k]; \quad \lim_{k\to\infty} \boldsymbol{p}[k] = \lim_{k\to\infty} \boldsymbol{F}^k \boldsymbol{p}[0] \approx \rho^k \boldsymbol{p}_\rho. \tag{2.13}$$

An iterative procedure based on the power iteration can in fact be efficiently implemented, because, as has been observed in [69],

$$[\boldsymbol{F}\boldsymbol{p}[k]]_i = \sum_{j\neq i} \gamma_i \frac{h_{ij}}{h_{ii}} p_j[k] = \frac{\gamma_i}{\frac{h_{ii}p_i[k]}{\sum_{j\neq i} h_{ij}p_j[k]}} p_i[k] = \frac{\gamma_i}{\Gamma_i(\boldsymbol{p}[k])} p_i[k], \tag{2.14}$$

where $\Gamma_i(\boldsymbol{p})$ is the Signal to Interference Ratio (SIR) due to the noiseless assumption. By (2.13), it is ensured that for sufficiently large k, the powers will result in a feasible allocation, if it exists. If there is no feasible allocation, then $\rho > 1$ and the powers diverge to infinity.

Transferring the same principle to the noise afflicted case $\boldsymbol{u} \neq 0$ results in an update equation of the form [54], [69], [80]

$$\boldsymbol{p}[k+1] = \boldsymbol{F}\boldsymbol{p}[k] + \boldsymbol{u}. \tag{2.15}$$

This can be expanded as [54], [69], [80]:

$$\boldsymbol{p}[k] = \boldsymbol{F}\left(\boldsymbol{F}\left(...(\boldsymbol{F}\boldsymbol{p}[0] + \boldsymbol{u})...+\boldsymbol{u}\right) + \boldsymbol{u} = \boldsymbol{F}^k\boldsymbol{p}[0] + \left(\sum_{l=0}^{k-1} \boldsymbol{F}^l\right)\boldsymbol{u}. \tag{2.16}$$

If $\rho(\boldsymbol{F}) < 1$, then $\lim_{k\to\infty} \boldsymbol{F}^k\boldsymbol{p}[0] = \boldsymbol{0}$ and $\sum_{l=0}^{k-1} \boldsymbol{F}^l$ forms a converging Neumann Series that is known to converge to $\lim_{k\to\infty} \sum_{l=0}^{k-1} \boldsymbol{F}^l = (\boldsymbol{I}-\boldsymbol{F})^{-1}$ [54], [69], [80]. That is,

$$\lim_{k\to\infty} \boldsymbol{p}[k] = (\boldsymbol{I}-\boldsymbol{F})^{-1}\boldsymbol{u} \;\Rightarrow\; \lim_{k\to\infty} (\boldsymbol{I}-\boldsymbol{F})\,\boldsymbol{p}[k] = \boldsymbol{u}. \tag{2.17}$$

Hence, for sufficiently large k, $\boldsymbol{p}[k]$ satisfies (2.9) and converges to $\boldsymbol{p}_p$. Due to the conical structure of $\mathcal{F}_P(\boldsymbol{\gamma})$, the vector $\boldsymbol{p}_p$ is the element-wise minimal power vector in $\mathcal{F}_P(\boldsymbol{\gamma})$ and hence minimal under any vector norm. Thus, (2.15) is known to solve the problem of finding the minimum power assignment for fixed SINR constraints [68], [69].

Similar to (2.14), iteration (2.15) has an intuitive technical interpretation as:

$$\boldsymbol{p}[k+1] = [\boldsymbol{F}\boldsymbol{p}[k] + \boldsymbol{u}]_i = \frac{\gamma_i}{\Gamma_i(\boldsymbol{p}[k])} p_i[k]. \tag{2.18}$$

The key property of the right hand side can be seen by assuming that all interfering powers remain fixed. In this case, plugging in the update rule (2.18) for $p_i[k+1]$ results in:

$$\frac{h_{ii}p_i[k+1]}{\sum_{j\neq i} h_{ij}p_j[k] + N_i} = \frac{\gamma_i}{\Gamma_i(\boldsymbol{p}[k])} \frac{h_{ii}p_i[k]}{\sum_{j\neq i} h_{ij}p_j[k] + N_i} = \gamma_i. \tag{2.19}$$

That is, transmitter i adapts its power such that, assuming interference fixed, the SINR target is achieved with equality. When all links use this update rule, links that achieve their SINR target, or even overshoot it, reduce their powers, whereas links that do not achieve their SINR targets increase their powers. A visual illustration of the update rule is given in Figure

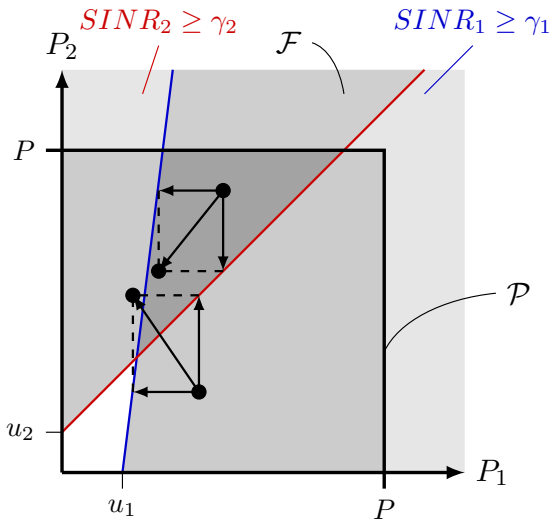

Figure 2.5: PCA update steps from two different starting points.

2.5, where the update step is shown from two different starting points. It can be fathomed that the iterations converge to the tip of the cone which forms $\mathcal{F}_P(\boldsymbol{\gamma})$.

Concluding, the PCA can be realized in a distributed fashion, as each link requires only its own target value and the currently achieved SINR to calculate its update. Further, it converges if, and only if, there exist feasible transmission powers. Among the feasible transmission powers, it converges to the tip of the cone that forms $\mathcal{F}_P(\boldsymbol{\gamma})$, hence the solution is the component-wise minimum among all feasible power vectors and the single Pareto-optimal, energy efficient point. Finally, it converges with linear convergence rate, with modulus $\rho(\boldsymbol{F})$ [54].

The presented PCA, often referred to as Foschini-Miljanic PCA (FM-PCA) [54], has been extensively investigated in literature. It has been shown to converge for both, synchronous [54] and asynchronous [70] power adaptation and several extensions have been proposed for robust power control [69], time-varying channels [81] and discrete power sets [72]. As it is well established and powerful, there is little to add in terms of research. It will become clear in Chapter 6 that it can well be used for D2D interference management.

The Feasible SINR Region

From the PC problem, which considers the inner loop optimization, structural conclusions for the outer loop optimization of setting appropriate SINR targets can be made. As the aim there is to optimize the target values with respect to a given metric, the chosen targets should allow feasible powers. If they would not, the targets could never be achieved, which would make the optimization obsolete. The optimization domain should thus be constrained to the set of feasible SINR values, $\mathcal{F}_\Gamma$, which can be defined as [6]

$$\mathcal{F}_\Gamma = \{\boldsymbol{\gamma} : \mathcal{P} \cap \mathcal{F}_P(\boldsymbol{\gamma}) \neq \emptyset\}\,. \tag{2.20}$$

So $\mathcal{F}_\Gamma$ contains all combinations of SINR targets, for which there exists a feasible power allocation in the valid power space.

In the noiseless case, the feasible SINR region $\mathcal{F}_\Gamma$ contains all SINR targets for which $\rho(\boldsymbol{F}(\boldsymbol{\gamma})) \leq 1$. In the noiseless case, $\mathcal{F}_\Gamma$ thus is entirely defined by the spectral radius. By interpreting the spectral radius as function of $\boldsymbol{\gamma}$, the feasible space can be interpreted as its sub-level set for a sub-level of one. In the noise-afflicted case, it is further constrained to those SINRs for which $\boldsymbol{p}_p \in \mathcal{P}$.

The exact structure of $\mathcal{F}_\Gamma$ is of interest for NUM problems because they define inherent properties of the targeted optimization [57]. The convexity properties are particularly in focus, because a convex $\mathcal{F}_\Gamma$ might lead to convex problems, which are known to be efficiently and decentrally solvable. Unfortunately, only few properties hold for $\mathcal{F}_\Gamma$ in general:

It is known that for any two non-negative matrices $\boldsymbol{A} \geq \boldsymbol{B}$, $\rho(\boldsymbol{A}) \geq \rho(\boldsymbol{B})$ holds [77]. From the definition of $\boldsymbol{F}$ it can be concluded that, for any two SINR target vectors $\boldsymbol{\gamma}_1 \geq \boldsymbol{\gamma}_2$,

$$\rho\left(\boldsymbol{F}(\boldsymbol{\gamma}_1)\right) = \rho\left(\boldsymbol{\Gamma}(\boldsymbol{\gamma}_1)\left(\boldsymbol{D}^{-1}\boldsymbol{H} - \boldsymbol{I}\right)\right) \geq \rho\left(\boldsymbol{\Gamma}(\boldsymbol{\gamma}_2)\left(\boldsymbol{D}^{-1}\boldsymbol{H} - \boldsymbol{I}\right)\right) = \rho\left(\boldsymbol{F}(\boldsymbol{\gamma}_2)\right). \tag{2.21}$$

It follows that $\mathcal{F}_\Gamma$ is downward comprehensive with $\boldsymbol{\gamma}$ and its complement, $\mathcal{F}_\Gamma^{-1}$, is upward comprehensive with $\boldsymbol{\gamma}$. That is, for any $\boldsymbol{\gamma}_1 \geq \boldsymbol{\gamma}_2$:

$$\boldsymbol{\gamma}_1 \in \mathcal{F}_\Gamma \;\Rightarrow\; \boldsymbol{\gamma}_2 \in \mathcal{F}_\Gamma; \quad \boldsymbol{\gamma}_2 \notin \mathcal{F}_\Gamma \;\Rightarrow\; \boldsymbol{\gamma}_1 \notin \mathcal{F}_\Gamma. \tag{2.22}$$

The same property can easily be shown to hold the noise-afflicted case. Further, it has been shown that when using a logarithmic transformation of the form $\gamma_i = e^{\tilde{\gamma}_i}$, then $\mathcal{F}_{\tilde{\boldsymbol{\gamma}}} = \{\tilde{\boldsymbol{\gamma}} : e^{\tilde{\gamma}} \in \mathcal{F}_\Gamma\}$ is a convex set with respect to $\tilde{\boldsymbol{\gamma}}$ [57], [73], [75], [82]. Formally, it holds for any two $\boldsymbol{\gamma}_1$, $\boldsymbol{\gamma}_2$ and $\alpha \in [0, 1]$ that

$$\boldsymbol{\gamma}_1, \boldsymbol{\gamma}_2 \in \mathcal{F}_\Gamma \;\Rightarrow\; \boldsymbol{\gamma}_1^{\alpha}\boldsymbol{\gamma}_2^{1-\alpha} \in \mathcal{F}_\Gamma. \tag{2.23}$$

In logarithmic scale, this is equivalent to

$$\tilde{\boldsymbol{\gamma}}_1, \tilde{\boldsymbol{\gamma}}_2 \in \mathcal{F}_{\tilde{\boldsymbol{\gamma}}} \;\Rightarrow\; \alpha\tilde{\boldsymbol{\gamma}}_1 + (1-\alpha)\tilde{\boldsymbol{\gamma}}_2 \in \mathcal{F}_{\tilde{\boldsymbol{\gamma}}}. \tag{2.24}$$

This log-convexity property has an impact on PC based NUM problems, which is discussed in the following.

Network Utility Maximization

After giving insight into the structural properties of the feasible SINR region $\mathcal{F}_\Gamma$ the loop can now be closed towards the NUM problems, which have the form of

$$\max_{\boldsymbol{\gamma}} U(\boldsymbol{\gamma}) = \sum_i U_i(\gamma_i) \text{ s.t. } \boldsymbol{\gamma} \in \mathcal{F}_\Gamma \tag{2.25}$$

For such optimization problems, the form of the utility and optimization domain are important properties. In particular, concave utilities in combination with convex domains create convex problems, that allow only one local and global optimum. Convex problems can be solved in polynomial time and often even allow decentralized implementations, which transfer to network algorithms. Non-convex problems, on the other hand, allow multiple local optima and mostly are harder to solve. Often these become non-deterministic, polynomial time (NP) complete or even NP hard.

It is thus important to observe the convexity properties of $U(\boldsymbol{\gamma})$ and $\mathcal{F}_\Gamma$. Because $\mathcal{F}_\Gamma$ is logarithmic-convex, the resulting NUM problems can be transformed into convex optimization problems if their utilities are log-concave, i.e., if $U(\boldsymbol{\gamma}_1^\alpha \boldsymbol{\gamma}_2^{1-\alpha}) \geq U(\boldsymbol{\gamma}_1)^\alpha U(\boldsymbol{\gamma}_2)^{1-\alpha}\ \forall \boldsymbol{\gamma}_1, \boldsymbol{\gamma}_2$ and $\alpha \in [0,1]$. This transforms to $U(e^{\tilde{\boldsymbol{\gamma}}})$ being concave in $\tilde{\boldsymbol{\gamma}}$. To create a convex problem, the variables then must simply be stated in logarithmic domain, i.e., the optimization must be done with respect to $\tilde{\boldsymbol{\gamma}}$ instead of $\boldsymbol{\gamma}$. The logarithmic transformation is sometimes claimed to reveal hidden convexity properties [57], [75].

The most popular class of utilities that does exhibit the log-convexity property are the α-fair rate-utilities. However, other popular problem types do not exhibit any hidden convexities, in particular not the sum-rate utility. Such utilities allow for local optima and hence often cannot be solved as efficiently. In some cases valid approximations for the rate function can render the sum-rate utility log-convex. Consider the approximations:

$$R_i = \log_2(1+\gamma_i) \approx \gamma_i \text{ for } \gamma_i \ll 1; \tag{2.26}$$

$$R_i = \log_2(1+\gamma_i) \approx \log_2(\gamma_i) \text{ for } \gamma_i \gg 1. \tag{2.27}$$

The first is called low-SINR approximation, as it holds for low SINR values, whereas the second is the high-SINR approximation. The low approximation creates linear utilities, which are log-convex and hence create non-convex NUM problem structures. However, the high approximation is linear in logarithmic domain and hence also log-concave. A sum-rate maximization under sufficiently high SINR targets thus creates a convex problem structure that can be solved efficiently.

Load-Spillage Framework

A well-known approach to solve the outer loop NUM for log-concave utilities is the load-spillage formulation introduced by Hande et al. [56], which is roughly sketched here. According to this framework, there are two indicator vectors $\boldsymbol{l}$ and $\boldsymbol{s}$ defined as

$$\boldsymbol{l} = \boldsymbol{F}\boldsymbol{p}_\rho \text{ and} \tag{2.28}$$

$$\boldsymbol{F}^T\boldsymbol{s} = \boldsymbol{s}\rho. \tag{2.29}$$

$\boldsymbol{l}$ and $\boldsymbol{s}$ are termed *interference load* and *interference spillage*. The terminology of interference load is intuitive, as it captures the relative interference of a link under use of $\boldsymbol{p}_\rho$. The term interference spillage becomes accessible when interpreting $\boldsymbol{s}$ as left eigenvalue of $\boldsymbol{F}$. According to the power iteration rule [79],

$$\lim_{k\to\infty} \mathbf{1}^T \left[\boldsymbol{F}^k \boldsymbol{p}\right] = \lim_{k\to\infty} \left[\mathbf{1}^T \boldsymbol{F}^k\right] \boldsymbol{p} \approx \rho^k \boldsymbol{s}^T \boldsymbol{p}$$

for any $\boldsymbol{p} \geq 0$. The left hand side of the expression can be interpreted as the sum of transmission powers after a very large number of PC iterations. Alternatively, it is the interference load after $k-1$ iterations. It reflects the aggregate amount of interference that is produced by the network in the long run to compensate a unit power "spilled" by link i's transmitter. Both, interference load and spillage are relative weights, because they are based on eigenvectors and hence unique only up to a scaling factor.

Load and spillage factors can be derived from Lagrangian multipliers using a primal-dual solution approach to the PC NUM problem. The interference management solution proposed in [56] results from several observations. First, it uses the fact that at optimality,

$$\boldsymbol{s} = \boldsymbol{F}^T \boldsymbol{l} \text{ and } \frac{s_i}{l_i} = \gamma_i \ \forall i \tag{2.30}$$

must hold. Second, the authors show that when keeping the load factors $\boldsymbol{l}$ fixed, associated SINR targets $\boldsymbol{\gamma}$ and spillage factors $\boldsymbol{s}$ can be calculated, such that load and spillage are the optimal Lagrange multipliers for $\boldsymbol{\gamma}$. Finally, an increasing direction for $\boldsymbol{l}$ is established, such that the associated $\boldsymbol{\gamma}$ create a larger utility. The increasing direction is given as:

$$\Delta l_i = \frac{U_i'(\gamma_i)\gamma_i}{q_i} - l_i, \text{ where } \boldsymbol{q} = (\boldsymbol{H} - \boldsymbol{D})\boldsymbol{p}_p. \tag{2.31}$$

q_i is the interference temperature at link i, using a power of $\boldsymbol{p}_p$. The proposed load-spillage algorithm [56] then assumes that the channel coefficients h_{ij} are known and creates an iterative procedure of the form: (1) Update $l_i := l_i + \alpha \Delta l_i$ at all links, for a fixed step-size α, and broadcast the resulting values. (2) Calculate s_i, γ_i from l_i. (3) Run the FM-PCA to identify $\boldsymbol{p}_p$ and $\boldsymbol{q}$. (4) Determine a new increasing direction Δl_i.

Note that the procedure assumes an FM-PCA to be run in step (3). This motivates that it is run on the outer loop and complies with the inner/outer loop structure. The Load-Spillage algorithm is known to converge towards an optimal solution for log-concave utility functions [56]. However, its implementation does not serve for D2D networks, as it assumes the channels known, which is not true for sidelinks. Nevertheless, the properties for its derivation, the entire power control theory framework, give a good starting point for D2D related interference management techniques, which will be leveraged in Chapter 6.

Concluding Remarks

Interference management has been identified as one of the key challenges in D2D enabled cellular networks. However, the used approaches in literature typically use a scheduling perspective and ignore major parts of dynamic power control, as will be shown in Section 6.2. The presented approach with Perron-Frobenius theory and inner-outer loop structure provides a good basis to leverage full power control, which will be shown to enable frequency reuse on a new order of magnitude in Chapter 6.

2.1.3 MAC Scheduling Model

The power control perspective presented in the previous section considers the impact of interference on achievable rates or other quality metrics but ignores higher layer properties, which are influenced by scheduling and routing decisions, as well as queuing effects. The model presented in this section, on the other hand, considers exactly these effects while abstracting interference. It has been well established in literature and is used to capture queue evolution in wireless networks. Details can be found in [83], which can be assumed as reference throughout the entire section.

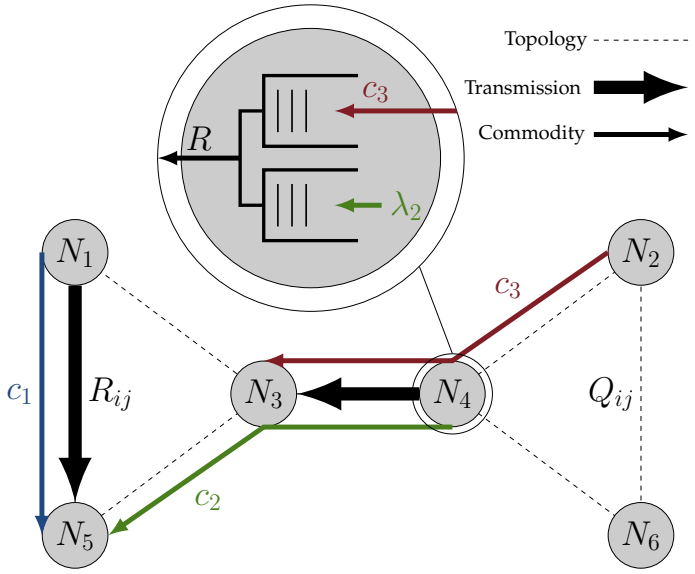

Figure 2.6: Depicted are a set of nodes, which transport data flows in a multi-hop fashion. All nodes maintain queues to transport data to their destination. Several nodes are connected with topology states Q_{ij}, shown with dashed lines, that indicate the possibility to transmit. Actual transmissions, given with bold arrows, decrease the queue of the transmitter node and increase that of the receiver node.

General Network Description

In this upper MAC layer perspective, the network is considered as a set of nodes $\mathcal{N}$, among which communication flows arise, as shown in Figure 2.6. From the nodes, a set of L MAC layer wireless links $\mathcal{L} \subseteq \mathcal{N} \times \mathcal{N}$ is formed over which data can be transmitted. Data flows are modeled as multi-commodity flows c_i, that may be transmitted over multiple hops. At the source node, a commodity arrives according to an assumed arrival process with expected time-average arrival rate of λ_i. Each node keeps a separate queue for all commodities passing through it. The back-log of a queue increases when data is received from other nodes or arrives from higher layers and decreases when data is transmitted over the wireless channel or passed to upper layers.

Transmissions are performed in consecutive time slots of length T, that are indexed with a variable $\tau \in \{0, 1, 2, ...\}$, where slot τ refers to the time interval $((\tau - 1)T, \tau T]$. Time slots can directly refer to their counterparts in a resource grid, but just as well model a super-frame that is composed of sub-slots. Wireless channel conditions are assumed to be fixed during a time slot but might change arbitrarily among different slots.

In each slot, the nodes can choose among a set of actions. Each action leads to defined data rate in the slot, depending on the current channel conditions and the action choices of other links. The goal is to transport the data towards their destination, for which the nodes can either be coordinated or act independently of each other.

Network State and Rate Function

The network is coupled by a topology state matrix $\boldsymbol{Q}[\tau] = \{Q_{mn}[\tau]\}\ \forall m, n \in \mathcal{N}$, indicated in Figure 2.6 with dashed lines, which is a collection of physical layer coupling information for each link $(m, n) \in \mathcal{L}$, respectively. The state can differ among different time slots, to model channel state evolution over time. Each link state $Q_{mn}[\tau]$ is taken from a possible state set $\mathcal{Q}$ that contains all allowed state values and may differ depending on the level of modeling detail. In a coarse model, e.g., $\mathcal{Q} = \{\text{ON}, \text{OFF}\}$ contains connectivity information only. In this case, $Q_{mn} = \text{ON}$ would denote that data can be transmitted from transmitter m to receiver n, whereas a state $Q_{mn} = \text{OFF}$ would indicate that there is no connectivity and no data can be transmitted.

Further, the network is associated with an action set $\mathcal{A}$ that contains the actions which a link can execute. The actions that are taken by link (m, n) at time τ are denoted with $A_{mn}[\tau] \in \mathcal{A}$ and can be gathered in the action matrix $\boldsymbol{A}[\tau] = \{A_{mn}[\tau]\}$. In the coarse model, the action set could be $\mathcal{A} = \{\text{TRANSMIT}, \text{IDLE}\}$. In general, idle links that do not transmit choose an idle action, which is denoted with A_0 throughout this thesis.

Both, state and action set are combined into a transmission rate function per link, $R_{mn} : \mathcal{A} \times \mathcal{Q} \mapsto \mathbb{R}_+$, which models the achieved rate for each combination of action set and channel state. The unit of the rate function can differ according to the exact model, typical units are bit per slot or packet per slot. In the given example, $R_{mn}(\text{ON}, \text{TRANSMIT}) = R$ would indicate the transmission of R bit per slot, whereas all other combinations would result in no transmission, i.e., $R_{mn}(\text{OFF}, \text{TRANSMIT}) = 0$, $R_{mn}(\text{ON}, \text{IDLE}) = 0$ and $R_{mn}(\text{OFF}, \text{IDLE}) = 0$. To shorten notation, refer to the rate at slot τ as $R_{mn}[\tau] = R_{mn}(\boldsymbol{A}[\tau], \boldsymbol{Q}[\tau])$, respectively. Further, the combination of all link rates achieved with a certain action matrix is denoted by the matrix $\boldsymbol{R}[\tau] = \boldsymbol{R}(\boldsymbol{A}[\tau], \boldsymbol{Q}[\tau])$, respectively.

A model of this type is appropriate to abstract the network layer from the exact physical properties of the devices and is applicable to a variety of scenarios. For a more fine grained model that is in compliance with the power control perspective presented in section 2.1.2, the state set $\mathcal{Q} = \mathbb{R}_+$ contains the attenuation coefficients of the wireless channel, i.e., the topology state matrix is $\boldsymbol{Q}[\tau] = \boldsymbol{H}[\tau]$, the channel matrix used from the power control perspective. The action set consists of a discrete set of Modulation and Coding Schemes (MCSs) in combination with an applied power, i.e., $\mathcal{A} = \mathcal{M} \times \mathcal{P}$, where $\mathcal{M} \in \{1, ..., M\}$ contains an index for each MCS to use and $\mathcal{P} = [0, p_{\text{max}}]$ is the allowed power set used in the previous section. Assuming a used bandwidth of W Hz and a slot length of T seconds per slot, the rate function $R_{mn}[\tau] = R_{mn}\left(\boldsymbol{p}[\tau], M_{mn}[\tau], \boldsymbol{H}[\tau]\right)$ from transmitter m to receiver n is defined as [84]:

$$R_{mn}[\tau] = R_{mn}\left(\boldsymbol{p}[\tau], M_m[\tau], \boldsymbol{H}[\tau]\right) = TW \log_2 \left(1 + C_m[\tau] \frac{h_{nm}[\tau] p_m[\tau]}{\sum\limits_{\substack{k \in \mathcal{L} \\ k \neq m}} h_{nk}[\tau] p_k[\tau] + N_n} \right), \quad (2.32)$$

where $C_m[\tau] \leq 1$ is a correction factor that depends on the MCS used by transmitter m. $R_{mn}[\tau]$ describes the amount of data that can be transported by link (m, n) in time slot τ,

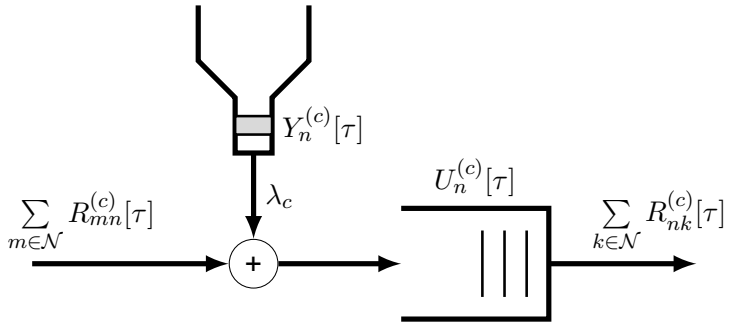

Figure 2.7: Input and output relations of a queue for commodity c, on node n. The input comprises of the data received from all other nodes and the data admitted at the current node, while the output comprises of all outgoing data. Note that according to the made assumptions, only one of the queue inputs can be active at each node.

using a certain MCS $M_m[\tau]$ and assuming an SINR according to a power vector $\boldsymbol{p}[\tau]$ with channel matrix $\boldsymbol{H}[\tau]$.

The model can be easily extended to heterogeneous topology state or action sets, where each device has a different action set to choose from. This can be incorporated by creating separate sets $\mathcal{Q}_{mn}$, $\mathcal{A}_{mn}$ that may differ per link and combining them into overall sets $\mathcal{Q} = \prod_{\mathcal{L}} \mathcal{Q}_{mn}$, $\mathcal{A} = \prod_{\mathcal{L}} \mathcal{A}_{mn}$, respectively, and can be used to model difference in device capabilities, e.g., transmission properties of BS versus those of UEs.

Data Admission and Queuing

Data admission considers the data arrival process at the source of each commodity. While data arrivals are in principle uncontrollable by the network, admission functions can be realized that control how much of the arriving data is injected into the MAC layer from higher layers. A special case of data admission is congestion control, where the admission targets the avoidance of congested links. However, admission can also be used for traffic shaping, e.g., for capping the maximum injected data rate or for creating certain traffic patterns, such as Token Bucket or Poisson traffic.

In the given model, it is assumed that all nodes maintain separate queues for all commodities passing through them and of which they are not the destination. The queues are assumed to have infinite length for simplicity. Each queue is subject to an arrival process and a service process, that depend on the actions taken in the network. The queue arrival process captures the combined effect of arrivals from higher layers and data admission for source nodes, as well as data reception from network transmissions. The service process models reduction in the queue backlog due to transmissions towards other links. At the destination node, data is assumed to be handed to higher layers immediately, corresponding to an infinitely large service rate.

Formally, the amount of data for commodity c, injected to the network at node n and slot τ, is denoted by the variable $Y_n^{(c)}[\tau] \in \mathbb{R}_+$. If $n \neq s_c$, $Y_n^{(c)}[\tau] = 0$ holds $\forall\tau$, i.e., only the source node can inject data. Each queue of node n for commodity c is described with a non-negative

backlog variable $B_n^{(c)}[\tau]$, which captures the amount of data present in the queue at slot τ. It is assumed that data is received and injected at the end of each time slot, after all transmissions have been performed. The queue backlog then evolves from slot to slot according to [83]:

$$B_n^{(c)}[\tau+1] = \left[B_n^{(c)}[\tau] - \sum_{(n,k)\in\mathcal{L}_c} R_{nk}^{(c)}[\tau] \right]^+ + Y_n^{(c)}[\tau] + \sum_{(k,n)\in\mathcal{L}_c} R_{kn}^{(c)}[\tau]. \tag{2.33}$$

That is, the backlog state of each queue firstly decreases by the amount of data that is transmitted to other nodes, but not below the value zero, then again increases by the amount of data that is received or admitted at the node. Together with the previously used rate function, queue evolution depends on the topology state, the actions taken and the data admission. The relation of the different variables and their role in the queue evolution is shown in Figure 2.7. Finally, define $D_c[\tau]$ to be the amount of data handed to the transport layer at d_c in slot τ, respectively.

Network State and Policies

The tuple $(\boldsymbol{Q}[\tau], \boldsymbol{B}[\tau])$ can be interpreted as network state at slot τ, which is out of the space $\mathcal{Q}\times\mathbb{R}_+$. The state space evolves from slot to slot according to given dynamics for the channel states and queues as discussed above. This evolution need not be deterministic - for example, the channel states can evolve according to a random process - but is definitely influenced by the action taken in each slot.

Define the history of channel states $\mathcal{H}_{\boldsymbol{Q}}[\tau] = \{..., \boldsymbol{Q}[\tau-1], \boldsymbol{Q}[\tau]\}$ and queue back-logs $\mathcal{H}_{\boldsymbol{B}}[\tau] = \{..., \boldsymbol{B}[\tau-1], \boldsymbol{B}[\tau]\}$ and admission decisions $\mathcal{H}_{\boldsymbol{Y}}[\tau] = \{..., \boldsymbol{Y}[\tau-1], \boldsymbol{Y}[\tau]\}$. Then a scheduling law can be defined as $\pi : \mathcal{H}_{\boldsymbol{Q}} \times \mathcal{H}_{\boldsymbol{B}} \mapsto \mathcal{A}$, which is a mapping from the state space $\mathcal{H}_{\boldsymbol{Q}} \times \mathcal{H}_{\boldsymbol{B}}$ to an action out of $\mathcal{A}$. This mapping can be deterministic or probabilistic, can depend on τ and can, but does not have to, incorporate the effect of reporting delays and estimation inaccuracies. The outcome of π is an action matrix $\boldsymbol{A}[\tau] := \pi(\mathcal{H}_{\boldsymbol{Q}}[\tau], \mathcal{H}_{\boldsymbol{B}}[\tau])$, which can be considered as schedule. Further, although π is treated from a global perspective, it might be realized by each link taking an independent action, i.e., in a decentralized fashion.

Similarly, define the history of admission decisions $\mathcal{H}_{Y_c}[\tau] = \{..., Y_c[\tau-1], Y_c[\tau]\}$ and received data $\mathcal{H}_{D_c}[\tau] = \{..., D_c[\tau-1], D_c[\tau]\}$. A congestion control policy $\varphi_c : \mathcal{H}_{Y_c} \times \mathcal{H}_{D_c} \mapsto \mathbb{R}_+$ defines how much data is admitted into the network at each source by using $Y_c[\tau] := \varphi_c(\mathcal{H}_{\boldsymbol{Q}}[\tau], \mathcal{H}_{\boldsymbol{B}}[\tau])$. Examples for such policies are sliding window protocols, whose window evolution can be formulated as function of the history of admissions and transport-layer receptions at the destination.

For fixed choice of π and $\varphi_c\ \forall c$, the whole network state evolution follows predetermined dynamics. While the channels $\boldsymbol{Q}[\tau]$ in general evolve according to stochastic processes, the evolution of $\boldsymbol{B}[\tau]$ depends on admissions, channel states and actions.

An overall performance metric on this abstraction level is network throughput, which is formally defined as:

$$\lambda_c = \lim_{t\to\infty} \frac{1}{t} \sum_{\tau=1}^{t} \mathbb{E}\{Y_c[\tau]\}. \tag{2.34}$$

A key interest lies in the ability of scheduling laws to satisfy throughput demands by transporting all injected data to the targeted destinations. The key notions related to this question are established in the following.

Per-Link Capacity Region

A key difficulty of designing scheduling laws lies in the time-varying nature of network evolution. The same action $\boldsymbol{A}$ can have different rate outcomes, depending on the current topology state $\boldsymbol{Q}[\tau]$, which evolves according to underlying statistics. Thus, a perfect action choice would assume $\boldsymbol{Q}[\tau]$ to be known at all time instances, and then deterministically choose the optimal actions based on the current realizations. However, even with full knowledge there is a fundamental limit on the achievable transmission rates. An interesting question thus is that, which transmission rates can actually be realized by appropriate scheduling, and how much data can be transported end-to-end over a network. To target this question, the notions of per-link capacity and transport capacity have been developed in literature, e.g. [83], which are introduced here.

The per-link capacity region contains all combinations of long-term, per-link rates that are actually achievable by at least one scheduling policy π. Assume for an instant that the topology state is fixed to $\boldsymbol{Q}[\tau] = \boldsymbol{Q}\ \forall\tau$. It is then known that when two action matrices $\boldsymbol{A}_1$, $\boldsymbol{A}_2$ are used for different time slots with relative frequencies α_1, α_2 such that $\alpha_1 + \alpha_2 = 1$, then the resulting long-term average rates are given by [83]

$$\lim_{t\to\infty} \frac{1}{t} \sum_{\tau=1}^{t} \boldsymbol{R}(\boldsymbol{A}[\tau], \boldsymbol{Q}) = \alpha_1 \boldsymbol{R}(\boldsymbol{A}_1, \boldsymbol{Q}) + \alpha_2 \boldsymbol{R}(\boldsymbol{A}_2, \boldsymbol{Q}). \tag{2.35}$$

That is, scheduling two actions with relative frequencies α_1, α_2 results in a long-term expected rate equal to the convex combination of $\boldsymbol{R}(\boldsymbol{A}_1, \boldsymbol{Q})$ and $\boldsymbol{R}(\boldsymbol{A}_2, \boldsymbol{Q})$. As this can be repeated for any actions out of $\mathcal{A}$, all convex combinations of single-action rates can be achieved by at least one scheduling policy π. On the other hand, any policy must lead to long-term average rates that are convex combinations of single-action rates:

$$\lim_{t\to\infty} \frac{1}{t} \sum_{\tau=1}^{t} \boldsymbol{R}(\boldsymbol{A}[\tau], \boldsymbol{Q}) = \lim_{t\to\infty} \frac{1}{t} \sum_{\tau=1}^{t} \boldsymbol{R}(\pi(\mathcal{H}_{\boldsymbol{Q}}[\tau], \mathcal{H}_{\boldsymbol{B}}[\tau]), \boldsymbol{Q}) = \sum_{\boldsymbol{A}_i \in \mathcal{A}} \alpha_i \boldsymbol{R}(\boldsymbol{A}_i, \boldsymbol{Q}). \tag{2.36}$$

As result, the long-term rates being convex combinations of per-link action rates is both, a necessary and sufficient condition for their realizability.

The capacity region $\mathcal{C}_{\boldsymbol{Q}}$ for a given topology state $\boldsymbol{Q}$ contains all realizable long-term rates under this state. From the preceding argumentation, $\mathcal{C}_{\boldsymbol{Q}}$ is known to be the union of all convex combinations of rates resulting from actions out of $\mathcal{A}$, which is the convex hull of rate vectors achieved by actions $\boldsymbol{A}_i \in \mathcal{A}$ [83]:

$$\mathcal{C}_{\boldsymbol{Q}} = \underset{\boldsymbol{A}_i \in \mathcal{A}}{\mathrm{Conv}} \{\boldsymbol{R}(\boldsymbol{A}_i, \boldsymbol{Q})\}. \tag{2.37}$$

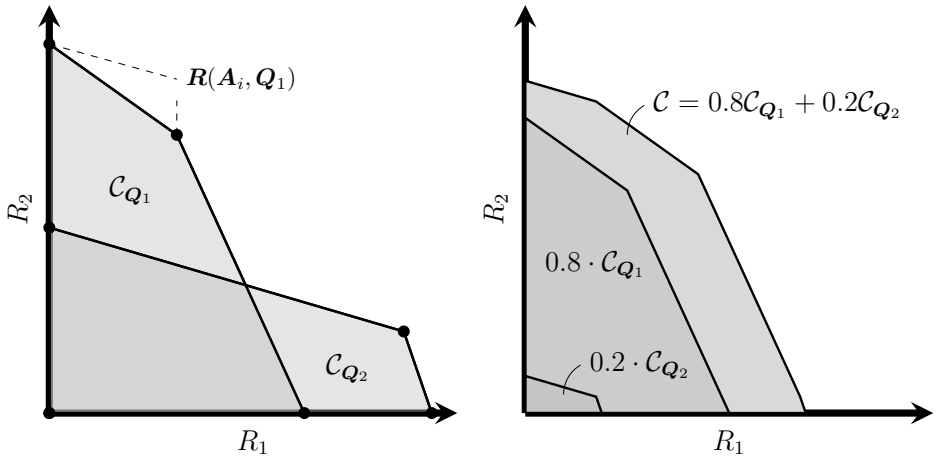

Figure 2.8: From actions to capacity region: The left figure shows the achieved rate vectors (R_1, R_2) for four different action combinations (A_0, A_0), (A_1, A_0), (A_0, A_1) and (A_1, A_1), and two different topology states $\boldsymbol{Q}_1$, $\boldsymbol{Q}_2$, together with their respective achievable rate region. The right hand side shows the generation of the overall capacity region, assuming that $\alpha_{\boldsymbol{Q}_1} = 0.8$ and $\alpha_{\boldsymbol{Q}_2} = 0.2$, respectively.

To incorporate variable topology states, assume that among all possible topologies, each state $\boldsymbol{Q}$ occurs with a relative frequency $\alpha_{\boldsymbol{Q}}$. As any topology state is available only $\alpha_{\boldsymbol{Q}}$ percent of time, the rate vectors in $\mathcal{C}_{\boldsymbol{Q}}$ can be chosen at most at this relative frequency. All capacity regions $\mathcal{C}_{\boldsymbol{Q}}$ are thus combined into a convex combination according to the fixed $\alpha_{\boldsymbol{Q}}$. So the overall capacity region is

$$\mathcal{C} = \sum_{\boldsymbol{Q} \in \mathcal{Q}} \alpha_{\boldsymbol{Q}} \mathcal{C}_{\boldsymbol{Q}} = \sum_{\boldsymbol{Q} \in \mathcal{Q}} \alpha_{\boldsymbol{Q}} \operatorname*{Conv}_{\boldsymbol{A}_i \in \mathcal{A}} \{\boldsymbol{R}(\boldsymbol{A}_i, \boldsymbol{Q})\}. \tag{2.38}$$

Here, $\alpha_{\boldsymbol{Q}} \mathcal{C}_{\boldsymbol{Q}}$ is a set containing any vector in $\mathcal{C}_{\boldsymbol{Q}}$, scaled by a factor $\alpha_{\boldsymbol{Q}}$. Further, the sum of two sets is interpreted as a new set, containing the sum of any element from the first with any element from the second.

The capacity region $\mathcal{C}$ mostly has a very complex structure, as it depends on the topology state statistics, and can only be explicitly generated for simple scenarios. An example for its' generation is shown in Figure 2.8, for two links, two topology states and four actions.

The definition of a capacity region simplifies notation in many cases and allows general structural statements, such as the conclusion that $\mathcal{C}$ is convex, closed and compact [83]. These statements play a role in NUM problems that are defined on this layer. Finally, assume a matrix $\overline{\boldsymbol{R}}$ of per-link long-term rates, then $\overline{\boldsymbol{R}} \in \mathcal{C}$ if, and only if, there exists a scheduling policy such that [83]:

$$\overline{\boldsymbol{R}} = \sum_{\boldsymbol{Q} \in \mathcal{Q}} \alpha_{\boldsymbol{Q}} \mathbb{E}\left\{\boldsymbol{R}[\tau] \mid \boldsymbol{Q}[\tau] = \boldsymbol{Q}\right\}, \tag{2.39}$$

where the elements of $\mathbb{E}\left\{\boldsymbol{R}[\tau] \mid \boldsymbol{Q}[\tau] = \boldsymbol{Q}\right\}$ contain the expectation of link rates under the considered policy, for given topology state $\boldsymbol{Q}$.

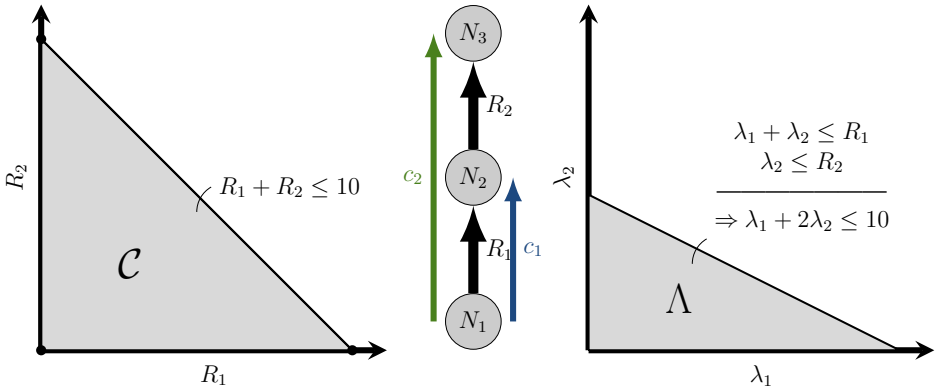

Figure 2.9: From MAC to transport capacity: A network with three nodes and two commodities is assumed as shown in the center. The left figure shows the assumed MAC layer capacity region, together with the generating capacity constraint. On the right is the resulting transport capacity region, which can be derived by combining the flow constraints with the MAC layer capacity constraint and maximizing λ_1 for each fixed λ_2.

Network Capacity Region

The single-hop data transmissions can be concatenated to form multi-hop, logical link data flows, which are modeled as commodity flows and indexed by an identifier $c \in \mathcal{K}$. Each commodity is associated with a source and destination node $s_c, d_c \in \mathcal{N}$ and is constrained to use a sub-set of the existing links, the allowed link set $\mathcal{L}_c \subseteq \mathcal{L}$, for data transport [83]. $\mathcal{L}_c$ can be used for routing, as it may contain a single path from s_c to d_c, or it may contain several, not necessarily disjoint paths for multi-path communication. In the extreme case it may contain all links of the network [83]. Each flow c is associated with an arrival process with expected value $\lambda_n^{(c)} \geq 0$ at node n. The data arrivals are stored in a local buffer, which is then served by the outgoing data rates.

For each commodity flow $c \in \mathcal{K}$ and link $(m,n) \in \mathcal{L}$ for given nodes $m, n \in \mathcal{N}$, a flow rate $R_{mn}^{(c)}[\tau]$ can be defined, that captures the amount of data from commodity c that is transported over link (m,n) at slot τ. $R_{mn}^{(c)}[\tau]$ is defined to be zero when $(m,n) \notin \mathcal{L}_c$, respectively. For all data to be transported to its destination node, flow rates must satisfy the constraint of

$$\sum_{c \in \mathcal{K}} R_{mn}^{(c)}[\tau] \leq R_{mn}[\tau], \quad \forall c, (m,n), \tau. \tag{2.40}$$

From the per-link capacity region, the network capacity region can be created, which is the set of all time-averaged, end-to-end logical link rates, i.e., all throughput rates, that can be supported by a scheduling policy for given network routes. The network capacity region is also sometimes called transport-layer capacity region [83], [85], or transport capacity [86], of a network. Formally, let $\lambda_n^{(c)}$ be an expected admission rate at which data of commodity $c \in \mathcal{K}$ is injected to the network at node $n \in \mathcal{N}$. Then the capacity region Λ is the set of all admission rates $\lambda_n^{(c)} \geq 0$, $\lambda_n^{(c)} = 0 \; \forall n \neq s_c$, such that there are a rate matrix $\overline{\boldsymbol{R}} \in \mathcal{C}$ and

multi-commodity flow variables $r_{nm}^{(c)}$ satisfying the constraints [83]:

$$\text{Flow Efficiency:} \quad r_{mn}^{(c)} \geq 0; \;\; r_{mm}^{(c)} = r_{d_c,m}^{(c)} = 0, \;\; \forall m,n \in \mathcal{N}, c \in \mathcal{K} \tag{2.41}$$

$$\text{Routing Constraint:} \quad r_{mn}^{(c)} = 0, \;\; \forall (m,n) \notin \mathcal{L}_c \tag{2.42}$$

$$\text{Flow Conservation:} \quad \sum_{l \in \mathcal{N}} r_{lm}^{(c)} + \lambda_m^{(c)} = \sum_{n \in \mathcal{N}} r_{mn}^{(c)}, \;\; \forall m \neq d_c \tag{2.43}$$

$$\text{Link Constraint:} \quad \sum_{c \in \mathcal{K}} r_{mn}^{(c)} \leq \overline{R}_{mn} \;\; \forall (m,n) \in \mathcal{L}; \;\; \overline{\boldsymbol{R}} \in \mathcal{C}. \tag{2.44}$$

The flow efficiency constraint guarantees that there are no negative rates, there is no self-communication and the destination node of a commodity does not forward data of the commodity. The routing constraint demands that commodities use only allowed links and the flow conservation ensures that any incoming data for non-destination nodes can be forwarded. Finally, the link constraint guarantees that the assigned rates are long-term achievable by a scheduling policy.

Together, the constraints model a fixed network with associated multi-commodity flow variables and link rates that can be supported in long-term by the wireless network. That is, the network capacity region Λ contains the set of all admission rates $\lambda_n^{(c)}$ for which a scheduling policy exists, that allows to transport all data to their designated targets in a multi-hop fashion for fixed routes. Transport capacity region and MAC capacity region differ in their generation, because the MAC region defines the link constraints for the transport region. In this sense, the transport capacity region can be interpreted as feasible region for transport layer flow variables. An example for a MAC capacity region and its related transport capacity is given in Figure 2.9.

Network Queue Stability

The presented model allows analysis of logical link traffic for different physical layer implementations and centralized or decentralized network architectures. Typically, the interest is in queue evolution under different traffic admission and scheduling decisions, which are analyzed for deterministic or probabilistic evolution of topology state matrices, and actions based on accurate, erroneous or outdated information. The targets vary from keeping all queue backlogs in the network bounded to minimizing delay, guaranteeing QoS or optimizing a general utility.

A queue backlog that is unbounded indicates that the network is in an overload situation and that not all traffic can be served. Hence, keeping all queue backlogs bounded can be considered as minimum requirement to guarantee network functionality. Boundedness is defined by the concept of queue stability [83]. According to this, a queue is called *strongly stable*, if

$$\lim_{t \to \infty} \sup \frac{1}{t} \sum_{\tau=1}^{t} \mathbb{E}\{U[\tau]\} < \infty. \tag{2.45}$$

In words, a queue is strongly stable if its time average expected backlog is upper bounded. Correspondingly, a network is called strongly stable, if all queues therein are strongly stable.

To analyze queue stability, data admission, reception and transmission are considered as stochastic processes, with a distribution that is most often unknown. Stability properties can already be established for rather mild assumptions on the processes, which are established in [83]. Processes that satisfy the required assumptions are called *admissible*. In particular, an admission process $Y[\tau]$ is called admissible with rate λ if [83]:

- The time average expected admission rate satisfies: $\lim_{t\to\infty} \frac{1}{t} \sum_{\tau=0}^{t-1} \mathbb{E}\{Y[\tau]\} = \lambda$.
- There exists a finite value $Y_{\max}$ such that $\mathbb{E}\{Y[\tau]^2 \mid \boldsymbol{H}[\tau]\} \leq Y_{\max}^2$, for all time slots τ, where $\boldsymbol{H}[\tau]$ represents the history of all events up to slot τ.
- For any $\delta > 0$, there exists an interval size T (that may depend on δ) such that for any initial time τ_0 the condition $\mathbb{E}\left\{\frac{1}{T}\sum_{k=0}^{T-1} Y[\tau_0+k] \mid \boldsymbol{H}[\tau_0]\right\} \leq \lambda + \delta$ holds.

In words, an admissible admission process has a well-defined time average expected value, approaches this value from above in average for a large enough time period, irrespective of the beginning of observation time, and has a bounded second order moment. Important examples for such admission processes are admission processes with finite burstiness and i.i.d. admission processes [83].

Similarly, a service process $R[\tau]$ is called admissible with time average service rate $\overline{R}$ if:

- The time average expected service rate satisfies: $\lim_{t\to\infty} \frac{1}{t} \sum_{\tau=0}^{t-1} \mathbb{E}\{R[\tau]\} = \overline{R}$.
- There exists an upper bound $R_{\max}$ such that $R[\tau] \leq R_{\max}$ for all τ.
- For and $\delta > 0$, there exists an interval size T (that may depend on δ) such that for any initial time τ_0 the condition $\mathbb{E}\left\{\frac{1}{T}\sum_{k=0}^{T-1} R[\tau_0+k] \mid \boldsymbol{H}[\tau_0]\right\} \geq \overline{R} - \delta$ holds.

Similar to an admission process, a service process is admissible if it has a well-defined time average expected value, approaches this value from below in average for a large enough time period, irrespective of the beginning of observation time, and is upper bounded by some value.

Using the above definitions, when an admission process is admissible with rate λ and a service process with rate $\overline{R}$, then [83]:

a) $\lambda \leq \overline{R}$ is a necessary condition for strong stability of a queue and

b) $\lambda < \overline{R}$ is a sufficient condition for strong stability.

Scheduler Stability Region

From the above notion of queue stability and admissible admission and service processes, the *stability region* of a scheduling policy can be defined. For this, denote the policy by an arbitrary identifier $*$. Then its stability region Λ_* is the set of all flow admission rates $\lambda_c \geq 0$ such that admissible admissions with expected value λ_c can be supported by the policy

with strongly stable queues. The formal definition is omitted here but is analog to that of the network capacity region, only that the rate matrix $\boldsymbol{R}$ is replaced by a matrix of admissible time average service rates $\overline{\boldsymbol{R}}$ that are supported by the policy.

The stability region of a scheduling policy contains all combinations of end-to-end commodity flow rates that are in fact long-term realizable by the policy. It can thus be interpreted as the portion of transport capacity that can be realized with a specific scheduling law. In contrast, the overall transport capacity itself contains all end-to-end rates that are realizable by at least one policy, i.e., is the union of the stability regions of all possible scheduling policies.

In general, the stability region of a scheduling policy should be as large as possible. It is known, and has been shown in [83], that the Dynamic Backpressure scheduling law has a stability region that equals the interior of the transport capacity. Backpressure scheduling thus is optimal in the sense that it can serve any demands that can be served at all.

Finally, we consider the border of the stability region, $\partial\Lambda_*$, which can also be

Known Scheduling Policies

There are several scheduling policies which are well-known and evaluated in this thesis. The schedulers are presented here for single-channel wireless systems with Time Division Multiple Access (TDMA) based scheduling without frequency reuse. Denote the empirical time-average transmission rate of each link with $\overline{R}_{mn}[\tau] = \frac{1}{\tau}\sum_{k=1}^{\tau} R_{mn}[\tau]$, and the estimate of the current, maximum achievable rate for link (m,n) with $R^*_{mn}[\tau] = \max_{A_i\in\mathcal{A}} R_{mn}(A_i, \boldsymbol{Q}[\tau])$. Further, let $A^*_{mn}[\tau] = \arg\max_{A_i\in\mathcal{A}} R_{mn}(A_i, \boldsymbol{Q}[\tau])$ be the action choice that maximizes link (m,n)'s rate and let A_0 be an action corresponding to no transmission.

Proportional Fair Scheduler [87]: For the Proportional Fair (PF) scheduler, interference free transmissions are assumed, i.e., only one link is allowed to transmit at a time. The scheduling law then is

$$A_{mn}[\tau] = \begin{cases} A^*_{mn}[\tau], & \text{if } (m,n) = \arg\max_{mn} R^*_{mn}[\tau]/\overline{R}_{mn}[\tau] \\ A_0, & \text{otherwise.} \end{cases} \tag{2.46}$$

In words, the PF scheduler schedules the link with the highest ratio of currently achievable rate to its empirical time-average. The policy thus schedules the link with the best channel quality, compared to its average channel. It is known to have good fairness properties for infinite queue backlogs and to converge to a proportionally fair point for high loads.

Maximum C/I Scheduler [88]: Just as the PF scheduler, the Maximum C/I scheduler assumes an interference free transmission. It schedules the link with the absolute highest transmission rate, i.e.,

$$A_{mn}[\tau] = \begin{cases} A^*_{mn}[\tau], & \text{if } (m,n) = \arg\max_{mn} R^*_{mn}[\tau] \\ A_0, & \text{otherwise.} \end{cases} \tag{2.47}$$

The Maximum C/I scheduler is known to maximize the sum-rate in interference free networks under full buffer assumption. However, it is known to become sub-optimal for less severe traffic back-log.

Dynamic Backpressure Scheduler [83]: In contrast to the previous schedulers, the Dynamic Backpressure (BP) scheduler is performed on a commodity basis. Further, it does not necessarily require an interference free transmission, however, it is restricted here to the interference free case for comparability. Consider the differential queue backlog of link (m, n) as

$$W^*_{mn}[\tau] = \left[\max_{\{c|(m,n)\in\mathcal{L}_c\}} \left[B^{(c)}_m[\tau] - B^{(c)}_n[\tau] \right] \right]^+ . \tag{2.48}$$

Then, the scheduled control action is

$$A_{mn}[\tau] = \begin{cases} A^*_{mn}[\tau], & \text{if } (m,n) = \arg\max_{mn} W^*_{mn}[\tau] R^*_{mn}[\tau] \\ A_0, & \text{otherwise.} \end{cases} \tag{2.49}$$

The quantity $W^*_{mn}[\tau]R^*_{mn}[\tau]$ is termed the *Backpressure* of the link. The BP scheduler is optimal in the sense that its stability region equals the interior of the network capacity region. That is, any input rates that can, at all, be stably supported can be supported by the BP scheduling policy. However, its properties in overload situations, with admission rates outside the stability region, are undefined.

Transport Layer Utility Maximization

Similar to the power control based NUM presented in Section 2.1.2, NUM problems can be defined on transport layer. Utility functions then take the form of $U(\boldsymbol{\lambda})$, where $\boldsymbol{\lambda}$ is a vector of admissible rates. Utility maximization problems on transport layer are simply defined by:

$$\begin{aligned} &\max_{\boldsymbol{\lambda}} U(\boldsymbol{\lambda}) \\ &\text{s.t.} \\ &\boldsymbol{\lambda} \in \Lambda_*, \end{aligned}$$

for a given, arbitrary scheduling policy $*$. Important utility functions on this level are:

- Weighted Sum-Throughput: $U(\boldsymbol{\lambda}) = \sum_c w_c \lambda_c$, $w_c \geq 0$;
- Proportional Fair Throughput: $U(\boldsymbol{\lambda}) = \sum_c \log(1 + \beta_c \lambda_c)$, $\beta_c > 0$;
- Sigmoidal: $U(\boldsymbol{\lambda}) = \sum_c (1 + e^{-t_c \lambda_c})^{-1}$, $t_c > 0$.

While the first function evaluates the throughput itself as utility, the second aims at a fair throughput maximization. The third utility is appropriate for limited throughput demands and is used, e.g., for video transmissions. Technically, transport layer utility maximization leads to rules for admission control, as the variables are the expected values of the admission processes. A powerful implementation structure for the solution of transport layer NUM problems is proposed in [83], which leverages the introduced BP scheduler. As this scheduler has a stability region equal to the interior of the transport region, the resulting problems can claim to optimize over all network throughputs that can, at all, be realized. Further, the transport region is known to be convex, closed and compact, hence the utilities easily

render the formulation convex. In particular, there are some very easy to implement admission rules which optimally solve important network utilities. These depend on the queue evolution of the underlying MAC layer. Assume that the admission rate is upper bounded as $Y_n^{(c)}[\tau] \leq \hat{Y}_{\max} \; \forall \tau$ and that there exists a fixed $V > 0$. Then, two important, optimal admission rules are [83]:

- Weighted Sum-Throughput: $Y_n^{(c)}[\tau] = \begin{cases} \hat{Y}_{\max} & \text{, if } w_c B_n^{(c)}[\tau] \leq V \\ 0 & \text{, otherwise} \end{cases}$
- Proportional Fair Throughput: $Y_n^{(c)}[\tau] = \min\left[\max\left[V/B_n^{(c)}[\tau] - 1/\beta, 0\right], \hat{Y}_{\max}\right]$.

As for sigmoidal utilities, they are non-concave and hence harder to optimize.

Concluding Remarks

The communication model presented in this section is general and can be adapted to many different networking scenarios. Its main strength lies in the fact that it is decoupled from the exact properties of MAC and Physical (PHY) layer, which can simply be exchanged in a modular fashion. In particular, it can be used for cellular networks and be easily modified to incorporate D2D communication over SLs. An application to the D2D use-case will be given in Section 2.2.3. Although not all aspects presented here are explicitly target of investigation in this thesis, a basic understanding of the overall coupling is required to correctly interpret results shown later.

2.1.4 The Resource Space

The resource usage of wireless networks in form of spectrum or Physical Resource Blocks (PRBs) is often of interest in wireless networks, because the amount of transmission resources is finite. For this aspect, most works follow an intuitive approach to evaluate the amount of used resources, e.g., by counting the number of used time- or frequency slots. Further, wireless resources mostly refer to the time and frequency dimension, whereas other communication aspects with resource like properties are often not recognized as such.

In this thesis, the benefit of using D2D communication will show to converge to a resource efficiency metric, which captures how much information can be transported with a finite set of transmission resources. To give a clean definition, the term "resource", as well as the "amount of resource" needs to be formally defined. However, even an intense literature search did not reveal a resource metric that would go beyond common, intuitive use. To ensure generality and the ability to transfer results to other context, a more formal approach to define the notion of resources and their measurement is developed in this section. The presented notion is novel and, to the best knowledge of the author, there is no comparable development in literature. Development of the presented resource measure thus must be seen as contribution of this thesis. The favored approach is based on mathematical measure theory and thus guarantees a metric that is consistent in itself. The used properties of measure theory are taken from [89], which can be considered as general reference throughout

this section. Commonly used resource metrics will be shown to comply with the proposed approach, further arguing in favor of its correctness.

The resource notion introduced here will be extensively used in Chapter 4, where the main contribution of D2D links towards a "good" system is investigated.

Resource Concept

The term "wireless transmission resource" in an abstract sense refers to transmitter and receiver settings that allow signal orthogonalization among different links. A setting thereby refers to the adjustment of certain communication parameters, such as the used frequency by adjusting filter settings or time slots by adjusting timing settings with respect to a reference frame. Transmissions that use different, non-overlapping spectrum, or time slots, do not interfere with each other, which leads to an increased communication quality. However, only a finite amount of such non-overlapping settings in terms of spectrum or time slots are available for transmission, due to the nature of time and technical or regulatory restrictions for usable frequency domain. When the amount of assumable settings is finite, they gain a resource like property and their use needs to be coordinated in a centralized or decentralized fashion, to not degrade networking performance.

While transmission resources most often refer to time and frequency, and in particular, their combination into PRBs for LTE-A networks, the concept is transferable to other technologies. For example, frequency hopping techniques can be used to leverage frequency diversity. In principle, hopping sequences can be designed in an orthogonal way and UEs that use orthogonal sequences will not interfere. However, only a finite amount of such orthogonal sequences exist. The set of orthogonal hopping sequences can be interpreted as a set of transmission resources, i.e., as a set of transmitter and receiver settings allowing orthogonalization. Similar aspects hold for preambles in the LTE Random Access Procedure (RAP) procedure. There, different codes are randomly used by links and can be decoded in an interference free fashion. The amount of usable codes is, again, limited and hence the codes can be interpreted as wireless transmission resources.

Different types of orthogonalization can be combined to create multi-dimensional resource structures. For example, transmissions on the same frequency in different time slots do not interfere, nor do transmissions at the same time but at different frequencies. By combining different orthogonalization techniques, an overall resource space is created and two links interfere whenever their used settings in this space overlap.

An important effect of resource use is created by spatial separation of the nodes. Spatial separation incurs resource-like properties: If the positions of users are sufficiently apart, or the material between links creates large enough attenuation, transmissions do not interfere, effectively creating an orthogonalization effect. However, in typical wireless set-ups, the position of nodes cannot be actively tuned, such that it is not treated as resource in this thesis. That is, different links that use the same resource on different positions are assumed to use the same resource, which might, or might not, lead to performance degradation due to interference. This creates an experienced mismatch of resource use: While each link that uses the same resource assumes to have full access to it, on a system level, all are actually using

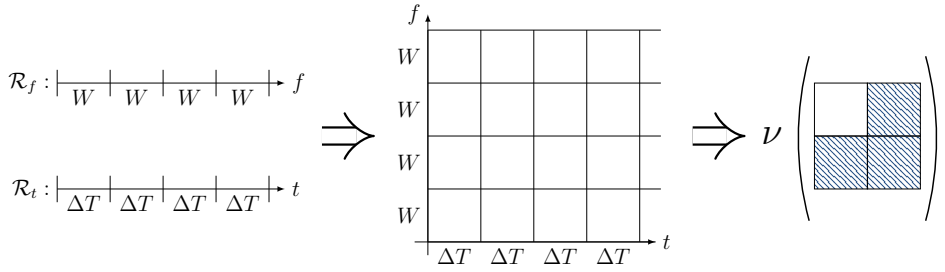

Figure 2.10: From resource dimensions to measures: The left part shows different resource dimensions decoupled. These are combined into an overall resource space, as shown in the middle part. On the combined resource space, a mathematical measure is defined, as shown on the right, which can identify an amount of used resource.

a single resource. That is, by leveraging spatial separation, the effective amount of usable resources can be increased.

In this section, a measure will be developed to capture the above effects in a mathematically clean fashion. While the definitions are abstract, it will be shown that they comply with intuitive use of resources.

Formal Definition

Formally, wireless transmission resources can be modeled by considering different resource dimensions $\mathcal{R}_i$, which are defined by a single underlying technology that allows separation of transmission signals. Formally, a resource dimension $\mathcal{R}_i$ is a set of assumable transmit-receive settings, such as transmission frequency ranges, time slots, hopping sequences or codes, where the use of the same setting incurs interference. Associated with each resource dimension is a locally finite mathematical measure $\nu_i : 2^{\mathcal{R}_i} \to \mathbb{R}_+$, which is a set function that reflects an amount of assumable settings and can be interpreted as an amount of resource. Natural choices for measures are Lebesgue measures for continuous resource dimensions, e.g., a frequency interval width or time interval length, and the counting measure for discrete resource dimensions, e.g., a number of simultaneously used codes or hopping sequences.

All dimensions are combined into the overall resource space $\mathcal{R} = \prod_i \mathcal{R}_i$, which is measured by the overall measure $\nu(r) = \prod_i \nu_i(r_i)\ \forall r \subseteq \mathcal{R}$, respectively. Note that if ν_i are measures on $\mathcal{R}_i\ \forall i$, then $\nu(r)$ is a product-measure on $\mathcal{R}$ [89]. An example for the commonly used time-frequency resource is shown in Figure 2.10. Any two resource subsets $\overline{\mathcal{R}}_k, \overline{\mathcal{R}}_l \subseteq \mathcal{R}$ indicate sets of usable resources. If they are disjoint in at least one used dimension, this leads to $\overline{\mathcal{R}}_k \cap \overline{\mathcal{R}}_l = \emptyset$ and indicates that transmissions on the subsets are interference free. Otherwise, there are at least some sub-parts of the used resources that interfere. By using such a resource measure, resource usage can be quantified for a large amount of scenarios with arbitrary technology, as long as the validity of the measures ν_i is ensured.

Resource measures are implicitly used in some well-known metrics for wireless transmission:

- The data rate refers to the amount of data transmitted within a certain time interval. This interval can be considered as time resource, with the length of the interval as

measure. The rate itself is the efficiency of data transmission with respect to the time resource.

- Spectral efficiency, on the other hand, denotes the transmitted data per time and spectrum. Here, implicitly a two-dimensional resource is assumed, where the amount of resource equals the spectrum width times slot length, which is the Lebesgue measure (i.e., volume) in a combined time-frequency space.

To make the abstract definition more accessible, it can be applied to the transmission resources of LTE-A networks, the PRBs. In LTE-A networks, the PRBs have a time and frequency dimension, which are standardized to fixed channel width of ± 90kHz around the center frequency f_c and a slot length of 1ms. PRBs are non-overlapping in either frequency or time, hence mutually disjoint, and all have the same size.

Formally, the resource space $\mathcal{R} = \mathcal{R}_t \times \mathcal{R}_f$ consists of the two dimensions time and frequency. Associated measures are the Lebesgue measures, i.e., the used frequency bandwidth and time duration of a signal. A transmission that uses a frequency range of W around center frequency f_c as $[f_c - W/2, f_c + W/2]$ for a time interval of $[t, t + T]$ uses a frequency resource of W and a time resource of T. By using the Lebesgue measure to measure an amount of resource for both dimensions, the size of a PRB becomes:

$$|\text{PRB}| = \nu\left([f_c - 90\text{kHz}, f_c + 90\text{kHz}]\right) \nu\left([\tau, (\tau + 1)\text{ms}]\right) = 180\text{kHz} \cdot 1\text{ms} = 180. \tag{2.50}$$

Because each resource has the same size, the total amount of used resources can be discretized. It is then given by the number of used resources times |PRB|, respectively.

While this short example shows that the very intuitive use of PRB counting falls into the presented generalized version, the linking to mathematical set theory allows generalization while still ensuring correctness of the used measures.

There are some further notions relating to per-link and system wide resource usage, which are formally developed in the following. The development follows the overall flow of: (1) Identifying whether a sub-part of a resource space is used; (2) Creating a measure for the amount of used resources; (3) Defining network-wide resource usage metrics.

Resource Usage Indication

Just as any mathematical measure, resource measures can be approximated arbitrarily close by appropriately defined indicator functions [89]. Indicator functions thus can serve as basic building block to derive appropriate measures. Here the indication determines, whether a considered resource element is part of a larger resource set. Consider a resource space $\mathcal{R}$ and a subset of this space, $\overline{\mathcal{R}} \subseteq \mathcal{R}$. Define the usage indicator $\delta_{\overline{\mathcal{R}}} : \mathcal{R} \to \{0, 1\}$ as

$$\delta_{\overline{\mathcal{R}}}(r) = \begin{cases} 1, & r \in \overline{\mathcal{R}} \\ 0, & r \notin \overline{\mathcal{R}} \end{cases}, \quad \forall r \in \mathcal{R}. \tag{2.51}$$

The usage indicator indicates whether a certain resource element, i.e., a single point in $\mathcal{R}$, is contained in a larger set $\overline{\mathcal{R}}$ or not. The measure of a resource is related to its indicator by the

Lebesgue integral with respect to the indicator function [89]:

$$\nu(\overline{\mathcal{R}}) = \int\limits_{r' \in \overline{\mathcal{R}}} 1 d\delta_{\mathcal{R}}(r') = \int\limits_{r' \in \mathcal{R}} \delta_{\overline{\mathcal{R}}}(r') d\delta_{\mathcal{R}}(r'). \tag{2.52}$$

Note that the left integral is over the space $\overline{\mathcal{R}}$ but considers how much of $\overline{\mathcal{R}}$ is in $\mathcal{R}$, whereas the right integral is over $\mathcal{R}$ but considers only those parts of $\mathcal{R}$ that are in $\overline{\mathcal{R}}$.

For fixed resource structures with disjoint partitions, e.g., the PRBs used in LTE, two resources either fully overlap or are disjoint. For this special structure, it makes sense to define an indicator on PRB basis, which identifies whether a PRB, say $\text{PRB}_k \subseteq \mathcal{R}$, is contained in another set of PRBs, $P = \cup_i \text{PRB}_i$ or not. This can be done as:

$$\delta_P(\text{PRB}_k) = \frac{\nu(\text{PRB}_k \cap P)}{\nu(\text{PRB}_k)} = \begin{cases} 1, & \text{PRB}_k \subseteq P \\ 0, & \text{else} \end{cases}. \tag{2.53}$$

Creating a resource measure from $\delta_P(\text{PRB}_k)$ yields a counting measure that corresponds to counting PRBs:

$$\nu_P(\overline{\mathcal{R}}) = \int\limits_{\text{PRB} \in P} \delta_{\overline{\mathcal{R}}}(\text{PRB}) d\delta_{\mathcal{R}}(\text{PRB}) = \text{\# used PRBs}. \tag{2.54}$$

This re-motivates the intuitive use of resource counting as formally correct. However, it is only one way of measuring an amount of resource.

Indication of Transmission Resources for a Set of Links

While the given definitions serve to measure the amount of resource of arbitrary sets, so far no relation was given to transmissions or wireless networking. Assume a set of links $\mathcal{L}$ that enforce transmissions with an action matrix $\boldsymbol{A}$, in compliance with the network model presented in Section 2.1.3. Consider that each action A_{mn} used by link $(m,n) \in \mathcal{L}$ is associated with a set of used transmission resources, $r(A_{mn}) \subseteq \mathcal{R}$. The resources used in overall by a set of links $\mathcal{L}$ then is $r(\boldsymbol{A}) = \bigcup_{mn} r(A_{mn})$. The indicator whether a resource element $r \in \mathcal{R}$ is used by one of the links in $\mathcal{L}$ is:

$$\begin{aligned} \delta_{r(\boldsymbol{A})}(\mathcal{L}, r) &= \max_{(m,n) \in \mathcal{L}} \delta_{r(A_{mn})}(r) \\ &= \begin{cases} 1, & \exists (m,n) \in \mathcal{L} : r \in r(A_{mn}) \\ 0, & \nexists (m,n) \in \mathcal{L} : r \in r(A_{mn}) \end{cases}. \end{aligned} \tag{2.55}$$

That is, $\delta_{\boldsymbol{A}}(\mathcal{L}, r)$ is one if at least on link uses r and zero otherwise. The same definition can be extended to PRB-based resources, by plugging δ_P into (2.55). This yields the indicator

$$\begin{aligned} \delta_P(\mathcal{L}) &= \max_{(m,n) \in \mathcal{L}} \delta_P(r(A_{mn})) \\ &= \begin{cases} 1, & \exists (m,n) \in \mathcal{L} : \text{PRB}_i \in r(A_{mn}) \\ 0, & \nexists (m,n) \in \mathcal{L} : \text{PRB}_i \in r(A_{mn}) \end{cases}. \end{aligned}$$

Network Wide Resource Use

The resource usage indication can be naturally leveraged to measure the amount of resources used by links in a network. For this, two different metrics exist, depending on the level at which resources are indicated. The metrics are referred to as the *effective* resource usage and the *system* resource usage in the following and in the remaining parts of this thesis.

Consider the scheduling perspective introduced in Section 2.1.3. Assume an arbitrary resource space $\mathcal{R}$ associated with an appropriate measure ν and denote by $r(A_i) \subseteq \mathcal{R}$, $A_i \in \mathcal{A}$ the set of resources used when an action A_i is performed. As the action A_0 is defined to be an idle action, define $r(A_0) = \emptyset$ for consistency.

Using these definitions, the effective amount of resources used by a set of links $\mathcal{L}$, assuming an action matrix $\boldsymbol{A}$, can be calculated as:

$$\begin{aligned} \nu^{\text{eff}}(\mathcal{L}, \boldsymbol{A}) &= \sum_{(m,n)\in\mathcal{L}} \nu(r(A_{mn})) = \sum_{(m,n)\in\mathcal{L}} \int_{r'\in\mathcal{R}} \delta_{r(A_{mn})}(r') d\delta_{\mathcal{R}}(r') && (2.56) \\ &= \int_{r'\in\mathcal{R}} \sum_{(m,n)\in\mathcal{L}} \delta_{r(A_{mn})}(r') d\delta_{\mathcal{R}}(r') = \int_{r'\in\mathcal{R}} \Sigma(\mathcal{L}, \boldsymbol{A}, r') d\delta_{\mathcal{R}}(r'). && (2.57) \end{aligned}$$

As seen in the first line, the effective resource usage is the sum of all per-link resource usages and is generated from the indicators of all single links. The indicators transform into an overall usage density function $\Sigma(\mathcal{L}, \boldsymbol{A}, r') = \sum_{(m,n)\in\mathcal{L}} \delta_{r(A_{mn})}(r')$, given in the second line, which evaluates the number of links using a resource element r'. $\nu^{\text{eff}}(\mathcal{L}, \boldsymbol{A})$ is a mathematical measure and thus a valid representation for an amount of used resources.

For the PRB resource structure, the effective resource usage turns into

$$\nu^{\text{eff}}(\mathcal{L}, \boldsymbol{A}) = |\text{PRB}| \sum_k \Sigma(\mathcal{L}, \boldsymbol{A}, \text{PRB}_k) = |\text{PRB}|\, \Sigma^{\text{eff}}(\mathcal{L}, \boldsymbol{A}), \tag{2.58}$$

where $\Sigma(\mathcal{L}, \boldsymbol{A}, \text{PRB}_k)$ reflects the number of links using PRB_k under action matrix $\boldsymbol{A}$ and $\Sigma^{\text{eff}}(\mathcal{L}, \boldsymbol{A})$ is the aggregate number of PRB usages in the network.

On the other hand, the system amount of resources used by a set of links can be simply defined using the indication for link sets, $\delta_{r(\boldsymbol{A})}(\mathcal{L}, r)$:

$$\nu^{\text{sys}}(\mathcal{L}, \boldsymbol{A}) = \int_{r'\in\mathcal{R}} \delta_{r(\boldsymbol{A})}(\mathcal{L}, r') d\delta_{\mathcal{R}}(r') = \int_{r'\in\mathcal{R}} \max_{(m,n)\in\mathcal{L}} \delta_{r(A_{mn})}(r') d\delta_{\mathcal{R}}(r').$$

For a PRB structure, this leads to

$$\begin{aligned} \nu^{\text{sys}}(\mathcal{L}, \boldsymbol{A}) &= |\text{PRB}| \sum_k \delta_{r(\boldsymbol{A})}(\mathcal{L}, \text{PRB}_k) \\ &= |\text{PRB}| \sum_k \max_{(m,n)\in\mathcal{L}} \delta_{r(A_{mn})}(\text{PRB}_k) = |\text{PRB}|\, \Sigma^{\text{sys}}(\mathcal{L}, \boldsymbol{A}), \end{aligned}$$

where $\delta_{\boldsymbol{A}}(\mathcal{L}, \text{PRB}_k)$ is the network wide resource indicator function and the system resource usage is $\Sigma^{\text{sys}}(\mathcal{L}, \boldsymbol{A}) = \sum_k \delta_{\boldsymbol{A}}(\mathcal{L}, \text{PRB}_k)$. Again, $\nu^{\text{sys}}(\mathcal{L}, \boldsymbol{A})$ is a mathematical measure and thus a valid representation for an amount of used resources.

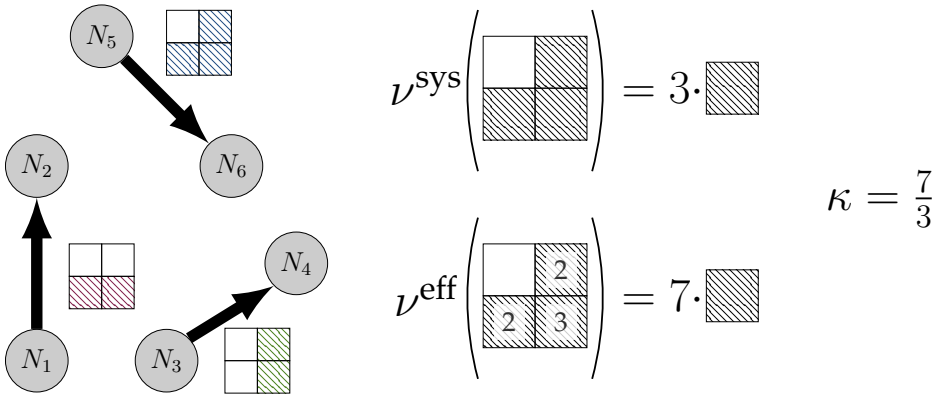

Figure 2.11: Effective resources, system resources and reuse factor, assuming a time-frequency resource structure with PRBs. The left part shows three links, together with their used PRBs, which are highlighted with colors. While the system resource measure ν^{sys} considers whether a PRB was used at all, the effective resource measure ν^{eff} incorporates the number of times it was used. The reuse factor κ captures the ratio of effective to system resource use.

Resource Reuse Factor

Both, system and effective resource usage refer to different metrics that are coupled by an important effect. When a resource is used several times in a wireless network, the effective resource usage can increase and hence the amount of available resources seems increased. This is in contrast to the actual availability of system resources, which remains constant. Resource reuse can thus be leveraged to effectively create more resources, or to use less resources. The effective increase in transmission resources can be captured by the reuse factor, which is explicitly given for PRB based resource spaces as:

$$\kappa(\mathcal{L}, \boldsymbol{A}) = \frac{\nu^{\text{eff}}(\mathcal{L}, \boldsymbol{A})}{\nu^{\text{sys}}(\mathcal{L}, \boldsymbol{A})} = \frac{|\text{PRB}| \sum_k \Sigma(\mathcal{L}, \boldsymbol{A}, \text{PRB}_k)}{|\text{PRB}| \sum_k \delta_{\text{PRB}_k}(\mathcal{L}, \boldsymbol{A})} = \frac{\Sigma^{\text{eff}}(\mathcal{L}, \boldsymbol{A})}{\Sigma^{\text{sys}}(\mathcal{L}, \boldsymbol{A})}. \tag{2.59}$$

An example for the relation among system resources, effective resources and resource reuse factor is given in Figure 2.11, respectively.

Concluding Remarks

The introduced formalization of transmission resources and reuse factor capture intuitive usage in a mathematically clean way. While the intuitive use is often encountered in related work, the formal introduction is novel and leads to an interesting perspective that is developed in this thesis. The used notions will be extensively used in Chapter 4, when the performance gain of D2D over cellular communication is investigated.

2.2 D2D System Description

After introducing the used models and some main properties, in this section the considered, D2D enabled cellular system will be formally described. Apart from mere operation of direct links, also the aspects of forming links are of interest, i.e., pairing devices and choosing communication modes, and will be modeled.

First, the used assumptions on used network types will be introduced in Section 2.2.1. Then, in Section 2.2.2, the formation of a D2D network will be modeled, starting from device positions and communication demands and yielding a set of links that must be operated to provide service. Finally, the underlying MAC structure will be modeled for an LTE-A network with D2D links in Section 2.2.3, by stating an overall utility maximization problem for MAC layer operation.

2.2.1 General Comment

The focus of this thesis is on in-band cellular D2D communication. The used models thus comply with the commonly used assumptions for cellular systems, with some variations that take into account the specific aspects of D2D links.

Throughout the development of this thesis, there is no real world implementation of D2D enhanced cellular systems except for few laboratory test-beds [90], [91]. However, standardization bodies are in progress of defining D2D communication aspects [31], [35], [92] and companies propose assumptions for just these [32]–[34]. Common assumptions are that D2D links should be treated similar to cellular uplinks, both in terms of management and transmission parameters, and should be operated using uplink transmission resources.

While this is not the only possible choice, it is motivated mainly by two aspects: First, UEs in general are designed to transmit with specific transmission parameters that may differ from those used by base stations. A common example is the use of Single-Channel Frequency Division Multiplex (SC-FDM) signals in the uplink, versus Orthogonal Frequency Division Multiplex (OFDM) in downlink. This use of different signals is motivated by different hardware requirements, that are optimized for cost in uplink and for spectral efficiency in downlink. Because UEs are the transmitters of SLs, the similarity is acknowledged in D2D modeling. Second, as frequency reuse is targeted, the BSs will receive increased interference when reusing uplink resources, whereas UEs would be subject to stronger interference on downlink resources. The common expectation is that BSs are more robust to interference, because of their use of more powerful hardware, leading to the conclusion that uplink resources should be targeted for reuse.

Although the assumptions are well motivated from an implementation perspective, the general problem types and properties used for uplink often also hold for downlink. The assumption of using uplink bands thus does not affect the generality of produced results.

Standardization of D2D links is performed with the target of deployment in 5G networks [15]. As for research, current 4G networks [93] are often assumed, where D2D links are treated similar to uplinks. The models used in this thesis particularly focus on an LTE-A network that is enhanced with SLs, however the freedom of changing system assumptions is taken whenever this seems beneficial for enabling side-links.

2.2.2 Model of Network Establishment

In the following, a typical action flow for the creation of D2D links is modeled, starting from device positioning and communication demands, via device pairing and mode selection to

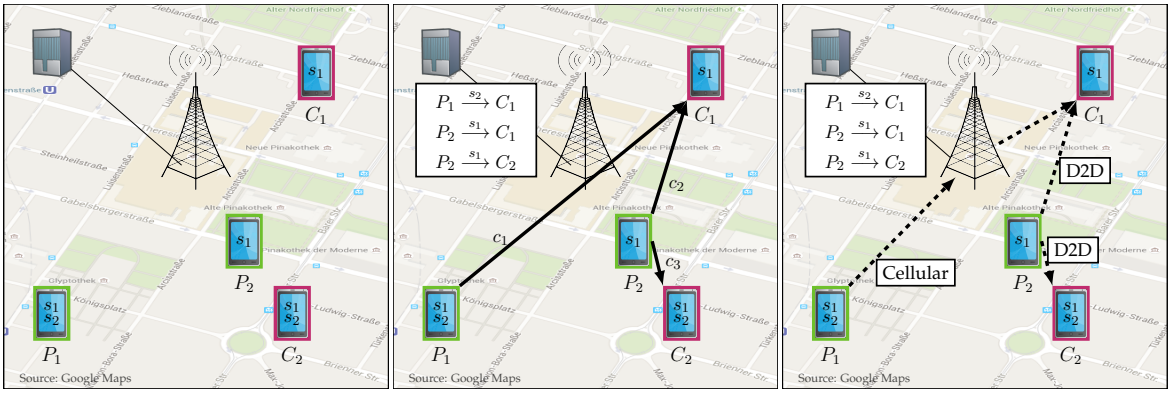

(a) (b) (c)

Figure 2.12: General flow of network establishment. As shown in Figure 2.12a, the network starts with nodes that either require (C_i) or provide (P_i) service, or both concurrently, which however is not depicted. The provisions and requirements are matched to create link pairs, among which traffic is generated as shown in Figure 2.12b. After the traffic is generated, some flows are handed off to direct mode, which is illustrated in Figure 2.12c.

the resulting network set-up with cellular and D2D links. The establishment of D2D links is mostly independent of the underlying MAC mechanisms and instead depends on stochastic distributions of devices and applications. The general considered flow for creating a network with D2D links, which is explained throughout this section, is illustrated in Figure 2.12.

Basic Network Set-Up

The cellular network is considered as a set of hardware devices, falling into two classes, that can communicate with each other wireless. The two device classes are the base stations (BSs), which are access points with two interfaces, one wired connection to the core network and a wireless interface, and the UEs, which are mobile stations that communicate only wireless. Tiered networks with small cells, femto-cells or wireless relay nodes are explicitly neglected in this set-up for simplicity.

Devices of both classes have random positions in space at each time instance. The positions of all devices are statistically independent of one another. Both device classes are thus modeled as homogeneous p.p.p.'s Φ_u and Φ_b, with distinct densities. The Poisson property is an intuitive assumption for UEs, but has also been shown realistic to model positions of BSs [51], [52]. Homogeneity, on the other hand, is an obvious simplification, as it does not take account for hot spots with increased density.

Network Service

Let Φ_u, Φ_b be the homogeneous p.p.p.'s of UEs and BSs, with device densities of λ_u and λ_b, respectively. Communication demands among devices are modeled by assuming a set of services that are offered and requested by arbitrary nodes out of the processes Φ_u and Φ_b. A device that initiates communication is hereby called the client, which requests a service, whereas the reacting device is called provider of the service.

The term "service" can denote any use-case that creates a traffic demand among two devices. It may relate to a dedicated communication demand, such as a voice call. Then, the caller is the client of a service, which is the service of establishing a voice connection to the callee. In this case, the callee is the unique provider device. A service may just as well be served by a number of providers. Assume, for example, a range extension scenario where UEs forward data streams of other UEs to a BS. Then all relays would be providers of such a relay service, whereas the source UEs would be the clients. Alternatively, the service could originate from higher layer applications, such as in distributed caching or gaming scenarios. Here, the providers are formed by all devices that offer caches, or host a game, whereas clients are all devices that request cache content or join a game.

Formally, each service is indicated by an identifier s and defined by the sets of provider and client nodes of the respective service. These node sets, $\mathcal{N}_p^{(s)}$ and $\mathcal{N}_c^{(s)}$, might either consist of predetermined device classes, such as BSs, or contain nodes randomly based on their device capabilities or installed applications. Note that a device can be part of several node sets if it provides or requests several services and might even be both, provider and client of the same service.

A particularly interesting example for D2D communication is that where $\mathcal{N}_p^{(s)}$ and $\mathcal{N}_c^{(s)}$ both contain only UEs, which are added probabilistically according to a certain distribution. This can be used to model services induced by higher layer applications, which create communication demands among UEs. Such applications might be installed at UEs only with certain probabilities, that are sufficiently independent of the UEs positions. Then, the node sets are created from the set of UEs by probabilistically adding each device to the node set independent of other nodes, i.e., by performing a thinning of the p.p.p Φ_u. For each service s, the node sets $\mathcal{N}_p^{(s)}$ and $\mathcal{N}_c^{(s)}$ can thus be described by homogeneous p.p.p.'s $\Phi_p^{(s)}$, $\Phi_c^{(s)}$, with device densities $\lambda_p^{(s)} = p_p^{(s)}\lambda_u$, $\lambda_c^{(s)} = p_c^{(s)}\lambda_u$, for the probabilities $p_p^{(s)}$, $p_c^{(s)}$, that a devices is provider or client of service s. Note that $\Phi_p^{(s)}$ and $\Phi_c^{(s)}$ are statistically independent if, and only if, the choice of being provider and client is done independently. In general, this property need not be guaranteed. In the following, only one service will be considered, such that the index s can be dropped for notational convenience.

The outcome of node positioning and thinning creates a network situation as depicted in Figure 2.12a, where a set of UEs exist in a cellular network that each proved or request certain services. In the figure, it was for better illustration assumed that devices can not be provider and client for different services simultaneously.

Device Paring

Once the node sets $\mathcal{N}_p$ and $\mathcal{N}_c$ are determined, the network can be considered divided into to sets of nodes with communication demands and offers. To create a satisfactory network state, demands and offers need to be matched, to form communication pairs. This is modeled with a pairing

$$P : (u_c, \Phi_p) \mapsto (u_c, u_p), \text{ for } u_c \in \Phi_c, \quad u_p \in \Phi_p \setminus u_c. \tag{2.60}$$

P matches any client with the set of providers and outputs a client-provider pair that will start communication.

Note that the pairing P can be realized in a variety of ways. It can be done on application layer, e.g., for gaming or caching scenarios, or the mapping might be decided in a network function that is run in data centers of the MNO. It might also be decided implicitly, e.g., by neighbor discovery among nodes on MAC level. Further, the resulting pairing might be a stochastic output or follow a deterministic law. Resulting pairs need not be in mutual communication range but can be located arbitrarily. The only required property is that the pairing creates transmitter-receiver pairs out of sets of nodes with communication demands.

Finally, the resulting pairs (u_c, u_p) are associated with a flow commodity $c \in \mathcal{K}$, as introduced in Section 2.1.3. One of the nodes u_c, u_p then is the source node s_c of the commodity, whereas the other is the destination d_c. The result of a device pairing step is depicted in Figure 2.12b, where the created pairs are shown in the box on the upper left.

Mode Selection

After all of the commodities, source and destination nodes are set, a mechanism decides with which communication mode the flow is realized, i.e., whether D2D communication should be used. Formally, each mode comprises of a set of MAC layer links that are established to transport the data. In particular, the two modes CM and DM are considered. Overlay and underlay decisions are here interpreted as scheduling decision, which is made independent of the mode selection itself.

Define the D2D sidelink as $\mathrm{SL}_c = (s_c, d_c)$, the uplink from s_c as $\mathrm{UL}_c = (s_c, b_s)$ and the downlink towards d_c as $\mathrm{DL}_c = (b_d, d_c)$, where b_s and b_d are the serving BSs of s_c and d_c, respectively. Note that $b_s \neq b_d$ might hold, in which case the data is transported from b_s to b_d via backhaul links. Each commodity is associated with a set of allowed routes $\mathcal{L}_c$, which is $\mathcal{L}_c^{(DM)} = \{\mathrm{SL}_c\}$ for the DM and $\mathcal{L}_c^{(CM)} = \{\mathrm{UL}_c, \mathrm{DL}_c\}$ for CM. As the interest here is in the wireless communication part, only wireless links are considered in $\mathcal{L}_c$.

Mode selection is modeled similar to device pairing, as a mapping

$$M : (s_c, d_c) \mapsto \{0, 1\}, \tag{2.61}$$

where the result $M = 1$ indicates that DM was chosen. According to the outcome, one of the link sets $\mathcal{L}_c^{(CM)}$, $\mathcal{L}_c^{(DM)}$ is added to $\mathcal{L}$ and set as allowed link set for commodity c. M thus determines the allowed link set for commodity c, as well as the resulting network topology. After this mode selection step, the introduced model entirely falls into the framework presented in Section 2.1.3. Similar to the device pairing, the mode selection mapping M can in principle be realized arbitrarily, e.g., by a function in the core network or by decentralized signaling methods, and can follow stochastic patterns or deterministic rules. Typically, it is assumed to be decided at one of the serving BSs.

Data Transport

With all pairing and mode selection decisions made, the participating nodes and allowed link sets are defined. Then, the network needs to be operated to transport all data with as good performance as possible. For this, a communication structure according to Sections

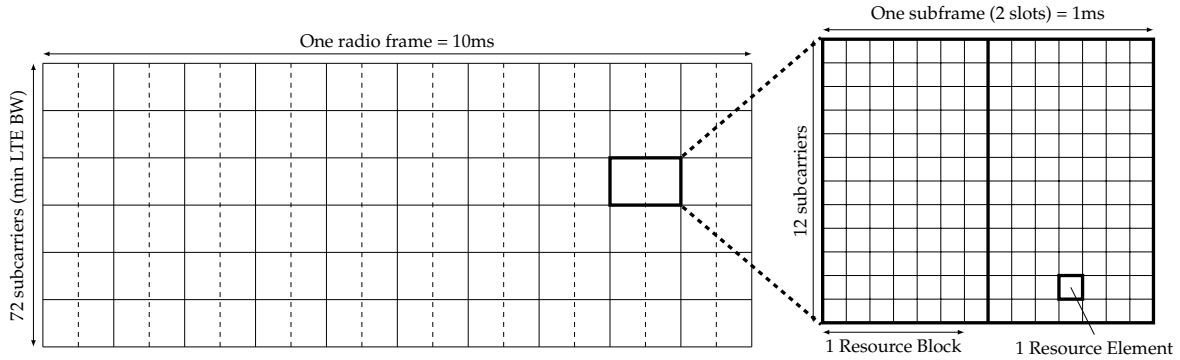

Figure 2.13: Structure of an LTE radio frame with a system bandwidth of 1.08 MHz.

2.1.2 and 2.1.3 is assumed. That is, each node has a separate queue for all commodities passing through it. Received or injected data is stored in the queue and acts modeled as arrival process to it. The wireless channel is abstracted into a combination of topology states $\boldsymbol{Q}$ and each link has a set of available actions gathered in the matrix $\boldsymbol{A}$. The combination of action with topology state lead to data rates R, that act as serving process to the commodity queues. It is assumed that all actions are decided at a scheduler, which is located at the BS and relies on backlog reports and channel reports by the UEs. Details of the exactly used model are given in the following section.

2.2.3 MAC Model

In this section, the MAC layer of the considered D2D scenario is modeled. As was stated already, D2D communication is typically assumed to use the same transmission settings as uplink communication, because D2D transmitters are UEs. Current standardization activities typically assume an LTE-A system, that is extended to incorporate sidelinks [31], [35], [92]. SLs can use uplink spectrum or an own, pre-defined part of the spectrum. In this thesis, the communication structure is modeled by that of an LTE-A cell, which simply incorporates direct links.

Transmission and Resource Structure

For transmission, it is assumed that downlink signals use Orthogonal Frequency Division Multiple Access (OFDMA), whereas uplink and sidelink use Single-Channel Frequency Division Multiple Access (SC-FDMA). The same transmission structure is also employed in LTE-A [59]. OFDMA and SC-FDMA differ in several aspects:

In OFDMA [59], a data block is distributed over several carriers. While independent, wireless symbols are created for all carriers, for encoding the symbols are considered as different dimensions of an overall OFDM-symbol, which spans several adjacent carriers. The waveforms are dimensioned such that there is no co-carrier interference, neglecting the need for guard bands. Finally, data on different carriers is de-modulated independently on each carrier, but de-coded in combination.

For SC-FDMA [59], data is again distributed over several modulation symbols, which are then combined by means of a Discrete Fourier Transformation (DFT). The result is a set of symbols that each spans several carriers. Compared to OFDMA, in SC-FDMA each carrier carries information of all modulation symbols, due to the DFT operation. This creates the effect that the overall transmission can be represented by an equivalent overall, virtual single channel transmission, although it is technically distributed over several, adjacent carriers [59].

SC-FDMA and OFDMA can be configured to use the same amount of carriers and bandwidth and thus can be combined into the same resource structure, which is leveraged in LTE, where the transmission resources are grouped in reference time frames. A reference frame defines the borders of a resource grid, as shown in Figure 2.13, with respect to which links can adjust their timings to not interfere with each other. An LTE frame is sub-divided into time-slots that are used for transmission. Similarly, the frequency domain is divided into sub-carriers. 12 of these sub-carriers in combination with two consecutive time-slots form a PRB, on which OFDM-symbols or SC-FDMA symbols can be transmitted. Typically, a radio frame has a duration of 10 ms, whereas a time-slot has one of 0.5 ms and a sub-carrier spans 15 kHz [59]. As a result, a PRB has a spectral width of 180 kHz and a duration of 1 ms. With the minimum specified bandwidth and frame duration, a radio frame contains 10 PRBs in time domain and 6 PRBs in spectral domain, i.e., 60 PRBs in total. However, several modes exist for the dimensioning of LTE frame structures, so the exact dimension might differ from case to case.

Typically, uplink and downlink communication is restricted to different parts of the LTE transmission resources. In principle, uplink and downlink resources can be configured to use different carriers or different time periods. The first is referred to as Frequency Division Duplex (FDD) mode, and is realized by placing uplink and downlink resources on different spectrum with an own frame for each. The latter is called Time Division Duplex (TDD) mode, where uplink and downlink resources use the same spectrum but alternate in time. TDD mode has the advantage that, due to the reciprocity of wireless channels, uplink channel information can also be used for downlink. However, FDD has the advantage of lower latency, because the time frames do not alternate in time. For the considered D2D scenario, TDD will prove to be better suited, which is why it is assumed throughout this thesis.

Transmission Parameters

On the level of abstraction used in this thesis, the underlying, physical transmission mechanisms are not altered. However, there exist defined interfaces that allow interaction with the physical transmission by means of scheduling, modulation and coding scheme selection and power control.

For each transmission on a single PRB, different parameters may be chosen to adapt to given channel conditions [59], [94]. First, different combinations of modulation formats and error coding schemes, called Modulation and Coding Schemes (MCSs) are available, that allow different levels of achievable data rates and reliability for given SINRs. The MCS combinations are associated with a Channel Quality Indicator (CQI) $q \in \mathbb{N}_+$, that takes integer

CQI Index	Modulation	Code Rate × 1024	Spectral Efficiency [bit/s·Hz]	CQI Index	Modulation	Code Rate × 1024	Spectral Efficiency [bit/s·Hz]
0	-	-	-	8	16-QAM	490	1.9141
1	QPSK	78	0.1523	9	16-QAM	616	2.4063
2	QPSK	120	0.2344	10	64-QAM	466	2.7305
3	QPSK	193	0.3770	11	64-QAM	567	3.3233
4	QPSK	308	0.6016	12	64-QAM	666	3.9023
5	QPSK	449	0.8770	13	64-QAM	772	4.5234
6	QPSK	602	1.1758	14	64-QAM	873	5.1152
7	16-QAM	378	1.4766	15	64-QAM	948	5.5547

Table 2.1: 4-bit CQI Table [94]

values within a defined range, e.g., $q \in \{0, 1, ..., 15\}$ [94]. While the CQI technically is a quality report, it directly refers to a preferred MCS, which it thus represents. A CQI value of 0 indicates being out-of-range on a considered sub-band and thus is associated with not transmitting at all. The other values indicate the use of Quadrature Phase Shift Keying (QPSK), 16-Quadrature Amplitude Modulation (QAM) or 64-QAM, in combination with different code rates [94]. By setting the CQI value, both transmitter and receiver will choose the appropriate modes to operate with the previously defined MCS. An example for such a mapping is given in Table 2.1.

As the transmission possibilities are orthogonalized by means of a resource grid in a reference time frame, the actual transmissions need to be coordinated to avoid interference. This is typically referred to as scheduling or resource allocation and assumed to take place at the BS. The outcome of a resource allocation decision is a schedule, where each active link is assigned an MCS to use on each PRB. The schedule is generally chosen to match a network-wide performance criterion, i.e., a utility function, and reported to the UEs in uplink, or simply used for transmission in downlink. In uplink, some constraints need to be considered due to the nature of the used SC-FDMA structure. While SC-FDM signals may spread several sub-bands, all used bands need to be localized, i.e., be continuous in frequency domain [59]. However, the exactly used sub-bands may change from one time slot to another. The combination of these possibilities and constraints renders uplink LTE scheduling a hard problem in general. To slightly relax the complexity, it will be assumed throughout this thesis that SC-FDM signals span only one sub-band at a time. For scheduling, this means that the resulting uplink schedules need to be chosen such that each UE uses one sub-band at most.

Along with fixed, defined MCS, the transmission power can be altered. Intuitively, for channels with large attenuation, larger powers should be used and for such with lower attenuation, powers can be reduced. Each node has a maximum transmission power that cannot be exceeded due to technical or regulatory constraints. In general, different transmission powers can be used for different PRBs. However, there are regulatory restrictions on how much power may be used on a single sub-band, as well as how much power may be used over several bands in total. For uplink signals, only one sub-band may be used in first place, hence both restrictions fall together. For downlink, however, the BS may use different channels at the same time and thus must comply with all power restrictions.

The combination of all restrictions for simultaneous sub-band use or transmission power

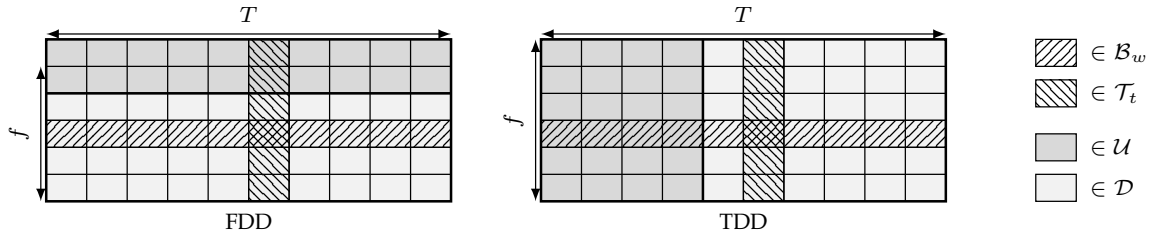

Figure 2.14: An FDD and a TDD LTE-Frame configuration. The colors and patterns highlight the used set definitions, i.e., the uplink/downlink PRB sets $\mathcal{U}$, $\mathcal{D}$ and the PRBs per sub-band and time slot, $\mathcal{B}_w$ and $\mathcal{T}_t$, respectively.

constraints often turn the optimization problems related to coordination of different links hard to solve, even for the interference free case. A significant amount of research is thus dedicated to this area of cellular networking. For D2D networks, the introduction of intracell-interference even tightens this aspect.

Modeling

The previously introduced aspects of LTE-A networking will now be formalized into a mathematic representation. Assume both, uplink and downlink LTE-frame to operate in a synchronous fashion, either in FDD-mode, in which they have the same time duration, or in TDD mode, where they are operated alternately. The union of uplink and downlink frame are considered as a frame slot of duration T and different slots are identified by the variable $\tau \in \mathbb{N}_+$. Frame slots are to be distinguished from the time slots within the resource grid. The latter are grouped by two, such that each PRB is referred to as time slot.

The transmission resources in a frame are indexed with an indicator $k \in \mathcal{R} = \{1, ..., K\}$, identifying the K different possible PRBs that reside either on uplink or downlink frame. To distinguish uplink from downlink, the resource space $\mathcal{R}$ is partitioned into an uplink PRB-set $\mathcal{U}$ and a disjoint downlink set $\mathcal{D}$, such that $\mathcal{U} \cap \mathcal{D} = \emptyset$ and $\mathcal{R} = \mathcal{U} \cup \mathcal{D}$ hold. The exact division can differ according to the used configuration for TDD or FDD and can be biased to have larger uplink or larger downlink sets, respectively.

Further, $\mathcal{R}$ can be considered partitioned into F disjoint PRB subsets per sub-band and Δ sub-sets per time slot. Each sub-set is associated with a set of PRBs $\mathcal{B}_w$ that reside on sub-band $w \in \{1, ..., W\}$, or PRBs $\mathcal{T}_t$ that are on time slot $t \in \{1, ..., \Delta\}$. Again, the sets $\mathcal{B}_w$ are disjoint and fully partition $\mathcal{R}$ and so do the sets $\mathcal{T}_t$, respectively.

The partition of resources into uplink and downlink sets, as well as frequency band and time slot sets, is shown in Figure 2.14 for better illustration.

During each frame-slot τ, which models the combination of one LTE uplink and downlink time frame, links can choose actions from one of the two action sets $\mathcal{A}_{\text{UL}}$ or $\mathcal{A}_{\text{DL}}$, depending on whether they are UEs or BSs. Assume that there are $C_{\text{UL}}, C_{\text{DL}} \in \mathbb{N}_+$ MCS schemes among which devices can choose for uplink and downlink transmissions. For any PRB $k \leq K$, let $\boldsymbol{x}_k^{\text{UL}} \in \{0,1\}^{C_{\text{UL}}}$ and $\boldsymbol{x}_k^{\text{DL}} \in \{0,1\}^{C_{\text{DL}}}$ be column vectors such that $x_{kq} = 1$ if MCS q is used on PRB k and zero otherwise. All vectors can be gathered in the matrices $\boldsymbol{X}^{\text{UL}} = \left[\boldsymbol{x}_1^{\text{UL}}, ..., \boldsymbol{x}_K^{\text{UL}}\right]^T$ and $\boldsymbol{X}^{\text{DL}} = \left[\boldsymbol{x}_1^{\text{DL}}, ..., \boldsymbol{x}_K^{\text{DL}}\right]^T$, respectively. Then the sets of allowed

MCS choices for uplink and downlink transmissions are given by:

$$\mathcal{M}^{\mathrm{UL}} = \left\{ \boldsymbol{X}^{\mathrm{UL}} : \sum_{q=1}^{C_{\mathrm{UL}}} x_{kq} \leq \mathbb{1}\{k \in \mathcal{U}\} \ \ \forall k; \quad \sum_{k \in \mathcal{T}_t} \sum_{q=1}^{C_{\mathrm{UL}}} x_{kq} \leq 1 \ \ \forall t \in \{1, ..., \Delta\} \right\}, \tag{2.62}$$

$$\mathcal{M}^{\mathrm{DL}} = \left\{ \boldsymbol{X}^{\mathrm{DL}} : \sum_{q=1}^{C_{\mathrm{DL}}} x_{kq} \leq \mathbb{1}\{k \in \mathcal{D}\} \right\}. \tag{2.63}$$

The set $\mathcal{M}^{\mathrm{UL}}$ contains all possible uplink MCS assignments. The first constraint ensures that PRBs on downlink bands are not used, whereas the second constraint ensures that per time slot, only one PRB is used. Similar holds for $\mathcal{M}^{\mathrm{DL}}$.

Along with $\mathcal{M}^{\mathrm{UL}}$ and $\mathcal{M}^{\mathrm{DL}}$, transmission powers can be chosen at the transmitters. Assume that on each PRB k, the transmitter m may assign a power $p_{k,m}$. The powers may then be grouped by either by transmitter, leading to the power vector $\boldsymbol{p}_m$ that contains all powers used by transmitter m, or by PRBs, creating a vector $\boldsymbol{p}_k$ that contains all transmit powers used by transmitters on a PRB k. The power vectors need to be chosen from valid power sets $\mathcal{P}^{\mathrm{UL}}$, $\mathcal{P}^{\mathrm{DL}}$, that may contain per-link, per-PRB or other spectral radiation constraints. Due to the diversity of demanded power constraints, the power sets are left as abstract sets here.

The overall action sets are composed from the introduced sets according to

$$\mathcal{A}_{\mathrm{UL}} = \mathcal{M}^{\mathrm{UL}} \times \mathcal{P}^{\mathrm{UL}}; \quad \mathcal{A}_{\mathrm{DL}} = \mathcal{M}^{\mathrm{DL}} \times \mathcal{P}^{\mathrm{DL}}. \tag{2.64}$$

In words, each transmitter may choose a set of MCS and transmission powers on the resource grid, according to the defined PRB usage and power constraints.

Apart from the action set, the network is described by its set of possible topology states. For each sub-channel, the topology state can be modeled using the scalar, real-valued attenuation coefficients introduced in Section 2.1.2. Thus, for each sub-band $w \in \{1, ..., W\}$, there is a channel matrix $\boldsymbol{H}_w \in \mathbb{R}_+^{|\mathcal{L}| \times |\mathcal{L}|}$ that captures the attenuation among all links. The system topology state then consists of W such channel matrices, i.e., $\boldsymbol{Q} = \{\boldsymbol{H}_1, ..., \boldsymbol{H}_W\}$, which are realizations of the overall, allowed set of topology states $\mathcal{Q} = \{\mathbb{R}_+^{|\mathcal{L}| \times |\mathcal{L}|}, ..., \mathbb{R}_+^{|\mathcal{L}| \times |\mathcal{L}|}\}$, respectively.

Action set and topology state are combined together into rate functions R, as defined in Section 2.1.3. For better nomenclature, assume that each link (m, n) is assigned an index i. The overall rate function $R_i[\tau]$ of a link i in frame τ, for given action matrix $\boldsymbol{A}[\tau]$ and a topology state $\boldsymbol{Q}[\tau]$, is:

$$R_i(\boldsymbol{A}[\tau], \boldsymbol{Q}[\tau]) = \sum_{k=1}^{K} \sum_{q=1}^{C} x_{kq}[\tau] R_q(\Gamma_i(\boldsymbol{H}_w[\tau], \boldsymbol{p}_k[\tau])), \text{ where } w \text{ s.t. } k \in \mathcal{B}_w.$$

R_q defines the rate function depending on the used MCS q and $\boldsymbol{H}_w$, $\boldsymbol{p}_k$ are the channel matrix of sub-band w and transmission power vector on PRB k. $\Gamma_i(\boldsymbol{H}_w, \boldsymbol{p}_k)$ is the SINR achieved by link i on the given PRB. The overall rate of link i thus is the sum of all per-PRB rates, which are defined by the MCS choices x_{kq}, respectively.

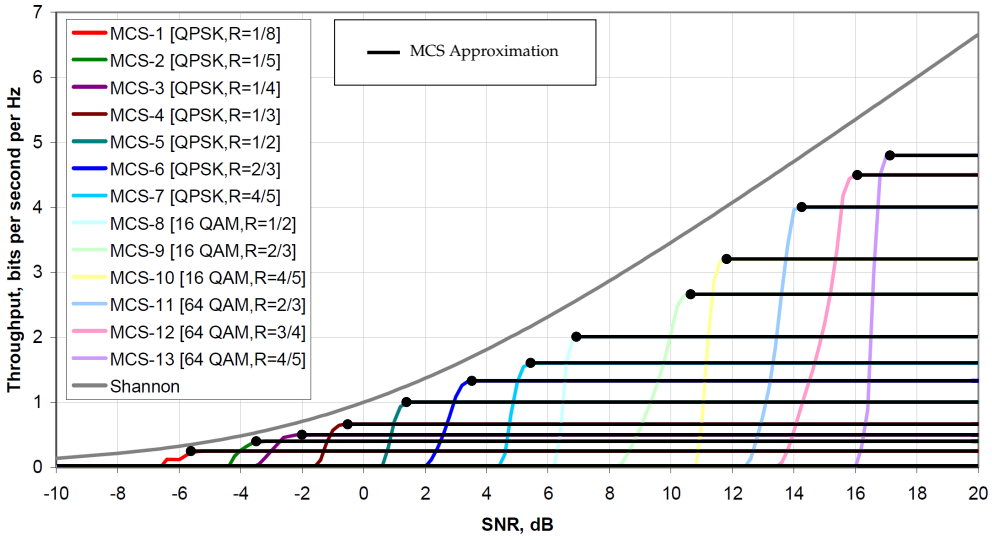

Figure 2.15: Used approximation for SINR to Rate mapping. The background is taken from [95] and shows the mapping of SINR to achievable rate for different MCSs. Enhanced in black are the used approximations per MCS, whereas in gray the maximum over all approximations is shown.

MAC Operation of D2D

Assuming the previously introduced nomenclature and definitions, the operation of a D2D enabled cellular network can be formulated as NUM problem. Here only the uplink is considered, as it is assumed that D2D sidelinks and cellular uplinks are operated on uplink bands, independent of the downlinks, which can be operated with legacy methods.

Formally, let utility $U_i(R_i) : \mathbb{R}_+ \mapsto \mathbb{R}$ be an arbitrary utility function, which reflects how desirable a certain instantaneous rate R_i is for communication. Because of the frame structure used in the considered LTE networks, an instantaneous rate is the accumulation of all rates on all PRBs, i.e.,

$$R_i = \sum_{k \in \mathcal{R}} R_i^{(k)}. \tag{2.65}$$

As introduced already in Section 2.2, uplink transmission is considered, combined with the assumption that SC-FDM signals do not span adjacent PRBs. PRB use thus is subject to the constraints that for each time slot t, only one of the PRBs in $\mathcal{T}_t$ is actually used. Further, only one MCS can be used on a PRB at a time.

The rate curves for different MCS in an LTE system, as they can be taken from measurements, are depicted in various colors in Figure 2.15. It can be seen that the relationships are highly non-linear and, more importantly, they have no tractable analytic formulations. In this thesis they are thus approximated as is shown in black in the figure: It is assumed that for each used MCS q, there is a distinct, minimum SINR target γ_q, above which the MCS yields constant rate and below which the rate is treated as zero. All SINR targets are collected in the target vector $\boldsymbol{\gamma}_t$. A second vector $\boldsymbol{r}_t$ is defined, where each element r_q contains the constant achievable data rate of an MCS, which is achieved whenever the SINR is larger or equal to γ_q. The choice of using an MCS q on PRB k is now indicated by a vector $\boldsymbol{x}_i^{(k)}$,

where each element corresponds to the MCS of a CQI value. Finally, an achieved SINR value $\gamma_i^{(k)}$ and a transmission power $p_i^{(k)}$ are introduced for every link on each PRB.

The general utility maximization problem can be formulated as follows:

$$\text{(D2D-NUM)} \qquad \max_{\boldsymbol{R},\boldsymbol{x},\boldsymbol{p},\boldsymbol{\gamma}} \sum_{i\in\mathcal{L}} U_i(R_i) \tag{2.66}$$

$$\text{s.t.}$$

$$0 \le R_i \le \sum_{k\in\mathcal{R}} R_i^{(k)} \tag{2.67}$$

$$- - - - - - - - - - - - - - - - - - -$$

$$R_i^{(k)} \le \boldsymbol{r}_t^T \boldsymbol{x}_i^{(k)} \qquad \forall i,k \tag{2.68}$$

$$\sum_{q=1}^{C_{\text{UL}}} x_{qi}^{(k)} \le \mathbb{1}\{k\in\mathcal{U}\} \qquad \forall i,k \tag{2.69}$$

$$\sum_{k\in\mathcal{T}_t} \sum_{q=1}^{C_{\text{UL}}} x_{qi}^{(k)} \le 1 \qquad \forall i,\mathcal{T}_t \tag{2.70}$$

$$x_{qi}^{(k)} \in \{0,1\} \qquad \forall i,q,k \tag{2.71}$$

$$- - - - - - - - - - - - - - - - - - -$$

$$\boldsymbol{\gamma}_t^T \boldsymbol{x}_i^{(k)} \le \gamma_i^{(k)} \qquad \forall i,k \tag{2.72}$$

$$\gamma_i^{(k)} \left(\sum_{j\neq i} \frac{h_{ij}}{h_{ii}} p_j^{(k)} + \frac{N_i}{h_{ii}} \right) \le p_i^{(k)} \qquad \forall i,k \tag{2.73}$$

$$[p_i^1, ..., p_i^K]^T \in \mathcal{P}_i \qquad \forall i \tag{2.74}$$

The intuition of this optimization problem is as follows: The utility (2.66) to be maximized evaluates the quality of the current network state as aggregation of all per-link utilities. Constraint (2.67) ensures that the evaluated rate does not exceed the actually accumulated one. Both together define an upper MAC layer perspective on the problem, as there is no information on the underlying MAC mechanisms, nor on the actually transported commodities.

In constraints (2.68)-(2.71), MCSs are set on each PRB. Constraint (2.68) guarantees that on each PRB, the assumed rate does not exceed that of the actually realized. The realized rate is set by the constant rate vector $\boldsymbol{r}_t$, among which one rate is chosen with $\boldsymbol{x}_i^{(k)}$. (2.69) restricts PRB use to the uplink band and (2.70) demands that on each time-slot, at most one frequency band is actually used and on each frequency band, only one MCS is chosen. (2.71) is an integer constraint for all $x_{qi}^{(k)}$. The four constraints together form a resource allocation perspective. The rate values $R_i^{(k)}$ thereby act as interface towards the upper layer MAC perspective.

Finally, equations (2.72)-(2.74) define the actual SINR targets, interference and power constraints on all PRBs. In particular, (2.72) ensures that the current SINR target satisfies that of the chosen MCS on each PRB. Variable $\boldsymbol{x}_i^{(k)}$ thereby serves as an interface to the resource allocation part, which is generated by associating the vectors $\boldsymbol{r}_t$ and $\boldsymbol{\gamma}_t$ such that the former contains the rates achieved with the SINR targets in the latter. The variables $\gamma_i^{(k)}$ can be interpreted as achieved SINRs, which is then realized with the powers $p_i^{(k)}$.

It can be seen, and is also indicated by the dashed lines between equations, that D2D-NUM is an overall, cross-layer optimization over several aspects of the MAC layer, namely

interference management, resource allocation and network utility maximization. Because the utility function is not clearly defined here, the resulting problem can assume a variety of properties only from changing the used utility. Further, some constraints can be adapted to other, related scenarios. For example, the PRB usage constraint (2.70) can be varied or dropped, if the transmitter capabilities allow to use several channels concurrently, or (2.74) can be adapted to incorporate maximum power constraints, spectral mask constraints or total power constraints, respectively. In the given formulation, constraint (2.73) alone renders the problem non-convex. It has been argued in Section 2.1.2 that it can be made convex by using a logarithmic transformation. However, this has an effect on the used utilities $U(r_i)$, which might be non-concave after transformation.

The presented NUM problem takes yet one of a multitude of possible forms, even though the utility itself is held abstract. In particular, for any LQ function $\psi(\Gamma_i)$ as introduced in Section 2.1.2, a set of utilities $U_i(\psi)$ can be defined and optimized in a similar fashion. The form shown in (2.66)-(2.74) gives only one example that will be investigated to get an insight into possible solution structures.

2.3 Simulations

To asses D2D with simulations, two different types of simulators are used throughout this thesis: Simulations based on Matlab and SimuLTE based simulations.

2.3.1 Matlab

One simulation type used in this thesis is based on the MATLAB computing environment, which is sold as commercial product by the company The Mathworks Inc. [96].

In the MATLAB computing environment, the focus is mostly on mathematical assessment of problems that occur in communication systems. The used models on this level thus mainly incorporate the mathematics, while important system aspects such as protocol interactions are neglected. To keep the simulation realism on an acceptable level, in general the communication channels, transmission powers and noise are generated according to realistic models, e.g. the WINNER II channel models [60]. The overall flow is to define system parameters, such as used frequency ranges, center frequencies, noise figures, resource structures and transmission power constraints. Then, devices are placed at spatial positions according to an assumed distribution and the channels among all devices are generated complying with a channel model. Once all parameters have been set, solution approaches for the targeted mathematical problems are run.

In general, MATLAB based simulations can be seen as first step to assess a problem. Solutions that work well in this mathematical environment can then be transfered to implementation in the more realistic, but also more error prone SimuLTE environment.

2.3.2 SimuLTE

The open source simulation framework SimuLTE [97] is based on the known event-based network simulator OMNeT++ [98]. SimuLTE implements major parts of the LTE stack in a standard compliant way, including the LTE Packet Data Convergence Protocol (PDCP) layer, the Radio Link Control (RLC) layer and the MAC layer.

On RLC layer, the Transparent Mode (TM), Unacknowledged Mode (UM) and Acknowledged Mode (AM) are implemented including higher layer packet fragmentation, complying with 3GPP specifications [99]. On the MAC layer, the MAC Packet Data Unit (PDU) and Control Element (CE) structure for Buffer Status Report (BSR) is supported and Hybrid Automatic Repeat Request (HARQ) is implemented, again standard compliant [100]. Further, a scheduling structure that is based on PRBs is implemented. For scheduling, SINR values are mapped to Transport Block Sizie (TBS) and codeword length, as defined in [101]. The exact TBS is determined according to MCS that vary from QPSK to 64-QAM. The MCS is selected according to CQI feedback, where the MCS is chosen for which the Block Error Rate (BLER) is closest to 0.1%.SimuLTE uses channel models standardized by the ITU-R M.2135-1 [61], implements shadowing and fading that can be turned on or off.

As D2D communication is not implemented by default, some enhancements needed to be added. In particular the BSR reporting structure for D2D links and channel quality identification needed to be changed and a mode selection functionality was added. For the reporting structure, each UE included additional MAC layer buffers for D2D SLs with an associated identifier for the target UE. The result was a set of link identifiers for each source-destination pair, which included uplink as special case that was targeted to the BS. BSR reporting and scheduling were then based on the link identifiers rather than uplink UEs, which the scheduler used before. Different schedulers were added to create a choice of options, including a channel aware PF scheduler and the BP scheduler [83]. Channel quality identification and mode selection functionality was introduced by adding channels among UEs, allowing the UEs to sniff ongoing transmissions and determine channel quality parameters. The results were signaled to the BS, which induced a mode selection choice. Mode change was realized by forwarding the traffic to the MAC layer buffer corresponding to the new recipient, i.e., to the conventional uplink buffer in CM or to the buffer for the targeted UE in DM. Realization of frequency reuse required change at a deeper level. In SimuLTE, interference is introduced by simply adding an external interference "device" that creates uniform interference on all channels. However, this proved to be insufficient for sophisticated interference coordination, as UEs themselves could not create interference among each other. To incorporate intra-cell interference, the all used PRBs were captured, together with the used transmission powers. Upon reception, the total interference plus noise power was determined and SINR was used to replace previous Signal to Noise Ratio (SNR) values.

Any upper layer functionality, e.g., Internet Protocol (IP), Transmission Control Protocol (TCP) or User Datagram Protocol (UDP) protocols, traffic generation, etc. were included using the INET framework for OMNeT++.

The combination of OMNeT++ with the standard-compliant implementation SimuLTE can be considered close to real systems. However, its use also induces many of the chal-

lenges that come with real implementations, such as cross-layer effects, delay and traffic shaping effects, that can be seen in simulation results. The use of SimuLTE was thus mostly the second step, which was based on results that had been verified to work in Matlab-based simulations.

Chapter 3

Scaling Laws of D2D Links

In this section, scaling laws for the expected number of established D2D links are investigated and the impact of device pairing and mode selection on the expected number is evaluated. The chapter bases on publication [1], in which the main results have been published for a one-serves-all service type. The results are extended to arbitrary service types in Section 3.5, which is a novel, unpublished contribution. Throughout this chapter, the action flow for creation of D2D links is assumed, which has been introduced in Section 2.2.2. This notion is combined with the stochastic geometry framework, of which basic properties have been reproduced in 2.1.1.

Although often taken for granted, the existence of sidelinks is, in fact, not a matter of course. In general, a series of prerequisites must be met for direct links to be established: (1) Local transmission opportunities must arise, i.e., there must be a sufficient spatial density of devices with mutual communication demands. (2) The devices must be paired correctly, i.e., be grouped into suitable communication pairs. (3) The operator's network must decide to offload the traffic of the communication pairs to the direct mode, instead of serving it by cellular communication. Any of these aspects, as well as their interplay, has an important influence on the amount of D2D communication links that can be assumed to exist. Identification of this influence is crucial to evaluate impact of direct links, as well as their enablers.

The influence is investigated by modeling the network as a stochastic distribution of nodes, with randomly distributed traffic demands, and creating an analytical model for the set-up procedure. The results are scaling laws for the spatial density of D2D links, general statements on the required penetration of D2D-enabled devices among all UEs, as well as the impact of device pairing and mode selection on the number of established direct links.

Related Work

The investigation of link establishment comprises a service level point of view that is not commonly used in D2D related research, which is focused on the PHY, MAC and networking layer [44], [49]. The few service level investigations with D2D context are related to distributed caching and consider how much and which types of information should be cached [102]–[105] and how the appropriate cache should be chosen for content delivery [106]. Technically, this corresponds to the device pairing step. The choice of the serving cache has a

direct influence on the chance of devices establishing a sidelink. However, in the mentioned works the question how many D2D flows are created by their proposed methods, which quantifies the impact of cache selection on D2D networks, is not discussed.

Mode selection is an intensively investigated research topic (c.f. references in [49]) that resides on networking layer because it can be interpreted as a routing problem. The correct criteria for mode selection, in terms of network sum-rate, energy efficiency and resource efficiency are investigated in literature. Again, the impact of mode selection on the number of established D2D flows is not quantified.

Peer discovery is also a related topic and considers the question how signaling methods should be designed for fast and energy efficient device discovery [107]–[111]. While this is related to both, mode selection and device pairing, the influence on the number of established D2D flows is also not investigated within this context.

It must be concluded that although much work exists on ways how to leverage D2D communication and how to manage it on PHY, MAC and networking layer, the question how many D2D flows are created by an application in a specific network realization seems completely unconsidered.

The aim of this chapter is to close this gap and provide analytic arguments for the impact of device densities, service penetration, device pairing and mode selection strategies on the spatial density of D2D flows established in a certain area.

3.1 Service Formulation

Consider a network where the UEs are described with a homogeneous p.p.p. Φ_u with density λ, as introduced in Section 2.1.1, and that follows the set-up flow given in Section 2.2.2. The points are located in a spatial observation area Ω. Assume that a set of local services $\mathcal{S}$ is present in the network, where a local service can be any application or use case generating MAC level traffic demands among UEs. Such a service could be induced, e.g., by a gaming application, by D2D enabled caches or by a protocol that provides relaying functionality. Assume further that S services exist in overall and that all UEs in the network will either be client or provider of a random subset of the available services, based on the personal preferences of their users.

Any UE is client of service s with probability $p_c^{(s)}$ and provider with probability $p_p^{(s)}$, where the probabilities are independent for all services. According to the stochastic geometry framework this performs a thinning of the p.p.p., such that the set of all clients and providers of service s will follow p.p.p.'s $\Phi_c^{(s)}$, $\Phi_p^{(s)}$, with density $\lambda_c^{(s)} = \lambda p_c^{(s)}$ and $\lambda_p^{(s)} = \lambda p_p^{(s)}$, respectively [50]. Due to the role that the parameters play in this context, $p_p^{(s)}$ will be called the *penetration* of service s, measured in percentage of devices that offer it, $\lambda_c^{(s)}$ the *popularity* of service s and $\lambda_p^{(s)}$ *availability* of s, measured in devices per square kilometer.

Using this distribution of nodes, two mappings $P : (u_c, \Phi_p) \mapsto (u_c, u_p)$, for $u_c \in \Phi_c,\ \ u_p \in \Phi_p \setminus u_c$ and $M : (s_c, d_c) \mapsto \{0, 1\}$ define the action flow that leads to establishing sidelinks in the network. The mapping P is called a pairing, as it chooses suitable devices among which traffic flows are established. Pairing can be done on any layer and corresponds to, e.g., cache

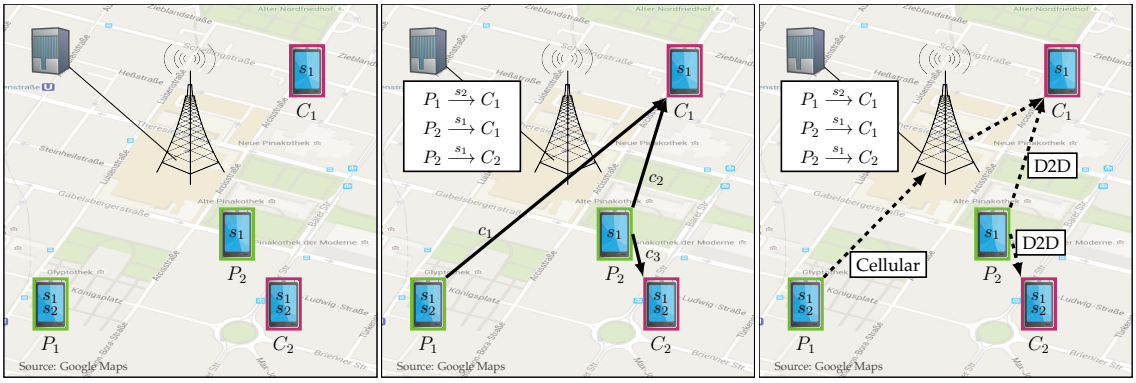

Figure 3.1: General flow of network establishment. As shown in Figure 3.1a, the network starts with nodes that either require (C_i) or provide (P_i) service. The provisions and requirements are matched to create link pairs, among which traffic is generated as shown in Figure 3.1b. After the traffic is generated, some flows are handed off to direct mode, which is illustrated in Figure 3.1c.

selection. The second mapping M is the mode selection, which chooses whether a flow is realized via the direct sidelink path $\mathcal{L}_c^{(\mathrm{DM})}$, in which case $M(s_c, d_c) = 1$ or with cellular communication over path $\mathcal{L}_c^{(\mathrm{CM})}$. Note that as $M(s_c, d_c)$ only depends on s_c and d_c, it is implicitly assumed that each communication pair chooses its mode independently of the other pairs.

From the given perspective, services can be classified by the types of pairings they allow. In particular, it is differentiated between the number of clients that a server can serve and the number of servers that a client can be served from. Four extreme cases exist, which are: (1) One-to-one mapping, i.e., each client can be served by one server and each server can serve one client. This is appropriate for unique sessions such as a data transmission among dedicated devices. (2) One-serves-all, i.e., any server can serve an arbitrary number of clients but each client can only be served by one server. This would be appropriate for relaying services, D2D multi-cast or for D2D internet gateways. (3) All-serve-one, i.e., any client can be served by an arbitrary number of servers which, however, can serve only one client. (4) Full-mesh, i.e., there are no constraints on client and server side. This last case is appropriate, e.g., for distributed caching scenarios, when clients can request different portions of data from different caches. Throughout this analysis, a one-serves-all model is assumed. However, it will be shown in Section 3.5 that its analysis also give strong arguments for the behavior of the other models.

3.1.1 Basic Effects

The following investigation is based on simulations, for which results are shown before the underlying properties are modeled and investigated analytically. While simulations in general have only limited realism, they are suitable to implement the axiomatically assumed action chain of node distribution, device pairing and mode selection given in the previous section.

The made simulations were produced with the open source simulator SimuLTE [97],

which is based on the known network simulation framework OMNeT++ [98] and has been described in more detail in Section 2.3. The simulation set-up is similar to Figure 3.1. In a single cell, UEs are deployed according to a p.p.p. and are managed by a BS. The UEs either provide or require a random subset of the services. The different services are modeled as different video files which are requested by the clients and served by the providers. The exact probabilities with which services are required or provided follow a Zipf distribution in s, i.e.,

$$p_{\{c,p\}}^{(s)} = \frac{s^{-\alpha}}{\sum_{k=1}^{S} k^{-\alpha}},$$

for an $\alpha \geq 0$. Zipf distributions are known to accurately model the distribution of web-caching and peer-to-peer piece selection [112], [113] and are simply assumed to describe the service popularity at this point. It will be seen that in fact, the results can be decoupled from their actual distribution, such that Zipf distributions can be assumed without loss of generality. In the core network of the operator, a server keeps track of all services present in the network. At the beginning of a simulation, each UE reports to the server its position and which services it provides or requires. The server pairs requirements with provisions and passes each client the identity of a provider according to the chosen pairing strategy. The client UEs then initiate the transport of video data.

During the video transport, the clients track the uplink signal of the providers to estimate the quality of a potential D2D link and report this quality to the BS. The BS then decides whether the session will be offloaded to a direct link, according to a chosen mode selection criterion. After all mode selection decisions have been made, the simulation stops, resulting in data on which links have been offloaded and which not.

The focus of investigations is on three mode selection criteria, which are taken from literature, and three pairing strategies. As device pairing is typically omitted in literature, no known strategies exist. Three prototypical strategies are defined here, which are:

- *Random Pairing*: Each client is paired with a random provider.
- *Nearest Pairing*: Each client is paired with the spatially nearest provider.
- *Farthest Pairing*: Each client is paired with the spatially farthest provider.

The *Random Pairing* strategy might occur when device pairs are formed over the top on application layer, without taking any information on the spatial topology into account. The *Nearest Pairing* should intuitively produce D2D pairs because the produced pairs tend to be spatially nearby, resulting in good channel conditions. The *Farthest Pairing* is introduced as an example of an *ill-designed* pairing, i.e., to capture the impact of wrong decisions on this level.

The considered mode selection criteria are:

- *ForceD2D*: The BS will offload traffic whenever it is possible, i.e., whenever the CQI of the direct link is larger than zero. This criterion is used, e.g., in [30], [114]–[119].

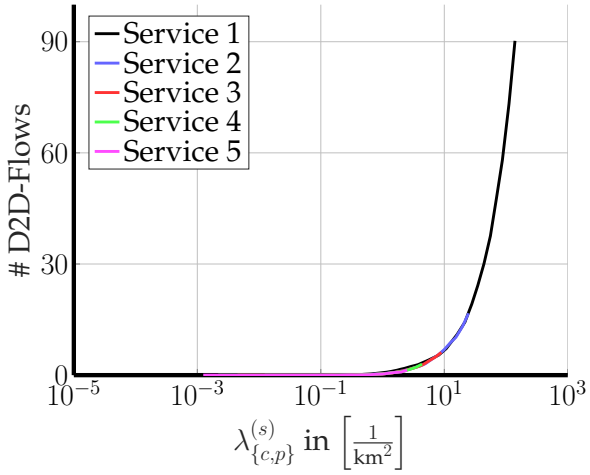

Figure 3.2: Mean number of D2D flows versus UE densities, for $S = 5$ services that are Zipf-distributed with $\alpha = 2.5$

- *Capacity*: The BS offloads sessions, if the capacity on the direct link is larger than the one of the cellular link. The capacity is here determined under the assumption that all resources are used exclusively by the considered link [119]–[121].
- *Resource Efficiency*: Sessions are offloaded only if the average achievable resource efficiency of the direct link is larger than the one using cellular communication [5]. Resource efficiency includes the fact that not all resources need to be used for some modes and is discussed in more detail in Chapter 4 and 5.

It must be stressed that even though the focus is on some pairing strategies and mode selection criteria, the developed framework can be transferred to any other pairing strategies and mode selection criterion, as long as they form valid mappings according to the given definitions.

The first simulation was performed using $S = 5$ total services, the *Nearest Pairing* strategy and *ForceD2D* mode selection. The client and server probabilities both follow a zipf distribution in s with parameter $\alpha = 2.5$. Figure 3.2 shows the resulting mean number of D2D flows versus the popularity/availability of UEs for the respective service, which are chosen to be equal. The results are averaged over 1000 runs, leading to confidence intervals that are small enough to be neglected. As can be seen, the curves for different services merge into an overall relationship between service popularities/availabilities $\lambda^{(s)}_{\{c,p\}}$ and number of D2D flows. The resulting relationship is independent of the exact service considered. Although intuitive, this result is interesting as all services were required and offered in parallel during the same simulation runs, even on the same UEs, and thus are coupled by resource constraints. The result has a very practical benefit: To capture the effects of service popularity and availability on the occurrence of D2D communication, it is sufficient to analyze the case of a single service with the service popularity λ_c, and service availability λ_p. A further conclusion is that not the probabilities $p^{(s)}_{\{c,p\}}$ are the essential parameters but popularity and availability, $\lambda^{(s)}_{\{c,p\}}$, are. The only interest in the client/server probabilities is due to the fact

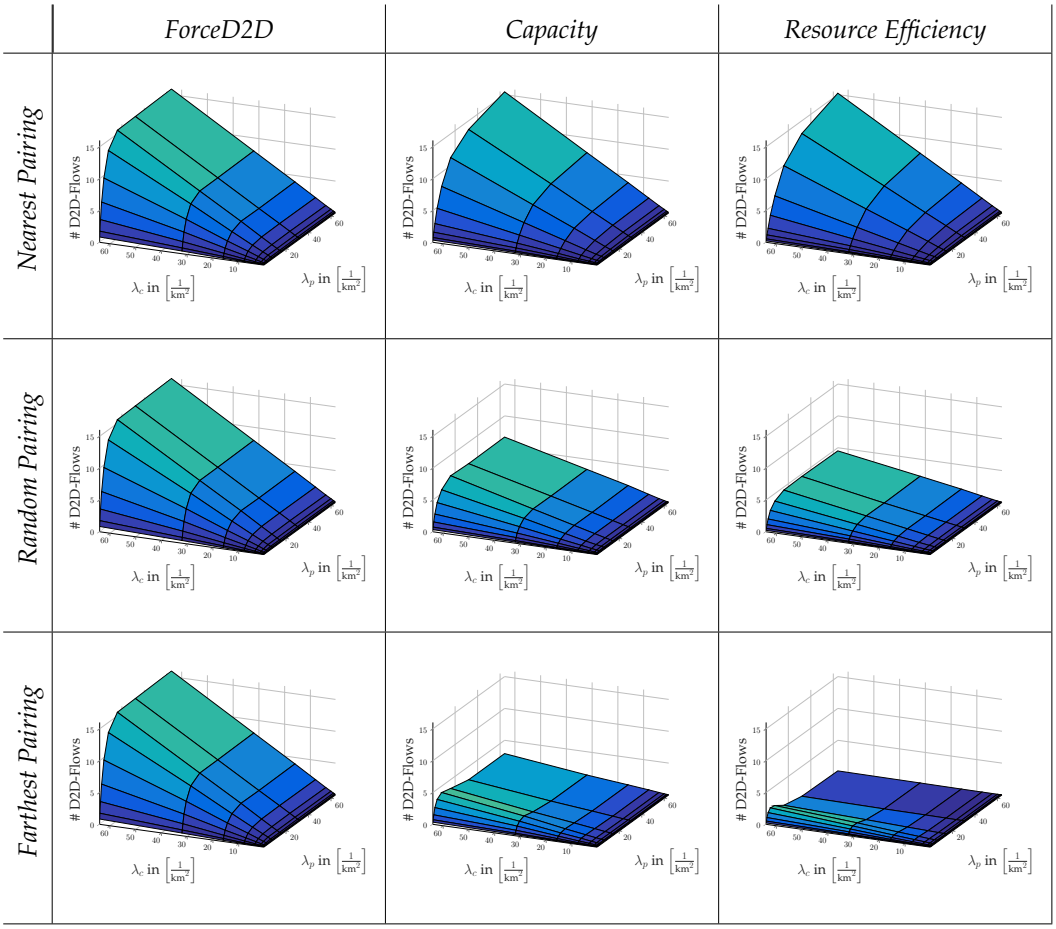

Figure 3.3: Mean number of occurring D2D-flows for different combinations of pairing, mode selection and UE densities. All results shown λ_c in $1/\text{km}^2$ on the x-axis, λ_p in $1/\text{km}^2$ on the y-axis and the mean number of D2D-flows on the z-axis.

that they create $\lambda_{\{c,p\}}^{(s)}$ out of λ. Finally, the result justifies the use of a Zipf distribution in retrospective: As the probabilities anyways lead to the same basic effect, the exact distribution of services on the devices does not have a main impact.

For the next result, popularity and availability for each considered combination of pairing strategy and mode selection criterion are varied, using powers of two from $0.25/\text{km}^2$ to $64/\text{km}^2$. The resulting number of D2D flows, again averaged over 1000 runs, is shown in the result grid of Figure 3.3. Each graph shows the popularity λ_c on the x-axis and the availability λ_p on the y-axis. The z-axis shows the mean number of resulting D2D flows. Several observations can be made: (1) There seems to be a linear relationship between the popularity λ_c and the number of offloaded flows in any case. The availability λ_p, on the other hand, has a rather undefined influence on the occurring flows, depending on the chosen combination of pairing strategy and mode selection. (2) In most cases, there seems to be a saturation effect on the number of flows versus availability. Closer investigations suggest the main property leading to this saturation effect to be that, while each client can produce one flow at most, each provider can in principle serve an arbitrary number of clients. Because of this, the number of D2D flows will increase less with λ_p if there is a large number of providers already.

(3) The *ForceD2D* mode selection behaves independently of the used pairing strategy. This is counter intuitive, because the *Farthest Pairing* should, e.g., produce less flows than the *Nearest Pairing*. (4) For *Capacity* and *Resource Efficiency* mode selections, the pairing strategy has a big influence on the resulting D2D-flows. The use of *Nearest Pairing* produces the most D2D-Flows, *Random Pairing* produces a number of flows that converges to a lower value. *Farthest Pairing*, however, shows a peak for low provider densities but produces less flows for high densities.

3.2 Modeling with Stochastic Geometry

In this section a mathematical model that captures the results presented in Section 3.1.1 is derived. For this, denote with $u_{\boldsymbol{c}}$ a client at the spatial position $\boldsymbol{c} \in \Omega$ and with $u_{\boldsymbol{p}}$ a provider at position $\boldsymbol{p} \in \Omega$. Considering given mappings P and M, define the set Π as:

$$\Pi = \{u_c \in \Phi_c : M(P(u_c, \Phi_p)) = 1\}. \tag{3.1}$$

Π is the set of client nodes that are offloaded to direct mode. The number of nodes in Π equals the number of D2D links. We can interpret the mapping $M(P(u_c, \Phi_p))$ as mark that is associated with each client node. Due to the given assumptions that M depends only on u_c, u_p and P maps each u_c to a $u_p \in \Phi_p$ independently, Π is a p.p.p. created from Φ_c by independent marking. However, note that Π need not be homogeneous. As described in Section 2.1.1, the density of clients that are in Π, i.e., the density of D2D links, is given by [50]

$$\lambda_{\text{D2D}} = \lambda_c \cdot P\{u_c \in \Pi\}, \tag{3.2}$$

where $P\{u_c \in \Pi\}$ is the overall probability that a client is in Π.

Say that $\neg E_{\Phi_p}(\mathcal{V})$ (Φ_p not empty on $\mathcal{V}$) if Φ_p has points in an area $\mathcal{V} \subseteq \Omega$. Conversely, there are no points in $\mathcal{V}$ if $E_{\Phi_p}(\mathcal{V})$. Further, define

$$\Pi_{\mathcal{V}} = \{u_c \in \Pi : (u_c, u_{\boldsymbol{p}}) = P(u_c, \Phi_p) \text{ with } \boldsymbol{p} \in \mathcal{V}\} \tag{3.3}$$

the set of clients that are offloaded with a provider in $\mathcal{V}$. Assume for an instant that there is exactly one client, $u_{\boldsymbol{c}}$, with a random position $\boldsymbol{c} \in \Omega$. A necessary condition for D2D to take place is that $\neg E_{\Phi_p}(\Omega)$ holds, i.e., there are providers in Ω. If $E_{\Phi_p}(\Omega)$, there can be no D2D flows, i.e., $P\{\Pi \mid E_{\Phi_p}(\Omega)\} = 0$. The following definitions are conditioned on the event that $\neg E_{\Phi_p}(\Omega)$ but, for ease of reading, the condition will be left out whenever it is clear from the context that it needs to be fulfilled. Keep in mind that the position of the client is uniformly distributed and assume for the moment that it has a fixed position $\boldsymbol{c}$. Consider that, if $\neg E_{\Phi_p}(\Omega)$, the pairing for $u_{\boldsymbol{c}}$ is performed by some function $P : (u_{\boldsymbol{c}}, \Phi_p) \mapsto (u_{\boldsymbol{c}}, u_{\boldsymbol{p}})$, following a set of rules that are either deterministic or probabilistic with respect to the UE positions. As the number and positions of the providers are random, keeping $\boldsymbol{c}$ fixed, there is a probability for each $\mathcal{V} \subseteq \Omega$ that the position $\boldsymbol{p}$ of the paired provider will be in $\mathcal{V}$. And if there is a probability, it has a probability density function $f_p(\boldsymbol{p} \mid \boldsymbol{c})$ that satisfies:

$$P\{\boldsymbol{p} \in \mathcal{V} \mid \boldsymbol{c}\} = \int_{\mathcal{V}} f_p(\boldsymbol{p} \mid \boldsymbol{c}) d\boldsymbol{p}. \tag{3.4}$$

Similarly, mode selection is performed by the mapping $M : (u_{\boldsymbol{c}}, u_{\boldsymbol{p}}) \mapsto \{0, 1\}$, which can behave according to deterministic or probabilistic rules. Given that $\boldsymbol{c}$ is fixed, there is a probability $P\{u_{\boldsymbol{c}} \in \Pi \mid \boldsymbol{p}, \boldsymbol{c}\}$ for each position $\boldsymbol{p}$, that a flow from a provider at $\boldsymbol{p}$ to a client at $\boldsymbol{c}$ will be offloaded. Thus, for a given set $\mathcal{V} \subseteq \Omega$ and fixed $\boldsymbol{c}$, the overall probability of a flow being offloaded and $\boldsymbol{p}$ being in $\mathcal{V}$, provided that there are providers in Ω, is

$$P\{u_{\boldsymbol{c}} \in \Pi_{\mathcal{V}} \mid \boldsymbol{c}, \neg E_{\Phi_p}(\Omega)\} = P\{u_{\boldsymbol{c}} \in \Pi \mid \boldsymbol{p}, \boldsymbol{c}\}\, P\{\boldsymbol{p} \in \mathcal{V} \mid \boldsymbol{c}\} = \int_{\mathcal{V}} P\{u_{\boldsymbol{c}} \in \Pi \mid \boldsymbol{p}, \boldsymbol{c}\}\, f_p(\boldsymbol{p} \mid \boldsymbol{c}) d\boldsymbol{p}.$$

Consider distance based mode selection strategies, which behave deterministic with respect to the UE positions. For deterministic mode selection, no matter how often the mode selection is run, its outcome will not change when $\boldsymbol{c}$, $\boldsymbol{p}$ stay fixed and hence $P\{u_{\boldsymbol{c}} \in \Pi \mid \boldsymbol{p}, \boldsymbol{c}\} \in \{0, 1\}\ \forall \boldsymbol{c}, \boldsymbol{p}$. A probabilistic mode selection would be one that depends on mutual interference among UEs. In this case, for each position pair $\boldsymbol{c}$, $\boldsymbol{p}$, the outcome of the mode selection might change, depending on the other UEs' positions. Then, the same flow could experience different mode selection results when the function is re-run and $P\{u_{\boldsymbol{c}} \in \Pi \mid u_{\boldsymbol{c}} \in\} \in [0, 1]$, where the probability is taken over all possible realizations of Φ_c, Φ_p.

Denote with $C(\boldsymbol{c}) = \{\boldsymbol{p} \in \Omega : P\{u_{\boldsymbol{c}} \in \Pi \mid \boldsymbol{p}, \boldsymbol{c}\} > 0\}$, the set of all positions with nonzero probability that a flow from a provider UE $u_{\boldsymbol{p}}$ is offloaded, when $\boldsymbol{c}$ is fixed. $C(\boldsymbol{c})$ plays the role of a *potential D2D service area*, as any provider must be in $C(\boldsymbol{c})$ to have a chance of serving a node $u_{\boldsymbol{c}}$ via D2D. Now, the main results of this section can be postulated:

Lemma 3.1. For any arbitrary pairing strategy and mode selection function, the probability of a flow being offloaded is:

$$P\{u_c \in \Pi\} = \frac{1}{\|\Omega\|} \int_{\Omega} P\{u_{\boldsymbol{c}} \in \Pi_{C(\boldsymbol{c})}\} d\boldsymbol{c} = E_{\boldsymbol{c}}\left\{P\{u_{\boldsymbol{c}} \in \Pi_{C(\boldsymbol{c})}\}\right\} \tag{3.5}$$

where $\|\Omega\|$ is the size of Ω and $E_{\boldsymbol{c}}\{\cdot\}$ is the expectation value w.r.t. $\boldsymbol{c}$. The right hand side gives the expected probability over all client positions, that a flow will be offloaded and the provider is in its service area $C(\boldsymbol{c})$.

Proof. By using probability theory, it holds that:

$$\begin{aligned}
& P\{u_c \in \Pi\} \overset{(1)}{=} P\{u_c \in \Pi \mid \neg E_{\Phi_p}(\Omega)\} P\{\neg E_{\Phi_p}(\Omega)\} \\
\overset{(2)}{=}\ & E_{\boldsymbol{c}}\left\{P\{u_{\boldsymbol{c}} \in \Pi_{\Omega} \mid \boldsymbol{c}, \neg E_{\Phi_p}(\Omega)\}\right\} \cdot P\{\neg E_{\Phi_p}(\Omega)\} \\
=\ & E_{\boldsymbol{c}}\left\{\int_{\Omega} P\{u_{\boldsymbol{c}} \in \Pi \mid \boldsymbol{p}, \boldsymbol{c}\}\, f_p(\boldsymbol{p} \mid \boldsymbol{c}) d\boldsymbol{p}\right\} P\{\neg E_{\Phi_p}(\Omega)\} \\
\overset{(3)}{=}\ & E_{\boldsymbol{c}}\left\{\int_{C(\boldsymbol{c})} P\{u_{\boldsymbol{c}} \in \Pi \mid \boldsymbol{p}, \boldsymbol{c}\}\, f_p(\boldsymbol{p} \mid \boldsymbol{c}) d\boldsymbol{p}\right\} P\{\neg E_{\Phi_p}(\Omega)\} \\
=\ & E_{\boldsymbol{c}}\left\{P\{u_{\boldsymbol{c}} \in \Pi_{C(\boldsymbol{c})} \mid \neg E_{\Phi_p}(\Omega)\}\right\} \cdot P\{\neg E_{\Phi_p}(\Omega)\} \\
\overset{(4)}{=}\ & E_{\boldsymbol{c}}\left\{P\{u_{\boldsymbol{c}} \in \Pi_{C(\boldsymbol{c})}\}\right\}
\end{aligned}$$

In steps (1) and (4) the law of total probabilities was used, together with the fact that $P\{u_c \in \Pi \mid E_{\Phi_p}(\Omega)\} = P\{u_{\boldsymbol{c}} \in \Pi_{C(\boldsymbol{c})} \mid E_{\Phi_p}(\Omega)\} = 0$. For step (2) it was leveraged that $\boldsymbol{c}$ is uniformly distributed and for (3) that $P\{u_{\boldsymbol{c}} \in \Pi \mid \boldsymbol{p}, \boldsymbol{c}\} = 0$ outside $C(\boldsymbol{c})$ by definition. □

Theorem 3.1. For any arbitrary pairing strategy and mode selection criterion, the density of occurring D2D flows takes the form of

$$\lambda_{\text{D2D}} = \lambda_c P_M(\lambda_p)\left(1 - e^{-\lambda_p \overline{C}}\right), \tag{3.6}$$

where $P_M(\lambda_p) = E_{\boldsymbol{c}}\left\{P\{u_{\boldsymbol{c}} \in \Pi_{C(\boldsymbol{c})} \mid \neg E_{\Phi_p}(C(\boldsymbol{c}))\}\right\}$. $P_M(\lambda_p)$ is the expected probability over all $\boldsymbol{c}$ that of a flow from paired devices is offloaded, given that there are servers in $C(\boldsymbol{c})$. $P_M(\lambda_p)$ can be interpreted as **compliance factor** of the pairing strategy with the mode selection function, because a badly performed device pairing will have a low probability of being offloaded, even if there are servers in the potential service area. $\overline{C} > 0$ is an appropriately chosen parameter that is induced by the mode selection function and that is called **effective size of the service area**.

Proof. By combining equations (3.2) and (3.5), it holds that

$$\begin{aligned}
\lambda_{\text{D2D}} &= \lambda_c \cdot P\{u_c \in \Pi\} = \lambda_c E_{\boldsymbol{c}}\left\{P\{u_{\boldsymbol{c}} \in \Pi_{C(\boldsymbol{c})}\}\right\} \\
&\overset{(1)}{=} \lambda_c E_{\boldsymbol{c}}\{P\{u_{\boldsymbol{c}} \in \Pi_{C(\boldsymbol{c})} \mid \neg E_{\Phi_p}(C(\boldsymbol{c}))\} \cdot P\{\neg E_{\Phi_p}(C(\boldsymbol{c}))\}\} \\
&= \lambda_c P_M(\lambda_p) \cdot E_{\boldsymbol{c}}\left\{P\{\neg E_{\Phi_p}(C(\boldsymbol{c}))\}\right\}
\end{aligned}$$

here we again use the law of total probabilities for step (1), together with the fact that $P\{u_{\boldsymbol{c}} \in \Pi_{C(\boldsymbol{c})} \mid E_{\Phi_p}(C(\boldsymbol{c}))\} = 0$.

The term $E_{\boldsymbol{c}}\left\{P\{\neg E_{\Phi_p}(C(\boldsymbol{c}))\}\right\}$ is the expected probability that there exists a provider with a nonzero offloading probability. As $\boldsymbol{c}$ is uniformly distributed,

$$\begin{aligned}
E_{\boldsymbol{c}}\left\{P\{\neg E_{\Phi_p}(C(\boldsymbol{c}))\}\right\} &= 1 - E_{\boldsymbol{c}}\left\{P\{E_{\Phi_p}(C(\boldsymbol{c}))\}\right\} \\
&= 1 - \frac{1}{\|\Omega\|}\int_{\Omega} P\{E_{\Phi_p}(C(\boldsymbol{c}))\} d\boldsymbol{c} \\
&\overset{(1)}{=} 1 - \frac{1}{\|\Omega\|}\int_{\Omega} e^{-\lambda_p \|C(\boldsymbol{c})\|} d\boldsymbol{c}.
\end{aligned} \tag{3.7}$$

$\|\cdot\|$ here denotes the size of an area and (1) is due to the Poisson property of Φ_p. As (3.7) is a continuous function of both, λ_p and $\|C(\boldsymbol{c})\|$, we can define a variable $\overline{C}$, such that

$$e^{-\lambda_p \overline{C}} = \frac{1}{\|\Omega\|}\int_{\Omega} e^{-\lambda_p \|C(\boldsymbol{c})\|} d\boldsymbol{c}. \tag{3.8}$$

However, as λ_p cannot be split from from $\|C(\boldsymbol{c})\|$ in the exponent of the right term, it is not clear whether one constant parameter $\overline{C}$ will fit for all λ_p. So consider two different p.p.p. Φ_p and Φ_p' with densities λ_p and λ_p', $\lambda_p < \lambda_p'$. As both, Φ_p and Φ_p', are p.p.p., Φ_p' can be imagined to be generated from Φ_p by adding the points of a third p.p.p. $\Delta\Phi_p$ that is independent from Φ_p and whose density $\Delta\lambda_p$ is such that $\lambda_p' = \lambda_p + \Delta\lambda_p$ [50]. Assume that each of the p.p.p.

can have independent $\overline{C}$, which is written as $\overline{C}_{\Phi_p}$, $\overline{C}_{\Phi'_p}$ and $\overline{C}_{\Delta\Phi_p}$, respectively. Then the result is:

$$\begin{aligned} e^{-\lambda'_p\overline{C}_{\Phi'_p}} &= \frac{1}{\|\Omega\|}\int_{\Omega} e^{-\lambda'_p\|C(\boldsymbol{c})\|}d\boldsymbol{c} \\ &= \frac{1}{\|\Omega\|}\int_{\Omega} e^{-(\lambda_p+\Delta\lambda_p)\|C(\boldsymbol{c})\|}d\boldsymbol{c} \\ &= E_{\boldsymbol{c}}\left\{P\left\{E_{\Phi_p}\right\}P\left\{E_{\Delta\Phi_p}\right\}\right\} \\ &= E_{\boldsymbol{c}}\left\{P\left\{E_{\Phi_p}\right\}\right\}E_{\boldsymbol{c}}\left\{P\left\{E_{\Delta\Phi_p}\right\}\right\} \\ &= e^{-\lambda_p\overline{C}_{\Phi_p}}e^{-\Delta\lambda_p\overline{C}_{\Delta\Phi_p}} \\ \Leftrightarrow \lambda'_p\overline{C}_{\Phi'_p} &= \lambda_p\overline{C}_{\Phi_p}+\Delta\lambda_p\overline{C}_{\Delta\Phi_p}. \end{aligned}$$

This is true for arbitrary λ'_p, λ_p, $\Delta\lambda'_p$, which is the case only if $\overline{C}_{\Phi'_p} = \overline{C}_{\Phi_p} = \overline{C}_{\Delta\Phi_p} = \overline{C}$, because $\lambda'_p = \lambda_p + \Delta\lambda_p$. □

3.3 Implications

In this section, the implications of Theorem 3.1 for understanding the impact of service popularity, service availability, mode selection and pairing are discussed.

3.3.1 Implications on Service Parameters

Consider the dependency of λ_{D2D} on λ_c and λ_p in equation (3.6). The dependency on λ_c is linear, which is consistent with the simulation results of Section 3.1.1. The dependency on λ_p, on the other hand, differs because the exact form of $P_M(\lambda_p)$, which is the compliance factor of pairing and mode selection, is unknown. Comparing (3.2) with (3.6), the probability that a client will be served via D2D is:

$$P_{\text{D2D}} = P\{u_c \in \Pi\} = P_M(\lambda_p)\left(1 - e^{-\lambda_p\overline{C}}\right). \tag{3.9}$$

That is, the probability of a flow becoming D2D is the probability that there is a provider from which a flow could be offloaded (i.e., that is in $C(\boldsymbol{c})$), times the probability that the pairing would choose such a provider to serve the client. For correct evaluation of P_{D2D}, knowledge on $P_M(\lambda_p)$ is necessary. However, as $P_M(\lambda_p) \in [0,1]$, we can definitely upper bound λ_{D2D} with:

$$\lambda_{\text{D2D}} \leq \lambda_c\left(1 - e^{-\lambda_p\overline{C}}\right). \tag{3.10}$$

The structure of this bound can in fact be observed in most of the results presented in Figure 3.3. In general, λ_{D2D} seems to converge exponentially with rate $\overline{C}$ when the service availability λ_p is increased. This important property states that the number of D2D flows always saturates with the number of provider UEs but not with that of client UEs.

3.3.2 Implications on Mode Selection

Consider the right factor in (3.6), $1 - e^{-\lambda_p \overline{C}}$. From a stochastic geometry point of view, it is the probability that Φ_p has points on an area of size $\overline{C}$. At the same time, indicated by (3.7), it is the expected probability that Φ_p has points on $C(\boldsymbol{c})$, which is why $\overline{C}$ is called the *effective size* of $C(\boldsymbol{c})$. It must be stressed that in general, $\overline{C} \geq E_{\boldsymbol{c}}\{\|C(\boldsymbol{c})\|\}$, which can be seen by applying Jensen's inequality to (3.8). An alternative interpretation, coming from a *coverage area* point of view, is that $1 - e^{-\lambda_p \overline{C}}$ describes the expected probability that a client is in the D2D coverage area of at least one provider. The value of $\overline{C}$ is determined by the area on which a mode selection strategy will actually allow offloading flows. A mode selection that offloads flows on a larger area will have a large $\overline{C}$, one that offloads only on a small area will have a low $\overline{C}$.

3.3.3 Implications on Pairing Strategy

Consider $P_M(\lambda_p) = E_{\boldsymbol{c}}\left\{P\{u_{\boldsymbol{c}} \in \Pi_{C(\boldsymbol{c})} \mid \neg E_{\Phi_p}(C(\boldsymbol{c}))\}\right\}$. By the definition of $C(\boldsymbol{c})$, if a flow is offloaded to D2D, its provider must be in $C(\boldsymbol{c})$. So explicitly, $P_M(\lambda_p)$ is the expected probability that a flow is offloaded to D2D, given that there are providers with nonzero offloading probability. Moreover, as discussed in Section 3.2, for a mode selection that follows deterministic rules, a flow will either definitely be offloaded or not offloaded, no matter how often the decision function will be run. In this case, as $P\{u_{\boldsymbol{c}} \in \Pi \mid \boldsymbol{p}, \boldsymbol{c}\} \in \{0, 1\}\ \forall \boldsymbol{p}$, $C(\boldsymbol{c})$ will contain all those points where a provider must be such that the flow will definitely be offloaded. In this case $P_M(\lambda_p)$ is the probability that the provider paired with $u_{\boldsymbol{c}}$ is in $C(\boldsymbol{c})$, given that there are providers in $C(\boldsymbol{c})$. For probabilistic mode selections, $P_M(\lambda_p)$ is the probability that the flow of two paired UEs will be offloaded to D2D, provided that there are pairs with nonzero offloading probability.

Because the UE pairs are chosen by the pairing strategy, $P_M(\lambda_p)$ is an indicator for how often the pairing strategy chooses UE pairs that will be offloaded, i.e., how well enables the sidelink option. P_M changes with λ_p even for the simple pairing strategies considered in Section 3.1.1. Consider, e.g., the *Nearest Pairing* strategy. The probability that the nearest devices will be offloaded to the D2D mode intuitively increases with λ_p, because the expected distance to the nearest provider decreases.

3.3.4 Compliance of Pairing and Mode Selection

The definition of P_M gives a tool to evaluate the compliance of the pairing and mode selection functions, a notion which is deepened in this section. Note that the spatial density of D2D flows produced by a pairing strategy with constant P_M would always be by a factor P_M below the upper bound (3.10). So $P_M(\lambda_p)$ can also be interpreted as a *degree of compliance* for the pairing strategy. Thus, the following definition can be made

Definition 3.1. Let $\mathcal{H}$ be the set of all possible pairing strategies, $\mathcal{M}$ the set of all mode selection functions and let $P^*_{\lambda_p} \in \mathcal{H}$ be a strategy such that, for a distinct λ_p, $P_{M^*_{\lambda_p}}(\lambda_p) \geq P_{M'}(\lambda_p)$ $\forall P' \in \mathcal{H}$. Define a pairing strategy P^* to be *fully compliant w.r.t.* $M \in \mathcal{M}$, if $P_{M^*}(\lambda_p) = P_{M^*_{\lambda_p}}(\lambda_p)\, \forall \lambda_p$.

Note that in general, compliance of a pairing strategy depends on the used mode selection because $P\{u_{\boldsymbol{c}} \in \Pi \mid \boldsymbol{c}, \boldsymbol{p}\}$ does. In the case of a deterministic mode selection function, a fully compliant pairing strategy will always choose a provider out of $C(\boldsymbol{c})$, if there is one. In this case, $P_{M^*}(\lambda_p) = 1$ can be achieved, as any flow from a provider in $C(\boldsymbol{c})$ will be offloaded with probability one. If the mode selection function has a probabilistic part, however, it might happen that $P_{M^*}(\lambda_p) < 1$ and yet, it is considered fully compliant, as there can be no better compliance.

Using the introduced notion of compliance, it makes sense to define an *a-posteriori* pairing strategy P_a that uses knowledge about $P\{u_{\boldsymbol{c}} \in \Pi \mid \boldsymbol{c}, \boldsymbol{p}\}$, i.e., the outcome of the mode selection, while pairing devices:

Definition 3.2. Define as *a-posteriori* pairing strategy a strategy that satisfies:

$$P_a(u_{\boldsymbol{c}}, \Phi_p) \in \left\{u_{\boldsymbol{p}'} : P\{u_{\boldsymbol{c}} \in \Pi \mid \boldsymbol{p}', \boldsymbol{c}\} \geq P\{u_{\boldsymbol{c}} \in \Pi \mid \boldsymbol{p}, \boldsymbol{c}\}\ \forall u_{\boldsymbol{p}} \in \Phi_p\right\}$$

Proposition 3.1. A pairing strategy is fully compliant if, and only if, it is an a-posteriori pairing strategy.

Proof. Consider an a-posteriori pairing P_a. From Definition 3.2 it is clear that P_a maximizes $P\{u_{\boldsymbol{c}} \in \Pi \mid \Phi_p, \boldsymbol{c}\}$ in every single network realization. From the definition of $C(\boldsymbol{c})$ it is clear that if there is a $u_{\boldsymbol{p}}$ in $C(\boldsymbol{c})$, M_a will choose a $u_{\boldsymbol{p}}$ inside. Hence, P_a maximizes $P_M(\lambda_p) = E_{\boldsymbol{c}}\left\{P\{u_{\boldsymbol{c}} \in \Pi_{C(\boldsymbol{c})} \mid \neg E_{\Phi_p}(C(\boldsymbol{c}))\}\right\}$ and is fully compliant. On the other hand, assume a strategy P' that is not an a-posteriori strategy and define $u_{\boldsymbol{p}'}$ to be the provider such that $(u_{\boldsymbol{c}}, u_{\boldsymbol{p}'}) = P'(u_{\boldsymbol{c}}, \Phi_p)$. Then, because it does not fulfill the definition, there are network realizations such that

$$\exists u_{\boldsymbol{p}} \neq u_{\boldsymbol{p}'}: \quad P\{u_{\boldsymbol{c}} \in \Pi \mid \boldsymbol{p}, \boldsymbol{c}\} > P\{u_{\boldsymbol{c}} \in \Pi \mid \boldsymbol{p}', \boldsymbol{c}\}. \tag{3.11}$$

By designing a pairing strategy P'' that chooses $u_{\boldsymbol{p}}$ whenever (3.11) holds, and $P'(u_{\boldsymbol{c}}, \Phi_p)$ otherwise, $P_{M''}(\lambda_p) > P_{M'}(\lambda_p)$ holds. Hence, M' is not fully compliant. □

The if and only if nature of Proposition 3.1 shows that whenever full compliance of pairing and mode selection is achieved, the solution to the mode selection, or more precisely $P\{u_{\boldsymbol{c}} \in \Pi \mid \boldsymbol{c}, \boldsymbol{p}\}$, must implicitly be considered already in the pairing step. While this can be achieved for special cases of mode selection, such as deterministic, distance dependent mode selection, there are many cases where it must be considered unrealistic. Typically, the mode selection will depend on channel qualities, probably even interference properties. Then, an implementation of P_a would in the worst case require evaluating $P\{u_{\boldsymbol{c}} \in \Pi \mid \boldsymbol{c}, \boldsymbol{p}\}$ for each potential combination of client and provider, which would cause a high overhead in terms of computational complexity, signaling effort and delay.

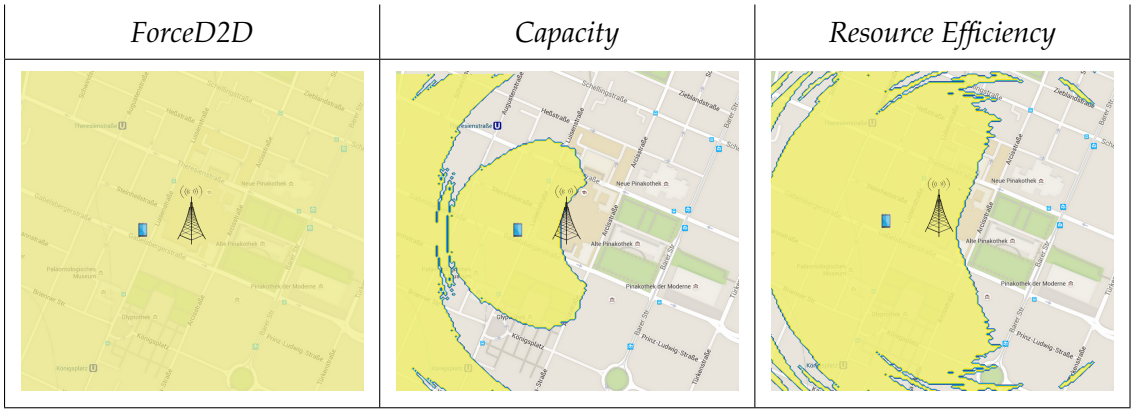

Figure 3.4: Example service areas for the mode selection criteria *ForceD2D*, *Capacity* and *ResourceEfficiency*. The service areas are highlighted with a yellow color.

On the other hand, there are more practical classifications of pairing strategies:

Definition 3.3. Consider an arbitrary pairing strategy $P \in \mathcal{H}$ and mode selection function $M \in \mathcal{M}$. P is called

- ...α-*compliant* with the used mode selection H, for some $\alpha > 0$, if $\lim_{\lambda_p \to \infty} P_M(\lambda_p) = \alpha$.
- ...*asymptotically compliant*, if in the limit, $\lim_{\lambda_p \to \infty} P_M(\lambda_p) = \lim_{\lambda_p \to \infty} P_{M^*}(\lambda_p)$.
- ...*non-compliant*, or *ill-designed*, in any other case.

The compliance and asymptotic behavior describes the quality of the pairing strategy in high density situations: α-compliance induces that, for sufficiently large λ_p, the density of D2D-Flows will constantly be by a factor α below (3.10). Asymptotic compliance means that, for large enough λ_p, the pairing will become compliant and non-compliance means that the pairing strategy is unrelated or badly related to the mode selection criterion. It is easy to show that any pairing strategy falls in either of the defined categories, so the classification performs a full partitioning of $\mathcal{H}$. Examples for asymptotic compliant, α-compliant and ill-designed pairing strategies will be given in Section 3.4.

3.4 Simulation Verification

The insights from Sections 3.2 and 3.3 will now be applied to explain the results from Section 3.1.1. First, the used mode selection criteria and pairing strategies are investigated, to deepen the understanding of their interaction. Then the produced results will be explained.

3.4.1 Compliance of Simulated Strategies

First, for the mode selection criteria *ForceD2D*, *Capacity* and *Resource Efficiency*, the types of service area that they create are investigated. For this, simulations are run by keeping a single client at a fixed position, sweeping a provider through the full considered area Ω and

evaluating, whether the resulting flow is offloaded or not. Figure 3.4 shows the resulting service areas for all three criteria. The *ForceD2D* criterion creates a rather circular service area around the client, whose radius is so large that it falls out of bounds in this simulation. So, any flow in Ω will definitely be offloaded by the *ForceD2D* function. The *Resource Efficiency* service area has been shown already in [4] to be biased towards the far part of the base station, which is found verified, and so is the *Capacity* service area, although it is a little smaller. Still, the direction of the bias depends on the exact position of the client with respect to the BS. In general, all three criteria fulfill two properties, which are given here without proof for the sake of brevity:

Proposition 3.2. Consider a time interval in which all channels remain constant. In this, all three mode selection criteria, *ForceD2D*, *Capacity* and *Resource Efficiency*, are deterministic with respect to $\boldsymbol{c}$, $\boldsymbol{p}$, i.e., $P\{u_{\boldsymbol{c}} \in \Pi \mid \boldsymbol{p}, \boldsymbol{c}\} \in \{0, 1\}$.

Further, assuming a UE distance $d = \|\boldsymbol{p} - \boldsymbol{c}\|$ and an arbitrary $b > 0$, all three criteria fulfill:

$$P\{\boldsymbol{p} \in C(\boldsymbol{c}) \mid d \leq b\} \geq P\{\boldsymbol{p} \in C(\boldsymbol{c}) \mid d > b\}. \tag{3.12}$$

The determinism property is given for a small time-scale, as all channel qualities remain fixed for given positions. So although channels in general will change, if pairing and mode selection are done on a sufficiently small time-scale, the latter can be treated as deterministic mapping. The second, distance based property originates from the statistical properties of wireless channels, which tend to become stronger for smaller distances. It can be seen from equation (3.12) that $C(\boldsymbol{c})$ will most likely contain an area around $\boldsymbol{c}$ for all three criteria. This is intuitive from a technical but not necessary from a mathematical viewpoint. Proposition 3.2 allows to define a class of *location-aware* mode selection functions $\mathcal{M}_L$:

Definition 3.4. Define $\mathcal{M}_L$ as the set of mode selection functions such that $P\{u_{\boldsymbol{c}} \in \Pi \mid \boldsymbol{p}, \boldsymbol{c}\} \in \{0, 1\}$ and $\forall b > 0$,

$$P\{\|\boldsymbol{p} - \boldsymbol{c}\| \mid \leq b\} \geq P\{\|\boldsymbol{p} - \boldsymbol{c}\| > b\}. \tag{3.13}$$

Assuming a mode selection $M \in \mathcal{M}_L$, the compliance of the strategies *Random Pairing*, *Nearest Pairing* and *Farthest Pairing* will now be investigated.

Proposition 3.3. The *Random Pairing*, $M_R(u_{\boldsymbol{c}}, \Phi_p)$, is α-compliant with any $M \in \mathcal{M}_L$, where the compliance factor is $\alpha = E_{\boldsymbol{c}}\{\|C(\boldsymbol{c})\|\} / \|\Omega\|$

Proof. As M_R chooses a random provider $u_{\boldsymbol{p}}$, $\boldsymbol{p}$ will be uniformly distributed in Ω. So for any fixed $\boldsymbol{c}$,

$$P\{\boldsymbol{p} \in C(\boldsymbol{c})\} = \frac{\|C(\boldsymbol{c})\|}{\|\Omega\|}.$$

As all $M \in \mathcal{M}_L$ are deterministic, the probability $P\{u_{\boldsymbol{c}} \in \Pi_{C(\boldsymbol{c})}\} = P\{\boldsymbol{p} \in C(\boldsymbol{c})\}$. So:

$$\begin{aligned} P_{M_R}(\lambda_p) &= E_{\boldsymbol{c}}\left\{P\{u_{\boldsymbol{c}} \in \Pi_{C(\boldsymbol{c})} \mid \neg E_{\Phi_p}(C(\boldsymbol{c}))\}\right\} \\ &= E_{\boldsymbol{c}}\left\{P\{u_{\boldsymbol{c}} \in \Pi_{C(\boldsymbol{c})}\}\right\} \\ &= E_{\boldsymbol{c}}\left\{P\{\boldsymbol{p} \in C(\boldsymbol{c})\}\right\} \\ &= \frac{E_{\boldsymbol{c}}\left\{\|C(\boldsymbol{c})\|\right\}}{\|\Omega\|} = \alpha \end{aligned}$$

□

It must be commented that, as only the determinism property of Proposition 3.2 was used in the preceding proof, M_R is in fact α-compliant with *any deterministic* mode selection. This is an important property because it states that although random pairing is not a sophisticated strategy, it is also not ill-designed for a broad class of mode selection criteria.

Proposition 3.4. The *Nearest Pairing*, $M_N(u_{\boldsymbol{c}}, \Phi_p)$, is α-compliant for any $M \in \mathcal{M}_L$.

Proof. Let $B(b, \boldsymbol{c})$ be a ball of radius b, with $\boldsymbol{c}$ in the center. The probability that $u_{\boldsymbol{p}}$ with $(u_{\boldsymbol{c}}, u_{\boldsymbol{p}}) = M_N(u_{\boldsymbol{c}}, \Phi_p)$ is in $B(b, \boldsymbol{c})$ is the probability that there is at least one provider in $B(b, \boldsymbol{c})$,

$$P\{\boldsymbol{p} \in B(b, \boldsymbol{c})\} = P\{d \leq b\} = 1 - e^{-\lambda_p \|B(b, \boldsymbol{c})\|},$$

and hence is strictly increasing with λ_p. As M is deterministic w.r.t. $\boldsymbol{c}$ and $\boldsymbol{p}$, $P\{u_{\boldsymbol{c}} \in \Pi_{C(\boldsymbol{c})}\} = P\{\boldsymbol{p} \in C(\boldsymbol{c})\}$. Combining the increasing property with (3.12) yields

$$\begin{aligned} P_{M_N}(\lambda_p) &= E_{\boldsymbol{c}}\left\{P\{\boldsymbol{p} \in C(\boldsymbol{c})\}\right\} \\ &= E_{\boldsymbol{c}}\{P\{\boldsymbol{p} \in C(\boldsymbol{c}) \mid d \leq b\} P\{d \leq b\} \\ &\quad + P\{\boldsymbol{p} \in C(\boldsymbol{c}) \mid d > b\} P\{d > b\}\}, \end{aligned}$$

which is strictly increasing with λ_p. As $P_{M_N}(\lambda_p)$ is upper bounded by $P_{M^*}(\lambda_p)$, $\lim_{\lambda_p \to \infty}(P_{M_N}(\lambda_p)) = \alpha$ must converge to a value. So $P_{M_N}(\lambda_p)$ is α-compliant. □

Proposition 3.5. The *Farthest Pairing*, $M_F(u_{\boldsymbol{c}}, \Phi_p)$, is ill-designed for any $M \in \mathcal{M}_L$.

Proof. For any ball $B(b, \boldsymbol{c})$ of radius b around $\boldsymbol{c}$, the probability that the farthest provider is inside $B(b, \boldsymbol{c})$ is the probability that there is no provider in $\Omega \setminus B(b, \boldsymbol{c})$, which is:

$$\begin{aligned} P\{u_{\boldsymbol{p}} \in B(b, \boldsymbol{c})\} &= P\{E_{\Phi_p}(\Omega \setminus B(b, \boldsymbol{c}))\} \\ &= e^{-\lambda_p \|\Omega \setminus B(b, \boldsymbol{c})\|}. \end{aligned}$$

As $P\{d \leq b\} = P\{u_{\boldsymbol{p}} \in B(b, \boldsymbol{c})\}$ is strictly decreasing with λ_p for any fixed b, so is $P_{M_F}(\lambda_p)$ according to the argumentation from Proposition 3.4. As $P\{\boldsymbol{p} \in C(\boldsymbol{c}) \mid d \leq b\}$ is upper bounded by one, $P_{M_F}(\lambda_p)$ is lower bounded by 0 and converges to a low value for increasing λ_p. $P_{M_N}(\lambda_p)$ is ill-designed. □

3.4.2 Interpretation of Simulation Results

After classifying the different pairing strategies, turn back towards the results from Figure 3.3:

It has been noted (1) that the spatial density of D2D-Flows increases linearly with λ_c in any case. This is verified by the theoretic development and is due to the Poisson nature of Φ_u. The influence of λ_p, on the other hand, depends on $P_M(\lambda_p)$.

The saturation effect (2) can be explained by considering the effective size of the service area, $\overline{C}$. The effect can be interpreted as a saturation of the probability that a client is in the D2D service area of a provider.

(3) The *ForceD2D* mode selection behaves independent of the choice of pairing strategies, which is because its service area $C(\boldsymbol{c})$ includes Ω for all $\boldsymbol{c}$, so any flow of two paired UEs will always be handed off. In this sense, *ForceD2D* forms an upper bound on the achievable number of D2D flows.

(4) The *Random Pairing* strategy converges to a rather low number of D2D flows for both, *Capacity* and *Resource Efficiency* mode selection. However, its convergence speed is analog to the one of the *ForceD2D* mode selection. This is because the *Random Pairing* strategy has a constant P_{M_R}, as shown in Proposition 3.3. The *Farthest Pairing* produces the least D2D flows because it is ill-designed. However, it can be seen that for low λ_p, the number of flows increases at first. This motivates that indeed, the $P_{M_F}(\lambda_p)$ has a higher value at first but decreases with increasing λ_p. Finally, for the *Nearest Pairing* strategy, the mean number of flows saturates significantly slower for the *Capacity* and *Resource Efficiency* mode selections than for the *ForceD2D* function. This can be explained by the fact that the effective size of the service area, $\overline{C}$, is smaller than for *ForceD2D* and that $P_{M_N}(\lambda_p)$ converges towards 1 but is significantly smaller for low λ_p.

3.5 Extensions

The presented investigations and results base on the assumption of a one-serves-all service type, where each client can be served by at most one provider but the providers can serve an arbitrary number of clients. This assumption reflects in the pairing function $P : (u_c, \Phi_p) \mapsto (u_c, u_p)$, for $u_c \in \Phi_c,\ \ u_p \in \Phi_p \setminus u_c$, which maps a single client to one out of a set of possible providers. In a similar fashion, the other service types can be assessed, which is briefly summarized in this section.

3.5.1 All-Serve-One Type Service

A mapping $P : (\Phi_c, u_p) \mapsto (u_c, u_p)$, for $u_p \in \Phi_p,\ \ u_c \in \Phi_c \setminus u_p$ models an all-serve-one type service, as it maps each provider to one out of a set of possible clients. For the all-serve-one service, an analysis can be done analogously to the one presented in the previous sections. This produces the same results, only that the indices of provider and client are exchanged. That is, Π then becomes the set of all providers that are offloaded to direct mode. Further, a D2D service area $C(\boldsymbol{p})$ for each provider can be formed, which contains all positions where a

client must be to have non-zero probability of being handed off to direct mode when paired. The density of D2D flows takes the form

$$\lambda_{\text{D2D}} = \lambda_p P_M(\lambda_c)\left(1 - e^{-\lambda_c \overline{C}}\right), \tag{3.14}$$

where $P_M(\lambda_c) = E_{\boldsymbol{p}}\left\{P\{u_{\boldsymbol{p}} \in \Pi_{C(\boldsymbol{p})} \mid \neg E_{\Phi_c}(C(\boldsymbol{p}))\}\right\}$ is the compliance factor of pairing and mode selection.

Due to the fact that a client position $\boldsymbol{c} \in C(\boldsymbol{p})$ if, and only if, $\boldsymbol{p} \in C(\boldsymbol{c})$, it holds that

$$P\{\neg E_{\Phi_p}(C(\boldsymbol{c}))\} = P\{\neg E_{\Phi_c}(C(\boldsymbol{p}))\}. \tag{3.15}$$

The expectation of the left probability with respect to all client positions has been shown to be of the form $\left(1 - e^{-\lambda_c \overline{C}}\right)$ for homogeneous p.p.p.'s in Theorem 3.1, where $\overline{C}$ is a unique parameter that is correct for all values of λ_c. Because the device positions are uniformly distributed for both, Φ_c and Φ_p, the results take the same form for all-serve-one types and even result in the same parameter $\overline{C}$.

3.5.2 Full-Mesh Type Service

In the extreme case of a full-mesh type service, where an arbitrary number of providers can serve each client and each provider can serve an arbitrary number of clients, the pairing step can be assumed to simply map each single client to all available providers. As Π is the set of all clients (or servers, respectively) that are handed off to direct mode, the number of direct links does not correspond to the density of Π anymore. However, the results of the one-serves-all type service can be applied by sequentially assuming each provider of a certain realization to be the only available. Formally, this corresponds to a series of sets Π_{u_p}, $u_p \in \Phi_p$ that contain those clients that would be handed off when only the considered provider u_p is available. As the pairing with respect to a single provider can only result in a single output, it has a compliance factor of one, which by equation (3.5) yields

$$\lambda_{\text{D2D}}^{(u_p)} = \lambda_c E_{\boldsymbol{c}}\left\{P\{\neg E_{\Phi_p}(C(\boldsymbol{c}))\}\right\} = \lambda_c E_{\boldsymbol{c}}\left\{P\{\boldsymbol{p} \in C(\boldsymbol{c}))\}\right\}. \tag{3.16}$$

By repeating this procedure for all $u_p \in \Phi_p$ and adding the densities,

$$\begin{aligned}
\lambda_{\text{D2D}} &= \sum_{u_p \in \Phi_p} \lambda_{\text{D2D}}^{(u_p)} = \sum_{u_p \in \Phi_p} \lambda_c E_{\boldsymbol{c}}\left\{P\{\boldsymbol{p} \in C(\boldsymbol{c}))\}\right\} \\
&= \lambda_c E_{\boldsymbol{c}}\left\{\sum_{u_p \in \Phi_p} P\{\boldsymbol{p} \in C(\boldsymbol{c}))\}\right\} \\
&\overset{(1)}{=} \lambda_c \lambda_p \overline{C}.
\end{aligned} \tag{3.17}$$

Equality (1) comes from the fact that the right part of the previous term is the expected number of providers in $C(\boldsymbol{c})$, over all client positions $\boldsymbol{c}$.

Service Type	λ_{D2D} w.r.t. λ_c, λ_p	λ_{D2D} w.r.t. λ, p_p, p_c	Upper Bounds
One-to-One	$\leq \min\{\lambda_p, \lambda_c\}$	$\leq \min\{p_p, p_c\}\lambda$	λ
One-Serves-All	$\lambda_c P_M(\lambda_p)\left(1 - e^{-\lambda_p \overline{C}}\right)$	$p_c \lambda P_M(\lambda, p_p)\left(1 - e^{-p_p \lambda \overline{C}}\right)$	$\lambda\left(1 - e^{-\lambda \overline{C}}\right)$
All-Serve-One	$\lambda_p P_M(\lambda_c)\left(1 - e^{-\lambda_c \overline{C}}\right)$	$p_p \lambda P_M(\lambda, p_c)\left(1 - e^{-p_c \lambda \overline{C}}\right)$	$\lambda\left(1 - e^{-\lambda \overline{C}}\right)$
Full-Mesh	$\lambda_c \lambda_p \overline{C}$	$p_p p_c \lambda^2 \overline{C}$	$\lambda^2 \overline{C}$

Table 3.1: Scaling laws for different service types

3.5.3 One-to-One Mapping

For a service with one-to-one mapping, little can be said in general because the pairing of each device depends on the pairings of all other devices. However, the number of D2D flows can be upper bounded by considering that the set of all possible one-to-one mappings is a subset of both, the set of all one-to-all mappings and all-to-one mappings. As the spatial density of D2D-flows for one-serves-all type services is upper bounded by λ_c and that for all-serve-one type services by λ_p, the density under one-to-one mapping can be upper bounded by

$$\lambda_{\text{D2D}} \leq \min\{\lambda_p, \lambda_c\}. \tag{3.18}$$

3.6 Lessons Learned

As conclusion, a short summary of the results is given. Investigated was the set-up flow of D2D links, under the axiomatic assumption that the devices are paired according to an arbitrary mapping and that mode selection chooses the communication with a mechanism that is deterministic or probabilistic with respect to the device positions but independent for each client-provider pair. As result, some core insights were gained:

(1) For each client (or provider) device, a D2D service area can be defined, which is the set of all positions where a provider (client) needs to reside to have a non-zero offloading probability. D2D flows can be set-up if, and only if, two devices are paired that are within their mutual service areas. The exact form of the service area depends on the mode selection strategy. Its' effective size is an indicator for how probable D2D communication is.

(2) The compliance of pairing and mode selection step has a key impact on expected number of D2D flows. That is, to successfully leverage the D2D option, the pairing step must already be aware of it. Compliance can be roughly grouped into the three categories of asymptotic compliance, α-compliance and non-compliance. A sufficient strategy for a large class of mode selection functions is to match devices with others chosen randomly from an area within maximum distance or to match the closest devices, which both provide α-compliance.

(3) For the different service types one-to-one mapping, one-serves-all, all-serve-one and full-mesh, different scaling laws can be derived, which are given in Table 3.1. In general, the

more degrees of freedom a service allows in terms of concurrent connections, the more D2D-flows can be expected. That is, full-mesh type services have the largest potential to lead to D2D connections, followed by one-serves-all and all-serve-one types. Services with one-to-one mappings can be expected to lead to D2D flows only for high device densities.

It must be stressed that the results were derived with loose assumptions on the actual system. In particular, they do not rely on any MAC layer system aspects such as device capabilities or overlay/underlay operation. Further they include single-cast and multi-cast application, because the latter can be modeled as a service where the multi-cast source is the provider and the sinks are the clients. The results are thus general and can be transferred to a variety of cases.

Chapter 4

Gains of D2D Communication

In this chapter, the gain of D2D communication compared to cellular uplink downlink communication is evaluated and the ability of network utility maximization (NUM) based network management to leverage it is discussed. A metric is proposed that captures the benefit of realizing communication over direct links, compared to cellular up- and downlink. The proposed metric is a transmission-resource efficiency, which extensively uses the notion of resource measures introduced in Section 2.1.4, as well the commodity flow perspective, queue stability, scheduled actions and policies, which were introduced in Section 2.1.3.

The presented notion of D2D-Gain and some properties of resource efficiency, such as the notion of schedule scaling, have been presented in publications [4], [5]. However, the presentation here is the first to be a mathematically clean and consistent derivation of all induced properties. In particular, the extension to arbitrary utility-resource efficiency, as well as the properties of resource efficiency presented in Section 4.4, are entirely novel and unpublished.

Related Work

In general, any communication between two UEs can be realized by using either the cellular mode (CM) comprising of uplink downlink communication or the direct mode (DM) with a single link. As the CM is always possible due to the assumption that all links are in coverage, it constitutes a fall-back solution and is clearly chosen when no direct connection can be established. Intuitively, when a link with a low connectivity on the sidelink is handed off to direct mode, its communication quality will degrade. On the other hand, when it is relatively strong, the communication can benefit from direct mode. The exact trade-off, when to choose which mode, is tightly coupled with the used quality metric for the overall network state.

The D2D-gains have been formulated by G. Fodor et al. [30], who postulate three types of gains originating from the use of direct links: The **Proximity-Gain** captures that two spatially close UEs may achieve higher data rates compared to cellular links. This is especially true for cell-edge UEs, which suffer from a weak uplink connectivity. The rate gain originates from strong sidelink channels and thus diminishes with increasing spatial distance of transmitter and receiver. The **Hop-Gain** refers to using less wireless transmission resources for transporting the same amount of data on the sidelink, compared to using a cellular link.

The main reason for this gain is that cellular communication uses two hops, the uplink and downlink. Thus, even when the achieved rate on the sidelink is not larger than that on the cellular link, resources are freed on either uplink or downlink frequency band, rendering D2D beneficial. The **Reuse-Gain** implies that radio resources may be used by several connections within the same cell. Resource reuse benefits from strong sidelink channels, which allows direct links to be more robust to interference than cellular links. Further, less transmission power can be used on sidelinks for an appropriate link quality, such that only little interference is created towards other, interfered links. The three gains have already been established in Chapter 1 and are illustrated in Figure 1.5.

Although the expectations for the benefits of D2D communication underlaying cellular networks are clearly defined, there is no common understanding on how to measure these benefits, which makes research of different authors hard to compare. The optimization metrics of work on resource allocation and mode selection, for example, include the sum-rate criterion [122], throughput [114], sum of transmission powers [123], maximum interference power [124], sum of interference power [121] and even spatial distance of nodes [125].

While a network can be optimized for any of these metrics, their use is mostly not clearly motivated but rather the result of an intuitive choice. Optimizing for different metrics can induce the outcome of different optimal solutions, rendering results hard to compare. A clear understanding on the main drivers for good D2D connections according to [30] is missing in literature, as the gains are typically only used as a conceptual argument, e.g., to give a high-level interpretation on the origin of a better performance, which was achieved with a proposed mechanism.

An investigation targeting the aspects that influence and enable the D2D gains in a more systematic way is presented in this chapter. In particular, it is shown in Section 4.1 that the sum-rate and sum-throughput metric, which arguably are the most commonly used metrics in literature, do not reflect the D2D gains in general. It is then argued throughout Section 4.2 that a flow-based resource efficiency captures the D2D gain. The misalignment of sum-throughput and sum-rate criterion with respect the D2D-gains gives rise to the question whether optimizing for rate is, at all, a good target for the D2D set-up. To gain an insight on this question, the resource efficiency metric is investigated more closely in Section 4.4. The focus thereby is on the relation of resource efficiency metrics to NUM problems, which are typically formulated to develop network management algorithms. As result, it is shown under which conditions utility maximization can leverage the targeted gains.

The notion of D2D-gains also has an impact on mode selection. Obviously, when it is possible to measure the achievable "gain" by using a direct link, this information can be leveraged to make good mode selection choices. The insights presented in the following are thus used to develop a mode selection strategy in Chapter 5.

4.1 The D2D-Gains

To capture the main properties of the D2D-gains, they are interpreted as specific quality aspects that can either be better or worse on the sidelink, compared to a cellular link. A

Figure 4.1: Coupling of the D2D-Gains by scheduling decisions

proximity-gain is considered positive when a larger data rate is achieved via D2D than via cellular communication and negative otherwise. The hop-gain is considered positive when less resources are used by the sidelink than by up- and downlink together and the reuse-gain increases with the number of times a resource is simultaneously used within a cell.

As has been observed already, many works in literature refer to optimization of sum-rate or sum-throughput of a network. A slight mismatch exists here in the use of terms, as the term "rate" is used for both, MAC layer per-hop rate and transport layer end-to-end rate, which however is referred to as throughput in this work. In general, both sum-rate and sum-throughput capture how much information is transported and are commonly accepted as an indicator for the ability of a network to serve user demands. The D2D gains, however, are only loosely coupled with data rates. In fact, when considering the original gain definitions, only maximizing the proximity-gain actually refers to maximizing rates. Further, the different gains are subject to scheduling choices, as the D2D and cellular links can be assigned more or less resources, leading to larger or smaller data rates, or more resources can be reused. Finally, the gains are tightly coupled by scheduling decisions in the following way: A D2D-link might be scheduled more resources and hence have a higher throughput than its corresponding cellular link. This would create a positive proximity-gain but might result in a negative hop-gain at the same time. On the other hand, the sidelink could also be assigned less resources, producing a positive hop-gain but a smaller proximity-gain. Proximity- and hop-gain are thus coupled by scheduling decisions in a negative way, i.e, a larger hop-gain in general induces a lower proximity-gain. A similar effect can be observed for the reuse-gain: If a resource is reused, this might produce a larger spectral efficiency, i.e., more traffic transported per time-frequency resource. On the other hand the introduced interference will reduce data rates of other links, thus lowering or increasing their proximity-gain, depending on which of uplink, downlink and sidelink is interfered more.

From this perspective, all gains are in fact coupled and subject to scheduling decisions, which also include the decision of reusing resources. The coupling is depicted in Figure 4.1. The question is how to trade off the different gain aspects to achieve an overall good state. In this context, the sum-rate and sum-throughput criterion do not fully capture the D2D gains as they neglect both, the resource usage and spectral efficiency aspect. Intuitively, the expected gains of D2D [30] are no gains in terms of rate or throughput, but system inherent gains that can be used to increase rate and throughput. However, they could just as well be used to minimize resource usage or other network utilities.

A simple but core observation is that the D2D-gains refer to end-to-end transported bits and the resources required to transport them. That is, for cellular links the throughput must be considered rather than the MAC layer per-hop rates for up- and downlink. The sum-rate criterion thus must be considered inappropriate to capture any aspect of D2D-gain, as up-

link and downlink each contribute to its metric. The sum-rate thus is biased towards cellular throughput where one piece of information is accounted for in both, up- and downlink hop.

4.2 Formal Definition of Resource Efficiency

The expected gains of D2D communication can be captured in two efficiency metrics: As will be argued, the combined effect of proximity-gain and hop-gain lead to the metric of logical link throughput per resource use. The reuse-gain, on the other hand, is captured by the achievable resource reuse in the network. All three can be combined into a pure resource-efficiency metric, as is proposed in this section.

Throughout Section 4.2, the resource efficiency will be introduced in a clean fashion. Different notions of resource efficiency and their mutual relations will be discussed. These notions will then be used in the remaining parts of Chapter 4 to assess the D2D-gains.

4.2.1 Throughput-Resource Efficiency

Consider a network consisting of a link set $\mathcal{L}$ that uses a resource space $\mathcal{R}$ with associated measure ν as introduced in section 2.1.4. Let $\lambda_n^{(c)}$ be the expected admission rate of commodity c at its' source node $n \in \mathcal{L}$ and let $\boldsymbol{A}$ be a fixed action matrix that can serve to transport all injected data with strongly stable queues, i.e., that satisfies constraints (2.41)-(2.44) from Section 2.1.3. Assume for the time being that action $\boldsymbol{A}$ is chosen in all time slots. Then define the network-wide throughput-resource efficiency as:

$$\mathrm{RE}_{\mathcal{L}}(\boldsymbol{A}) = \frac{\sum_{n\in\mathcal{N}}\sum_{c\in\mathcal{K}} \lambda_n^{(c)}}{\nu^{\mathrm{sys}}(\mathcal{L},\boldsymbol{A})} = \frac{\sum_{n\in\mathcal{N}} \lambda_n}{\nu^{\mathrm{sys}}(\mathcal{L},\boldsymbol{A})}, \tag{4.1}$$

where $\lambda_n = \sum_{c\in\mathcal{K}} \lambda_n^{(c)}$ is the total throughput originating from link n. The sum in the numerator is the sum-throughput of the network, whereas the denominator is the system resource usage defined in section 2.1.4, which counts a resource once if it is used by at least one link. The resource efficiency thus relates the sum-throughput that is achieved using a fixed amount of resources with just this amount of resources.

Considering equation (4.1), in general the throughput can be assumed to be non-decreasing with system resource use.[1] Efficiency can thus be increased by increasing the throughput over-proportionally to the resource use or by over-proportionally freeing resources with respect to throughput reduction. Both directions can be achieved by introducing resource reuse, either by increasing the throughput while using resources several times or by rescheduling links to achieve the same throughput using less resources.

Let $\nu_n(\boldsymbol{A}) = \sum_{(m,n)\in\mathcal{L}} \nu(A_{mn})$ be the effective amount of resources used by node n and $\nu^{\mathrm{eff}}(\mathcal{L},\boldsymbol{A})$ the system wide effective resource usage, which counts each resource by the number of times it is used in the network. The network wide resource efficiency can then be

[1] While this assumption does not strictly hold, e.g., when interference effects occur, it will generally be induced by correct network management.

reformulated to a weighted per-node resource efficiency as follows:

$$\begin{aligned} \mathrm{RE}_{\mathcal{L}}(\boldsymbol{A}) &= \frac{\nu^{\mathrm{eff}}(\mathcal{L},\boldsymbol{A})}{\nu^{\mathrm{sys}}(\mathcal{L},\boldsymbol{A})}\frac{\sum\limits_{n\in\mathcal{N}}\lambda_n}{\nu^{\mathrm{eff}}(\mathcal{L},\boldsymbol{A})} = \kappa(\mathcal{L},\boldsymbol{A})\sum_{n\in\mathcal{N}}\frac{\nu_n(\boldsymbol{A})}{\nu^{\mathrm{eff}}(\mathcal{L},\boldsymbol{A})}\frac{\lambda_n}{\nu_n(\boldsymbol{A})} \\ &= \kappa(\mathcal{L},\boldsymbol{A})\sum_{n\in\mathcal{N}} w_n(\boldsymbol{A})\mathrm{RE}_n(\boldsymbol{A}). \end{aligned} \tag{4.2}$$

That is, the network wide resource efficiency can be decomposed into the components of reuse factor $\kappa(\mathcal{L},\boldsymbol{A}) = \nu^{\mathrm{eff}}(\mathcal{L},\boldsymbol{A})/\nu^{\mathrm{sys}}(\mathcal{L},\boldsymbol{A})$ and a weighted sum of per-node resource efficiencies, where the weights $w_n(\boldsymbol{A}) = \nu_n(\boldsymbol{A})/\nu^{\mathrm{eff}}(\mathcal{L},\boldsymbol{A})$ are according to their relative, effective resource usage.

By combining (4.1) with (4.2), an interesting relationship between the sum-throughput criterion and resource efficiency can be revealed:

$$\sum_{n\in\mathcal{N}}\lambda_n = \nu^{\mathrm{sys}}(\mathcal{L},\boldsymbol{A})\mathrm{RE}_{\mathcal{L}}(\boldsymbol{A}) = \nu^{\mathrm{eff}}(\mathcal{L},\boldsymbol{A})\sum_{n\in\mathcal{N}} w_n(\boldsymbol{A})\mathrm{RE}_n(\boldsymbol{A}). \tag{4.3}$$

Equation (4.3) reveals two ways to increase the sum-throughput of the network: Either $\nu^{\mathrm{sys}}(\mathcal{L},\boldsymbol{A})$ can be increased, which corresponds to increasing the overall used resources, or $\mathrm{RE}_{\mathcal{L}}(\boldsymbol{A})$ can be increased, which corresponds to using resources more efficiently. The former solution is straightforward and, in fact, often used in wireless networks, where the amount of usable frequency is constantly increased by standardization bodies. However, at some point the usable resources always remain limited, in which case the increase of efficiency becomes interesting. This increase can be achieved by creating as much "effective" resource as possible, i.e., by increasing the reuse factor, or by increasing the weighted efficiency of all nodes in the network. To increase the weighted efficiency, flows must be appropriately routed and scheduled. An increase of reuse factor typically decreases the per-link resource efficiencies due to interference, so a good trade-off between both aspects needs to be found.

4.2.2 Long-Term Resource Efficiency

The resource efficiency can be extended from that of a single action matrix, i.e., fixed schedule, to the long-term achieved efficiency of a dynamic scheduler. For this, let $\boldsymbol{S} = \{\boldsymbol{A}[0],\boldsymbol{A}[1],...,\boldsymbol{A}[\tau],...\}$ be an infinite sequence of action matrices generated by a dynamic scheduler, and let the flow variables $\lambda^{(c)}$ be stably supported by $\boldsymbol{S}$. Assume an observation interval of T time slots, such that $\tau \in \{1,...,T\}$. The long-term achieved resource efficiency of $\boldsymbol{S}$ then is:

$$\mathrm{RE}_{\mathcal{L}}(\boldsymbol{S}) = \lim_{T\to\infty}\frac{\sum\limits_{n\in\mathcal{N}}\lambda_n}{\frac{1}{T}\sum\limits_{\tau=1}^{T}\nu^{\mathrm{sys}}(\mathcal{L},\boldsymbol{A}[\tau])} = \frac{\sum\limits_{n\in\mathcal{N}}\lambda_n}{\overline{\nu}^{\mathrm{sys}}(\mathcal{L},\boldsymbol{S})}, \tag{4.4}$$

where $\overline{\nu}^{\mathrm{sys}}(\mathcal{L},\boldsymbol{S})$ is the time-averaged expected value of the system resource usage with action sequence $\boldsymbol{S}$. Note that (4.4) takes a form analog to (4.1). Because equations (4.2) and (4.3) are mere reformulations of (4.1), they can be analogously derived for (4.4) by defining

the time averages

$$\overline{\nu}^{\text{eff}}(\mathcal{L},\boldsymbol{S}) = \lim_{T\to\infty}\frac{1}{T}\sum_{\tau=1}^{T}\nu^{\text{eff}}(\mathcal{L},\boldsymbol{A}[\tau]), \quad \overline{\nu}_n(\boldsymbol{S}) = \lim_{T\to\infty}\frac{1}{T}\sum_{\tau=1}^{T}\nu_n(\boldsymbol{A}[\tau]), \tag{4.5}$$

leading to the equations

$$\text{RE}_{\mathcal{L}}(\boldsymbol{S}) = \overline{\kappa}(\mathcal{L},\boldsymbol{S})\sum_{n\in\mathcal{N}}\overline{w}_n(\boldsymbol{S})\text{RE}_n(\boldsymbol{S}), \tag{4.6}$$

$$\sum_{n\in\mathcal{N}}\lambda_n = \overline{\nu}^{\text{sys}}(\mathcal{L},\boldsymbol{S})\text{RE}_{\mathcal{L}}(\boldsymbol{S}) = \overline{\nu}^{\text{eff}}(\mathcal{L},\boldsymbol{S})\sum_{n\in\mathcal{N}}\overline{w}_n(\boldsymbol{S})\text{RE}_n(\boldsymbol{S}) \tag{4.7}$$

with the expected time-average reuse factor $\overline{\kappa}(\mathcal{L},\boldsymbol{S}) = \overline{\nu}^{\text{eff}}(\mathcal{L},\boldsymbol{S})/\overline{\nu}^{\text{sys}}(\mathcal{L},\boldsymbol{S})$ and the expected time-average relative resource usages $\overline{w}_n(\boldsymbol{A}) = \overline{\nu}_n(\boldsymbol{A})/\overline{\nu}^{\text{eff}}_{\mathcal{L}}(\boldsymbol{A})$

4.2.3 Link- and Flow-Rate Based Resource Efficiency

Similar to throughput based resource efficiency, a link-rate resource efficiency can be defined. Both are related but measure slightly different things. Whereas the throughput based efficiency measures the end-to-end transported information per resource use, the link rate efficiency refers to the MAC-layer sum-rate delivered per resource. An amount of throughput thus may be counted several times in the link-rate metric, if it is transported over multiple hops. Denote by $\overline{R}_{mn}$ the time averaged expectation of link (m,n)'s data rate assuming the action sequence $\boldsymbol{S}$. Then the link-rate resource efficiency is defined as:

$$\begin{aligned}\text{RE}^{\text{MAC}}_{\mathcal{L}}(\boldsymbol{S}) &= \frac{\sum_{(m,n)\in\mathcal{L}}\overline{R}_{mn}}{\overline{\nu}^{\text{sys}}(\mathcal{L},\boldsymbol{S})} = \overline{\kappa}(\mathcal{L},\boldsymbol{S})\frac{\sum_{(m,n)\in\mathcal{L}}\overline{R}_{mn}}{\overline{\nu}^{\text{eff}}(\mathcal{L},\boldsymbol{S})} = \overline{\kappa}(\mathcal{L},\boldsymbol{S})\sum_{(m,n)\in\mathcal{L}}\frac{\overline{\nu}_{mn}(\boldsymbol{S})}{\overline{\nu}^{\text{eff}}(\mathcal{L},\boldsymbol{S})}\frac{\overline{R}_{mn}}{\overline{\nu}_{mn}(\boldsymbol{S})} \\ &= \overline{\kappa}(\mathcal{L},\boldsymbol{S})\sum_{(m,n)\in\mathcal{L}}\overline{w}_{mn}(\boldsymbol{S})\text{RE}_{mn}(\boldsymbol{S}),\end{aligned} \tag{4.8}$$

where $\overline{w}_{mn} = \overline{\nu}_{mn}(\boldsymbol{S})/\overline{\nu}^{\text{eff}}(\mathcal{L},\boldsymbol{S})$ is the system-wide, relative effective resource usage of link (m,n). An analog transformation can be made on throughput basis. Assume that $\overline{R}_{mn} = \sum_{c:(m,n)\in\mathcal{L}_c}\overline{R}_c$, where $\overline{R}_c$ is the time-averaged expected value of data from flow c transported over link (m,n). It holds for the link's resource efficiency that:

$$\begin{aligned}\text{RE}_{mn}(\boldsymbol{S}) &= \frac{\overline{R}_{mn}}{\overline{\nu}_{mn}(\boldsymbol{S})} = \sum_{c:(m,n)\in\mathcal{L}_c}\frac{\overline{R}_c}{\overline{\nu}_{mn}(\boldsymbol{S})} = \sum_{c:(m,n)\in\mathcal{L}_c}\frac{\overline{R}_c}{\overline{R}_{mn}}\frac{\overline{R}_{mn}}{\overline{\nu}_{mn}(\boldsymbol{S})} \\ &= \sum_{c:(m,n)\in\mathcal{L}_c}\frac{\frac{\overline{R}_c}{\overline{R}_{mn}}\overline{\nu}_{mn}(\boldsymbol{S})}{\overline{\nu}_{mn}(\boldsymbol{S})}\text{RE}^{(c)}_{mn}(\boldsymbol{S}) = \sum_{c:(m,n)\in\mathcal{L}_c}\frac{\overline{\nu}^{(c)}_{mn}(\boldsymbol{S})}{\overline{\nu}_{mn}(\boldsymbol{S})}\text{RE}^{(c)}_{mn}(\boldsymbol{S}),\end{aligned} \tag{4.9}$$

where $\text{RE}^{(c)}_{mn}(\boldsymbol{S}) = \overline{R}_{mn}/\overline{\nu}_{mn}(\boldsymbol{S})$ is the same for all flows that pass through link (m,n). The term $\overline{\nu}^{(c)}_{mn}(\boldsymbol{S}) = \overline{\nu}_{mn}(\boldsymbol{S})\cdot\overline{R}_c/\overline{R}_{mn}$ can be interpreted as the resource usage of flow c on link (m,n), respectively. The last form can be interpreted similar to (4.8) as weighted efficiency per flow, where the weights are the relative resource usage. From the reformulation, the

intuition follows that all flows using a single link transmit at the same efficiency but use resources according to their relative rates on the link. This interpretation can be verified by the relation that the rate-resource efficiency times amount of used resources should yield the achieved data rate:

$$\overline{\nu}_{mn}^{(c)}(\boldsymbol{S})\mathrm{RE}_{mn}^{(c)}(\boldsymbol{S}) = \frac{\overline{R}_c}{\overline{R}_{mn}}\overline{\nu}_{mn}(\boldsymbol{S})\mathrm{RE}_{mn}^{(c)}(\boldsymbol{S}) = \overline{R}_c. \tag{4.10}$$

Plugging (4.9) into (4.8) yields the following equation for system-wide resource efficiency:

$$\begin{aligned}
\mathrm{RE}_{\mathcal{L}}^{\mathrm{MAC}}(\boldsymbol{S}) &= \overline{\kappa}(\mathcal{L},\boldsymbol{S}) \sum_{(m,n)\in\mathcal{L}} \overline{w}_{mn}(\boldsymbol{S}) \sum_{c:(m,n)\in\mathcal{L}_c} \frac{\overline{\nu}_{mn}^{(c)}(\boldsymbol{S})}{\overline{\nu}_{mn}(\boldsymbol{S})}\mathrm{RE}_{mn}^{(c)}(\boldsymbol{S}) \\
&= \overline{\kappa}(\mathcal{L},\boldsymbol{S}) \sum_{(m,n)\in\mathcal{L}} \sum_{c:(m,n)\in\mathcal{L}_c} \frac{\overline{\nu}_{mn}^{(c)}(\boldsymbol{S})}{\overline{\nu}^{\mathrm{eff}}(\mathcal{L},\boldsymbol{S})}\mathrm{RE}_{mn}^{(c)}(\boldsymbol{S}) \\
&= \frac{\sum_{c\in\mathcal{K}}\sum_{(m,n)\in\mathcal{L}_c}\overline{R}_c}{\overline{\nu}^{\mathrm{sys}}(\mathcal{L},\boldsymbol{S})} = \frac{\sum_{c\in\mathcal{K}}\overline{R}_c\sum_{(m,n)\in\mathcal{L}_c}1}{\overline{\nu}^{\mathrm{sys}}(\mathcal{L},\boldsymbol{S})}.
\end{aligned} \tag{4.11}$$

The first equality in the last line was achieved by re-arranging the summands to flip the sums, using (4.10) and using that $\overline{\kappa}(\mathcal{L},\boldsymbol{S}) = \overline{\nu}^{\mathrm{eff}}(\mathcal{L},\boldsymbol{S})/\overline{\nu}^{\mathrm{sys}}(\mathcal{L},\boldsymbol{S})$, respectively. The second equality comes from flow conservation, by which the infinite time-horizon, average rate of a flow over different links is equal. Equation (4.11) shows the difference among the usage of MAC layer link rates and end-to-end throughput for resource efficiency metrics, which lies in the fact that the link-rate resource efficiency counts the data of a single flow by the multiplicity of the hops used. This distorting multiplicity exactly motivates why resource efficiency, and in later instance also the D2D-Gains, should be evaluated on throughput basis and not on a per-hop rate basis.

4.2.4 Flow-Rate Based Resource Efficiency

A side-effect of the presented considerations is that they give a consistent definition for the resource use of a flow on a link, which can be used reformulate the throughput resource efficiency into a flow formulation. By using the definition of $\overline{\nu}_{mn}^{(c)}(\boldsymbol{S})$, the effective amount resources used by a flow $c \in \mathcal{K}$ in a network can be defined as

$$\overline{\nu}_c(\boldsymbol{S}) = \sum_{(m,n)\in\mathcal{L}_c} \overline{\nu}_{mn}^{(c)}(\boldsymbol{S}) = \sum_{(m,n)\in\mathcal{L}_c} \overline{\nu}_{mn}(\boldsymbol{S})\cdot\overline{R}_c/\overline{R}_{mn} = \overline{R}_c \sum_{(m,n)\in\mathcal{L}_c} \frac{1}{\mathrm{RE}_{mn}(\boldsymbol{S})}. \tag{4.12}$$

In words, it is the sum of resources used by the flow on links that it traverses, using the definition of per-hop resource usage by a flow, which was developed above. It can further be calculated only by knowing the throughput $\overline{R}_c$ and the MAC-layer rate-resource efficiencies of each link, as given on the right hand side. This definition of resource usage is consistent, as the total number of resources is given by

$$\sum_{c\in\mathcal{K}}\overline{\nu}_c(\boldsymbol{S}) = \sum_{c\in\mathcal{K}}\sum_{(m,n)\in\mathcal{L}_c}\overline{\nu}_{mn}(\boldsymbol{S})\cdot\overline{R}_c/\overline{R}_{mn} = \sum_{(m,n)\in\mathcal{L}}\overline{\nu}_{mn}(\boldsymbol{S})\frac{\sum_{c:(m,n)\in\mathcal{L}_c}\overline{R}_c}{\overline{R}_{mn}} = \overline{\nu}^{\mathrm{eff}}(\mathcal{L},\boldsymbol{S}),$$

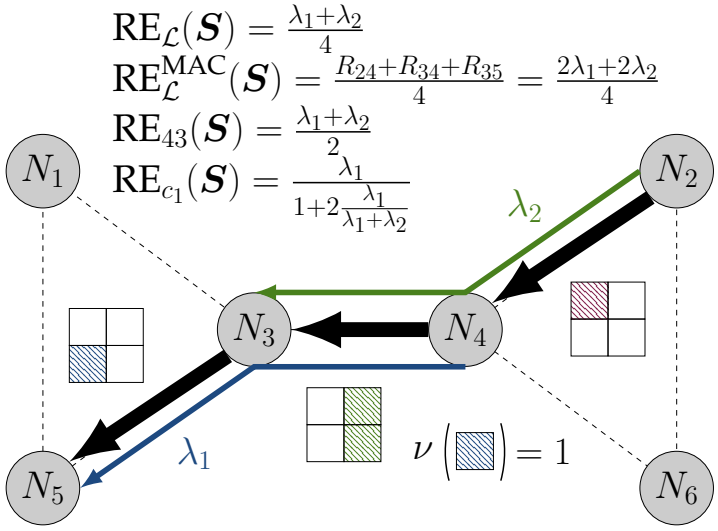

Figure 4.2: Comparison of different resource efficiency definitions for an example network, which uses a fixed schedule on four resources at all time slots. Filled squares indicate resource use. It is assumed that each resource has a measure of one.

where it was used that $\overline{R}_{mn} = \sum_{c:(m,n)\in\mathcal{L}_c} \overline{R}_c$. That is, by using this definition of per-flow resource usage, the total amount of effective resources are correctly represented. Because $\overline{R}_c = \lambda_c$, the throughput-resource efficiency of a flow c can be re-written into

$$\mathrm{RE}_c(\boldsymbol{S}) = \frac{\lambda_c}{\overline{\nu}_c(\boldsymbol{S})} = \left(\sum_{(m,n)\in\mathcal{L}_c} \frac{1}{\mathrm{RE}_{mn}(\boldsymbol{S})} \right)^{-1} . \tag{4.13}$$

The flow formulation of the network-wide resource efficiency then results in

$$\begin{aligned} \mathrm{RE}_{\mathcal{L}}(\boldsymbol{S}) &= \overline{\kappa}(\mathcal{L},\boldsymbol{S}) \frac{\sum_{c\in\mathcal{K}} \lambda_c}{\overline{\nu}^{\mathrm{eff}}(\mathcal{L},\boldsymbol{S})} = \overline{\kappa}(\mathcal{L},\boldsymbol{S}) \sum_{c\in\mathcal{K}} \frac{\overline{\nu}_c(\boldsymbol{S})}{\overline{\nu}^{\mathrm{eff}}(\mathcal{L},\boldsymbol{S})} \mathrm{RE}_c(\boldsymbol{S}) \\ &= \overline{\kappa}(\mathcal{L},\boldsymbol{S}) \sum_{c\in\mathcal{K}} \overline{w}_c \left(\sum_{(m,n)\in\mathcal{L}_c} \frac{1}{\mathrm{RE}_{mn}(\boldsymbol{S})} \right)^{-1} . \end{aligned} \tag{4.14}$$

As can be seen, a resource efficiency can consistently be defined on several levels without contradiction and can actually be calculated knowing network parameters such as MAC-layer rates and resource usage and end-to-end throughput. The relation of all defined resource efficiency is depicted for better illustration in Figure 4.2. The notions derived in this Section will be used in the following to discuss properties of the D2D-gain.

4.3 Resource Efficiency and D2D-Gains

The reason for defining and investigating resource efficiency metrics in the previous sections is that they can be used to capture the three RAN-gains of D2D, proximity-, hop- and reuse-gain. When traffic flows are realized by different communication modes, i.e., cellular or D2D

mode, this corresponds to routing them through the network on different paths. The D2D mode thereby refers to a direct, one-hop route between source and destination, whereas the cellular mode refers to a two-hop path passing through an uplink to and a downlink from a base station.

Consider two routing link sets $\mathcal{L}_c^{\text{CM}}$ and $\mathcal{L}_c^{\text{DM}}$ for each flow $c \in \mathcal{K}$, where the first link set refers to a flow being realized by cellular mode and the second by direct mode. Further, let $\mathcal{L}^{\text{CM}} = \{\mathcal{L}_1^{\text{CM}}, ..., \mathcal{L}_K^{\text{CM}}\}$ denote the topology where all flows are solely realized by cellular mode, whereas $\mathcal{L}^*$ is a topology where some flows are offloaded to direct mode. Assume flow variables λ_n^{CM} and λ_n^* that are within the stability region of a scheduler, with $\boldsymbol{S}^{\text{CM}}$ and $\boldsymbol{S}^*$ being two action sequences after mode selection choices have been made. The flow variables need not necessarily be equal across different modes and neither do the action sequences. The D2D-gains can then be captured by the relative resource efficiency increase as:

$$G_{\text{D2D}} = \frac{\text{RE}_{\mathcal{L}^*}(\boldsymbol{S}^*)}{\text{RE}_{\mathcal{L}^{\text{CM}}}(\boldsymbol{S}^{\text{CM}})} = \frac{\sum\limits_{n\in\mathcal{N}} \lambda_n^*}{\sum\limits_{n\in\mathcal{N}} \lambda_n^{\text{CM}}} \frac{\overline{\nu}^{\text{eff}}(\mathcal{L}^{\text{CM}}, \boldsymbol{S}^{\text{CM}})}{\overline{\nu}^{\text{eff}}(\mathcal{L}^*, \boldsymbol{S}^*)} \frac{\overline{\kappa}^*(\mathcal{L}^*, \boldsymbol{S}^*)}{\overline{\kappa}^{\text{CM}}(\mathcal{L}^{\text{CM}}, \boldsymbol{S}^{\text{CM}})} = G_P \cdot G_H \cdot G_R,$$

$$\text{with} \qquad G_P = \frac{\sum\limits_{n\in\mathcal{N}} \lambda_n^*}{\sum\limits_{n\in\mathcal{N}} \lambda_n^{\text{CM}}};\ G_H = \frac{\overline{\nu}^{\text{eff}}(\mathcal{L}^{\text{CM}}, \boldsymbol{S}^{\text{CM}})}{\overline{\nu}^{\text{eff}}(\mathcal{L}^*, \boldsymbol{S}^*)};\ G_R = \frac{\overline{\kappa}^*(\mathcal{L}^*, \boldsymbol{S}^*)}{\overline{\kappa}^{\text{CM}}(\mathcal{L}^{\text{CM}}, \boldsymbol{S}^{\text{CM}})}. \tag{4.15}$$

G_{D2D} can be decomposed into three factors G_P, G_H and G_R, respectively. G_P captures the relative sum-throughput increase that is realized after the mode selection has been done, compared to serving all throughput with cellular communication. It can thus be interpreted as the proximity-gain of D2D. G_H reflects how much more resource is used by cellular communication compared to the offloaded situation and hence corresponds to the hop-gain. Finally, G_R is the relative increase of reuse-factor, introduced by allowing reuse from D2D links, and hence is the reuse-gain. All gains together are traded off to form the overall D2D-gain, which captures the overall effect of how efficiently system transmission resources are used to serve all demands in the network.

An example for the trade-off of the different gain aspects is shown in Figure 4.3. On the left hand side, a potential D2D flow is shown in cellular mode, together with another ongoing uplink transmission. While the uplink is assigned two transmission resources and achieves a rate of two, the potential D2D flow is assigned the remaining uplink resource and achieves a rate of one. This is in spite of free downlink resources, because the uplink is the transmission bottle-neck. On the right hand side, the flow is offloaded to direct mode. The sidelink is allowed to use all downlink resource and, due to advantageous channels, can also reuse all resources of the uplink transmission. The decrease in uplink quality due to interference is made up for by assigning more resources, such that it still achieves its target rate. The question here is, how to consistently evaluate which situation is more beneficial. To give an answer, the three gains aspects can be evaluated: In direct mode, the sum-throughput is six, compared to a sum-throughput of three in cellular mode, yielding a proximity-gain of two. On the other hand, effectively, nine resources are used due to frequency reuse, which is more than twice as many as in cellular mode, creating a hop-gain of 0.44. Finally, in direct mode a cellular reuse factor of 1.5 is achieved, compared to no reuse in cellular mode, resulting in

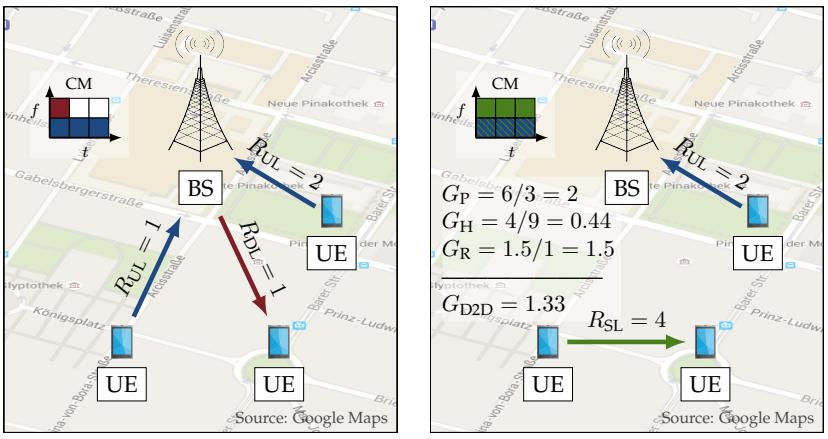

Figure 4.3: An example for the trade-off of different gain aspects. The left figure shows a cellular realization of all flows, while on the right side one flow is offloaded to direct mode. The quantities R_{UL}, R_{DL} and R_{SL} denote the achieved rates in fictive rate units, while the resource grid in the upper left depicts the resource usage, where the color of each resource matches that of the link types using it. The right figure further shows an example gain calculation.

a reuse-gain of 1.5. Altogether, the positive proximity-gain and reuse-gain more than cancel the negative hop-gain out, leading to an overall-gain factor of 1.3. This factor expresses that in direct mode, the six available system resources are used 1.3 times more efficiently than in cellular mode.

Several special cases exist, that correspond to special system designs: (1) For overlay D2D-communication within a single network cell, there is no resource reuse and hence, $\overline{\nu}^{\text{eff}}(\boldsymbol{S}) = \overline{\nu}^{\text{sys}}(\boldsymbol{S})\ \forall \boldsymbol{S}$, leading to $\overline{\kappa}^{*}(\mathcal{L}^{*}, \boldsymbol{S}^{*}) = \overline{\kappa}^{\text{CM}}(\mathcal{L}^{\text{CM}}, \boldsymbol{S}^{\text{CM}}) = 1$ and $G_R = 1$. That is, there is no reuse-gain. (2) When the achieved throughputs remain fixed, $\lambda_n^{*} = \lambda_n^{\text{CM}}\ \forall n \in \mathcal{N}$, e.g., because the applications use constant bit-rate, then $G_P = 1$. In this case no proximity-gain can be leveraged because possible traffic increases are not matched by increasing demands. (3) In a single-cell overlay D2D-network with elastic traffic demands, the throughput will be increased until all resources are fully utilized. In this case, $\overline{\nu}^{\text{eff}}(\mathcal{L}^{\text{CM}}, \boldsymbol{S}^{\text{CM}}) = \overline{\nu}^{\text{eff}}(\mathcal{L}^{*}, \boldsymbol{S}^{*})$ and $G_H = 1$. Note that only in the case of $G_H = G_R = 1$, i.e., for overlay D2D networks with elastic traffic demands, maximizing the D2D-gain in fact corresponds to maximizing the sum-throughput. In all other cases, there is always a trade-off among throughput, resource usage and resource reuse. This is in contrast to research on D2D networks, which mainly focuses on maximizing throughput.

The D2D-gain perspective has a direct influence on mode selection, as intuitively flows with a D2D-gain larger than one should use the direct mode rather than cellular mode. On the other hand, the gain itself depends on the dynamics of the scheduler. A scheduler that acts against SLs, for some reason, will never produce a D2D-gain, even if it would be possible to produce one. As the typically implemented schedulers are not actively designed to maximize the D2D-gain but rather to maximize a network utility, it must be asked how suitable current NUM based schedulers are to leverage the D2D option. This is particularly the case considering that often schedulers target throughput maximization, which was shown here to only partly match with the gain expectations for D2D links. With this in mind, it makes

sense to further investigate the interplay between resource efficiency and scheduling, which will be in focus in the remaining parts of this chapter.

4.3.1 Utility-Based D2D-Gains

The D2D-gain can be abstracted for use with any throughput-dependent utility function, which makes it easier to relate it to NUM based schedulers. Assume a utility of the form

$$U(\boldsymbol{\lambda}) = \sum_n U_n(\lambda_n); \;\; \boldsymbol{\lambda} = [\lambda_1, ..., \lambda_N]^T, \tag{4.16}$$

where λ_n is the expected admission rate with which data is injected into the wireless part of the network. If not stated differently, the $U_n(\lambda_n)$ are assumed to be strictly monotonically increasing with λ_n. Such utility functions are often used on network layer to model user satisfaction with rate for applications such as voice or video transmissions, or rate fairness. A utility-resource efficiency can be defined as

$$\mathrm{RE}^{\mathrm{U}}_{\mathcal{L}}(\boldsymbol{S}) = \lim_{T\to\infty} \frac{\sum\limits_{n\in\mathcal{N}} U_n(\lambda_n)}{\frac{1}{T}\sum\limits_{\tau=1}^{T} \nu^{\mathrm{sys}}(\mathcal{L}, \boldsymbol{A}[\tau])} = \frac{\sum\limits_{n\in\mathcal{N}} U_n(\lambda_n)}{\overline{\nu}^{\mathrm{sys}}(\mathcal{L}, \boldsymbol{S})}. \tag{4.17}$$

Correspondingly, the utility based D2D-gain becomes

$$G^{\mathrm{U}}_{\mathrm{D2D}} = \frac{\mathrm{RE}^{\mathrm{U}}_{\mathcal{L}^*}(\boldsymbol{S}^*)}{\mathrm{RE}^{\mathrm{U}}_{\mathcal{L}^{\mathrm{CM}}}(\boldsymbol{S}^{\mathrm{CM}})} = \frac{\sum\limits_{n\in\mathcal{N}} U_n(\lambda_n^*)}{\sum\limits_{n\in\mathcal{N}} U_n(\lambda_n^{\mathrm{CM}})} \frac{\overline{\nu}^{\mathrm{eff}}(\mathcal{L}^{\mathrm{CM}}, \boldsymbol{S}^{\mathrm{CM}})}{\overline{\nu}^{\mathrm{eff}}(\mathcal{L}^*, \boldsymbol{S}^*)} \frac{\overline{\kappa}^*(\mathcal{L}^*, \boldsymbol{S}^*)}{\overline{\kappa}^{\mathrm{CM}}(\mathcal{L}^{\mathrm{CM}}, \boldsymbol{S}^{\mathrm{CM}})} = G^{\mathrm{U}}_P \cdot G_H \cdot G_R$$

The only difference with respect to (4.15) lies in the proximity-gain G^{U}_P, which is now measured by an arbitrary utility function instead of throughput. The actual D2D-gain can be considered as special case by choosing sum throughput as utility function.

4.4 Resource Efficiency of Schedulers

As has been argued in Section 4.3, the commonly targeted gain of introducing D2D communication into a cellular network originates from its property to allow more efficient resource use. However, this makes D2D communication prone to improperly designed network management. When flows are handed off to direct mode without taking into account their impact on the achievable system efficiency, D2D might actually degrade networking performance, negating the gains it was supposed to create.

Also, a scheduler that does not target efficient use of resources might not be able to leverage the D2D-gains. If this is true, the scheduling task needs to be shifted from maximizing data rates to maximizing throughput-efficiencies. An understanding of the efficiency metric is thus required to evaluate the impact of scheduling and offloading and to identify ways to properly design both functions. As the resource efficiency has not formally been defined in literature before, the impact of scheduling on resource efficiency is unknown and thus developed here.

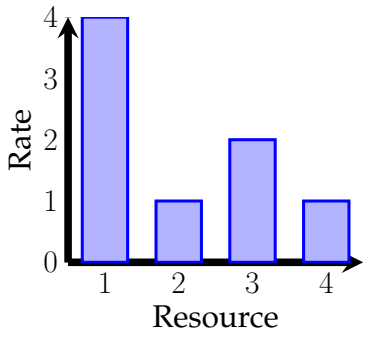

Target Rate	2	4	6	8
Max. Eff.	4	4	3	2
Min. Eff	1	1.33	1.71	2

Figure 4.4: Maximum achievable and minimum required efficiency for given example with four transmission resources.

The main intuition formalized in this section is illustrated in Figure 4.4 for better initial understanding. On the left, the achievable rate on four different transmission resources (channels, PRBs,...) is shown. As the achievable rate differs per resource, clearly the use of different resources creates varying rate-resource efficiencies. Now assume that the resources can be used at different relative frequencies over arbitrary many time slots. Then, using only a single resource for a certain fraction of slots and not transmitting for the remaining fraction would lead to a decreased average rate. The resource efficiency, however, would be left unchanged because the resource use is reduced proportionally. By leveraging this, the largest achievable and least required efficiency to realize an average rate is shown on the right side: An average rate of two can be achieved by using resource one on half of the slots, yielding a rate-efficiency of four per resource use, or by using resources two and four on all time slots, resulting in a rate-efficiency of one. By the same logic, the remaining efficiencies follow.

From the sequence, three interesting observations can be made: (1) The largest achievable efficiency decreases with targeted rate. (2) The least required efficiency increases with targeted rate. (3) Both have the same value at the maximum targeted rate. This effect is a basic behavior of efficiency metrics that will be formalized in the following sections. It will be shown to hold for arbitrary utility functions, as long as they are strictly increasing with rates.

4.4.1 Definitions and Assumptions

Throughout this chapter, it is assumed that the network topology state is given as an infinite time-horizon set of topology matrices, $\boldsymbol{Q} = \{\boldsymbol{Q}[0], \boldsymbol{Q}[1], ..., \boldsymbol{Q}[\tau], ...\}$. Let $\boldsymbol{S} = \{\boldsymbol{A}[0], \boldsymbol{A}[1], ..., \boldsymbol{A}[\tau], ...\}$ be an infinite time-horizon action sequence generated by a scheduling policy and let $\Lambda(\boldsymbol{S}, \boldsymbol{Q})$ be its associated stability region, i.e., the set of all flow admission rates that can be stably supported assuming $\boldsymbol{S}$ and $\boldsymbol{Q}$ given. For notational convenience, $\Lambda(\boldsymbol{S}, \boldsymbol{Q})$ is abbreviated to Λ when the dependency on $\boldsymbol{S}$ and $\boldsymbol{Q}$ is clear. The sequence $\boldsymbol{S}$ is one of a set $\mathcal{S}$ of possible, infinite time-horizon sequences. Consider a utility function $U(\boldsymbol{\lambda})$ for a given $\boldsymbol{\lambda} \in \Lambda$, that is strictly increasing with $\boldsymbol{\lambda}$, and let $\overline{\nu}^{\text{sys}}(\boldsymbol{S})$ be the time averaged amount of system resources used by sequence $\boldsymbol{S}$. Then the utility based resource efficiency,

achieved by sequence $\boldsymbol{S}$ with traffic input $\boldsymbol{\lambda}$ is

$$\mathrm{RE}^U(\boldsymbol{S},\boldsymbol{\lambda}) = \frac{U(\boldsymbol{\lambda})}{\overline{\nu}^{\mathrm{sys}}(\boldsymbol{S})}. \tag{4.18}$$

Define tuples of the form $(\boldsymbol{S},\boldsymbol{\lambda}) \in \mathcal{S}\times\Lambda$, where $\mathcal{S}\times\Lambda = \{(\boldsymbol{S},\boldsymbol{\lambda}) : \boldsymbol{S}\in\mathcal{S}, \boldsymbol{\lambda}\in\Lambda(\boldsymbol{S},\boldsymbol{Q})\}$, i.e., tuples of action sequences and admission rates from their stability region. Then, for finite values of U and V, define the following sets:

$$\underline{\mathcal{S}}(U) = \{(\boldsymbol{S},\boldsymbol{\lambda})\in\mathcal{S}\times\Lambda : U(\boldsymbol{\lambda})\geq U\}; \tag{4.19}$$

$$\mathcal{S}(U) = \{(\boldsymbol{S},\boldsymbol{\lambda})\in\mathcal{S}\times\Lambda : U(\boldsymbol{\lambda}) = U\}; \tag{4.20}$$

$$\overline{\mathcal{S}}(V) = \{(\boldsymbol{S},\boldsymbol{\lambda})\in\mathcal{S}\times\Lambda : \overline{\nu}^{\mathrm{sys}}(\boldsymbol{S})\leq V\}; \tag{4.21}$$

$$\mathcal{S}(V) = \{(\boldsymbol{S},\boldsymbol{\lambda})\in\mathcal{S}\times\Lambda : \overline{\nu}^{\mathrm{sys}}(\boldsymbol{S}) = V\}; \tag{4.22}$$

$$\mathcal{S}^*_{\mathrm{RE}} = \left\{(\boldsymbol{S},\boldsymbol{\lambda})\in\mathcal{S}\times\Lambda : \mathrm{RE}^U(\boldsymbol{S},\boldsymbol{\lambda}) = \max_{\mathcal{S}\times\Lambda}\mathrm{RE}^U(\boldsymbol{S},\boldsymbol{\lambda})\right\}. \tag{4.23}$$

In words, $\underline{\mathcal{S}}(U)$ is the set of all sequences and throughput vectors that support a utility level of at least U, $\mathcal{S}(U)$ is the set of sequences and throughputs that exactly achieve U, $\overline{\mathcal{S}}(V)$ is the set that require at most V resources on average, $\mathcal{S}(V)$ the set that require exactly V resources on average and $\mathcal{S}^*_{\mathrm{RE}}$ is the set of all sequences and throughputs that maximize the utility based resource efficiency.

4.4.2 Sequence Scaling

Consider an action sequence $\boldsymbol{S}$ that can stably support admissible admission rates with mean of $\boldsymbol{\lambda}$. Further, imagine another sequence $\boldsymbol{S}_\alpha$ such that $\boldsymbol{A}_\alpha[\tau] = \boldsymbol{A}[\tau]\in\boldsymbol{S}$ with probability α and $\boldsymbol{A}_\alpha[\tau] = \boldsymbol{A}_0$ with probability $1-\alpha$, independently at each time slot. Per definition of an idle action, $\boldsymbol{R}(\boldsymbol{A}_0) = 0$ and hence, $\boldsymbol{S}_\alpha$ is able to realize the throughput of $\alpha\boldsymbol{\lambda}$ if, and only if, $\boldsymbol{S}$ can realize $\boldsymbol{\lambda}$, i.e., $\Lambda_\alpha = \alpha\Lambda$ holds. As further $\nu^{\mathrm{sys}}(\boldsymbol{A}_0) = 0$ holds, $\boldsymbol{S}_\alpha$ will realize a long term resource usage of $\overline{\nu}^{\mathrm{sys}}(\boldsymbol{S}_\alpha) = \alpha\overline{\nu}^{\mathrm{sys}}(\boldsymbol{S})$.

Sequence $\boldsymbol{S}_\alpha$ is called a *downscaled version* of $\boldsymbol{S}$, respectively, as it scales both, resource usage and throughput by a factor α. The utility based resource efficiency of $\boldsymbol{S}_\alpha$ then is

$$\mathrm{RE}^U(\boldsymbol{S}_\alpha,\alpha\boldsymbol{\lambda}) = \frac{U(\alpha\boldsymbol{\lambda})}{\overline{\nu}^{\mathrm{sys}}(\boldsymbol{S}_\alpha)} = \frac{U(\alpha\boldsymbol{\lambda})}{\alpha\overline{\nu}^{\mathrm{sys}}(\boldsymbol{S})}. \tag{4.24}$$

The effect of sequence scaling on the achieved resource efficiency depends on the form of the utility function. Define the class of scale-invariant utilities, for which $U(\alpha\boldsymbol{\lambda}) = \alpha U(\boldsymbol{\lambda})\ \forall\boldsymbol{\lambda}$. Examples for such utilities are the sum-throughput, weighted sum-throughput or max-min fair throughput. For scale-invariant utilities, clearly sequence downscaling does not change the achieved resource efficiency:

$$\mathrm{RE}^U(\boldsymbol{S}_\alpha,\alpha\boldsymbol{\lambda}) = \frac{U(\alpha\boldsymbol{\lambda})}{\alpha\overline{\nu}^{\mathrm{sys}}(\boldsymbol{S})} = \frac{\alpha U(\boldsymbol{\lambda})}{\alpha\overline{\nu}^{\mathrm{sys}}(\boldsymbol{S})} = \mathrm{RE}^U(\boldsymbol{S},\boldsymbol{\lambda}). \tag{4.25}$$

In particular, this holds for the throughput based resource efficiency, which was originally used to define the D2D-gain. While it does not hold for general utilities, some laws can be established to hold in general, which is done in the next section.

4.4.3 Resource Efficiency Laws

The previous definitions can be used to establish the following laws for resource efficiency:

Proposition 4.1 (Weak Law of Non-Increasing and Non-Decreasing Resource Efficiency)**.** Consider an arbitrary utility $U(\boldsymbol{\lambda})$, two utility target levels U_1, U_2, $U_1 \geq U_2$ and their associated tuple sets $\underline{\mathcal{S}}_{U_1}$, $\underline{\mathcal{S}}_{U_2}$. Then it holds that

$$\begin{aligned} \sup_{\underline{\mathcal{S}}_{U_1}} \mathrm{RE}^U(\boldsymbol{S},\boldsymbol{\lambda}) &\leq \sup_{\underline{\mathcal{S}}_{U_2}} \mathrm{RE}^U(\boldsymbol{S},\boldsymbol{\lambda}) \\ \inf_{\underline{\mathcal{S}}_{U_1}} \mathrm{RE}^U(\boldsymbol{S},\boldsymbol{\lambda}) &\geq \inf_{\underline{\mathcal{S}}_{U_2}} \mathrm{RE}^U(\boldsymbol{S},\boldsymbol{\lambda}). \end{aligned}$$

Proof. Due to their definition, $\underline{\mathcal{S}}_{U_1} \subseteq \underline{\mathcal{S}}_{U_2}$. Hence, the efficiency maximizer/minimizer among all sequences and flow values in $\underline{\mathcal{S}}_{U_1}$ is also contained in $\underline{\mathcal{S}}_{U_2}$, respectively. So the supremum and infinum among $\underline{\mathcal{S}}_{U_2}$ must be at least as large or low as that of $\underline{\mathcal{S}}_{U_1}$. □

Proposition 4.1 is simple but gives an interesting view on the resource efficiency of sequences, as it states that the maximum achievable efficiency cannot increase when the demanded utility increases. Further, it states that the minimum required efficiency to realize a utility value cannot decrease with increasing value. This holds true for any sequence and utility. The intuitive notion is that for lower utility demands, the schedulers have more options how to realize the flow transport. This gives the freedom to use an inefficient schedule that barely realizes the flows, or to use a highly efficient one that over-achieves the demanded flow utilities. By increasing utility demands, less sequences are available to realize the flow transport, yielding the result.

The efficiency laws can be strengthened for special types of utility functions. For this, call a utility sub-linearly scalable if $\forall\boldsymbol{\lambda}$, $\alpha \geq 1$, $U(\boldsymbol{\lambda}) \leq U(\alpha\boldsymbol{\lambda}) \leq \alpha U(\boldsymbol{\lambda})$ and super-linearly scalable if $\forall\boldsymbol{\lambda}$, $\alpha \geq 1$, $U(\boldsymbol{\lambda}) \leq \alpha U(\boldsymbol{\lambda}) \leq U(\alpha\boldsymbol{\lambda})$. Then, the following holds:

Proposition 4.2 (Strong Law of Non-Increasing and Non-Decreasing Resource Efficiency)**.** Consider an arbitrary utility $U(\boldsymbol{\lambda})$, two utility target levels U_1, U_2, $U_1 \geq U_2$ and their associated tuple sets $\mathcal{S}_{U_1}$, $\mathcal{S}_{U_2}$. Then it holds that

$$\begin{aligned} \sup_{\mathcal{S}_{U_1}} \mathrm{RE}^U(\boldsymbol{S},\boldsymbol{\lambda}) &\leq \sup_{\mathcal{S}_{U_2}} \mathrm{RE}^U(\boldsymbol{S},\boldsymbol{\lambda}) \text{ for sub-linearly scalable } U(\boldsymbol{\lambda}), \\ \inf_{\mathcal{S}_{U_1}} \mathrm{RE}^U(\boldsymbol{S},\boldsymbol{\lambda}) &\geq \inf_{\mathcal{S}_{U_2}} \mathrm{RE}^U(\boldsymbol{S},\boldsymbol{\lambda}) \text{ for super-linearly scalable } U(\boldsymbol{\lambda}). \end{aligned}$$

Proof. Note that the main difference with respect to Propositions 4.1 lies in the used tuple sets. Assume a sub-linearly scalable utility $U(\boldsymbol{\lambda})$ and a tuple $(\boldsymbol{S}_1, \boldsymbol{\lambda}_1) \in \mathcal{S}_{U_1}$. Due to its scalability nature, $\alpha U(\boldsymbol{\lambda}) \leq U(\alpha\boldsymbol{\lambda})\ \forall\alpha \leq 1$ can be deduced. Because $U(\alpha\boldsymbol{\lambda})$ is monotonically increasing with α, there exists an $\alpha \leq 1$ such that $U(\alpha\boldsymbol{\lambda}_1) = U_2$. As $\alpha \leq 1$, $U(\alpha\boldsymbol{\lambda}_1) \geq \alpha U(\boldsymbol{\lambda}_1) = \alpha U_1$ holds. Now $\boldsymbol{S}_1$ can be down-scaled to $\boldsymbol{S}_\alpha$, leading to

$$\mathrm{RE}^U(\boldsymbol{S}_\alpha, \alpha\boldsymbol{\lambda}_1) = \frac{U(\alpha\boldsymbol{\lambda}_1)}{\overline{\nu}^{\mathrm{sys}}_{\boldsymbol{S}_\alpha}(\alpha\boldsymbol{\lambda}_1)} \geq \frac{\alpha U(\boldsymbol{\lambda}_1)}{\alpha\overline{\nu}^{\mathrm{sys}}_{\boldsymbol{S}_1}(\boldsymbol{\lambda}_1)} = \frac{U(\boldsymbol{\lambda}_1)}{\overline{\nu}^{\mathrm{sys}}_{\boldsymbol{S}_1}(\boldsymbol{\lambda}_1)} = \mathrm{RE}^{\boldsymbol{S}_1}_U(\boldsymbol{\lambda}_1). \tag{4.26}$$

However, the tuple $(\boldsymbol{S}_\alpha, \alpha\boldsymbol{\lambda}_1)$ is in $\mathcal{S}_{U_2}$ because $\alpha\boldsymbol{\lambda}_1 \in \Lambda_\alpha$ and α was chosen such that $U(\alpha\boldsymbol{\lambda}_1) = U_2$. Hence for any efficiency that is achieved by a tuple in $\mathcal{S}_{U_1}$ a tuple in $\mathcal{S}_{U_2}$ can be found with at least as large efficiency. This leads to the first result. By following the same proof outline for super-linearly scalable utilities, the $\geq$ in (4.26) is replaced by a $\leq$, yielding the second result. □

The difference between Propositions 4.1 and 4.2 mainly lies in the used sets $\overline{\mathcal{S}}_U$ and $\mathcal{S}_U$. While $\overline{\mathcal{S}}_U$ allows that the efficiency maximizer over-achieves the required utility levels U, for $\mathcal{S}_U$ all utilities need to be exactly achieved. So the result of Proposition 4.2 is the stronger one, as it states that the required efficiency to achieve *exactly* a utility level cannot decrease and the maximum possible cannot increase with the utility level. A special case is again formed by the scale invariant utilities such as weighted sum-throughput or max-min fairness. These are both, super-linearly and sub-linearly scalable at the same time, hence the supremum and infinum rule both apply at the same time.

Propositions 4.1 and 4.2 motivate that as utilities increase, the variety of efficiencies that action sequences may have to realize them narrows down. This view is completed by the property that large enough utility values can only be achieved by a single resource efficiency, which is established in the following.

Lemma 4.1 (Usable Resource Boundedness)**.** Let $\overline{U} = \sup_{\mathcal{S}\times\Lambda} U(\boldsymbol{\lambda}) < \infty$ be a finite, maximum achievable utility over all possible schedule sequences. Then, there is a resource bound $\overline{V} \geq 0$ such that

$$\forall V' \geq \overline{V}, \quad \sup_{\overline{\mathcal{S}}(V')\times\Lambda} U(\boldsymbol{\lambda}) = \overline{U}. \tag{4.27}$$

Proof. Assume that the converse would hold, i.e.,

$$\begin{aligned} &\nexists \overline{V} \geq 0 \text{ s.t. } \forall V' \geq \overline{V}, \quad \sup_{\overline{\mathcal{S}}(V')\times\Lambda} U(\boldsymbol{\lambda}) = \overline{U} \\ \Leftrightarrow \quad &\forall \overline{U} > 0 \;\; \exists V', (\boldsymbol{S}', \boldsymbol{\lambda}') \in \overline{\mathcal{S}}(V'), \text{ s.t. } U(\boldsymbol{\lambda}') > \overline{U}. \end{aligned} \tag{4.28}$$

As result, $\sup_{\mathcal{S}\times\Lambda} U(\boldsymbol{\lambda}) = \infty$, which contradicts the assumption of $\overline{U}$ to be finite. □

The intuition of Lemma 4.1 is that there always is a maximum amount of usable resources. The most intuitive example for such a bound is that there are only finite transmission resources in overall, i.e., each possible action uses only a finite amount in first place. However, other examples would be resources that are not usable due to the topology state, e.g., channels that are in deep fade, which yield zero rate and hence are not reasonably usable by a link. While in this case, it is in principle possible to use such a channel, it would not increase the utility to do so. Another example would be a multi-hop flow with a bottleneck link. Here, the non-bottleneck links cannot fully use all resources in a reasonable manner, as this would simply increase the queue backlog at the bottleneck link but not serve to deliver a larger throughput. Full resource use would then not increase the utility. In light of these considerations, Lemma 4.1 states the existence of an upper resource bound $\overline{V}$, beyond which utility cannot be increased anymore, even if technically, more resources were available.

Proposition 4.3 (Efficiency Limits for Large Utilities)**.** Let $\overline{U} = \sup_{\mathcal{S}\times\Lambda} U(\boldsymbol{\lambda})$ be the maximum achievable utility over all possible schedule sequences and let

$$\overline{V} = \inf\left\{V' : \sup_{\overline{\mathcal{S}}(V')\times\Lambda} U(\boldsymbol{\lambda}) = \overline{U}\right\} \tag{4.29}$$

be the usable resource bound introduced in Lemma 4.1. Then

$$\lim_{U\to\overline{U}} \inf_{\underline{\mathcal{S}}_U\cap\overline{\mathcal{S}}(\overline{V})} \mathrm{RE}^U(\boldsymbol{S},\boldsymbol{\lambda}) = \lim_{U\to\overline{U}} \sup_{\underline{\mathcal{S}}_U\cap\overline{\mathcal{S}}(\overline{V})} \mathrm{RE}^U(\boldsymbol{S},\boldsymbol{\lambda}). \tag{4.30}$$

Proof. Assume $(\boldsymbol{S},\boldsymbol{\lambda})$ such that $\overline{\nu}^{\mathrm{sys}}(\boldsymbol{S}) < \overline{V}$. By the definition of $\overline{V}$ as smallest resource bound to allow utility $\overline{U}$, $U(\boldsymbol{\lambda}) < \overline{U}$ must hold. As consequence

$$\lim_{U\to\overline{U}} \inf_{\underline{\mathcal{S}}_U\cap\overline{\mathcal{S}}(\overline{V})} \overline{\nu}^{\mathrm{sys}}(\boldsymbol{S}) \to \overline{V}. \tag{4.31}$$

This yields

$$\lim_{U\to\overline{U}} \inf_{\underline{\mathcal{S}}_U} \mathrm{RE}^U(\boldsymbol{S},\boldsymbol{\lambda}) = \lim_{U\to\overline{U}} \inf_{\underline{\mathcal{S}}_U} \frac{U(\boldsymbol{\lambda})}{\overline{\nu}^{\mathrm{sys}}(\boldsymbol{S})} = \frac{\overline{U}}{\overline{V}} = \lim_{U\to\overline{U}} \sup_{\underline{\mathcal{S}}_U} \frac{U(\boldsymbol{\lambda})}{\overline{\nu}^{\mathrm{sys}}(\boldsymbol{S})} = \lim_{U\to\overline{U}} \sup_{\underline{\mathcal{S}}_U} \mathrm{RE}^U(\boldsymbol{S},\boldsymbol{\lambda}).$$

□

In words, Proposition 4.3 states that when utility values approach the border of the achievable, assuming that resources are used only in a "reasonable" manner in the sense of Lemma 4.1, such that only resources are used which can actually increase the utility, then all sequences realizing the demanded utility achieve the same resource efficiency. As corollary, the only reason why an action sequence should achieve the maximum achievable utility and not the given resource efficiency would be that it uses resources which do not contribute towards a utility increase.

The combination of the presented propositions gives the following view on the relation between utility levels, usable resources and their efficiency, which is illustrated in Figure 4.5: For any achievable utility target, there is not one sequence but a possibly unbounded set of infinite time-horizon action sequences that can achieve it. In contrast to the cardinality of this set of sequences, the set of resource efficiencies that can be attained while achieving a utility target is bounded. The larger the utility values become, the more resources are required to achieve them, thus the set of available sequences decreases in size. Due to this decrease, the infinum of required efficiency to achieve a utility level increases and the supremum of achievable efficiency decreases with the level. At the maximum achievable utility level, all resources are needed to attain it and thus the set of achievable efficiency values diminishes to a single point.

The properties are shown in Figure 4.5 for the rate-resource efficiency and a utility-resource efficiency, where the utility is a sigmoid function shown on the lower left. The sigmoid function has the interesting property that it is super-linearly scalable for small rates

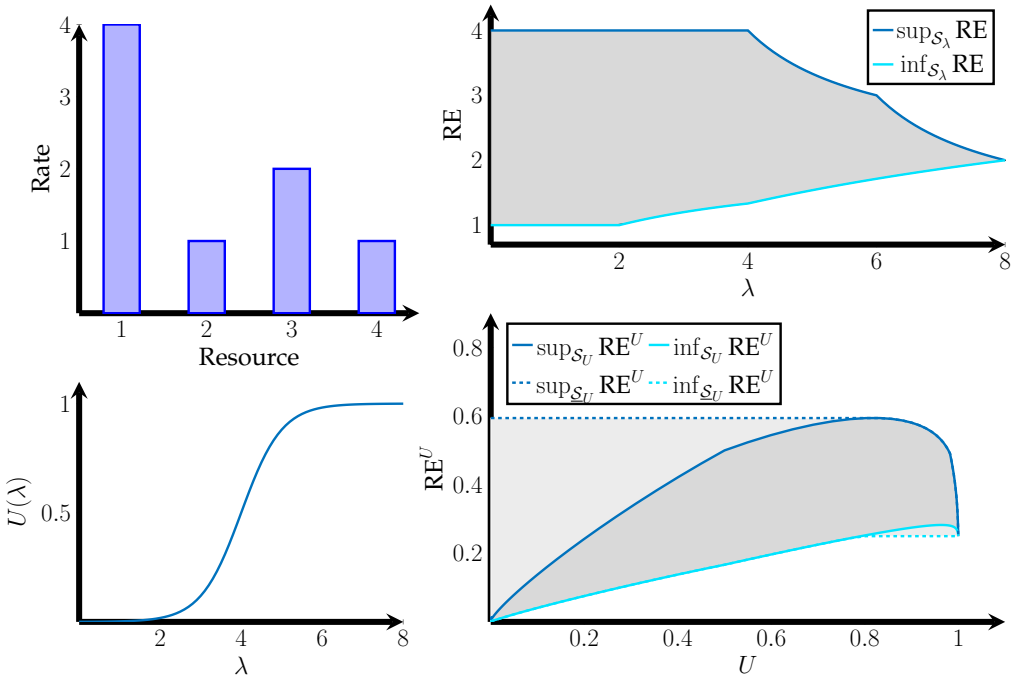

Figure 4.5: Example for previously proven results. The upper left shows usage efficiencies of four different transmission resources and on the lower left the considered sigmoid utility function is depicted. On the right, upper bound and lower bound for rate-resource efficiencies and utility-resource efficiencies is shown.

and sub-linearly scalable for large rates. For resources and achievable rates, the same structure as in Figure 4.4 is assumed and shown on the upper left. The upper right graph shows an upper and lower bound on the rate-resource efficiency. As the rate is scale-invariant and thus both, super-linearly and sub-linearly scalable, the strong laws of Proposition 4.2 hold for all inputs. On the lower right graph, upper and lower bound on the utility-resource efficiencies in set $\mathcal{S}_U$ is given in solid lines, whereas the upper and lower bound on $\underline{\mathcal{S}}_U$ are given in dashed lines. As the sigmoid function is super-linearly scalable below a rate of 4.7, that yields a utility of 0.8, the strong law holds for the lower bound up to this value. Above a rate of 4.7, for a utility larger than 0.8, the sigmoid function is sub-linearly scalable and hence the strong law holds for the upper bound. In the regions where the strong law does not hold, the dashed lines indicated that still the weak laws hold. The intuition behind the weak laws is that to achieve a utility of, e.g., at least $U \geq 0.5$, the largest achievable efficiency would be attained by targeting a utility of 0.8. Correspondingly, the lowest efficiency possible to achieve a utility of at least $U \geq 0.9$ would be to target a utility of 1. For both, rate and utility based efficiency, the upper and lower bound fall together for the maximum attainable utility value. The reason is that at this point, simply all resources need to be used, so there is only one achievable efficiency value in first place.

4.4.4 Ways to Maximize Resource Efficiency

The results of section 4.4.3 motivate that utility maximizing schedulers are not automatically suitable to achieve a large resource efficiency, as they aim at realizing a utility of maximal

value $\overline{U}$ while neglecting the associated resource use. For lower utility targets, more efficient sequences might be available but not employed by the scheduler, for the simple reason that the realized sequence achieves the utility target as well. An example for such a case would be a throughput maximizing scheduler that serves a single traffic flow with bursty, but low admission rate. Instead of delaying the flow service to efficiently use only strong channels, the scheduler will probably assign as many resources as possible to the flow after its burst, to maximize the throughput. These resources, however, may also contain some with low quality, as long as they are available and help to increase the instantaneous throughput, which results in a worse resource efficiency.

It has been argued that the D2D-gains are equivalent to an increase in a system resource efficiency. However, improperly designed schedulers might not be able to leverage the gains if they do not schedule efficiently. This might lead to the effect that even though communication mode is chosen to enable good, efficient communication, the employed schedulers are unable to leverage this quality increase. Thus, in this section ways to leverage resource efficiency are explored. The target is to find ways to dynamically create resource efficient sequences and is achieved by establishing two properties. Consider the set $\mathcal{S}^*_{\text{RE}}$ defined in section 4.4.1, which contains all tuples of action sequences and flow variables that achieve maximal resource efficiency for a given utility $U(\boldsymbol{\lambda})$.

Proposition 4.4 (Efficiency by Resource Minimization)**.** Let $(\boldsymbol{S}^*, \boldsymbol{\lambda}^*) \in \mathcal{S}^*_{\text{RE}}$, $U^* = U(\boldsymbol{\lambda}^*)$ and

$$(\boldsymbol{S}^*_V, \boldsymbol{\lambda}^*_V) = \arg \min_{\boldsymbol{S}\in\mathcal{S},\boldsymbol{\lambda}\in\Lambda} \overline{\nu}^{\text{sys}}(\boldsymbol{S}) \quad \text{s.t.} \quad U(\boldsymbol{\lambda}) \geq U^*. \tag{4.32}$$

Then $(\boldsymbol{S}^*_V, \boldsymbol{\lambda}^*_V) \in \mathcal{S}^*_{\text{RE}}$, i.e., $(\boldsymbol{S}^*_V, \boldsymbol{\lambda}^*_V)$ maximizes the resource efficiency over $\mathcal{S}$.

Proof. First, observe that the minimization in fact is over the set $\underline{\mathcal{S}}_{U^*}$ and that $(\boldsymbol{S}^*, \boldsymbol{\lambda}^*)$, from which U^* is derived, is both in $\underline{\mathcal{S}}_{U^*}$ and $\mathcal{S}_{U^*}$. Correspondingly, $\underline{\mathcal{S}}_{U^*} \supseteq \mathcal{S}_{U^*}$ contains a global efficiency maximizer and any efficiency maximizer among $\underline{\mathcal{S}}_{U^*}$ must also be in $\mathcal{S}^*_{\text{RE}}$. Further, for all $(\boldsymbol{S}, \boldsymbol{\lambda}) \in \underline{\mathcal{S}}_{U^*}$ for which $U(\boldsymbol{\lambda}) > U^*$ holds, $\overline{\nu}^{\text{sys}}(\boldsymbol{S}) > \overline{\nu}^{\text{sys}}(\boldsymbol{S}^*)$ must hold. Otherwise, if $\overline{\nu}^{\text{sys}}(\boldsymbol{S}) \leq \overline{\nu}^{\text{sys}}(\boldsymbol{S}^*)$ would hold,

$$\text{RE}^U(\boldsymbol{S}, \boldsymbol{\lambda}) = \frac{U(\boldsymbol{\lambda})}{\overline{\nu}^{\text{sys}}(\boldsymbol{S})} > \frac{U(\boldsymbol{\lambda}^*)}{\overline{\nu}^{\text{sys}}(\boldsymbol{S})} \geq \frac{U(\boldsymbol{\lambda}^*)}{\overline{\nu}^{\text{sys}}(\boldsymbol{S}^*)} = \text{RE}^U(\boldsymbol{S}^*, \boldsymbol{\lambda}^*), \tag{4.33}$$

which is impossible due to the definition of $(\boldsymbol{S}^*, \boldsymbol{\lambda}^*)$ as global efficiency maximizer. Because $(\boldsymbol{S}^*, \boldsymbol{\lambda}^*)$ is in the optimization domain $\underline{\mathcal{S}}_{U^*}$ of (4.32) and has a resource usage of $\overline{\nu}^{\text{sys}}(\boldsymbol{S}^*)$, a solution with $\overline{\nu}^{\text{sys}}(\boldsymbol{S}) > \overline{\nu}^{\text{sys}}(\boldsymbol{S}^*)$ must be sub-optimal to problem (4.32), which targets minimizing resources. Because $U(\boldsymbol{\lambda}) > U^*$ leads to $\overline{\nu}^{\text{sys}}(\boldsymbol{S}) > \overline{\nu}^{\text{sys}}(\boldsymbol{S}^*)$, the solution to (4.32) must yield $U(\boldsymbol{\lambda}^*_V) = U^*$, i.e., $(\boldsymbol{S}^*_V, \boldsymbol{\lambda}^*_V) \in \mathcal{S}_{U^*}$. However, the efficiency maximizer among all $\mathcal{S}_{U^*}$ is the tuple that achieves minimal $\overline{\nu}^{\text{sys}}(\boldsymbol{S})$, as all achieved utilities in the set are equal. Hence is achieved by $(\boldsymbol{S}^*_V, \boldsymbol{\lambda}^*_V)$. □

The intuitive explanation of Proposition 4.4 is that the maximum efficiency can be achieved by minimizing resources with minimum utility constraints, if the utility targets are well defined. Similarly can be done the reverse way:

Proposition 4.5 (Efficiency by Utility Maximization)**.** Let $(\boldsymbol{S}^*, \boldsymbol{\lambda}^*) \in \mathcal{S}^*_{\text{RE}}$, $V^* = \overline{\nu}^{\text{sys}}(\boldsymbol{S}^*)$ and

$$(\boldsymbol{S}^*_U, \boldsymbol{\lambda}^*_U) = \arg \max_{\boldsymbol{S} \in \mathcal{S}, \boldsymbol{\lambda} \in \Lambda} U(\boldsymbol{\lambda}) \quad \text{s.t.} \quad \overline{\nu}^{\text{sys}}(\boldsymbol{S}) \leq V^*. \tag{4.34}$$

Then $(\boldsymbol{S}^*_U, \boldsymbol{\lambda}^*_U) \in \mathcal{S}^*_{\text{RE}}$, i.e., $(\boldsymbol{S}^*_U, \boldsymbol{\lambda}^*_U)$ maximizes the resource efficiency over $\mathcal{S}$.

Proof. First, observe that the maximization in fact is over the set $\overline{\mathcal{S}}_{V^*}$ and that $(\boldsymbol{S}^*, \boldsymbol{\lambda}^*)$, from which V^* is derived, is both in $\overline{\mathcal{S}}_{V^*}$ and $\mathcal{S}_{V^*}$. Correspondingly, $\overline{\mathcal{S}}_{V^*}$ contains a global efficiency maximizer and any efficiency maximizer among $\overline{\mathcal{S}}_{V^*}$ must also be in $\mathcal{S}^*_{\text{RE}}$. Further, for all $(\boldsymbol{S}, \boldsymbol{\lambda}) \in \overline{\mathcal{S}}_{V^*}$ for which $\overline{\nu}^{\text{sys}}(\boldsymbol{S}) < V^*$ holds, $U(\boldsymbol{\lambda}) < U(\boldsymbol{\lambda}^*)$ must hold. Otherwise, if $U(\boldsymbol{\lambda}) \geq U(\boldsymbol{\lambda}^*)$ would hold,

$$\text{RE}^U(\boldsymbol{S}, \boldsymbol{\lambda}) = \frac{U(\boldsymbol{\lambda})}{\overline{\nu}^{\text{sys}}(\boldsymbol{S})} \geq \frac{U(\boldsymbol{\lambda}^*)}{\overline{\nu}^{\text{sys}}(\boldsymbol{S})} > \frac{U(\boldsymbol{\lambda}^*)}{\overline{\nu}^{\text{sys}}(\boldsymbol{S}^*)} = \text{RE}^U(\boldsymbol{S}^*, \boldsymbol{\lambda}^*), \tag{4.35}$$

which is impossible due to the definition of $(\boldsymbol{S}^*, \boldsymbol{\lambda}^*)$ as global efficiency maximizer. Because $(\boldsymbol{S}^*, \boldsymbol{\lambda}^*)$ is in the optimization domain $\overline{\mathcal{S}}_{V^*}$ of (4.34) and achieves a utility of $U(\boldsymbol{\lambda}^*)$, any solution with $U(\boldsymbol{\lambda}) < U(\boldsymbol{\lambda}^*)$ must be sub-optimal to problem (4.34), which targets maximizing utility. Because $\overline{\nu}^{\text{sys}}(\boldsymbol{S}) < V^*$ leads to $U(\boldsymbol{\lambda}) < U(\boldsymbol{\lambda}^*)$, solution to (4.34) must satisfy $\overline{\nu}^{\text{sys}}(\boldsymbol{\lambda}^*_U) = V^*$, i.e., $(\boldsymbol{S}^*_U, \boldsymbol{\lambda}^*_U) \in \mathcal{S}_{V^*}$. However, the efficiency maximizer among all $\mathcal{S}_{V^*}$ is the tuple that achieves maximal $U(\boldsymbol{\lambda})$, as all used resources in the set are equal. Hence is achieved by $(\boldsymbol{S}^*_U, \boldsymbol{\lambda}^*_U)$. □

Analog to Proposition 4.4, Proposition 4.5 shows that utility maximizing schedulers are to some extent suitable to create resource efficiency, as long as the resources are bounded to a correct value. Both propositions can be summarized in the following corollary:

Corollary 4.1 (Max-Min Characterization of Resource Efficient Points)**.** Consider any tuple $(\boldsymbol{S}^*, \boldsymbol{\lambda}^*) \in \mathcal{S}^*_{\text{RE}}$. Then, $(\boldsymbol{S}^*, \boldsymbol{\lambda}^*)$ is a solution to both,

$$\min_{\boldsymbol{S} \in \mathcal{S}, \boldsymbol{\lambda} \in \Lambda} \overline{\nu}^{\text{sys}}(\boldsymbol{S}) \quad \text{s.t.} \quad U(\boldsymbol{\lambda}) \geq U^* = U(\boldsymbol{\lambda}^*) \text{ and} \tag{4.36}$$

$$\max_{\boldsymbol{S} \in \mathcal{S}, \boldsymbol{\lambda} \in \Lambda} U(\boldsymbol{\lambda}) \quad \text{s.t.} \quad \overline{\nu}^{\text{sys}}(\boldsymbol{S}) \leq V^* = \overline{\nu}^{\text{sys}}(\boldsymbol{S}^*). \tag{4.37}$$

The impact of these insights on resource efficient scheduling is given in the following Section.

4.4.5 Resource Efficient Scheduling

Although utility maximizing schedulers are not in general suitable to maximize resource efficiency, the results from the previous section suggest a way how they can be leveraged to do so by posing the right utility constraints U^* or resource constraints V^*. However, the determination of U^* and V^* pose a challenge in itself, as both denote the optimal choice of utility or resource constraint. While the full evaluation of ways to identify U^* or V^* is out of the scope of this work, two particular special cases shall be investigated, for which their determination is possible.

4.4.5.1 Elastic Traffic Demands

The first special case is one where all traffic sources create elastic traffic. While traffic "elasticity" is not concisely defined with respect to mathematics, it is often claimed to hold for TCP traffic, which dynamically adapts to the available throughput to transport as much data as possible. To comply with this notion, in this thesis traffic is considered elastic if the admission control generates a traffic vector $\boldsymbol{\lambda} \in \partial\Lambda_\pi$, that is at the border of the schedulers' stability region, which is defined as

$$\partial\Lambda_\pi = \{\boldsymbol{\lambda} \in \Lambda_\pi : \nexists \boldsymbol{\lambda}' \in \Lambda_\pi \text{ with } \boldsymbol{\lambda}' \neq \boldsymbol{\lambda},\ \ \boldsymbol{\lambda}' \geq \boldsymbol{\lambda}\}. \tag{4.38}$$

Elastic traffic then adapts itself towards a point in $\partial\Lambda_\pi$, by adapting to the available throughput rate and increasing the throughput as much as possible. For such policies, the following can be argued:

Lemma 4.2. Assume any two $(\boldsymbol{S}_1, \boldsymbol{\lambda}_1), (\boldsymbol{S}_2, \boldsymbol{\lambda}_2) \in \mathcal{S} \times \Lambda$ and $\boldsymbol{\lambda}_1, \boldsymbol{\lambda}_2 \in \partial\Lambda_\pi$ for a given scheduler π. Then $\overline{\nu}^{\text{sys}}(\boldsymbol{S}_1) = \overline{\nu}^{\text{sys}}(\boldsymbol{S}_2)$.

Proof. Without loss of generality, assume that $\overline{\nu}^{\text{sys}}(\boldsymbol{S}_1) < \overline{\nu}^{\text{sys}}(\boldsymbol{S}_2)$. Then, as it the network supports the use of $\overline{\nu}^{\text{sys}}(\boldsymbol{S}_2)$ resources, a sequence $\boldsymbol{S}_1'$ can be created with $\overline{\nu}^{\text{sys}}(\boldsymbol{S}_1') > \overline{\nu}^{\text{sys}}(\boldsymbol{S}_1)$, allowing for a feasible vector $\boldsymbol{\lambda}_1' \neq \boldsymbol{\lambda}_1$, $\boldsymbol{\lambda}_1' \geq \boldsymbol{\lambda}_1$. Hence, $\boldsymbol{\lambda}_1 \notin \partial\Lambda_\pi$, which leads to a contradiction on the assumption. □

The use of this Lemma allows the establishment of:

Proposition 4.6 (Efficiency Maximization for Elastic Traffic)**.** Assume a utility $U(\boldsymbol{\lambda})$ that is strictly increasing with $\boldsymbol{\lambda}$ and consider the problem

$$\max_{\boldsymbol{\lambda} \in \Lambda_\pi} U(\boldsymbol{\lambda}). \tag{4.39}$$

Then any $(\boldsymbol{S}, \boldsymbol{\lambda}) \in \mathcal{S} \times \Lambda$ solving (4.39) optimally also solves the problem

$$\max_{\mathcal{S} \times \Lambda} \text{RE}^U(\boldsymbol{S}, \boldsymbol{\lambda}) \text{ s.t. } \boldsymbol{\lambda} \in \partial\Lambda_\pi. \tag{4.40}$$

Proof. Because $U(\boldsymbol{\lambda})$ is strictly increasing with $\boldsymbol{\lambda}$, the optimal solution $\boldsymbol{\lambda}^*$ to (4.39) must be in $\partial\Lambda_\pi$, otherwise there were a feasible $\boldsymbol{\lambda}' \neq \boldsymbol{\lambda}^*$, $\boldsymbol{\lambda}' \geq \boldsymbol{\lambda}^*$ leading to $U(\boldsymbol{\lambda}') > U(\boldsymbol{\lambda}^*)$. On the other hand, according to Lemma 4.2 the resources required to realize any throughput in $\partial\Lambda_\pi$ is equal. As result, the solution to (4.40) is achieved by simply maximizing $U(\boldsymbol{\lambda})$ over $\partial\Lambda_\pi$, i.e., must also solve (4.39). □

Proposition 4.6 creates an important intuition for elastic traffic. It can be assumed that transport-layer admission control is often agnostic to the underlying network, as it is done in an end-to-end fashion. If such admission control creates elastic traffic, i.e., will result in a throughput at the border of the feasible region, then the remaining degrees of freedom only lie in the actual trade-off point on the border that is chosen. In this case, utility maximization will also lead to an optimal resource efficiency. The most important example for elastic traffic generation are TCP protocols, which in fact are used in the majority of networks.

4.4.5.2 Static Traffic Demands

Static traffic considers cases when the transmission data of a flow is produced at a constant rate. In this case, providing more throughput to the flow than it produces does not provide any benefit, as the increased throughput cannot be leveraged. On the other hand, many constant bit-rate cases require that the throughput is fully served to achieve a satisfactory performance. Consider a network with only constant bit-rate traffic of $\overline{\boldsymbol{\lambda}}$. Then, for a $C > 0$ the associated utility can be formulated as

$$U(\boldsymbol{\lambda}) = \begin{cases} C & \text{if } \boldsymbol{\lambda} \geq \overline{\boldsymbol{\lambda}}, \\ -\infty & \text{otherwise.} \end{cases} \tag{4.41}$$

For such a utility, it is easy to argue the following:

Proposition 4.7 (Efficiency Maximization for Static Traffic)**.** Consider a utility $U(\boldsymbol{\lambda})$ according to (4.41) and assume that the network can serve $\overline{\boldsymbol{\lambda}}$. Then, efficiency is maximized by solving

$$\min_{\mathcal{S}\times\Lambda} \overline{\nu}^{\text{sys}}(\boldsymbol{S}) \quad \text{s.t.} \quad U(\boldsymbol{\lambda}) \geq C. \tag{4.42}$$

Proof. Any solution with $U(\boldsymbol{\lambda}) < C$ has an efficiency value of minus infinity and hence cannot be optimal. On the other hand, as any feasible solution creates the same utility C, this utility must also be the optimal utility according to Proposition 4.4. □

As result, for constant bit-rate traffic, efficiency is maximized by searching for the minimum amount of resources required to serve all data rates.

4.5 Lessons Learned for D2D

The insights gained throughout this chapter can be summarized in a few key statements.

First, it was argued that the D2D-gains cannot directly be captured with sum-rate or sum-throughput metrics, which are generally used by respective literature, as these neglect the hop-and reuse gain. It was argued in an intuitive fashion that a resource-efficiency metric is more appropriate. A formal resource-efficiency metric was developed from very basic notion of transmission resources, by introducing a mathematical measure to capture an amount of used resources and combining this with the concept of achievable throughput and stability regions. It was shown that indeed, by formulating the efficiency increase introduced by D2D-communication, the three gain types proximity-gain, hop-gain and reuse-gain can be re-motivated.

As no knowledge on utility-resource metrics was present in literature, fundamental properties were derived on how efficiency scales with different utility function types. The resulting interpretation was that each utility target can be realized by a multitude of possible action sequences, with different resource efficiencies. However, for increasing utility demands, the lowest required resource efficiency tends to increase, whereas the maximum achievable

tends to decrease. This effect maximizes at the largest feasible utility target, which can be achieved only with a single resource efficiency.

Further, possibilities to maximize resource efficiency were investigated, yielding the result that it can be done by resource minimization with utility constraints or utility maximization with resource constraints, as long as the constraints are chosen correctly. Using these results, arguments for correct D2D management under different system assumptions can be made:

(1) Assume a network with elastic traffic demands, where the admission of flows is dynamically increased to maximize a certain utility that is strictly increasing with rate. It is known that such traffic types operate at the border of the transport region, as any traffic within the interior has a point on the border with larger utility. It was shown that for such traffic, the used resources always remain the same, as any freed resources will simply create a larger demand. In such a system there is no hop-gain and consequently, resource efficiency maximization equals utility maximization. The best-known example for elastic traffic is TCP traffic, which refers to a widely used set of congestion control algorithms.

(2) Consider a network with constant bit-rate traffic, where all flows only inject a limited, fixed amount of data. If the injected traffic rates are in the transport region, all of the data will be delivered to the receivers. In this case, the achieved utility will remain the same for all different mode choices for which the rates are in the transport region. Hence, there is no proximity-gain and consequently, utility maximization does not serve to leverage the D2D-gain. In this case, efficiency maximization is achieved by resource use minimization.

It must thus be argued that while network utility maximization can indeed help to increase resource efficiency and provide a D2D-gain, this is not the case in general, with the most prominent counter-example being constant bit-rate traffic. The results of this chapter can directly be used to motivate two types of mode selection problems. In the first, the communication modes should be found such that an achievable network utility is maximized. The second considers mode selection such that the required resources to serve all flows are minimized.

Chapter 5

Mode Selection Strategies

In this chapter, mode selection strategies are developed to decide, which communication flows should use the sidelink option and which should use cellular links. Following the insights of Chapter 4, by which utility maximization is not always a good option, two schemes are developed, one based on resource efficiency and one on network utility maximization (NUM). The resource efficiency based mode selection has been published in [5], while the utility based mode selection is novel. Both proposed solutions use the MAC scheduling model, which has been introduced in 2.1.3.

Mode selection is a core aspect in D2D-enabled cellular networks. It considers the question, by which communication mode a certain flow should be realized in the cellular network. In general, there are three possible modes: (1) The cellular mode (CM), in which a flow uses the uplink and downlink hop, i.e., is relayed by the base station. (2) The dedicated direct mode (DM). Here, the communication is direct but uses dedicated transmission resources. (3) The D2D Reuse Mode (RM), sometimes also shared mode, is a direct communication where resources are allowed to be reused within a cell. The DM is also referred to as *overlay* D2D, whereas the RM is known as *underlay*.

A typical mode selection scenario is illustrated in Figure 5.1: Several UEs are present in a network cell, with traffic demands among them. The data transport is coordinated by a scheduler that runs on the BS and coordinates transmissions among MAC layer links. In this set-up, a mode selection strategy is to be developed, i.e., a function that decides for each flow the mode by which it will be realized. In principle, the decision of CM versus DM can be seen as a routing problem, because the flow will either be routed directly from source to destination of the flow or through the infrastructure node. The decision of DM versus RM, on the other hand, is a scheduling problem that depends on interference properties in the network. In particular, a sidelink could also only partly reuse resources of another link, whereas other resources are reused from a third link or in an overlay fashion. In this case, the link would only partly be in RM and partly in DM.

State of Research

In literature, a large variety of use cases and mode combinations are considered, which are well summarized in [49]. According to this survey, the major part of research is dedicated

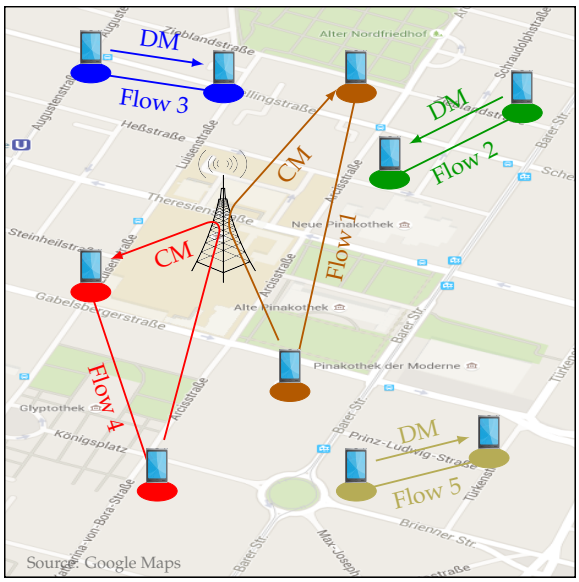

Figure 5.1: Example setup of the overlay D2D mode selection problem. Flows between UEs occur in the cell, indicated by connected circles. The eNodeB needs to decide which flows use the CM and which the DM.

to static mode selection, which is decided on a slow time-scale. Only few works [126], [127] consider dynamic mode selection, which is at the time scale of scheduling decisions. Decision strategies take into account the path-loss [128], spatial distances among nodes and BSs [129], [130], channel qualities [131]–[134] and mutual interference [114], [115], among others.

The considered scenarios found in literature typically vary, and so do the made system assumptions. For example, the authors of [115] assume a Wideband Code Division Multiple Access (WCDMA) system, where all links interfere. Mode selection can then be performed similar to interference aware BS association [76]. In contrast, the work in [114] assumes an LTE like transmission structure, further that both UEs of the sidelink have the same distance to the BS and a fixed distance among each other, and that the cellular mode uses the same resources as the side-link, split into uplink and downlink by equal parts. Clearly, both methods cannot be compared already due to the used system model. Even worse, the provided methods depend much on the strong assumptions and are hardly applicable when they change.

Nevertheless, some approaches re-appear across different works and thus can be generalized. A number of works target maximizing the capacity of each offloaded link unilaterally [114], [130], whereas others intuitively take account for the hop-gain [119], [120], which is typically assumed to be 0.5. Further, for comparison it is often considered to force all links into cellular mode or direct mode [119], [130], [135].

For distance based mode selection schemes, a general variant has been proposed in [130], [136]. Here, a general distance-based mode selection is considered, with tunable distance threshold. Links are then offloaded to DM whenever their distance is smaller than the threshold. It is argued that this strategy is also comparable to link gain based schemes, as the expected link gain deterministically depends on the distance.

In this thesis, a similar generalization approach is taken for rate-based mode selection

schemes. Assume that the maximum achievable long-term average rate over the sidelink, uplink and downlink are $\overline{R}^*_{\mathrm{SL}}$, $\overline{R}^*_{\mathrm{UL}}$ and $\overline{R}^*_{\mathrm{DL}}$, respectively. Observe that the achievable long-term average throughput in cellular mode is the minimum of the uplink and downlink rate. Then, define the general mode selection strategy as:

Mode Selection 5.1 (General Mode Selection (G-MS))**.** Choose DM, if

$$\overline{R}^*_{\mathrm{SL}} > \alpha \cdot \min\{\overline{R}^*_{\mathrm{UL}}, \overline{R}^*_{\mathrm{DL}}\} \tag{5.1}$$

for a fixed $\alpha \geq 0$. Else, choose CM.

The right hand side of the scheme is the achievable throughput in cellular mode, whereas the left is the achievable throughput in direct mode. Many mode selection schemes found in literature take the form of Mode Selection 5.1. For $\alpha = 0$, DM is chosen whenever there is a connectivity over the SL. This is typically referred to as the *ForceD2D* scheme [119], [130], [135]. When $\alpha \to \infty$, DM will never be chosen, which is the *ForceCellular* scheme [119], [130], [135]. With $\alpha = 1$, DM is chosen whenever the D2D throughput is larger than the cellular link throughput, which is called the *Capacity* scheme [114], [130]. When the CM throughput is corrected to be half of the cellular capacity to account for the hop-gain [119], [120], which is related to as the *Rate* scheme, $\alpha = 0.5$.

While this general mode selection scheme does not entirely match any of the solutions proposed in literature, it comes very close. Considering the difference in assumed system models, it must thus be considered a good exemplary scheme that can be re-applied depending on the differing, exact system set-up.

5.1 Resource Efficiency Based Mode Selection

In Chapter 4 it was motivated that the proximity-, hop- and reuse-gain can be captured by a flow-based resource efficiency metric. This metric thus gives a concrete analytical measure for Fodors' gains and has an immediate impact on mode selection, which is leveraged in this section. A mode selection strategy is developed which chooses the DM if the D2D-Gain is estimated to be larger than one and the CM otherwise. The accuracy of estimation is investigated and the scheme is thoroughly evaluated with simulations.

The aim of the considered mode selection is to maximize the resource efficiency for D2D communication with constant bit-rate traffic. It has been argued in Chapter 4 that especially in this case, utility maximization cannot properly leverage the direct link option, as it does not consider resource use. Because tractable ways for interference management were not available at the time of development, it assumes an overlay D2D communication scenario.

From the resource efficiency discussion in Chapter 4, DM should be chosen only when it creates a larger system-wide resource efficiency than the CM. Formally, for each flow the choice is between the cellular path represented by the routing link set $\mathcal{L}^{\mathrm{C}}_c$, which contains one uplink and one downlink hop, and the direct path $\mathcal{L}^{\mathrm{D}}_c$, which contains one direct hop only. All per-flow link sets are combined into an overall link set $\mathcal{L}_{\mathcal{K}} = \{\mathcal{L}_1, ..., \mathcal{L}_K\} \in \mathcal{L}^{\mathrm{MS}} =$

$\prod_{c\in\mathcal{K}} \mathcal{L}_c$, where $\mathcal{L}_c = \{\mathcal{L}_c^{\mathrm{C}}, \mathcal{L}_c^{\mathrm{D}}\}$. The abstracted definition of the mode selection problem is:

$$\text{(MS)} \quad \max_{\mathcal{L}_\mathcal{K}\in\mathcal{L}^{\mathrm{MS}}} \mathrm{RE}_{\mathcal{L}_\mathcal{K}}(\boldsymbol{S}). \tag{5.2}$$

That is, the MS problem considers for a given, infinite time-horizon schedule sequence $\boldsymbol{S}$, which route among $\{\mathcal{L}_c^{\mathrm{C}}, \mathcal{L}_c^{\mathrm{D}}\}$ each flow should use to maximize the expected value of the rate based resource efficiency. Although the formulation of the problem is short, it has a complex inherent structure. First, it depends on the used scheduling sequence, which is often dynamically produced depending on channel and queue evolution and hence must be considered unknown. Second, there is a mutual dependency among chosen communication modes, i.e., the set $\mathcal{L}_\mathcal{K}$, and the schedule sequence $\boldsymbol{S}$, which creates resource efficiencies that are hard to predict.

5.1.1 Problem Assessment

To make the MS problem more tractable, some reformulations are done. First, observe that the reuse factor $\overline{\kappa}(\mathcal{L}, \boldsymbol{S}) = 1$ because the overlay case is considered, leading to $\overline{\nu}^{\mathrm{eff}}(\mathcal{L}, \boldsymbol{S}) = \overline{\nu}^{\mathrm{sys}}(\mathcal{L}, \boldsymbol{S})$, respectively. By using the notion of per-flow resources $\overline{\nu}_c(\boldsymbol{S})$, which was introduced in (4.12) and associates a transport-layer flow with a number of used resources, and using the equality $\overline{\nu}^{\mathrm{eff}}(\mathcal{L}, \boldsymbol{S}) = \sum_c \overline{\nu}_c(\boldsymbol{S})$, the resulting expression for resource efficiency can be expressed per flow c:

$$\mathrm{RE}_{\mathcal{L}}(\boldsymbol{S}) = \frac{\sum_{c\in\mathcal{K}} \lambda_c}{\overline{\nu}^{\mathrm{sys}}(\mathcal{L}, \boldsymbol{S})} = \frac{\sum_{c\in\mathcal{K}} \lambda_c}{\overline{\nu}^{\mathrm{eff}}(\mathcal{L}, \boldsymbol{S})} = \frac{\sum_{c\in\mathcal{K}} \lambda_c}{\sum_{c'\neq c} \overline{\nu}_{c'}(\boldsymbol{S}) + \overline{\nu}_c(\boldsymbol{S})}. \tag{5.3}$$

As the expected admission rates λ_c are assumed fixed, they do not change with a mode switch and induce a proximity-gain of $G_P = 1$. In addition to the reuse-gain being $G_R = 1$ for the considered overlay case, the only remaining gain dimension here is the hop-gain.

From (5.3) it is clear that for fixed λ_c, maximizing the efficiency breaks down to reducing the average resource use per flow. This reduction is beneficial for the overall resource efficiency and has no trade-offs, as there is no further coupling among links. Due to this, each link can be optimized independently of other links. This is a simple conclusion that, however, is only possible due to the clean definition of a resource use per flow, which has been introduced in Chapter 4. In fact, it is not so clearly visible from an intuitive per-link resource use perspective.

Although the reduction to decisions per single link already reduce complexity significantly, the dynamics of scheduling is still not easy to estimate a priori. Thus, in this section, the behavior will be estimated based on channel measurements and achievable rates. While this is simpler than a full on-line evaluation, it is not clear how well the resource efficiency of a flow can be predicted from the achievable rates, because the dynamics of the scheduler are ignored. Thus, one focus of the presented investigation is to quantify the quality of this prediction.

5.1.2 Proposed Mode Selection

Let $\mathrm{UL}_c, \mathrm{DL}_c, \mathrm{SL}_c \in \mathcal{L}$ denote the uplink, downlink and sidelink of a potential D2D flow c, let $\boldsymbol{Q} = \{\boldsymbol{Q}[0], \boldsymbol{Q}[1], ..., \boldsymbol{Q}[\tau], ...\}$ be an infinite time-horizon topology state process and let $\overline{R}_l^* = \max_{\boldsymbol{A}_i \in \mathcal{A}} \mathrm{E}\{R_l(\boldsymbol{A}_i, \boldsymbol{Q})\}$ be the maximum possible, expected link rate on link $l \in \mathcal{L}$ assuming a single action $\boldsymbol{A}_l^* = \arg\max_{\boldsymbol{A}_i \in \mathcal{A}} \mathrm{E}\{R_l(\boldsymbol{A}_i, \boldsymbol{Q})\}$. $\boldsymbol{A}_l^*$ is, in fact, an exclusive action of a single link l, because overlay communication is considered. Note that $\overline{R}_l^*$ is achieved when l uses all available resources within a frame. Further, let $\mathrm{RE}_l^* = \overline{R}_l^* / \nu_l(\boldsymbol{A}_l^*)$ be the resource efficiency achieved when $\overline{R}_l^*$ is scheduled.

Now consider what throughput and resource efficiencies can be expected in either of the modes. The expected, achievable throughput in direct mode is $\lambda_c^{\mathrm{D}} = \overline{R}_{\mathrm{SL}}^*$. The expected throughput in cellular mode is $\lambda_c^{\mathrm{C}} = \min\{\overline{R}_{\mathrm{UL}}^*, \overline{R}_{\mathrm{DL}}^*\}$. The amount of resources necessary to achieve the both throughputs can be calculated as:

$$\begin{aligned} \overline{\nu}_c^{\mathrm{D}} &= \nu(\boldsymbol{A}_{\mathrm{SL}}^*), \\ \overline{\nu}_c^{\mathrm{C}} &= \overline{\nu}_{\mathrm{UL}} + \overline{\nu}_{\mathrm{DL}} = \lambda_c^{\mathrm{C}} \left(\frac{1}{\mathrm{RE}_{\mathrm{UL}}^*} + \frac{1}{\mathrm{RE}_{\mathrm{DL}}^*} \right). \end{aligned}$$

The resources of the CM are calculated according to equation (4.12). The intuition is that on the CM path, each hop will use only the percentage of resources necessary to achieve λ_c^{C}. In general, as one of UL or DL will be the bottle-neck link, the other one will not need to use all its available resources. For the CM, the downlink hop will typically achieve a much higher rate per resource, due to the larger power of BSs compared to UEs. Thus, in general only few of the used resources reside on downlink bands.

After these introductory considerations, the proposed mode selection scheme is:

Mode Selection 5.2 (*Resource Efficiency* Mode Selection (RE-MS))**.** Choose DM for flow c, if

$$\mathrm{RE}_c^{\mathrm{D}} = \frac{\lambda_c^{\mathrm{D}}}{\overline{\nu}_c^{\mathrm{D}}} > \frac{\lambda_c^{\mathrm{C}}}{\overline{\nu}_c^{\mathrm{C}}} = \mathrm{RE}_c^{\mathrm{C}} \tag{5.4}$$

Else, choose CM.

5.1.3 Analysis of RE-MS

Mode Selection 5.2 does not depend on the used scheduler but performs a rather simple evaluation of link qualities, aiming at resource efficiency maximization. The impact and quality of the RE-MS depends on the used scheduling policy and on its ability to leverage the increased efficiency. In this context, schedulers can be classified by considering whether they leverage resource diversity or not. For this, define $\pi_{l,k}$ to be the relative frequency of frames in which link l is scheduled on PRB_k. Further, let $\overline{r}_{l,k}$ be the average rate with which link l can use PRB_k. Then consider two classes of schedule sequences:

Definition 5.1 (Diversity-leveraging sequences)**.** Assume two PRBs k, m on which link $l \in \mathcal{L}$ achieves the average rates $\overline{r}_{l,k}$, $\overline{r}_{l,m}$. Then, the set of diversity-leveraging sequences is the set of action sequences:

$$\mathcal{S}_L = \{\boldsymbol{S} : \pi_{l,k} > \pi_{l,m} \Leftrightarrow \overline{r}_{l,k} > \overline{r}_{l,m} \ \ \forall k, m \in \mathcal{R}, l \in \mathcal{L}\}.$$

Definition 5.2 (Diversity-agnostic sequences)**.** The set of diversity agnostic sequences is the set of action sequences:

$$\mathcal{S}_A = \{\boldsymbol{S} : \pi_{l,k} = \pi_l \ \ \forall k \in \mathcal{R}, l \in \mathcal{L}\}.$$

With diversity-leveraging schedule sequences, a link will be assigned PRBs with larger efficiency more often than PRBs with lower efficiency. For diversity agnostic schedulers, the PRB allocation is independent of per-resource efficiency. A diversity agnostic schedule sequence would be, e.g., one that assigns an amount of PRBs to links but chooses the exact assigned PRBs randomly. A scheduler is called diversity-leveraging or diversity-agnostic when it generates diversity-leveraging or diversity-agnostic sequences, respectively. The considered schedulers *Maximum C/I* and *Backpressure*, which have been formally introduced in Section 2.1.3, leverage channel diversity and thus produce diversity leveraging sequences. On the other hand, the *Proportional Fair* scheduler can be implemented in a diversity leveraging way but is diversity agnostic in its original definition, which does not consider the channel states per PRB. In this work, it is implemented in a diversity agnostic way to show the impact.

By the definition of diversity agnostic schedulers, and taking into account the definition of sequence scaling from Section 4.4.2, it can be realized that from a per-link perspective, all diversity agnostic sequences behave as scaled versions of each other: For any sequence $\boldsymbol{S}$, it holds that

$$\overline{R}_l = \mathrm{E}\{R_l(\boldsymbol{S}, \boldsymbol{Q})\} = \sum_{k=1}^{K} \pi_{l,k} \overline{r}_{l,k}; \qquad \overline{\nu}_l = \mathrm{E}\{\nu_l(\boldsymbol{S})\} = |\mathrm{PRB}| \sum_{k=1}^{K} \pi_{l,k}, \tag{5.5}$$

where $\overline{r}_{l,k}$ is the expected rate of link l on PRB k. Now assume two sequences $\boldsymbol{S}_1$, $\boldsymbol{S}_2 \in \mathcal{S}_A$ with relative usage frequencies $\pi_l^{(1)}$, $\pi_l^{(2)}$. Then, the produced rates and resource usages behave as:

$$\overline{R}_l^{(2)} = \pi_l^{(2)} \sum_{k \in \mathcal{R}} \overline{r}_{l,k} = \alpha \pi_l^{(1)} \sum_{k \in \mathcal{R}} \overline{r}_{l,k} = \alpha \overline{R}_l^{(1)}, \tag{5.6}$$

$$\overline{\nu}_l^{(2)} = K \cdot \pi_l^{(2)} |\mathrm{PRB}| = \alpha K \cdot \pi_l^{(1)} |\mathrm{PRB}| = \alpha \overline{\nu}_l^{(1)}, \tag{5.7}$$

where $\alpha = \pi_l^{(2)} / \pi_l^{(1)}$. This is exactly the behavior of a scaled scheduling sequence. A consequence is the following corollary:

Corollary 5.1. All sequences $\boldsymbol{S} \in \mathcal{S}_A$ achieve the same resource efficiency over a single link.

Proof. For any $\boldsymbol{S}_1$, $\boldsymbol{S}_2 \in \mathcal{S}_A$ with relative usage frequencies $\pi_l^{(1)}$, $\pi_l^{(2)}$ it holds that

$$\mathrm{RE}_l(\boldsymbol{S}^{(2)}, \boldsymbol{Q}) = \frac{\overline{R}_l^{(2)}}{\overline{\nu}_l^{(2)}} = \frac{\alpha \overline{R}_l^{(1)}}{\alpha \overline{\nu}_l^{(1)}} = \mathrm{RE}_l(\boldsymbol{S}^{(1)}, \boldsymbol{Q}). \tag{5.8}$$

□

By re-considering the proposed mode selection, it becomes clear that it in fact evaluates the resource efficiency of a diversity-agnostic schedule sequence, as it is based on the

constant use of a single action $\boldsymbol{A}_l^*$, leading to a relative frequency of one. Hence, it will correctly estimate the efficiency gain of any diversity-agnostic scheduler and is optimal when used with such schedulers, e.g., when used with the *Proportional Fair* scheduler. The question arises, whether the proposed mode selection is also suitable for use with diversity leveraging schedulers. This is investigated with the following Proposition:

Proposition 5.1 (Leveraging diversity improves efficiency)**.** Let $\boldsymbol{S}_L \in \mathcal{S}_L$ and $\boldsymbol{S}_A \in \mathcal{S}_A$. Then, $\mathrm{RE}(\boldsymbol{S}_L) \geq \mathrm{RE}(\boldsymbol{S}_A)$.

Proof. Consider an arbitrary link l. For any $\boldsymbol{S}_A \in \mathcal{S}_A$, consider a scaled version $\boldsymbol{S}_A^{(\alpha_l)}$ with factor α_l such that $\alpha_l \overline{\nu}_l^A = \overline{\nu}_l^L$. According to (5.5)

$$\sum_{k \in \mathcal{R}} \pi_{l,k}^L = \frac{\overline{\nu}_l^L}{|\mathrm{PRB}|} = \frac{\alpha_l \overline{\nu}_l^A}{|\mathrm{PRB}|} = \sum_{k \in \mathcal{R}} \alpha_l \pi_l^A. \tag{5.9}$$

For the achieved long term rates on l, it follows that

$$\overline{R}_l^L = \sum_{k \in \mathcal{R}} \pi_{l,k}^L \overline{r}_{l,k} \geq \sum_{k \in \mathcal{R}} \alpha_l \pi_l^A \overline{r}_{l,k} = \alpha_l \overline{R}_l^A, \tag{5.10}$$

because both sides can be interpreted as scaled, convex combination of per-PRB rates, the left gives more weight to PRBs with large rates by definition and both, $\pi_{l,k}^L$ and $\alpha_l \pi_{l,k}^A$ sum up to the same value. Combining these two results yields:

$$\mathrm{RE}_l(\boldsymbol{S}_L) = \frac{\overline{R}_l^L}{|\mathrm{PRB}| \sum\limits_{k \in \mathcal{R}} \pi_{l,k}^L} \geq \frac{\alpha_l \overline{R}_l^A}{\alpha_l |\mathrm{PRB}| \sum\limits_{k \in \mathcal{R}} \pi_l^A} = \mathrm{RE}_l(\boldsymbol{S}_A). \ \forall l \in \mathcal{L} \tag{5.11}$$

For traffic demands that are within the stability regions of both, $\boldsymbol{S}_L$ and $\boldsymbol{S}_A$, the transported traffic over a link is given as $\overline{R}_l^L = \sum_{c: l \in \mathcal{L}_c} \lambda_c = \overline{R}_l^A$. The higher efficiency of $\boldsymbol{S}_L$ thus must be due to less resource use:

$$\overline{\nu}_l^L = \frac{\overline{R}_l^L}{\mathrm{RE}_l(\boldsymbol{S}_L)} \leq \frac{\overline{R}_l^A}{\mathrm{RE}_l(\boldsymbol{S}_A)} = \overline{\nu}_l^A. \ \forall l \in \mathcal{L} \tag{5.12}$$

As the result holds for any link $l \in \mathcal{L}$, $\boldsymbol{S}_L$ will use less resources on each single link of the network while achieving the same rates, hence $\mathrm{RE}(\boldsymbol{S}_L) \geq \mathrm{RE}(\boldsymbol{S}_A)$ must hold. □

Proposition 5.1 states that the efficiency of any diversity-leveraging scheduler is lower bounded by that of any diversity-agnostic scheduler. Equality among the resource efficiencies holds when there is no channel diversity to be leveraged, i.e., when $\overline{r}_{l,k} = \overline{r}_l$ $\forall k \in \mathcal{R}, l \in \mathcal{L}$, as then equality holds for equation (5.10). Since the lower bound will be achieved in this case, the bound is tight. For traffic demands outside the stability region, schedulers will choose a point on its boundary according to their designed utility target [83]. In this case the realized long term rates per link might differ for different schedulers and hence the previous argumentation does not hold any more. Proposition 5.1 proves that although *Resource Efficiency* Mode Selection assumes a diversity-agnostic scheduler, it also optimizes a tight lower bound of diversity-leveraging schedulers, when operated within their stability region.

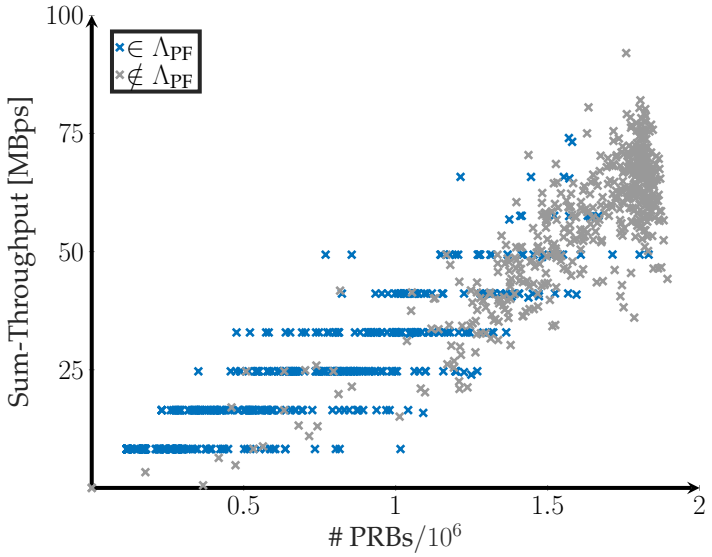

Figure 5.2: Scatterplot of sum-throughput and required PRBs for a Proportional Fair Scheduler and $\lambda = 2000$ kBps.

5.1.4 Simulation

In this section, the interplay of the considered schedulers and mode selection schemes is compared by means of simulation, using the OMNeT++ based framework introduced in Section 2.3.

The simulations consider the single cell overlay D2D set-up illustrated in Figure 5.1. A random number of UE-pairs are deployed in a single cell, whose number and positions follow a poisson point process with density 20 km^{-2}. A data flow, modeled by a video transmission, appears between each of the UE pairs. The eNodeB decides, according to a chosen mode selection scheme, which of the flows will be offloaded to DM and which reside in CM. After all decisions have been made, the transmissions continue for 20 seconds simulation time.

During simulation, the overall number of transmitted byte and the PRB usage are recorded for uplink, downlink and direct links. Each combination of the schedulers *Proportional Fair*, *Maximum C/I* and *Backpressure* with the mode selection schemes *ForceD2D*, *ForceCellular*, *Capacity*, *Rate* and *Resource Efficiency* are simulated. The input data rate used for video transmission at each link are varied from 0.8 kbit/s to 3.2 Mbit/s in exponential steps and for each configuration, 1000 Monte-Carlo runs are performed.

For each run, a value pair of sum-throughput and required resource usage is output. 1000 samples of such pairs are shown in Figure 5.2 for a Proportional Fair Scheduler and an injection rate of $\lambda = 2000$ kBps at all nodes. In the plot, two types of points are shown in blue and gray, respectively. For blue points, the injected traffic is identified to lie within the stability region of the proportional fair scheduler, whereas the queue sizes grow unbounded for gray points, which indicates that they lie outside the stability region.

The blue points appear on regular levels. This is due to the different numbers of users

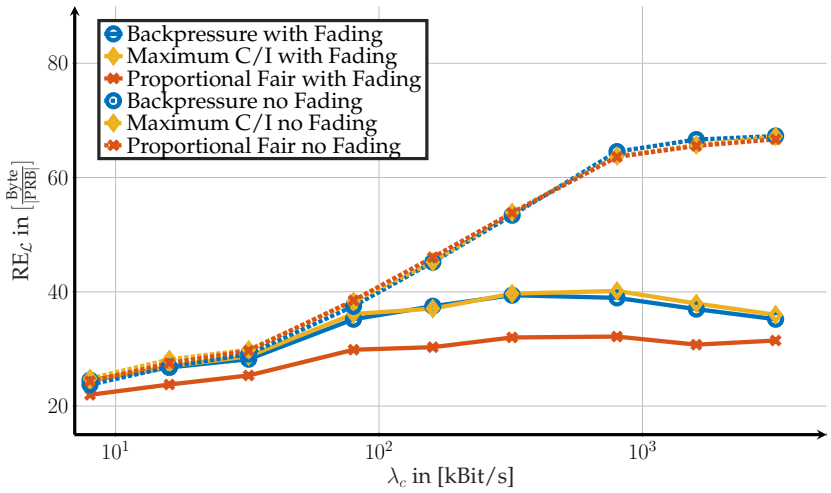

Figure 5.3: Input rates versus achieved resource efficiency (Transported Byte per PRB and Cell) for different schedulers, using the *Resource Efficiency* mode selection. The dotted lines represent scenarios with fading turned off.

per run, which all insert the same throughput into the network, while their number is determined randomly according to a Poisson distribution. However, the points are shifted arbitrarily on the x-axis, which indicates that they are scheduled with different resource efficiencies. The differing efficiencies originate from different channel gains and, in second instance, from random node positions.

The gray points do not comply with the leveled structure. In general it can be seen that the larger the number of users, the more points lie outside the stability region. The effect here is that, as the traffic is outside the stability region, the Proportional Fair Scheduler trades the rates off towards a rate-fair point. The exact point differs from run to run and hence does the achieved sum-throughput of the network.

The effect of finding a rate-fair point, while desirable from a fairness perspective, is not desired to evaluate the resource efficiency. As the different scheduler types target the different utilities of sum-rate, proportional fairness and queue stability, their difference in throughput-resource efficiency across different operation points is so large that no general statement on the impact of mode selection schemes can be done. Thus, the subsequent analysis considers only those sub-parts of data that lie within the stability region of all three investigated schedulers.

In Figure 5.3 the network wide resource efficiencies achieved by different schedulers after using the *Resource Efficiency* mode selection scheme are compared. Similar results are achieved using the other mode selection schemes, which is why they are not explicitly shown. Two cases are illustrated, one with fading turned off in the simulator and one with fading turned on. In general, fading reduces the channel quality independently on each channel, i.e., no fading means no frequency diversity. It can be seen in Figure 5.3 that with frequency diversity, the diversity leveraging schedulers *Maximum C/I* and *Backpressure* achieve a larger resource efficiency than the diversity agnostic scheduler *Proportional Fair*. This had been predicted by Proposition 5.1. It also gives a notion that the efficiency roughly

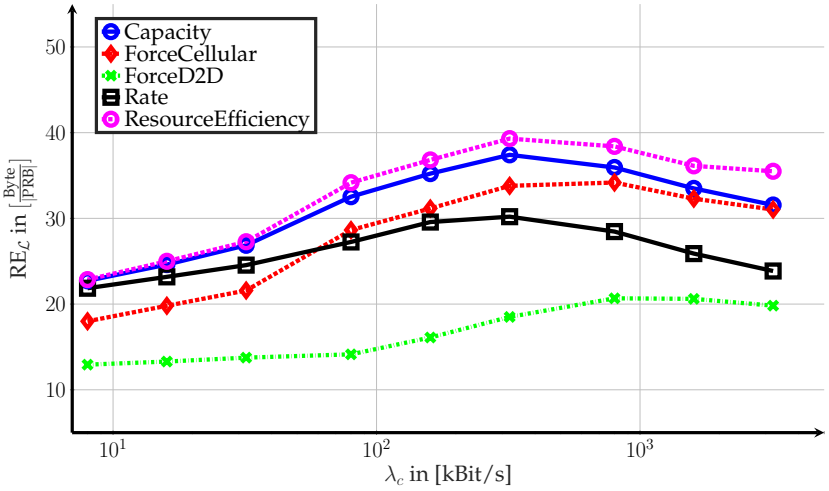

Figure 5.4: Input rates versus achieved resource efficiency for different mode selection schemes, using the Backpressure scheduler.

increases with the throughput optimality of the schedulers. On the other hand, without frequency diversity, all schedulers achieve the same resource efficiency, which is the equality case of Proposition 5.1.

Further, the resource efficiencies produced by different mode selection schemes in combination with all schedulers are compared. The comparison is qualitatively the same for all schedulers, which is why only those of the *Backpressure* scheduler are shown, while the remaining results are given in Appendix C. The input rate versus average resource efficiencies after mode selection with different schemes are shown in Figure 5.4. The proposed scheme, *Resource Efficiency*, produces the largest resource efficiency inside the stability region, followed by *Capacity*. For small input rates, all *Resource Efficiency*, *ForceCellular* and *Rate* scheme perform similarly well. However, *Rate* is overtaken by *ForceCellular* as the input rates increase and for large rates *ForceCellular* performs equally well as *Capacity*. The *ForceD2D* scheme performs worst throughout the whole parameter space. The reason is that in the considered simulation set-up, this scheme produces a high amount of D2D links with low channel qualities, which can only be scheduled inefficiently.

In general, the *Rate* scheme over-estimates the hop-gain, as it assumes that DM uses half the resource of CM, and will tend to choose the DM too often, which produces serious drawbacks for larger input rates. The *Capacity* scheme, on the other hand, does not consider the hop-gain at all and hence is too conservative with offloading. The proposed *Resource Efficiency* scheme estimates the resource efficiency better over the entire considered search space and hence finds the better trade-offs.

5.2 Network Utility Optimal Mode Selection

The next presented mode selection scheme is based on network utility maximization, which is performed on transport layer. It implicitly assumes a MAC layer that is capable of creating

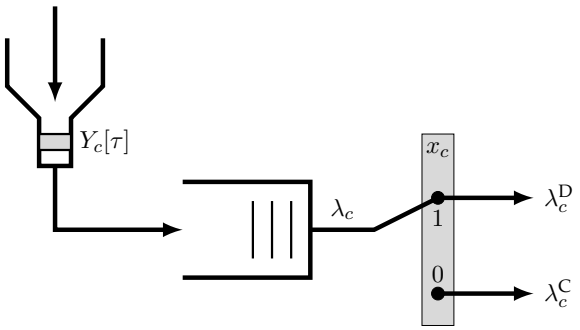

Figure 5.5: Inner structure of s_c. The mode selection problem is considered as "flow steering" problem, where the option is among direct and cellular path. Depending on x_c, the output of the MAC-layer queue must comply with cellular or direct throughput.

a large stability region, such as the BP scheduler does.

Consider a set of data flows $\mathcal{K}$, which have UEs s_c and d_c as source and destination for all $c \in \mathcal{K}$, and a network utility function $U(\boldsymbol{\lambda})$ with $\boldsymbol{\lambda} \in \mathbb{R}_+^{|\mathcal{K}|}$ that reflects the perceived quality of the achieved throughputs λ_c. For each of the flows, the decision needs to be made whether it should be served in CM or DM, respectively. Assume that for each mode, the flow can achieve a throughput of λ_c^{C} and λ_c^{D} and introduce a decision variable per flow, $x_c \in \{0, 1\}$, with $x_c = 1$ if, and only if, the flow is in DM. Depending on the made decision, the achieved throughput of flow c is upper bounded as $\lambda_c \leq \lambda_c^{\mathrm{C}}$ or $\lambda_c \leq \lambda_c^{\mathrm{D}}$. Using this formulation, mode selection can be formulated as NUM problem of the form:

$$\text{(MS-NUM)} \qquad \max_{\boldsymbol{\lambda}, \boldsymbol{x}, \boldsymbol{\lambda}^{\mathrm{C}}, \boldsymbol{\lambda}^{\mathrm{D}}} U(\boldsymbol{\lambda}) \tag{5.13}$$

$$\text{s.t.}$$

$$\lambda_c x_c \leq \lambda_c^{\mathrm{D}} \ \ \forall c, \tag{5.14}$$

$$\lambda_c (1 - x_c) \leq \lambda_c^{\mathrm{C}} \ \ \forall c, \tag{5.15}$$

$$[\boldsymbol{\lambda}^{\mathrm{C}}; \boldsymbol{\lambda}^{\mathrm{D}}] \in \Lambda, \tag{5.16}$$

$$x_c \in \{0, 1\}, \lambda_c \geq 0 \ \ \forall c \in \mathcal{K}. \tag{5.17}$$

Depending on the decision variable x_c, the throughput of flow c must either comply with that of DM in (5.14) or that of CM in (5.15). Condition (5.16) ensures that all flows are within the transport region. Note that if CM is chosen, λ_c^{D} may assume the value of zero independent of λ_c, while in the other case, λ_c^{C} may. The formulation of MS-NUM follows an intuition of flow steering that is shown in Figure 5.5: Depending on x_c, the traffic at s_c is routed over the cellular path, hence connected with λ_c^{C}, or over the direct path, providing λ_c^{D}. Note that MS-NUM is a mixed-integer nonlinear problem (MINLP). Condition (5.16) is convex, because the transport region Λ is known to be. However, Conditions (5.14) and (5.15) have a combinatorial nature and the properties of $U(\boldsymbol{\lambda})$ are undefined. Note however, that if $\boldsymbol{\lambda}$ and $\boldsymbol{x}$ are kept fixed, the remaining problem is convex. This can be leveraged with a Generalized Benders Decomposition (GBD).

Introduction of Generalized Benders Decomposition

A formal introduction of GBD is given in Appendix B. The core idea of the Generalized Benders Decomposition is the notion of *complicating variables*. These are variables which, if fixed, render the remaining problem "easy" by allowing the application of known solutions or standard techniques. By leveraging this, complex problem structures can be decomposed into easier to solve sub-problems. In mixed-integer problems, the integer variables are typically considered as complicating and the decomposition produces an integer problem and a continuous one.

GBD based algorithms use an outer and inner optimization loop. The inner optimization, called *primal problem*, solves the problem with fixed complicating variables, or a feasibility problem if the fixed complicating variables render the problem infeasible. In the outer optimization, called *relaxed master problem*, an approximation of the outer target function and its solution space is generated, based on the solution of the primal problem. The complicating variables are then optimized with respect to this outer optimization.

Both, inner and outer optimization are run alternately with the variables of the other optimization kept fixed. Each solution of the primal problem creates a constraint for the relaxed master problem, thus further re-fining it.

5.2.1 Application of GBD to MS-NUM

Applying the GBD to the MS-NUM problem, it makes sense to define the variables $\boldsymbol{\lambda}$ and $\boldsymbol{x}$ as complicating. Then, the decomposition produces three problems, a primal problem, a feasibility problem and a master problem.

Primal and Feasibility Problem

The primal problem reads

$$\text{(P-MS)} \qquad \max_{\boldsymbol{\lambda}^{\mathrm{C}},\boldsymbol{\lambda}^{\mathrm{D}}} U(\boldsymbol{\lambda}^{(k)}) \tag{5.18}$$

$$\text{s.t.}$$

$$\lambda_c^{(k)} x_c^{(k)} \leq \lambda_c^{\mathrm{D}} \ \ \forall c, \tag{5.19}$$

$$\lambda_c^{(k)} (1 - x_c^{(k)}) \leq \lambda_c^{\mathrm{C}} \ \ \forall c, \tag{5.20}$$

$$[\boldsymbol{\lambda}^{\mathrm{C}}; \boldsymbol{\lambda}^{\mathrm{D}}] \in \Lambda, \tag{5.21}$$

where the superset (k) indicates the k'th choice of complicating variables, which are kept constant during optimization. A prerequisite for correctness of the GBD is that the primal problem is convex, such that strong duality holds. It can be verified that this is true for P-MS, because the optimizing function is constant and all constraints are convex. If the set

complicating variables render P-MS infeasible, a feasibility problem is solved:

$$\text{(F-MS)} \qquad \min_{\boldsymbol{z},\boldsymbol{\lambda}^{\mathrm{C}},\boldsymbol{\lambda}^{\mathrm{D}}} \|\boldsymbol{z}\| \tag{5.22}$$

$$\text{s.t.}$$

$$\lambda_c^{(k)} x_c^{(k)} - \lambda_c^{\mathrm{D}} \leq z_c^{\mathrm{D}} \ \ \forall c, \tag{5.23}$$

$$\lambda_c^{(k)} (1 - x_c^{(k)}) - \lambda_c^{\mathrm{C}} \leq z_c^{\mathrm{C}} \ \ \forall c, \tag{5.24}$$

$$[\boldsymbol{\lambda}^{\mathrm{C}}; \boldsymbol{\lambda}^{\mathrm{D}}] \in \Lambda, \ \ \boldsymbol{z} \geq \mathbf{0} \tag{5.25}$$

$\boldsymbol{z}$ therein is a slack variable of the form $\boldsymbol{z} = [\boldsymbol{z}^{\mathrm{C}}; \boldsymbol{z}^{\mathrm{D}}]$. F-MS aims at finding a solution as close to feasibility as possible, with respect to a defined norm $\|\boldsymbol{z}\|$. The complicating variables are, again, kept fixed.

Now consider the P-MS. Because the complicating variables are constant, so is the utility, so any feasible point is in fact also optimal. Due to this, it is sufficient to solve the feasibility problem: If it results in a solution with $\|\boldsymbol{z}\| = 0$, the result is an optimal solution to the P-MS. If not, it is an optimal solution of the F-MS.

The F-MS can further be re-fined. First, the sum-norm $\|\boldsymbol{z}\|_1$ is chosen, as it creates linear, decomposable problem structures. Further, observe that at optimality, (5.23) and (5.24) must be tight, i.e.,

$$\lambda_c^{(k)} x_c^{(k)} - \lambda_c^{\mathrm{D}} = z_c^{\mathrm{D}}, \text{ and } \lambda_c^{(k)} (1 - x_c^{(k)}) - \lambda_c^{\mathrm{C}} = z_c^{\mathrm{C}} \tag{5.26}$$

must hold[1]. Substituting this relationship into the conditions $z_c^{\mathrm{C}} \geq 0$, $z_c^{\mathrm{D}} \geq 0$ yields

$$\lambda_c^{\mathrm{D}} \leq \lambda_c^{(k)} x_c^{(k)} \text{ and } \lambda_c^{\mathrm{C}} \leq \lambda_c^{(k)} (1 - x_c^{(k)}).$$

As direct consequence, the optimal value of λ_c^{D} is zero if $x_c^{(k)} = 0$ and that of λ_c^{C} is zero if $x_c^{(k)} = 1$. By choosing a sum-norm $\|\cdot\|_1$ for (5.18), substituting (5.26) into it and considering that $\lambda_c^{(k)}$, $x_c^{(k)}$ are kept constant yields the equivalent problem

$$\max_{\boldsymbol{\lambda}^{\mathrm{C}},\boldsymbol{\lambda}^{\mathrm{D}}} \sum_c \lambda_c^{\mathrm{C}} + \sum_c \lambda_c^{\mathrm{D}}$$

$$\text{s.t.}$$

$$\lambda_c^{\mathrm{D}} \leq \lambda_c^{(k)} x_c^{(k)},$$

$$\lambda_c^{\mathrm{C}} \leq \lambda_c^{(k)} (1 - x_c^{(k)}),$$

$$[\boldsymbol{\lambda}^{\mathrm{C}}; \boldsymbol{\lambda}^{\mathrm{D}}] \in \Lambda.$$

This is a sum-throughput maximization, where each link uses the chosen mode and under the condition that no throughput exceeds a set target value $\lambda_c^{(k)}$. Problems of this type have been extensively studied in literature under arbitrary networking scenarios, c.f. [83]. In particular, by applying the results of [83, Chap. 5.2.2], which have been reproduced in Section 2.1.3, sum-throughput maximization without constraints can be optimally solved when using the BP scheduler and admitting traffic according to a simple threshold rule, which states

[1] Technically, it can happen that the conditions are not tight when $\lambda_c^{(k)} x_c^{(k)} - \lambda_c^{\mathrm{D}} < 0$, $\lambda_c^{(k)} (1 - x_c^{(k)}) - \lambda_c^{\mathrm{C}} < 0$ $\forall c$. However, in this case there always also are feasible, hence optimal, smaller λ_c^{D}, λ_c^{C} that make the conditions tight.

that traffic should not be added whenever the queue backlog exceeds a defined threshold but can be admitted arbitrarily otherwise. The upper bounds on average throughput can be realized by using a token-bucket type admission control, with infinite bucket size and token generation rate of $\lambda_c^{(k)}$. When doing so and combining this admission with the BP scheduler, the optimal values of λ_c^{C}, λ_c^{D} are the empirically measured, achieved throughputs in the chosen mode.

The Lagrange function of the F-MS is used to generate outer approximations for the master problem, with multipliers fixed at their optimal values. Taking the original formulation, the Lagrange function is:

$$\begin{aligned} L &= \sum_c \left(z_c^{\mathrm{C}} + z_c^{\mathrm{D}}\right) + \sum_c q_c^{\mathrm{C}} \left(\lambda_c^{(k)}(1-x_c^{(k)}) - \lambda_c^{\mathrm{C}} - z_c^{\mathrm{C}}\right) + \sum_c q_c^{\mathrm{D}} \left(\lambda_c^{(k)} x_c^{(k)} - \lambda_c^{\mathrm{D}} - z_c^{\mathrm{D}}\right) \\ &\quad - \sum_c \varepsilon_c^{\mathrm{C}} z_c^{\mathrm{C}} - \sum_c \varepsilon_c^{\mathrm{D}} z_c^{\mathrm{D}}. \end{aligned}$$

The variables q_c^{C}, q_c^{D}, $\varepsilon_c^{\mathrm{C}}$, $\varepsilon_c^{\mathrm{D}}$ therein are Lagrange multipliers and the condition $[\boldsymbol{\lambda}^{\mathrm{C}}; \boldsymbol{\lambda}^{\mathrm{D}}] \in \Lambda$ was implicitly assumed, i.e., not included into the Lagrange function. As the problem is convex and Slaters' constraint qualification is guaranteed to hold, any Karush-Kuhn-Tucker (KKT) point is a global optimum. The KKT conditions yield

$$1 = q_c^{\mathrm{C}} + \varepsilon_c^{\mathrm{C}}; \;\; 1 = q_c^{\mathrm{D}} + \varepsilon_c^{\mathrm{D}}. \tag{5.27}$$

From these and the complementary slackness conditions, it can be concluded that if, for any mode, $z_c^{\mathrm{C/D}} > 0$, then the corresponding $\varepsilon_c^{\mathrm{C/D}} = 0$ and $q_c^{\mathrm{C/D}} = 1$. On the other hand, if $z_c^{\mathrm{C/D}} = 0$ then $\varepsilon_c^{\mathrm{C/D}}$ and $q_c^{\mathrm{C/D}}$ will take values between zero and one. The optimal values of $\varepsilon_c^{\mathrm{C/D}}$ and $q_c^{\mathrm{C/D}}$ can then be found by a dual ascent algorithm. By using that $\lambda_c^{(k)}(1-x_c^{(k)}) - \lambda_c^{\mathrm{C}} - z_c^{\mathrm{C}} = 0$ must be tight at optimality, the multipliers $\varepsilon_c^{\mathrm{C/D}}$ are adapted according to the rule

$$\begin{aligned} \varepsilon_c^{\mathrm{C}}[k+1] &= \left[\varepsilon_c^{\mathrm{C}}[k] + \delta(\lambda_c^{(k)}(1-x_c^{(k)}) - \lambda_c^{\mathrm{C}})\right]^{[0,1]}, \\ \varepsilon_c^{\mathrm{D}}[k+1] &= \left[\varepsilon_c^{\mathrm{D}}[k] + \delta(\lambda_c^{(k)} x_c^{(k)} - \lambda_c^{\mathrm{D}})\right]^{[0,1]}, \end{aligned}$$

where $\delta > 0$ is a fixed step-size and $[\cdot]^{[0,1]} = \max\{\min\{\cdot, 1\}, 0\}$ is the projection onto $[0,1]$. After sufficient time, the multipliers $q_c^{\mathrm{C/D}}$ can be identified as $q_c^{\mathrm{C/D}} := 1 - \varepsilon_c^{\mathrm{C/D}}$, respectively

The Master Problem

The resulting approximation for the master problem takes the form of $\xi(\boldsymbol{\lambda}, \boldsymbol{x}) \leq 0$, where $\xi(\boldsymbol{\lambda}, \boldsymbol{x})$ is the Lagrange function with constant, optimally chosen multipliers, minimized over $\boldsymbol{\lambda}^{\mathrm{C}}$, $\boldsymbol{\lambda}^{\mathrm{D}}$. By using that, as shown in Appendix B, the variables $z_c = 0$ are assumed for creating $\xi(\boldsymbol{\lambda}, \boldsymbol{x})$, it becomes:

$$\begin{aligned} \xi(\boldsymbol{\lambda}, \boldsymbol{x}) &= \min_{[\boldsymbol{\lambda}^{\mathrm{C}}; \boldsymbol{\lambda}^{\mathrm{D}}] \in \Lambda} \left[\sum_c \lambda_c \left(q_c^{\mathrm{D}} x_c + q_c^{\mathrm{C}}(1-x_c)\right) - \sum_c \left(q_c^{\mathrm{D}} \lambda_c^{\mathrm{D}} + q_c^{\mathrm{C}} \lambda_c^{\mathrm{C}}\right)\right] \\ &= \sum_c \lambda_c \left(q_c^{\mathrm{D}} x_c + q_c^{\mathrm{C}}(1-x_c)\right) - \max_{[\boldsymbol{\lambda}^{\mathrm{C}}; \boldsymbol{\lambda}^{\mathrm{D}}] \in \Lambda} \left[\sum_c \left(q_c^{\mathrm{D}} \lambda_c^{\mathrm{D}} + q_c^{\mathrm{C}} \lambda_c^{\mathrm{C}}\right)\right] \\ &= \sum_c \lambda_c \left(q_c^{\mathrm{D}} x_c + q_c^{\mathrm{C}}(1-x_c)\right) - R, \end{aligned}$$

where $R = \max_{[\boldsymbol{\lambda}^{\mathrm{C}};\boldsymbol{\lambda}^{\mathrm{D}}]\in\Lambda} \left[\sum_c \left(q_c^{\mathrm{D}}\lambda_c^{\mathrm{D}} + q_c^{\mathrm{C}}\lambda_c^{\mathrm{C}}\right)\right]$ can be calculated from the solution of the F-MS. Note that due to the additivity of the different terms, the primal optimization is completely decoupled from the complicating variables for fixed multipliers. So the optimal value of the minimization does not change when $\boldsymbol{\lambda}$, $\boldsymbol{x}$ change.

All approximations form constraints for the master problem, which then takes the following form:

$$\begin{aligned} \text{(M-MS)} \qquad & \max_{\boldsymbol{\lambda},\boldsymbol{x}} U(\boldsymbol{\lambda}) \\ & \text{s.t.} \\ & \sum_c q_{c,k}^{\mathrm{D}}\lambda_c x_c + q_{c,k}^{\mathrm{C}}\lambda_c(1-x_c) \le R_k \ \ \forall k \\ & x_c \in \{0,1\}, \lambda_c \ge 0 \ \ \forall c \in \mathcal{K}. \end{aligned}$$

The constraints are, in fact, sum-throughput constraints on those throughputs and modes which did not achieve their target during the k'th instance of F-MS. For all modes that did achieve their target throughputs, the optimal multipliers are zero. The constraints can be interpreted as outer approximations on the transport region Λ. The algorithmic statement of the GBD demands that M-MS and F-MS are solved in an alternating fashion. Each solution outcome of the M-MS then creates an optimistic rate target for the F-MS, whereas the F-MS generates a new constraint for the M-MS in return. As result, the application of the GBD results in an outer approximation algorithm.

Due to the binary nature of $\boldsymbol{x}$, the master problem M-MS has a combinatorial nature. However, it can be relaxed to a continuous problem without losing optimality. For this, define

$$\overline{r}_c^{\mathrm{D}} = \lambda_c x_c; \ \ \overline{r}_c^{\mathrm{C}} = \lambda_c(1-x_c); \ \ r_c^{\mathrm{D}} = \overline{r}_c^{\mathrm{D}} x_c = \lambda_c x_c^2; \ \ r_c^{\mathrm{C}} = \overline{r}_c^{\mathrm{C}}(1-x_c) = \lambda_c(1-x_c)^2 \tag{5.28}$$

and observe that $\lambda_c = \overline{r}_c^{\mathrm{D}} + \overline{r}_c^{\mathrm{C}} = r_c^{\mathrm{D}} + r_c^{\mathrm{C}}$ due to $x_c \in \{0,1\}$. The integer constraint $x_c \in \{0,1\}$ can be re-written into $x_c(1-x_c) = 0$, which transfers to the newly defined variables as:

$$\overline{r}_c^{\mathrm{D}} \cdot \overline{r}_c^{\mathrm{C}} = 0; \ \ r_c^{\mathrm{D}} \cdot r_c^{\mathrm{C}} = 0. \tag{5.29}$$

Now, the integer constraint can be relaxed to $x \in [0,1]$, which transfers to

$$x_c(1-x_c) \ge 0 \ \ \Rightarrow \ \ r_c^{\mathrm{D}} \cdot r_c^{\mathrm{C}} \ge 0 \ \ \Rightarrow \ \ r_c^{\mathrm{D}} \ge 0, \ \ r_c^{\mathrm{C}} \ge 0. \tag{5.30}$$

Based on these results, the following Proposition can be established:

Proposition 5.2. When relaxing x_c to $x_c \in [0,1]$, there always is an optimal solution of M-MS with $x_c \in \{0,1\}$.

Proof. First, note that relaxing x_c can be re-written into an equivalent optimization over x_c,

$\overline{r}_c^{\mathrm{D}}$ and $\overline{r}_c^{\mathrm{C}}$ of the form

$$\begin{aligned} &\max_{\boldsymbol{\lambda},\boldsymbol{r}^{\mathrm{D}},\boldsymbol{r}^{\mathrm{C}}} U(\boldsymbol{\lambda}) \\ &\text{s.t.} \\ &\lambda_c = x_c\overline{r}_c^{\mathrm{D}} + (1-x_c)\overline{r}_c^{\mathrm{C}} \;\; \forall c \\ &\sum_c q_{c,k}^{\mathrm{D}}\overline{r}_c^{\mathrm{D}} + \sum_c q_{c,k}^{\mathrm{C}}\overline{r}_c^{\mathrm{C}} \leq R_k \;\; \forall k \\ &\overline{r}_c^{\mathrm{D}}, \overline{r}_c^{\mathrm{C}}, \lambda_c \geq 0; \;\; x_c \in [0,1] \;\; \forall c \in \mathcal{K}. \end{aligned}$$

Consider an optimal outcome x_c^* with $0 < x_c^* < 1$. If $U(\boldsymbol{\lambda})$ is strictly increasing with λ_c, then the result obviously holds: Either the optimal values $\overline{r}_c^{\mathrm{D}*} = \overline{r}_c^{\mathrm{C}*}$, in which case any x_c is optimal. Or one of the values $\overline{r}_c^{\mathrm{D}*}$, $\overline{r}_c^{\mathrm{C}*}$ is larger, then there is a value $0 < x_c' < x_c^*$ or $x_c^* < x_c'' < 1$ that realizes a larger λ_c, which contradicts the assumption on optimal x_c^*. Now assume that $U(\boldsymbol{\lambda})$ is not strictly increasing with λ_c and that one of the optimal rate values is larger, e.g., $\overline{r}_c^{\mathrm{D}*} \geq \overline{r}_c^{\mathrm{C}*}$. In this case, for any optimal x_c^* with $0 < x_c^* < 1$, $\overline{r}_c^{\mathrm{D}*}$ can be reduced to the value $\hat{r}_c^{\mathrm{D}} = \overline{r}_c^{\mathrm{D}*}x_c^* + \overline{r}_c^{\mathrm{C}*}(1-x_c^*)$ without violating any constraints. The solution $x_c^* := 1$, $\overline{r}_c^{\mathrm{D}*} := \hat{r}_c^{\mathrm{D}}$ then leads to the same λ_c and hence is also optimal. An analog argumentation holds when $\overline{r}_c^{\mathrm{D}*} \leq \overline{r}_c^{\mathrm{C}*}$. □

The intuition of the proposition is that either the solution of the relaxed M-MS is on integer space or, if not, it is sufficient to chose the mode which has the larger optimal value of $\overline{r}_c^{\mathrm{D}*}$, $\overline{r}_c^{\mathrm{C}*}$. If both modes are tied, a random mode may be chosen. Combining all results, the relaxed M-MS can be re-written as:

$$\begin{aligned} \text{(RM-MS)} \qquad &\max_{\boldsymbol{\lambda},\boldsymbol{r}^{\mathrm{D}},\boldsymbol{r}^{\mathrm{C}}} U(\boldsymbol{\lambda}) \\ &\text{s.t.} \\ &\lambda_c \leq r_c^{\mathrm{D}} + r_c^{\mathrm{C}} \;\; \forall c \\ &\sum_c q_{c,k}^{\mathrm{D}} r_c^{\mathrm{D}} + \sum_c q_{c,k}^{\mathrm{C}} r_c^{\mathrm{C}} \leq R_k \;\; \forall k \\ &r_c^{\mathrm{D}}, r_c^{\mathrm{C}}, \lambda_c \geq 0 \;\; \forall c \in \mathcal{K}. \end{aligned}$$

5.2.2 Utility Optimal Mode Selection

The results are now combined into a formal algorithmic statement. As stated already, the master problem and feasibility problem are solved alternately. While the master problem is explicitly formulated, the feasibility problem is solved decentralized by combining the BP scheduler with token-bucket traffic shaping, which uses a token generation rate of λ_c^*, and a queue-based threshold admission rule. It is assumed that the master problem is solved after fixed time intervals ΔT, which are mode selection intervals within which modes are kept constant.

In the given form, the master problem needs to be solved at a central instance, which is referred to as central coordinator (CC). The CC might be the BS, but might just as well be located somewhere in the core network or on an edge-cloud. The proposed algorithm is given in Algorithm 1. As the first instances of the RM-MS can yield an unbounded result, it can

Algorithm 1 Utility Optimal Mode Selection

Choose uility $U(\boldsymbol{\lambda})$, set MS interval ΔT.
Initialize RM-MS as:
$\max_{\boldsymbol{\lambda}, \boldsymbol{r}^{\mathrm{D}}, \boldsymbol{r}^{\mathrm{C}}} U(\boldsymbol{\lambda})$ s.t. $\lambda_c \leq r_c^{\mathrm{D}} + r_c^{\mathrm{C}} \ \forall c$.
Set $\varepsilon \geq 0$, UB $:= \infty$, LB $:= -\infty$
while UB $-$ LB $> \varepsilon$ **do**
  Solve RM-MS, yielding $\boldsymbol{\lambda}^*$, $\boldsymbol{r}^{\mathrm{D}*}$, $\boldsymbol{r}^{\mathrm{C}*}$.
  Set UB $= \min\{\mathrm{UB}, U(\boldsymbol{\lambda}^*)\}$
  Set $x_c^* = \mathbb{1}\{r_c^{\mathrm{D}} \geq r_c^{\mathrm{C}}\} \ \forall c$.
  Set $\lambda_c^* = r_c^{\mathrm{D}} x_c + r_c^{\mathrm{C}}(1 - x_c) \ \forall c$.
  Notify all links of $\boldsymbol{x}^*$, $\boldsymbol{\lambda}^*$.
  Let links operate with traffic input λ_c^* for time ΔT.
  Links identify $q_{c,k}^{\mathrm{C}}$, $q_{c,k}^{\mathrm{D}}$ and report their achieved r_c^{C}, r_c^{D}.
  Add constraint to M-MS:
  $\sum_c q_{c,k}^{\mathrm{D}} r_c^{\mathrm{D}} + \sum_c q_{c,k}^{\mathrm{C}} r_c^{\mathrm{C}} \leq R_k$
  Set LB $= \max\{\mathrm{LB}, U(\boldsymbol{r}^{\mathrm{C}} + \boldsymbol{r}^{\mathrm{D}})\}$
end while
Output: $\boldsymbol{\lambda}^*$, $\boldsymbol{x}^*$

make sense to upper bound all λ_c by an optimistic upper bound, e.g., the maximum achievable throughput when all resources are assigned to the outgoing link. This can increase the convergence speed because otherwise, unused modes will always seem to provide the better utilities at first. As for complexity analysis, the only statement that can be made for GBD is that it converges to the optimal solution within a finite number of iterations.

Unfortunately, due to time and space restrictions, a proper investigation of convergence properties with simulation is out of scope. However, from purely algorithmic perspective, the proposed structure has strong properties. First, it is valid for any type of utility function, as long as the utility is with respect to end-to-end throughput. The exact form of used utility might turn the master problem hard to solve if it is not well defined. However, the mode selection algorithm will yield optimal result whenever the master problem is optimally solved. The second strong property is that the optimality of mode selection is independent of the underlying MAC and PHY mechanisms, provided that some assumptions hold: It was assumed that the BP scheduler is used, which is known to have a stability region that equals the interior of the transport capacity region. For the BP scheduler to have this property, it is assumed that the underlying scheduling problems can optimally solve the weighted sum-rate utility, in the defined action space of the MAC layer. Under these assumptions, optimality can in principle be claimed for cellular networks with OFDMA, SC-FDMA, WCDMA, with single-antenna or multi-antenna capabilities and could even be claimed for out-band D2D. For any other scheduler type apart from the BP, the proposed mode selection converges to optimum within the stability region of the scheduler, provided that it is convex. While this is true for some known schedulers, e.g., the Maximum C/I scheduler, others, such as the Proportional Fair scheduler, are known to produce non-convex stability regions [83].

5.3 Lessons Learned

Two different approaches for mode selection were considered, one targeting resource efficiency maximization for constant bit-rate traffic and the other targeting utility maximization for elastic traffic demands.

For the resource efficient mode selection, which targets resource reduction, simple channel measurements are used, as other, tractable formulations were not available at the time of development. The impact and accuracy of this mode selection was thoroughly investigated with simulations. It could be shown that the proposed scheme induces less resource usage for constant bit-rate traffic and that it optimizes a tight lower bound for all diversity leveraging schedulers.

The second, utility maximizing mode selection was based on an application of the GBD, which results in an outer approximation algorithm for the transport region. It induces a semi-distributed management structure, which consists of a simple threshold based queue admission control at all UEs and a centralized optimization at a CC. The scheme can be claimed to result in an optimal mode constellation with respect to any throughput based utility of choice, provided that the utility is optimally maximized over a convex optimization space.

Chapter 6

Reuse Management

One major benefit seen in D2D communication is that, due to the expected short range of links, transmission powers can be reduced. This can be leveraged to allow the reuse of transmission resources within a cell. However, managing reuse is challenging because it introduces intracell-interference into the cellular system. The main difficulties come from the non-linearity of interference coupling, as well as the structure of direct links, which induces that the base station is not part of communication itself and hence must manage interference remotely.

In this section, several aspects of interference management in D2D networks are investigated. First, methods to evaluate whether frequency reuse is possible among a set of given links are developed in Section 6.1. These have been published in [6]. Then, the Reuse Maximization Problem (RMP) is introduced in Section 6.2, which is the problem how to maximize the number of links on a single communication channel, subject to SINR constraints. The RMP captures a core problem of interference aware scheduling, which is the impact of binary link activation and de-activation on dynamic power control problems. Results on the RMP follow the publications [2], [7]. While the RMP in itself solves the problem of admission control onto a single communication channel, it is also suitable to capture the general impact of optimizing mixed-integer NUM problems with interference constraints and dynamic power control. Correspondingly, the results of RMP are related to general utility maximization and applied to the overall D2D-NUM problem presented in Section 2.2.3. While this adaptation is novel, it has been submitted to [8]. All considered problems are investigated assuming full power control capabilities at the UEs and rely on the power control perspective, of which the main intuition was given in Section 2.1.2.

In literature, feasible reuse is mostly achieved by introducing spatial reuse constraints or interference power thresholds, c.f. [44]. However, these approaches often neglect the existing work on dynamic power control [55], [57], as introduced in Section 2.1.2, which provides insights on inherent properties of interference. In contrast to existing works, dynamic power control is assumed as a key ingredient in this chapter. In general, frequency reuse on a single channel is investigated, which creates problem structures that are complex enough to solve. However, possible extensions to multi-channel reuse are often straightforward and discussed whenever appropriate.

6.1 Reuse Feasibility Estimation

To perform appropriate scheduling and frequency reuse, as initial step it must be taken into account whether it is at all possible to achieve minimum signal quality targets for a set of links in spite of mutual interference. Clearly, if SINR constraints of links exclude each other, an infeasible problem instance is generated for following network optimizations, i.e., power control or scheduling mechanisms. Validating reuse feasibility thus is a core first step that, however, is assumed to be fulfilled more often than it is actually targeted.

Due to the dynamics expected for D2D communication and the associated network optimization, feasibility information needs to be acquired as fast as possible. In particular, some optimization approaches might even use this information as intermediary indicator for link activation decision, that is run regularly within outer-loop problems. In this section, it is investigated how to check for reuse feasibility fast under dynamic power control. Two algorithms are developed and evaluated in terms of speed, accuracy and control overhead.

6.1.1 State of the Art

The problem of determining reuse feasibility resembles call admission control problems, which have been investigated for voice networks with full power control. However, these have not been transferred to context of D2D-communication, where mostly power control capabilities are not properly leveraged.

Prior work on power control feasibility in wireless networks [78], [137]–[140] has been developed as a basis for call-admission control. The well-known FM-PCA [54] is often assumed in this context because it is known to converge if and only if the reuse situation is feasible. The works presented in [78], [137]–[139] assume a set-up where several links are active already, whose PCA has converged, and new links seek admission to a channel: In [78], Bambos et al. propose that all links which want to reuse a channel send a low-power probing tone and wait for the active PCAs to re-converge. From the interference produced by the re-converged PCAs, reuse feasibility is determined. The authors of [137] and [138] follow this approach, using a discriminant [137] and the spectral radius [138] as feasibility criterion. Kučera et al. [139] investigate the dynamics of the Foschini-Miljanic PCA and use observations of its convergence speed to calculate the spectral radius before convergence of the PCA. The algorithm developed in [139] is shown to outperform those in [78], [137], [138]. Lin et al. [140] show how the feasibility problem can be transformed into a linear program. While this is preferable from an algorithmic perspective, it has the drawback that the introduced formulation cannot be well implemented in a distributed fashion.

The work on call admission control can also be used to test for reuse feasibility in the D2D scenario. However, current work evaluates reuse feasibility incorrectly when constrained transmission powers make reuse impossible. This recognized in [137], [138], but not solved, and [78], [139] and [140] completely neglect power constraints.

6.1.2 System Model & Basic Properties

Throughout this section, the notation and variables of the power control network model is assumed, which has been introduced in Section 2.1.2. Consider a set of wireless links, that are targeted to reuse a certain transmission resource, i.e., a frequency channel or even a single PRB in an LTE time-frequency grid.

Assume an arbitrary LQ-constraint $\psi(\Gamma_i) \geq \psi_i$ for a link-quality function $\psi(\Gamma) \in \Psi$ or $\phi(\Gamma_i) \leq \phi_i$ for $\phi(\Gamma) \in \Upsilon$, as defined in Section 2.1.2, following the approach of [57]. The LQ-constraint is required for a link to achieve satisfactory transmission quality. From the definitions in Section 2.1.2, it is bijectively mappable to an SINR constraint of the form $\Gamma_i(\boldsymbol{p}) \geq \gamma_i$. The corresponding SINR targets can be used to define a relative gain matrix $\boldsymbol{F}$ [55], [57] and feasible power region $\mathcal{F}_{\boldsymbol{p}}$ as presented in (2.9)-(2.11).

Using this model, the target is to develop an algorithm which evaluates the function:

$$\delta\left\{\mathcal{F}_{\boldsymbol{p}} \cap \mathcal{P} = \emptyset\right\} = \begin{cases} 1, & \text{if } \mathcal{F}_{\boldsymbol{p}} \cap \mathcal{P} = \emptyset \\ 0, & \text{if } \mathcal{F}_{\boldsymbol{p}} \cap \mathcal{P} \neq \emptyset, \end{cases} \tag{6.1}$$

where $\mathcal{P}$ contains all allowed power vectors that comply with device capabilities. The indicator function checks for reuse feasibility and can be used for admission control decisions into the network. Clearly, if $\delta\left\{\mathcal{F}_{\boldsymbol{p}} \cap \mathcal{P} = \emptyset\right\} = 0$, then it would be inappropriate to let the targeted set of links reuse a resource, because the links cannot be guaranteed to achieve their targeted qualities.

Two cases can make frequency reuse impossible: First, $\mathcal{F}_{\boldsymbol{p}}$ can be empty. This is the case when $\rho(\boldsymbol{F}) > 1$, i.e., the half-spaces have no intersection for $\boldsymbol{p} \geq \boldsymbol{0}$. Second, $\boldsymbol{p}_p$ can violate the maximum power constraint. In this case, the situation is feasible in principle but at least one sender cannot use enough transmission power to assume a state in $\mathcal{F}_{\boldsymbol{p}}$. Refer to $\mathcal{F}_{\boldsymbol{p}} = \emptyset$ as the first type of infeasibility and $\mathcal{F}_{\boldsymbol{p}} \neq \emptyset$, $\mathcal{F}_{\boldsymbol{p}} \cap \mathcal{P} = \emptyset$ as the second type, respectively. The second type holds if and only if $\boldsymbol{p}_p \not\leq \boldsymbol{p}_{\max}$, and further if $\rho(\boldsymbol{F}) \geq 1$, respectively.

The state of the art solutions discussed in section 6.1.1 aim at calculating $\rho(\boldsymbol{F})$ and do not solve the second type of infeasibility. This leads to wrong feasibility statements, as will be shown in section 6.1.5.

For the following investigation, it is assumed that all links use a power-constrained Foschini-Miljanic PCA, i.e., update their powers according to the rule:

$$\boldsymbol{p}[k+1] \quad = \quad \min\{\boldsymbol{F}\boldsymbol{p}[k] + \boldsymbol{u}, \boldsymbol{p}_{\max}\}. \tag{6.2}$$

As can be seen from the further development, the presented algorithms could in principle use any PCA that converges towards $\boldsymbol{p}_p$, such as [69].

6.1.3 Mathematical Solution

Several mathematical possibilities to evaluate reuse feasibility with maximum power constraints are now discussed. In Section 6.1.4, the approaches are developed into algorithms.

A natural solution to determine reuse feasibility is to calculate $\rho(\boldsymbol{F})$ and $\boldsymbol{p}_p$ and then check for $\rho(\boldsymbol{F}) < 1$ and $\boldsymbol{p}_p \leq \boldsymbol{p}_{\max}$. Efficient algorithms exist for the calculation of both,

however, a lot of information needs to be obtained, namely all channel gains, noise figures, maximum transmission powers and SINR requirements, causing much overhead. This approach will be considered as "brute-force reference" although it is deemed to be impractical for a real world setup.

The first made observation is based on the following result from nonnegative matrix theory [77]: Define

$$r_{\boldsymbol{F}}(\boldsymbol{p}) = \min_{p_i \neq 0} \frac{(\boldsymbol{F}\boldsymbol{p})_i}{p_i}, \quad s_{\boldsymbol{F}}(\boldsymbol{p}) = \max_{p_i \neq 0} \frac{(\boldsymbol{F}\boldsymbol{p})_i}{p_i}. \tag{6.3}$$

$r_{\boldsymbol{F}}(\boldsymbol{p})$ is the minimal and $s_{\boldsymbol{F}}(\boldsymbol{p})$ the maximal factor by which $\boldsymbol{F}$ distorts the components of $\boldsymbol{p}$, i.e., $r_{\boldsymbol{F}}(\boldsymbol{p}) \cdot \boldsymbol{p} \leq \boldsymbol{F}\boldsymbol{p} \leq s_{\boldsymbol{F}}(\boldsymbol{p}) \cdot \boldsymbol{p}$ holds for $\boldsymbol{p} > 0$. Then, for all $\boldsymbol{p} > 0$ [77]:

$$r_{\boldsymbol{F}}(\boldsymbol{p}) \leq \rho(\boldsymbol{F}) \text{ and } s_{\boldsymbol{F}}(\boldsymbol{p}) \geq \rho(\boldsymbol{F}). \tag{6.4}$$

Equality is achieved in (6.4) for both, $r_{\boldsymbol{F}}(\boldsymbol{p})$ and $s_{\boldsymbol{F}}(\boldsymbol{p})$ when $\boldsymbol{p} = \boldsymbol{p}_\rho$ is the dominant eigenvector of $\boldsymbol{F}$, i.e., the eigenvector to the largest modulus eigenvalue. Applying this result, it is used that $(\boldsymbol{F}\boldsymbol{p})_i = p_i\gamma_i/\Gamma_i(\boldsymbol{p})$ in (6.3), which leads to:

$$\rho(\boldsymbol{F}) \geq \min_i \frac{\gamma_i}{\Gamma_i(\boldsymbol{p})} \ \forall \boldsymbol{p}, \quad \rho(\boldsymbol{F}) \leq \max_i \frac{\gamma_i}{\Gamma_i(\boldsymbol{p})} \ \forall \boldsymbol{p}. \tag{6.5}$$

This leads to the following proposition:

Proposition 6.1. If, for some $\boldsymbol{p} \geq \boldsymbol{0}$, all SIRs meet the SINR constraint then $\mathcal{F}_{\boldsymbol{p}} \neq \emptyset$. If no SIR meets the SINR constraint then $\mathcal{F}_{\boldsymbol{p}} = \emptyset$.

Proof. If all SIRs meet the SINR constraint, $1 \geq \max_i \gamma_i/\Gamma_i(\boldsymbol{p}) \geq \rho(\boldsymbol{F})$, hence $\mathcal{F}_{\boldsymbol{p}} \neq \emptyset$. If no SIR meets the SINR constraint, $1 < \min_i \gamma_i/\Gamma_i(\boldsymbol{p}) \leq \rho(\boldsymbol{F})$, hence $\mathcal{F}_{\boldsymbol{p}} = \emptyset$. □

Proposition 6.1 can be used to check if the half-spaces of $\mathcal{F}_{\boldsymbol{p}}$ have an intersection or not and detect the first type of infeasibility. However, it cannot be used to determine the second type of infeasibility. For the second type, it needs to be verified whether $\boldsymbol{p}_p$ is in $\mathcal{P}$ or not. This can be done using the following proposition:

Proposition 6.2. If, for some $\boldsymbol{0} \leq \boldsymbol{p} \leq \boldsymbol{p}_{\max}$, all SINR-constraints are met, $\mathcal{F}_{\boldsymbol{p}} \cap \mathcal{P} \neq \emptyset$. If $\Gamma_i \leq \gamma_i \ \forall i$ and $p_i = p_{\max,i}$, $\Gamma_i < \gamma_i$ for some i, $\mathcal{F}_{\boldsymbol{p}} \cap \mathcal{P} = \emptyset$.

Proof. Note that $\Gamma_i \gtreqless \gamma_i \ \forall i$ corresponds to $(\boldsymbol{I} - \boldsymbol{F})\,\boldsymbol{p} \gtreqless \boldsymbol{u}$. So if the first part holds, $\boldsymbol{p}$ is in $\mathcal{F}_{\boldsymbol{p}}$ and $\mathcal{P}$, hence $\mathcal{F}_{\boldsymbol{p}} \cap \mathcal{P} \neq \emptyset$. For the second part, observe that any $\boldsymbol{p}$ for which $(\boldsymbol{I} - \boldsymbol{F})\,\boldsymbol{p} \leq \boldsymbol{u}$ holds can be written as $\boldsymbol{p} = \boldsymbol{p}_p - \boldsymbol{p}_h$ for a $\boldsymbol{p}_h$ with $(\boldsymbol{I} - \boldsymbol{F})\,\boldsymbol{p}_h \geq 0$ as defined in Section 2.1.2. Then $\boldsymbol{p} \leq \boldsymbol{p}_p$ because $\boldsymbol{p}_h \geq 0$. If $p_i = p_{\max,i}$ and $\Gamma_i < \gamma_i$ holds for some i, then $p_{\max,i} < p_{p,i}$, hence $\boldsymbol{p}_p \not\leq \boldsymbol{p}_{\max}$ and $\mathcal{F}_{\boldsymbol{p}} \cap \mathcal{P} = \emptyset$. □

Proposition 6.1 and 6.2 will be combined into a algorithm in Section 6.1.4. For the next observation, consider the Foschini-Miljanic PCA in (6.2) and notice that it can be seen as a mathematical power iteration on $\boldsymbol{F}$ with a constant added on each iteration. Following this interpretation, it can be seen that the spectral radius of a matrix can be calculated from a

power iteration in combination with the Rayleigh-quotient [141]. In particular, let $\boldsymbol{p}[k]$ be a power iteration of the form $\boldsymbol{p}[k+1] = \boldsymbol{F}\boldsymbol{p}[k]$, then for $k \to \infty$, $\boldsymbol{p}$ converges towards the dominant eigenvector of $\boldsymbol{F}$:

$$\lim_{k\to\infty} \boldsymbol{p}[k] = \lim_{k\to\infty} \boldsymbol{F}^k \boldsymbol{p}(0) = \lim_{k\to\infty} \lambda_1^k \boldsymbol{v}_1, \tag{6.6}$$

for the maximum modulus eigenvalue $\lambda_1 (= \rho(\boldsymbol{F}))$ and its corresponding eigenvector $\boldsymbol{v}_1$. It is known that after sufficient iterations the Rayleigh-quotient $R_{\boldsymbol{F}}(\boldsymbol{p}[k])$ provides a "good" estimate of the eigenvalue [141], because:

$$\lim_{k\to\infty} R_{\boldsymbol{F}}(\boldsymbol{p}[k]) = \lim_{k\to\infty} \frac{\boldsymbol{p}^T[k]\boldsymbol{F}\boldsymbol{p}[k]}{\|\boldsymbol{p}[k]\|^2} = \frac{\lambda_1^{2k+1}\|\boldsymbol{v}_1\|^2}{\lambda_1^{2k}\|\boldsymbol{v}_1\|^2} = \lambda_1. \tag{6.7}$$

Applying this to the current scenario, $R_{\boldsymbol{F}}(\boldsymbol{p}[k])$ can be used to estimate $\rho(\boldsymbol{F})$. This estimation has in principle been found also by Kučera et al. in [139], although they did not develop their algorithm from this perspective, as it can be seen as a special case of their Theorem 4. However, it can only be used for calculation of $\rho(\boldsymbol{F})$ and not to detect the second type of infeasibility, which is due to $\boldsymbol{p}_p \not\leq \boldsymbol{p}_{\max}$. The method can be enhanced by calculating the Rayleigh-quotient not with the noiseless version of $\boldsymbol{p}[k+1]$ but the version including the normalized noise $\boldsymbol{u}$. This leads to a feasibility test of:

$$T_{\boldsymbol{F}}(\boldsymbol{p}[k]) \quad = \quad \frac{\boldsymbol{p}^T[k]\left(\boldsymbol{F}\boldsymbol{p}[k] + \boldsymbol{u}\right)}{\|\boldsymbol{p}[k]\|^2}. \tag{6.8}$$

It will now be shown how this test behaves for feasible and infeasible situations.

Proposition 6.3.

$$\lim_{k\to\infty} T_{\boldsymbol{F}}(\boldsymbol{p}[k]) = \begin{cases} 1, & \text{if } \rho(\boldsymbol{F}) \leq 1 \text{ and } \boldsymbol{p}_p \leq \boldsymbol{p}_{\max} \\ c, & \text{else} \end{cases}$$

with $c \in (1, \rho(\boldsymbol{F})]$ greater than one.

Proof. First, the case without maximum transmission powers will be considered, afterwards the their influence will be discussed. Consider that $\boldsymbol{p}[k]$ can be re-written as $\boldsymbol{p}[k] = \boldsymbol{p}_p + \Delta\boldsymbol{p}[k]$ and $\boldsymbol{p}_p = \boldsymbol{F}\boldsymbol{p}_p + \boldsymbol{u}$ by definition. Because $\boldsymbol{F}(\boldsymbol{p}_p + \Delta\boldsymbol{p}[k]) + \boldsymbol{u} = \boldsymbol{p}_p + \boldsymbol{F}\Delta\boldsymbol{p}[k]$, limit (6.6) applies to $\Delta\boldsymbol{p}[k]$ and (6.8) turns into:

$$\begin{aligned} \lim_{k\to\infty} T_{\boldsymbol{F}}(\boldsymbol{p}[k]) &= \lim_{k\to\infty} \frac{(\boldsymbol{p}_p + \Delta\boldsymbol{p}[k])^T\left(\boldsymbol{F}(\boldsymbol{p}_p + \Delta\boldsymbol{p}[k]) + \boldsymbol{u}\right)}{\|\boldsymbol{p}_p + \Delta\boldsymbol{p}[k]\|^2} \\ &= \lim_{k\to\infty} \frac{(\boldsymbol{p}_p + \lambda_1^k\boldsymbol{v}_1)^T(\boldsymbol{p}_p + \lambda_1^{k+1}\boldsymbol{v}_1)}{\|\boldsymbol{p}_p + \lambda_1^k\boldsymbol{v}_1\|^2} \\ &= \lim_{k\to\infty} \frac{\|\boldsymbol{p}_p\|^2 + (1+\lambda_1)\lambda_1^k\boldsymbol{p}_p^T\boldsymbol{v}_1 + \lambda_1^{2k+1}\|\boldsymbol{v}_1\|^2}{\|\boldsymbol{p}_p\|^2 + 2\lambda_1^k\boldsymbol{p}_p^T\boldsymbol{v}_1 + \lambda_1^{2k}\|\boldsymbol{v}_1\|^2}. \end{aligned} \tag{6.9}$$

It can be seen from (6.9) that if $\lambda_1 \leq 1$, then $\lim_{k\to\infty} T_{\boldsymbol{F}}(\boldsymbol{p}[k]) = 1$ and if $\lambda_1 > 1$, then $\lim_{k\to\infty} T_{\boldsymbol{F}}(\boldsymbol{p}[k]) = \lambda_1$.

Algorithm 2 Direct Measurement Test (DMT) Algorithm

1: BS broadcasts p_T, $\mathcal{S}$ and T_S.
2: All senders report $p_{\text{max},i}$ to BS.
3: **for** $i = 1$ to L **do**
4: Sender i sends with p_T at TTI $T_S + \Delta\text{TTI}_i(\mathcal{S})$.
5: All receivers calculate and store h_{ij}.
6: **end for**
7: All receivers report their h_{ij}'s and N_i to BS.
8: BS calculates $\rho(\boldsymbol{F})$, $\boldsymbol{p}_p$ and checks for $\boldsymbol{p}_p \leq \boldsymbol{p}_{\text{max}}$.
9: If $\rho(\boldsymbol{F}) < 1$ and $\boldsymbol{p}_p \leq \boldsymbol{p}_{\text{max}}$, reuse is feasible.

When $\lambda_1 \leq 1$ but $\boldsymbol{p}_p \nleq \boldsymbol{p}_{\text{max}}$, the PCA will still converge, but to a vector that does not fulfill (6.37) [137]. However, as it does converge at all,

$$\boldsymbol{p}[k+1] = \min\{\boldsymbol{F}\boldsymbol{p}[k] + \boldsymbol{u}, \boldsymbol{p}_{\text{max}}\} \approx \boldsymbol{p}[k] \tag{6.10}$$

will hold for some sufficient large k, meaning that all links will either achieve their requirement with equality or reach their transmit power limit $p_{\text{max},i}$. $\boldsymbol{p}[k]$ will hence satisfy $\boldsymbol{p}[k] \leq \boldsymbol{F}\boldsymbol{p}[k] + \boldsymbol{u}$ element-wise. As all vector elements are nonnegative,

$$\lim_{k\to\infty} T_{\boldsymbol{F}}(\boldsymbol{p}[k]) = \lim_{k\to\infty} \frac{\boldsymbol{p}^T[k](\boldsymbol{F}\boldsymbol{p}[k] + \boldsymbol{u})}{\boldsymbol{p}^T[k]\boldsymbol{p}[k]} > 1. \tag{6.11}$$

As conclusion, if $\lambda_1 \leq 1$ and $\boldsymbol{p}_p \leq \boldsymbol{p}_{\text{max}}$, $T_{\boldsymbol{F}}(\boldsymbol{p}[k])$ converges to 1, if $\lambda_1 \leq 1$ and $\boldsymbol{p}_p \nleq \boldsymbol{p}_{\text{max}}$ it converges to a value in $(0, \lambda_1)$ and otherwise it converges to λ_1, which was stated. □

6.1.4 Proposed Algorithms

Based on the discussion in Section 6.1.3, testing algorithms will now be developed. For this, consider a cellular wireless system with LTE-like transmission resource structure, with separate transmission- and control-channels that can be used differently at each Transmission Time Interval (TTI). Compared to the discussed references, where arriving calls seek admission to a channel, it is assumed that a controller, e.g., the BS, wants to check the reuse feasibility of a predefined set of links at a certain time instant. This check is considered to happen on a regular basis and the output to be used for scheduling decisions of the BS, for frequency reuse decisions or other admission related tasks. In set-ups with a high spatial density of D2D-links reusing resources, control channels might form a bottleneck as they cannot be easily reused. Because of this, the control overhead produced by introduced algorithms are of interest and included in the evaluations. Control traffic is assumed to be collision free and one message is assumed to carry b byte per transported numeric value, such that the accuracy of numeric representation can be tuned towards desired precision.

Algorithm 3 Rayleigh-Quotient Test (RQT) Algorithm

1: BS broadcasts p_T, T_S and I.
2: **for** $k = 1$ to I **do**
3: All senders transmit with $p_i[k]$.
4: All receivers report $\gamma_i/\Gamma_i(k)$ back to sender.
5: **if** $k < I$ **then**
6: Senders set $p_i[k+1] = \min\{\frac{p_i[k]\gamma_i}{\Gamma_i(k)}, p_{\max,i}\}$
7: **end if**
8: **end for**
9: Senders report $p_i[I]$ and $\gamma_i/\Gamma_i(\boldsymbol{p}[I])$ back to BS.
10: BS calculates $T_{\boldsymbol{F}}(\boldsymbol{p}[I])$.
11: If $T_{\boldsymbol{F}}(\boldsymbol{p}[I]) \leq 1$ reuse is feasible, else infeasible.

Direct Measurement Test (DMT) Algorithm

The Direct Measurement Test Algorithm implements the "brute-force reference" mentioned in Section 6.1.3. The BS defines a transmit power p_T, a probing order $\mathcal{S}$ and a start time T_S. $\Delta\text{TTI}_i(\mathcal{S})$ is the relative TTI offset of link i w.r.t. T_S, based on $\mathcal{S}$. The algorithm is described in Algorithm 2.

Assuming that all probing- and control-messages take one TTI for transmission, the algorithm will make a feasibility statement $L + 2$ TTIs after T_S. Control messages are sent in lines 1, 2 and 7 carrying different quantities of numeric values. $|\mathcal{S}| = L$ is assumed, as well as that every receiver reports all L channel gains. So the number control bytes sent is

$$\text{CB}_{\text{DMT}}(L) = (L+2)b + Lb + L(L+1)b = \Omega(bL^2). \tag{6.12}$$

Although some optimization can be done, e.g., $\mathcal{S}$ or $p_{\max,i}$ might be pre-defined, the main contributor to channel usage, which is the channel report by the receivers, cannot be circumvented.

Rayleigh-Quotient Test (RQT) Algorithm

The following algorithm is based on Proposition 6.3. It is used that $(\boldsymbol{F}\boldsymbol{p} + \boldsymbol{u})_i = p_i\gamma_i/\Gamma_i(\boldsymbol{p})$ and hence:

$$T_{\boldsymbol{F}}(\boldsymbol{p}[k]) = \frac{\sum_{i=1}^{L} p_i[k]^2\gamma_i/\Gamma_i(\boldsymbol{p}[k])}{\sum_{i=1}^{L} p_i[k]^2}. \tag{6.13}$$

Alternatively, $R_{\boldsymbol{F}}(\boldsymbol{p}[k])$ can be used, in which case Γ_i becomes the SIR. All links use PCA (6.2) and receivers feed information back to their senders using control channels. The BS defines an initial transmission power p_T that all senders use, a starting time T_S and a number of power-control iterations $I \geq 1$. The algorithm is described as Algorithm 3.

Again assuming that all probing- and control-messages (including feedback from receivers to transmitters) take one TTI, the algorithm will make a feasibility statement $2I + 1$ TTIs after T_S. As Proposition 6.3 holds in the limit, the feasibility statement made after I

Algorithm 4 SI(N)R-Bound Test (SBT) Algorithm

1: BS broadcasts p_T and T_S.
2: **loop**
3: All senders transmit with $p_i[k]$.
4: Receivers set $\beta_i = \begin{cases} 1, \gamma_i \leq \Gamma_i(k) < \gamma_i + \Delta\gamma \\ \gamma_i/\Gamma_i(k), \text{else} \end{cases}$
5: Receivers report β_i back to sender.
6: Receivers report T1, T2 and T3 to BS
7: Senders set $p_i[k+1] = \min\{p_i[k] \cdot \beta_i, p_{\max,i}\}$
8: **end loop**
9: BS receives no outage message within an iteration: Feasible
10: T2 by all links **or** T3: Infeasible

iterations is only true with a probability, depending on how well the PCA has converged. Control messages are sent at lines 1, 4 and 9. So the number of control bytes sent is:

$$\mathrm{CB}_{\mathrm{RQT}}(L, I) = 3b + LIb + 2Lb = \Omega(bIL). \tag{6.14}$$

The conclusion is that the RQT Algorithm will cause less control traffic than the DMT Algorithm, as long as $I < L$. However, when $I > L/2$, the DMT Algorithm will finish faster.

SI(N)R-Bound Test (SBT) Algorithm

The third algorithm uses Proposition 6.1 and 6.2. The PCA (6.2) is adapted such that powers are not updated if their SINR is within a threshold $\Delta\gamma$ above γ_i, which enforces an earlier convergence behavior. All links use the adapted PCA and report outage events to the BS, waiting for the algorithm to converge. Three outage events are defined:

- Type 1 outage (T1) refers to the SINR being below the target threshold.
- Type 2 outage (T2) indicates the SIR being below the SINR target and
- Type 3 outage (T3) denotes a T1 outage combined with that no further SINR change is observed over different iterations.

According to Proposition 6.1, if all UEs report T2 iteration, reuse is assumed infeasible. If no UE reports any event all, it is assumed feasible. Following Proposition 6.2, if a UEs reports a T3 outage, this result is interpreted as infeasible. Again, the BS defines an initial transmit power p_T and a starting time T_S. The algorithm is described as Algorithm 4.

Because neither the duration of the SBT Algorithm, nor the number of messages per iteration are deterministic, an analytical derivation of convergence speed and control overhead of the SBT lgorithm is not performed.

Parameter	Value
Cell Radius	500m
Maximum Tx.	26 dBm
Max. D2D-Dist.	50m
Channel Model	ITU-R M.2135-1
Noise Power	-94.5 dBm
SINR constraint γ_i	10 dB $\forall i \in \mathcal{L}$
$\Delta\gamma$	0.5 in linear domain

Table 6.1: Simulation Parameters

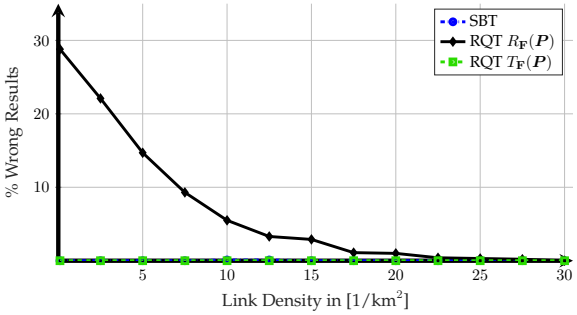

Figure 6.1: Percentage of Wrong Results

6.1.5 Simulative Evaluation

In this section, simulation results for the proposed algorithms are presented. The results were generated using the SimuLTE-framework [97] of the OMNeT++ simulator. A single cell D2D setup of an urban macro cell is assumed, containing one randomly positioned cellular uplink user and a set of D2D links. The number and position of D2D senders follow a p.p.p. of defined density and D2D receivers are placed uniformly distributed within a radius of 50 m of their transmitter. Further used simulation parameters are summarized in Table 6.1. At a predefined time instant, the BS tests the reuse feasibility of all links with the proposed algorithms. The algorithms are compared against the DMT Algorithm and algorithm A1 from [139], which is implemented like the RQT Algorithm using $R_{\boldsymbol{F}}(\boldsymbol{p}[k])$.

In Figure 6.1 the percentage of wrong results produced by the tests, after convergence, is compared for different user densities. Convergence is here assumed at the first TTI after which the feasibility result of the respective algorithm does not change anymore. The DMT Algorithm was used as reference for the true result. It can be seen that the SBT Algorithm and the RQT Algorithm with $T_{\boldsymbol{F}}(\boldsymbol{p}[k])$ always produce the correct result after sufficient iterations, whereas the RQT Algorithm with $R_{\boldsymbol{F}}(\boldsymbol{p}[k])$ can produce a significant amount of wrong results. A further investigation shows that all wrong results of $R_{\boldsymbol{F}}(\boldsymbol{p}[k])$ are false positive and in particular due to maximum power violations. This proves that the second type of infeasibility is not evaluated correctly by $R_{\boldsymbol{F}}(\boldsymbol{p})$.

Figure 6.2a shows the mean number of TTIs needed for convergence by the algorithms. It can be seen that the DMT Algorithm behaves deterministic according to the analysis from Section 6.1.4. The RQT Algorithms converge after 3-4 TTIs, i.e., 1-2 PCA iterations, for all densities. For high densities the RQT Algorithms converge slightly faster because the setups become clearly infeasible. The SBT Algorithm takes longest to converge for low D2D-link densities but saturates for higher densities.

The number of bytes sent on control channels until convergence is shown in Figure 6.2b. Here, $b = 1$ was assumed. The control traffic produced by the DMT Algorithm increases quadratically, as predicted in section 6.1.4. The traffic produced by the RQT Algorithms grows linearly, which is consistent with Figure 6.2a, as the average required iterations stay nearly constant but the average number of links increases linearly. The SBT Algorithm produces the least control traffic for large parts of the considered parameter range. This is notable because it also takes longest to converge. The reason for the low control traffic produced

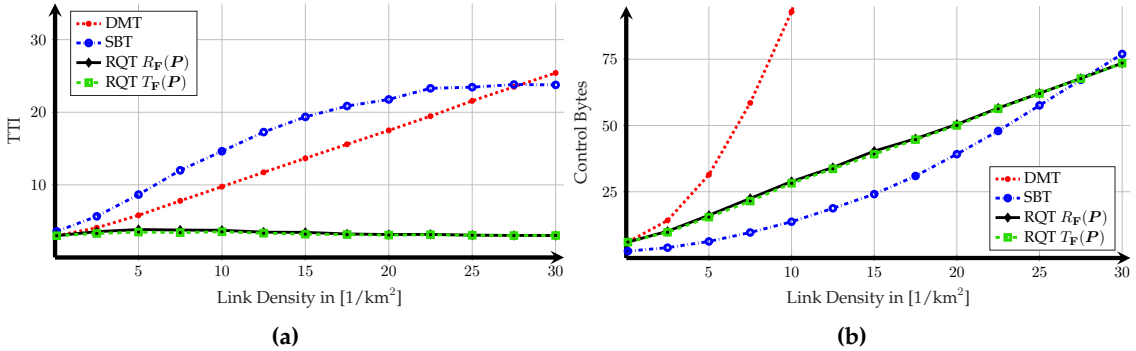

Figure 6.2: 6.2a Shows the convergence speed of the algorithms, whereas 6.2b shows the number of bytes sent on control channels until convergence.

by the SBT Algorithm is that UEs only send upon SINR/SIR outage events. So only a subset of the UEs actually sends reports and in overall, the reports sum up to be less than the regular reports produced by the other algorithms.

The conclusion is that both proposed algorithms, RQT and SBT, meet the target of reliable feasibility statements. The RQT Algorithm is very fast and makes reliable statements after few TTI but causes control traffic in amount linear to the number of participating links. The SBT Algorithm, on the other hand, is rather slow in convergence but produces less control traffic in overall and significantly less per TTI.

6.2 The Reuse Maximization Problem

Interference management in D2D enabled cellular networks comprises aspects of power control based NUM and scheduling. Both problem types have already been extensively investigated in different wireless network structures. In a D2D network, the main challenge is that the organizing entity, which is the BS, does not automatically have access to all required information, such as channel gains. This motivates the need for distributed, or semi-distributed organization to avoid control traffic. While power control based NUM problems are decentralizable for some utilities, the scheduling part adds a combinatorial nature that is hard to tackle in a distributed fashion. However, the good news is that D2D networks do not have to be entirely decentralized, as the BS enables a central coordination which can realize the required centralized tasks. One of the main questions thus is to what extent NUM problems can be decentralized and which parts should be centrally implemented.

Many research works have been dedicated to D2D interference management in the context of NUM problems. Common assumptions in literature are that transmission powers stay fixed or follow simple channel inversion rules and that the number of D2D links that are allowed to reuse a channel is upper bounded by one or two.

While the restriction to one- or two-fold reuse eases the management effort, it also neglects the actual potential of frequency reuse. In previous works [7], [142], [143], by allowing an arbitrary number of reuses, up to 40-fold frequency reuse in a cell could be achieved. Although the exact number depends on many parameters, such as the cell size, average link

distance and targeted SINR, the conclusion is that reuse could in fact be by orders of magnitude larger than often targeted.

The restriction to fixed transmission powers is often done with the comment that including full power control capabilities creates an MINLP structure, which is considered intractably complex for solution, in particular when full centralization is not possible. On the other hand, fixed powers induce sub-optimal behavior. If the powers are fixed at a too low value, the resulting interference constraints are very tight. This can hinder frequency reuse that would be possible if larger power were used. If the powers are fixed too large, it might produce much interference towards other links, again preventing reuse. Finding the right trade-off is a task that can be solved only with dynamic power control.

As for the considered network structure, a two-stage approach is commonly assumed, consisting of an admission control step and an optimization step. During the admission control a set of links is determined that may use a certain channel in spite of mutual interference, whereas the optimization step targets the actual operation in terms of power control and/or scheduling decisions. Both steps can either be solved separately or together in a full-scale optimization and are tightly intertwined, as the admission control can either target to ensure the feasibility of the subsequent problem or already target the achievable utilities themselves, up to the extreme case where it uses the optimal solution of the subsequent problem already for the admission decision. Design and quality of the admission step thus has a major influence on solution quality, as it defines the subsequent problem space. However, its impact is typically not properly investigated.

In this section, a core problem of D2D frequency reuse is targeted, which is termed the Reuse Maximization Problem (RMP). The RMP targets activating as many links as possible on a single resource assuming full power control, subject to the constraint that each active link is guaranteed a target SINR. The motivation for analyzing the RMP is two-fold. First, it targets the admission step, by allowing as much frequency reuse as possible. Second, it is related to a variety of D2D set-ups, as will be shown in Sections 6.2.1 and 6.5, and its analysis creates a fundamental understanding of frequency reuse with full power control. From an algorithmic perspective, it captures the impact of binary link activation in interference-coupled communication systems, paving the way to the solution of general mixed-integer NUM problems with interference constraints.

6.2.1 Problem Formulation

There exist several D2D-scenario types for which RMPs can be formulated, the difference amongst which has to be stressed to maintain credibility of the used problem statement. Mostly in literature, the D2D underlay scenario is considered, in which cellular users are protected from interference caused by D2D links. In this case, D2D links act similarly to cognitive radio links but are coordinated by the base station. However, some works consider set-ups where the D2D links require protection from interference [49]. Examples are MTC or vehicular communication links, which can also be realized with D2D. Further, as suggested in [30], D2D links could also share a resource pool solely among themselves. While this technically is an overlay scenario, here reuse can be performed among D2D links. In any of these

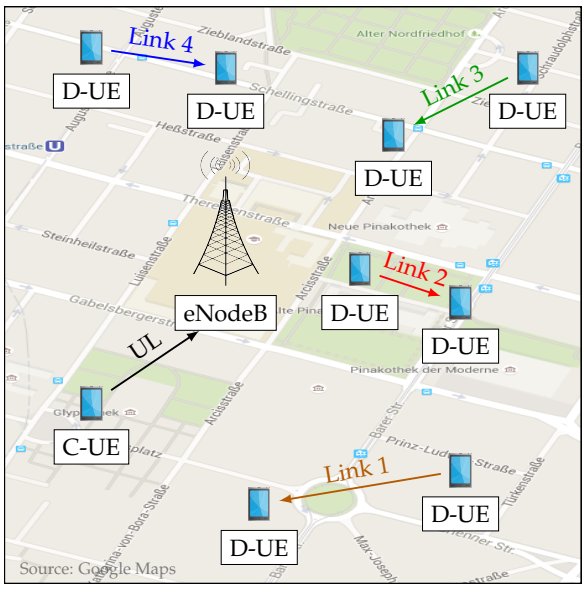

Figure 6.3: Example setup of the frequency reuse maximization problem. The considered question is, which of the present links should be activated such that a maximum number of links is active on the same transmission resource, while all achieve individual minimum quality constraints.

cases, both cellular and D2D links require to maintain a minimum SINR for communication, either for a guaranteed link quality or to have at least basic connectivity. In all scenarios, reuse maximization is the problem how to find the largest set of links that can achieve their SINR constraints in spite of mutual interference. Although the different scenario types are thought different in literature, the underlying problem structure is the same and will induce similar communication structures. Thus, it makes sense to formulate a problem that is capable of incorporating these scenarios as special cases.

The considered set-up is a single channel in a single cell of a cellular network, as shown in Figure 6.3. It is assumed that there is one cellular link and a number of D2D sidelinks, that all have full power control capabilities and can choose either to be active on a considered channel or not. In this set-up the task is to choose a set of links such that the reuse factor on a single channel is maximized, while all active links must maintain a certain SINR threshold.

Mathematically, the problem is formulated using the power control formulation, which is introduced in Section 2.1.2: Assume L wireless links that are gathered in the link set $\mathcal{L}$. For sufficient communication quality, each link requires a minimum SINR $\Gamma_i(\boldsymbol{p}) \geq \gamma_i$, where the powers are taken from an allowed power set $\mathcal{P} = \{\boldsymbol{p} : 0 \leq p_i \leq p_{\max,i} \ \forall i\}$. For each link, introduce an activation indicator $x_i \in \{0, 1\}$ that is zero when link i is inactive and one when it is active. All activation parameters are gathered in a vector $\boldsymbol{x} = [x_1, ..., x_N]^T$. The Reuse Maximization Problem (RMP) is formulated as:

$$\begin{aligned} \text{(RMP)} \qquad & \max_{\boldsymbol{x},\boldsymbol{p}} \sum_{i\in\mathcal{L}} x_i \\ & \text{s.t.} \\ & \Gamma_i(\boldsymbol{p}) \geq \gamma_i x_i \ \ \forall i \\ & \boldsymbol{p} \in \mathcal{P}; \ \ \boldsymbol{x} \in \{0,1\}^L \end{aligned} \tag{6.15}$$

The target is to maximize the number of active links under the condition that all SINR constraints are met, while all transmitters choose powers out of the valid set $\mathcal{P}$. By choosing $x_i = 0$ the corresponding SINR condition is inactivated, hence the SINR of link i is unconstrained.

Note that the RMP can be applied to a variety of use-cases with minor variation. It can be applied to D2D communication underlaying cellular uplink or downlink, or to reuse management among D2D links only, by adapting the link set $\mathcal{L}$. Protection of links, e.g., the underlayed cellular links, can be established by adding the constraint $x_i = 1$ for the corresponding link. Multi-channel reuse maximization as typically found in literature can be formulated by adding constraints of form (6.15) for each channel and adding further constraints, e.g., that all links should use at most one channel, or that not more than a maximum number of links should reuse a certain channel. Finally, note that the RMP also has connections to the D2D-NUM (2.66) itself, which can be implemented by replacing the first line with $\sum_{i\in\mathcal{L}} U_i(\gamma_i)x_i$, where $U_i(\gamma_i)$ is a utility value associated with γ_i. Utility maximization is explicitly not investigated here, as one of the targets is to capture the undisturbed effect of interference, which is not to be traded off against a utility. However, all stated problems are related and lead to the same algorithmic structure, which is investigated.

6.2.2 Related Work

The RMP is typically introduced as admission control step for D2D networks, which ensures that sufficient link quality can be guaranteed before a network utility maximization is performed. Further, it closely matches the problem of Call Admission Control (CAC) in voice networks. The closest related work for both, D2D and CAC are summarized in the following.

D2D Related Work

In D2D-context, there exist investigations with direct connections to the RMP, as well as more generally related NUM approaches.

Liu et al. [142] considered utility maximization with SINR guarantees and power control, allowing an arbitrary number of reusing D2D-links. Although their target was not to maximize reuse, their solution includes an admission control step that aims at adding as many D2D links as possible to a single channel.

In [143], Sun et al. investigated an RMP with fixed transmission powers. They transformed SINR constraints into an equivalent maximum interference threshold and generated a conflict graph by constructing edges whenever one link acts as dominant interferer, i.e., whenever one link alone is sufficient to violate the interference constraint of another one. By this, the authors transformed the problem into a maximum independent set problem for which they proposed a heuristic.

Another approach was proposed by Lee et al. [144]. In this work, the authors maximized reuse among D2D links, again assuming pre-set transmission powers and transforming SINR constraints into maximum interference constraints. By considering fading as unknown, they interpreted the received interference as a random variable. A link combination was consid-

ered feasible if all SINR constraints hold with a minimum probability. The RMP was formulated as set multi-covering problem on a graph, for which a greedy and an approximate algorithm were proposed and compared. The approach was later extended by Kuhnle et al. [145], who investigated online algorithms for solving the set multi-covering problem.

Elhami et al. [146] formulated reuse maximization as minimization of utilized resources with SINR constraints, assuming fixed powers. A contention graph was constructed using the disk graph interference model and inverted to create an allowed reuse graph. On the latter graph, the authors formulated reuse maximization as maximum clique problem for which they proposed two solution approaches.

Finally, Esmat et al. [147] considered resource sharing for sum-rate maximization with power control. They proposed a two stage approach, where the first stage is a greedy reuse maximization with maximum interference constraint, considering mutual channel coefficients.

Other D2D-related works in literature are more loosely related to the RMP. The works [122], [133], [148]–[155] investigate resource allocation for utility maximization, either with one-fold [122], [133], [148]–[150], [154] or multi-fold [151]–[153], [155] frequency reuse. Utility maximization and reuse maximization have a tight relation but differ in the used utility function, which is the number of active links for the latter. Among the mentioned works, [133], [148], [153], [155] consider power control while fixing the reuse partners and only [153] combines this with multiple reuse of a cellular resource. The adopted method throughout works [133], [148], [155] is to calculate optimal powers for each possible link combination and evaluate the achievable utility, before optimizing. [153] constrains reuse to those link sets where reuse among each combination of two links is possible, which is again tested by calculating optimal powers. All works leverage the fact that optimal powers can be calculated in closed form for one-fold reuse, which does not hold for the multi-reuse case. The use of optimal transmission powers for admission is a good example for the mentioned extreme case, where an optimal solution of the subsequent problem is used already for admission.

It can be concluded that most of the above approaches assume transmission powers to be fixed during the admission control steps, and hence have a different problem structure than the one investigated here, or rely on closed form solutions to the power control problem, which cannot be given for multi-reuse cases.

Admission Control Related Work

Problems similar to the investigated RMP have been investigated in the context of CAC, the main solutions of which are summarized here. In general, reuse maximization can be performed by activating links or sets of links, as well as by deactivating links or sets of links [156]. In [53], J. Zander proposes a Stepwise Removal Algorithm (SRA), where the link with the largest maximum of both, row sum and column sum of the relative gain matrix is deactivated step-by-step, until a feasible solution is found. Andersin et al. propose the SMART criterion in [156], which deactivates those links that will reduce the sum of elements in the gain matrix most, and prove this to outperform the SRA. Xiao et al. propose the call admission control scheme Δ-CAC, in which inactive links use low-power probing tones to determine

whether they can become active [137]. Links are therein activated if a certain discriminant, Δ, is larger than zero. Chen et al. [157] propose a decentralized two-phase link selection algorithm that extends [137]. In this algorithm, the dynamics of the Distributed Constrained Power Control (DCPC) [67] are used to determine a first feasible set, which is then extended by repeatedly executing the Δ-CAC algorithm with random links. The focus of [157] is not to provide an optimal solution but to create a completely decentralized algorithm and, correspondingly, the proposed approach creates a sub-optimal result. Finally, Lee et al. use a heuristic for D2D reuse link selection in [158] where those links are deactivated, whose column vectors in the relative gain matrix have a maximal 2-norm. For this last work, however, the performance of the link selection is not in focus and hence not evaluated.

Considering the above works, most solutions are derived from non-negative matrix theory or use a power control approach. The works [53], [156], [158] can be interpreted to use matrix norms to indicate the severity of interference. Correspondingly, the links with largest impact on the norm are reduced. In contrast, the remaining works [137], [157] rely on the convergence of power control algorithms to maximize the number of active links.

6.2.3 Properties of the RMP

Now follows an analysis of the RMP, which comprises of two parts: The first part in this section and Section 6.2.4 establishes properties that will be used for algorithm design in Section 6.4.1. In this section, the RMP is transformed into a relaxed and interference limited form. Two interpretations of the relaxed problem are given, a graph theoretic and an optimization based one. After properties that are known for the resulting formulation are presented, it is shown in that the RMP is tightly connected to finding those links that minimize the spectral radius of the relative gain matrix. This corresponds to finding the links with the best conditioned interference situation. By analyzing how to find these links the main point of view on the RMP is established: Necessary optimality conditions are given and the relative interference pressure is introduced, which is a parameter that indicates the local impact of a link on the spectral radius.

The Relaxed RMP

The RMP is an MINLP and hence has one of the hardest possible algorithmic problem structures. It will now be reformulated such that it becomes more tractable for analytic investigation. First, the integer constraint of the x_i is relaxed and instead $x_i \in [0,1]\ \forall i$ is demanded. This neglects the mixed-integer part and turns the problem into a nonlinear problem (NLP). Further, it is made compatible with use of the relative gain matrix, which constitutes a standard perspective used in power control theory [55], [57]. For this, the SINR constraint (6.15) of the RMP is transformed into:

$$p_i \geq x_i \left(\sum_{j \neq i} \gamma_i \frac{h_{ij}}{h_{ii}} p_j + \gamma_i \frac{N_i}{h_{ii}} \right) \quad \forall i \quad \Leftrightarrow \quad \boldsymbol{p} \geq \boldsymbol{X}(\boldsymbol{x}) \left(\boldsymbol{F}\boldsymbol{p} + \boldsymbol{u} \right). \tag{6.16}$$

$\boldsymbol{X}(\boldsymbol{x})$ therein is a diagonal matrix with entries $[\boldsymbol{X}(\boldsymbol{x})]_{ii} = x_i$, $\boldsymbol{F}$ is a relative gain matrix with entries $[\boldsymbol{F}]_{ij} = \gamma_i h_{ij}/h_{ii}$ if $i \neq j$ and zero otherwise and $\boldsymbol{u}$ is a vector with entries

$u_i = \gamma_i N_i / h_{ii}$. The complexity is reduced even further by relaxing (6.16) to the interference limited case. That is, it is assumed that compared to interference power, the noise power is negligible so approximately $N_i \approx 0 \; \forall i$ can be assumed, leading to $\boldsymbol{u} \approx \boldsymbol{0}$. It is known that this case exists only in the limit. However, it is proven particularly powerful for analytical investigation as it captures the case of *pure* interference. The impact of noise and integer constraints will be discussed in Sections 6.2.4. After all transformations, the relaxed RMP (R-RMP) reads

$$\begin{aligned} \text{(R-RMP)} \qquad & \max_{\boldsymbol{x},\boldsymbol{p}} \sum_{i \in \mathcal{L}} x_i \\ & \text{s.t.} \\ & \boldsymbol{p} \geq \boldsymbol{X}(\boldsymbol{x}) \boldsymbol{F} \boldsymbol{p} \\ & \boldsymbol{p} \in \mathcal{P}; \;\; \boldsymbol{x} \in [0,1]^L. \end{aligned} \tag{6.17}$$

Known Properties Related to the R-RMP

Problems with constraints similar to (6.17) are known to fall under the framework of Perron-Frobenius Theory [57], [77], which is well established but cannot be considered common knowledge in networking community. In this section, an overview over related properties is given that have been identified in literature within the last two decades:

The matrix $\boldsymbol{X}(\boldsymbol{x})\boldsymbol{F}$ has only positive or zero elements, i.e., is a non-negative matrix. According to the Perron-Frobenius Theorem for non-negative matrices, the maximum-norm eigenvalue ρ of $\boldsymbol{X}(\boldsymbol{x})\boldsymbol{F}$ is real and positive. This eigenvalue thus is equal to the matrix's spectral radius $\rho(\boldsymbol{X}(\boldsymbol{x})\boldsymbol{F})$ [77].

The eigenvector associated with the maximum eigenvalue, which is denoted with $\boldsymbol{p}_\rho$, is further known to have only positive elements and hence is a valid power vector if it is in $\mathcal{P}$. The application of the Perron-Frobenius Theorem to power control problems gives the result that an inequation of the form $\boldsymbol{p} \geq \boldsymbol{X}(\boldsymbol{x})\boldsymbol{F}\boldsymbol{p}$ can be satisfied if, and only if, $\rho(\boldsymbol{X}(\boldsymbol{x})\boldsymbol{F}) \leq 1$ [53], [77]. Feasibility of the power control problem thus entirely depends on channel gains and SINR targets but not on the actually used powers. Power control algorithms that will find feasible powers whenever $\rho(\boldsymbol{X}(\boldsymbol{x})\boldsymbol{F}) \leq 1$ exist and are well-known [54], [67], [69].

As corollary, the set of feasible $\boldsymbol{x}$ with gain matrix $\boldsymbol{F}$ can be defined according to (2.7) as

$$\mathcal{F}_x = \{\boldsymbol{x} \in [0,1]^L \mid \exists \boldsymbol{p} \in \mathcal{P} : \boldsymbol{p} \geq \boldsymbol{X}(\boldsymbol{x})\boldsymbol{F}\boldsymbol{p}\} = \{\boldsymbol{x} \in [0,1]^L : \rho(\boldsymbol{X}(\boldsymbol{x})\boldsymbol{F}) \leq 1\} \tag{6.18}$$

$\mathcal{F}_x$ can be interpreted as sub-level set of the function $\rho(\boldsymbol{x}) = \rho(\boldsymbol{X}(\boldsymbol{x})\boldsymbol{F})$ with respect to $\boldsymbol{x}$ for a sub-level of one. Demanding $\boldsymbol{p} \geq \boldsymbol{X}(\boldsymbol{x})\boldsymbol{F}\boldsymbol{p}$ in the R-RMP in fact corresponds to demanding $\boldsymbol{x} \in \mathcal{F}_x$, as a feasible power exists if and only if the latter is true. Power control could thus be completely neglected for the R-RMP, considering that finding feasible powers is a solved problem. However, $\mathcal{F}_x$ is known only implicitly, so constraining $\boldsymbol{x}$ to $\mathcal{F}_x$ is impractical for real optimization.

From the definition of $\boldsymbol{X}(\boldsymbol{x})\boldsymbol{F}$, structural properties introduced for the feasible SINR region $\mathcal{F}_\gamma$ in Section 2.1.2 transfer to $\mathcal{F}_x$. $\mathcal{F}_x$ can be shown to be convex with respect to logarithmically scaled activation variables $\tilde{x}_i = \log(x_i)$ [57]. A matrix-vector product can be

interpreted element-wise as:

$$[\boldsymbol{X}(\boldsymbol{x})\boldsymbol{F}\boldsymbol{p}]_i = x_i \frac{\gamma_i}{\Gamma_i(\boldsymbol{p})} p_i, \tag{6.19}$$

which relates to the PC problem. Further, let $\mathcal{A} = \{k \in \mathcal{L} : x_k > 0\}$ be the set of active links. Then it holds $\forall \boldsymbol{p} > 0$ that [57], [77]

$$\max_{i \in \mathcal{A}} x_i \frac{\gamma_i}{\Gamma_i(\boldsymbol{p})} \geq \rho(\boldsymbol{X}(\boldsymbol{x})\boldsymbol{F}) \geq \min_{i \in \mathcal{A}} x_i \frac{\gamma_i}{\Gamma_i(\boldsymbol{p})}, \tag{6.20}$$

with equality if and only if $\boldsymbol{p} = \boldsymbol{p}_\rho$. Equation (6.20) shows that the achievable max-min SINR offset factor $\Gamma_i(\boldsymbol{p})/\gamma_i$ becomes larger when $\rho(\boldsymbol{X}(\boldsymbol{x})\boldsymbol{F})$ decreases, which indicates an achievable robustness with respect to the SINR targets. Further, it is known that the size of the feasible power set $\mathcal{F}_{\boldsymbol{p}} = \{\boldsymbol{p} : \Gamma_i(\boldsymbol{p}) \geq x_i \gamma_i \ \ \forall i\}$ increases with decreasing spectral radius $\rho(\boldsymbol{X}(\boldsymbol{x})\boldsymbol{F})$. Due to this, the spectral radius can be considered as indicator for the *condition* of interference situation in the network. A lower radius indicates a better interference condition and vice versa.

Applying the load-spillage formulation of [56] to the RMP results in

$$\boldsymbol{l}_\rho = \boldsymbol{X}(\boldsymbol{x})\boldsymbol{F}\boldsymbol{p}_\rho \text{ and } \left(\boldsymbol{X}(\boldsymbol{x})\boldsymbol{F}\right)^T \boldsymbol{s}_\rho = \boldsymbol{s}_\rho \rho(\boldsymbol{x}). \tag{6.21}$$

Finally, let $\boldsymbol{p}_\rho, \boldsymbol{s}_\rho$ be the right and left eigenvectors of $\boldsymbol{X}(\boldsymbol{x})\boldsymbol{F}$ corresponding to $\rho(\boldsymbol{x})$, scaled such that $\boldsymbol{s}_\rho^T \boldsymbol{p}_\rho = 1$. Then [56]

$$\frac{\partial \rho(\boldsymbol{x})}{\partial x_i} = s_{\rho,i} \cdot [\boldsymbol{F}\boldsymbol{p}_\rho]_i \,; \ \ \frac{\partial \rho(\tilde{\boldsymbol{x}})}{\partial \tilde{x}_i} = s_{\rho,i} \cdot [\boldsymbol{X}(\boldsymbol{x})\boldsymbol{F}\boldsymbol{p}_\rho]_i = s_{\rho,i} l_{\rho,i}. \tag{6.22}$$

Graph-Theoretic Interpretation of the R-RMP

Apart from the optimization problem of given in Section 6.2.3, the R-RMP also has a connection to graph theory that is leveraged in Section 6.3:

For any given network, define $\mathcal{G}_{\boldsymbol{F}} = \{\mathcal{V}, E\}$ to be a graph with node set $\mathcal{V} = \mathcal{L}$ and edge set $E = \mathcal{L} \times \mathcal{L}$. Define the weights of edges $w : E \to \mathbb{R}_+$ as $w(e_{ij}) = f_{ij} \ \forall e_{ij} \in E$ Then the gain matrix $\boldsymbol{F}$ can be interpreted as adjacency matrix of $\mathcal{G}_{\boldsymbol{F}}$. From this perspective, the R-RMP becomes the problem of finding the node-maximal sub-graph of $\mathcal{G}_{\boldsymbol{F}}$, such that the spectral radius of its adjacency matrix is smaller than one. This problem has been investigated from a mathematical point of view, e.g., in [159].

The Spectral Radius Minimization Problem (SRMP)

Related to the RMP optimization problem is its' feasibility problem [160], which is the problem of finding a feasible point for a pre-defined utility level, or a point as close to feasibility as possible if there is no such point. From the background of Perron-Frobenius Theory, a feasibility problem can be defined in the following way, termed the Spectral Radius Minimization

Problem (SRMP):

$$\text{(SRMP)} \qquad \min_{\boldsymbol{x},\boldsymbol{p},c} c \tag{6.23}$$

$$\text{s.t.}$$

$$c\boldsymbol{p} \geq \boldsymbol{X}(\boldsymbol{x})\boldsymbol{F}\boldsymbol{p} \tag{6.24}$$

$$\sum_{i\in\mathcal{L}} x_i \geq K \tag{6.25}$$

$$\boldsymbol{p} \in \mathcal{P}; \;\; \boldsymbol{x} \in [0,1]^L$$

Note that the relaxed constraints of the R-RMP are incorporated here. A version for the original RMP can be created analogously. Condition (6.24) can be interpreted in the light of (6.19) as $c \geq x_i\gamma_i/\Gamma_i(\boldsymbol{p})\ \forall i$. The utility (6.23) in combination with (6.24) realizes a min-max problem structure on $x_i\gamma_i/\Gamma_i(\boldsymbol{p})$, whereas (6.25) ensures an activation level of at least K. By property (6.20), the optimal value of c will equal the spectral radius of the matrix $\boldsymbol{X}(\boldsymbol{x})\boldsymbol{F}$. Because the radius is strictly increasing with x_i, constraint (6.25) will be tight at optimality. As result, the SRMP aims at finding that activation vector $\boldsymbol{x}$ with activation level K that has the smallest spectral radius. This can also be interpreted in a way that it aims at finding the link activation vector with best conditioned interference coupling. The SRMP can also be interpreted as minimization of the maximum-norm $\|\cdot\|_\infty$ on slack-variables of the SINR-constraints, which will be detailed in Section 6.4.3. A feasibility problem of the shown form can be used to solve the R-RMP by adapting K, for example using a bisection search.

Lagrangian and KKT-Conditions of the SRMP

The SRMP allows a particularly insightful interpretation of the involved parameters and properties form an optimization perspective, which is developed here. These parameters and properties transfer from SRMP to R-RMP but the SRMP gives a clearer view, which is why it is used here.

The SRMP has a non-convex structure and in general possesses several local minima. In the form given above, constraint (6.24) is non-convex in the combined $\boldsymbol{p}$-$\boldsymbol{x}$-c space. By using the *hidden convexity* as proposed in [57], [75], [161], (6.24) can be turned into a convex constraint. For this, logarithmically scaled variables $\tilde{x}_i = \log(x_i)$ and $\tilde{p}_i = \log(p_i)$ are used. However, although this convexifies (6.24), condition (6.25) then turns into

$$\sum_{i\in\mathcal{L}} \exp(\tilde{x}_i) \geq K, \tag{6.26}$$

which again is a non-convex condition. By applying results from [57], it can be shown that there is no variable transformation such that all constraints are convex at the same time. That is, there is no hidden convexity in the SRMP. In spite of this misfortune, necessary optimality conditions exist, in particular the KKT conditions, which at least indicate local optimality. The Lagrange function associated with SRMP is

$$L(c,\boldsymbol{p},\boldsymbol{x},\boldsymbol{\eta},\mu) = c + \boldsymbol{\eta}^T\left(\boldsymbol{X}(\boldsymbol{x})\boldsymbol{F}\boldsymbol{p} - c\boldsymbol{p}\right) + \mu\left(K - \sum_{i\in\mathcal{L}} x_i\right), \tag{6.27}$$

where $\boldsymbol{\eta} \geq 0$ and $\mu \geq 0$ are multipliers and it was implicitly assumed that $\boldsymbol{p} \in \mathcal{P}$ and $\mathbf{0} \leq \boldsymbol{x} \leq \mathbf{1}$. A point is a KKT-point and hence locally optimal if it satisfies the conditions:

$$\boldsymbol{\eta}^T \boldsymbol{p} = 1; \quad \boldsymbol{\eta}^T \boldsymbol{X}(\boldsymbol{x}) \boldsymbol{F} = c\boldsymbol{\eta}^T; \quad \eta_i \left[\boldsymbol{F}\boldsymbol{p}\right]_i = \mu \ \ \forall i. \tag{6.28}$$

The complementary slackness conditions are:

$$\eta_i \left(x_i \sum_{j \neq i} f_{ij} p_j - c p_i \right) = 0 \ \ \forall i; \quad \mu \left(K - \sum_{i \in \mathcal{L}} x_i \right) = 0. \tag{6.29}$$

Note that the conditions remain the same when a logarithmic transformation is used. $\boldsymbol{p}$ and $\boldsymbol{x}$ have been assumed to be taken from their allowed spaces for notational brevity. However, adding constraints for adds slack variables that change the last KKT condition to

$$\eta_i \left[\boldsymbol{F}\boldsymbol{p}\right]_i = \begin{cases} \geq \mu, & \text{if } x = 0, \\ = \mu, & \text{if } x \in (0,1), \\ \leq \mu, & \text{if } x = 1, \end{cases} \quad \forall i \tag{6.30}$$

and creates analogous conditions for the powers p_i when they are on their lower and upper bounds.

Considering the middle optimality condition of (6.28), the conclusion is that at any locally optimal point, $c^* = \rho(\boldsymbol{X}(\boldsymbol{x})\boldsymbol{F})$ is the spectral radius and $\boldsymbol{\eta}^* = \boldsymbol{s}_\rho \geq \mathbf{0}$ is the spillage. Further, $\eta_i^* > 0 \ \forall i \in \mathcal{A}$ and (6.29) imply $p_i^* = p_{\rho,i}$ for $i \in \mathcal{A}$ and $p_i^* = 0$ otherwise. Also $\mu^* > 0$ holds from (6.30), which implies $\sum_{i \in \mathcal{L}} x_i^* = K$ by (6.29).

Relative Interference Pressure

Condition (6.30) has a particularly insightful interpretation. From the above conclusions and equation (6.22), in any locally optimal point the term $m_i = \eta_i^* \left[\boldsymbol{F}\boldsymbol{p}^*\right]_i$ is the product of interference load and spillage, which equals the derivative of the spectral radius. This is consistent, considering that the aim was to minimize $\rho(\boldsymbol{x})$ in first place. Because condition (6.30) was derived from setting $\partial L(c, \boldsymbol{p}, \boldsymbol{x}, \boldsymbol{\eta}, \mu)/\partial x_i = 0$, intuitively, x_i should be decreased to minimize $\rho(\boldsymbol{x})$ whenever $m_i > \mu$, i.e., $\partial L(c, \boldsymbol{p}, \boldsymbol{x}, \boldsymbol{\eta}, \mu)/\partial x_i > 0$ and increased when $m_i < \mu$.

The values of m_i and μ thus have a force-field interpretation: m_i is a system inherent parameter that captures the local impact of link activation on interference condition. It holds that $m_i \geq 0$ and $m_i = 0$ if, and only if, $x_i = 0$. The parameter m_i thus acts as deactivating force, that pulls the x_i towards zero. μ, on the other hand, is a parameter of choice that counters the effect of m_i. It acts as applied force, driving the links active. A general notion of this is depicted in Figure 6.4 for an instance of $\rho(\boldsymbol{x})$. To make the parameters m_i and μ intuitively accessible, m_i is called the *relative interference pressure*, which can be imagined as a deactivating force in the network. Correspondingly, the multiplier μ is an *activation pressure*, which is an employed force that activates links.

While the considered SRMP is a very specific problem formulation, similar force-field interpretations can be used for a multitude of interference management problems and also for

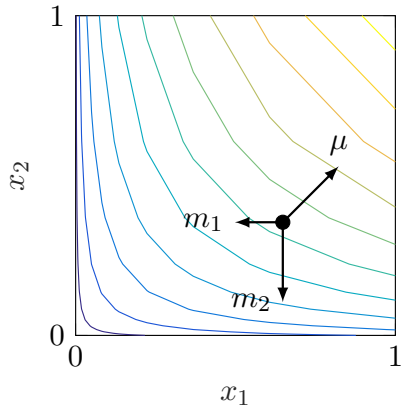

Figure 6.4: Force Field interpretation of interference pressure. The background shows height lines of the spectral radius, which is a concave function of $\boldsymbol{x}$. At the point marked with a dot, different values of m_i "pull" the links towards deactivation, with different force. The multiplier μ acts as activation force that applies to all links with same strength.

the R-RMP, because it is derived from the SINR condition. It is presented here for the SRMP because the interpretation becomes particularly clear. For other, more general interference management problems, the applied activation pressure will differ for each link and depend on the used utility function, whereas the interference pressure takes the same form as for the SRMP. The main difficulty of interference management lies in the non-linear behavior of the pressure, which is mainly driven by the fact that the spectral radius is a concave function [57].

6.2.4 Impacts of Relaxation

Now the impact of non-zero noise will be discussed. Further, the suspicion is motivated that the effect of binary link activation on the spectral radius can be bounded only by trivial bounds, which is the main driver of complexity.

Impact of Non-Zero Noise

So far, noise was assumed to be negligible. When noise becomes non-negligible, it slightly changes the problem structure. With noise, the spectral radius itself is only partly a good indicator for the condition of an interference situation. In fact, it looses its quality with increasing impact of the relative noise values u_i. However, important characteristics can be transferred from the noise-free to the noise-afflicted case: i) In the noise-afflicted case, a feasibility problem similar to the SRMP can be defined as max-min-SINR problem, only that the optimal solution is not attained anymore by $\boldsymbol{p}_\rho$ given in (6.20) but by some other $\boldsymbol{p}^*$. ii) The introduction of noise creates an affine version of (6.24) and hence does not change the convexity properties of the considered problems. iii) The main change is in the KKT-optimality conditions of SRMP which become $c^* = \Gamma_i(\boldsymbol{p}^*)/\gamma_i \; \forall i$, i.e., the maximum factor by which all SINRs can jointly be increased over their target. $\boldsymbol{\eta}^* = \boldsymbol{s}_\rho$ remains the spillage vector and

(6.30) turns into

$$m_i = s_{\rho,i}\left[\boldsymbol{F}\boldsymbol{p} + \boldsymbol{u}\right]_i \gtreqless \mu \;\; \forall i. \tag{6.31}$$

This quantity can still be interpreted as interference pressure, only that noise is included in the load factor in brackets. By this, the interference load is effectively turned into an interference plus noise load, which still complies with the force field interpretation.

Impact of Binary Activation

In the previous sections it was assumed that $x_i \in [0,1]\ \forall i$, neglecting the integer parts of the originally targeted RMP. This allowed to gain insights on the internal problem structure, as technically, on binary space no gradient exists and in general, no optimality conditions hold. However, relaxation is not necessarily suitable for optimization because the result might induce "partially active" links with $0 < x_i < 1$. Optimally mapping $\boldsymbol{x}$ back to integer space is, again, a non-trivial problem. Mere rounding does not provide good solutions and a full search around an optimal point has exponential complexity. Further, standard optimization techniques such as primal-dual based algorithms show bad convergence behaviors for the relaxed problem in preliminary investigations, thus even failing at finding locally optimal points of the R-RMP efficiently. On the other hand, as soon as the x_i are restricted to integer solutions, not even local optima might be found, because these are not guaranteed to be on integer domain.

One possibility to create tractable integer formulations is the use of outer approximations for the feasible activation region $\mathcal{F}_x$. Such approximations can be used to turn the activation problem into a purely integer problem that is independent of the power vector $\boldsymbol{p}$. A straightforward way to create outer approximations is to leverage the hidden convexity and transform $\boldsymbol{x}$ and $\boldsymbol{p}$ into logarithmic domain. Because $\rho(\boldsymbol{X}(\tilde{\boldsymbol{x}})\boldsymbol{F})$ is convex, it can be approximated in this domain as maximum over linear approximation functions $\hat{\rho}^{(k)}(\tilde{\boldsymbol{x}})$, which relate as $\hat{\rho}^{(k)}(\tilde{\boldsymbol{x}}) \leq \rho(\tilde{\boldsymbol{x}})\ \forall k$. For each $\hat{\rho}^{(k)}(\tilde{\boldsymbol{x}})$, a sub-level set $\hat{\mathcal{F}}_x^{(k)} = \{\boldsymbol{x} : \hat{\rho}^{(k)}(\log(\boldsymbol{x})) = \hat{\rho}^{(k)}(\tilde{\boldsymbol{x}}) \leq 1\}$ can be created, yielding

$$\mathcal{F}_x = \{\boldsymbol{x} : \rho(\boldsymbol{x}) \leq 1\} \subseteq \bigcap_k \hat{\mathcal{F}}_x^{(k)} \tag{6.32}$$

The $\hat{\rho}^{(k)}(\boldsymbol{x})$ can be created by a first order Taylor series of $\rho(\boldsymbol{X}(\tilde{\boldsymbol{x}})\boldsymbol{F})$ as

$$\hat{\rho}^{(k)}(\boldsymbol{x}) = \rho^{(k)} + \sum_{i=1}^{L} m_i^{(k)} \left(\tilde{x}_i - \tilde{x}_i^{(k)}\right) = \rho^{(k)} + \sum_{i=1}^{L} m_i^{(k)} \log(x_i / x_i^{(k)}). \tag{6.33}$$

Here, $\rho^{(k)} = \rho(\boldsymbol{X}(\boldsymbol{x}^{(k)})\boldsymbol{F})$ is an estimate of the spectral radius at $\boldsymbol{x}^{(k)}$, while $m_i^{(k)}$ is the interference pressure at $\boldsymbol{x}^{(k)}$ and ensures that the derivative of $\hat{\rho}^{(k)}(\boldsymbol{x}^{(k)})$ matches that of $\rho(\boldsymbol{X}(\boldsymbol{x}^{(k)})\boldsymbol{F})$.

Considering (6.33), the logarithmic form of $\hat{\rho}^{(k)}(\boldsymbol{x})$ has problematic issues. First, inactivating links creates $x_i = 0$, which is not in the domain of $\hat{\rho}^{(k)}(\boldsymbol{x})$. Second, when $x_i \to 0$, or equivalently $\tilde{x}_i \to -\infty$, the value of any approximation with $m_i^{(k)} > 0$ will grow unbounded to $-\infty$. However, a pressure $m_i^{(k)} > 0$ is generated by any $x_i^{(k)} > 0$, i.e., by any link that is not fully inactive. On the other hand when $m_i^{(k)} = 0$, which is generated by $x_i^{(k)} = 0$, then

changing x_i will not change the value of $\hat{\rho}^{(k)}(\boldsymbol{x})$, meaning that $\hat{\rho}^{(k)}(\boldsymbol{x})$ does not contain any information on x_i.

Because of this structure, when the set $\mathcal{A}^{(k)} = \{i : x_i^{(k)} > 0\}$ is considered, which contains all links that have been active to generate approximation k, then setting any $x_i = 0$ for $i \in \mathcal{A}^{(k)}$ will induce $\hat{\rho} \to -\infty$ and hence create an activation vector in $\hat{\mathcal{F}}_x^{(k)}$. Further, setting any $x_i > 0$ for $i \notin \mathcal{A}^{(k)}$ will not change $\hat{\rho}^{(k)}(\boldsymbol{x})$ at all. So when any number of links $i \notin \mathcal{A}^{(k)}$ are added to any proper sub-set of $\mathcal{A}^{(k)}$, the result will be in $\hat{\mathcal{F}}_x^{(k)}$. $\hat{\mathcal{F}}_x^{(k)}$ thus only excludes an infeasible $\mathcal{A}^{(k)}$ and all its super-sets. This exclusion is trivial, as $\rho(\boldsymbol{X}(\boldsymbol{x})\boldsymbol{F})$ known to be strictly increasing with $x_i \; \forall i$, hence supersets of an infeasible set must trivially be infeasible.

Although a formal proof is not yet given, investigations done for the assessment of this problem strongly indicate that a logarithmic transformation is the closest approximation of $\hat{\rho}(\boldsymbol{x})$ that is valid for all possible channel realizations and on the entire domain of $\boldsymbol{x}$. If this is true, it must be concluded that binary activation and deactivation of links create singularities that render bounds of their impact on the spectral radius trivial. The main complexity of the RMP comes from this property, as the search space cannot be properly bounded and thus remains very large.

6.2.5 Complexity Analysis of the RMP

A complexity statement for the RMP can be given by relating it to graph theory. Assume the graph $\mathcal{G}_{\boldsymbol{F}} = \{\mathcal{V}, E\}$ to be as defined in the graph-theoretic interpretation of the R-RMP. That is, $\mathcal{V} = \mathcal{L}$ is the node set and $E = \mathcal{L} \times \mathcal{L}$ the edge set with associated weights of $w : E \to \mathbb{R}_+$, $w(e_{ij}) = f_{ij} \; \forall e_{ij} \in E$. $\boldsymbol{F}$ can be interpreted as adjacency matrix of $\mathcal{G}_{\boldsymbol{F}}$.

Theorem 6.1. The RMP is NP-complete.

Proof. The proof can be done analogously to the NP-completeness proof shown in [162]. Consider the graph $\mathcal{G}_{\boldsymbol{F}}$ with $\boldsymbol{F}$ as adjacency matrix. The RMP can be reduced to the noiseless case of $N_i = 0 \; \forall i$, in which $\rho(\boldsymbol{F}) \leq 1$ is necessary and sufficient for feasibility. The noiseless case can thus be re-stated as maximizing the number of links such that the spectral radius of $\boldsymbol{F}$ is smaller than one. In the graph perspective, deactivating a link corresponds to removing its node from $\mathcal{G}_{\boldsymbol{F}}$ and the RMP corresponds to finding the maximum subgraph of $\mathcal{G}_{\boldsymbol{F}}$ with spectral radius smaller than one. Define a property on the graph as $\Pi(\mathcal{G}_{\boldsymbol{F}}) : \rho(\boldsymbol{F}) \leq 1$. The property $\Pi(\mathcal{G}_{\boldsymbol{F}})$ is non-trivial, i.e., it is true and false for infinitely many graphs. It further is *hereditary*, i.e., if a graph satisfies $\Pi(\mathcal{G}_{\boldsymbol{F}})$, so do all its sub-graphs. This is true because $\rho(\boldsymbol{F})$ strictly decreases when a link is deactivated. So $\Pi(\mathcal{G}_{\boldsymbol{F}})$ is a non-trivial, hereditary property and the RMP corresponds to finding a maximum sub-graph of $\mathcal{G}_{\boldsymbol{F}}$ that satisfies $\Pi(\mathcal{G}_{\boldsymbol{F}})$. It has been shown [163] that any maximum sub-graph problem with non-trivial, hereditary property can by default be reduced to the satisfiability problem, which is NP-complete. As result, the RMP with noise can be reduced to the noiseless RMP and via this to the satisfiability problem, which renders it NP-complete. □

6.2.6 Impact on Complexity of Related Problems

The NP-completeness serves as catalyzer to assess the complexity of several other, related problems:

Proposition 6.4. The mixed-integer NUM-problem of the form

$$\begin{aligned} \text{(MI-NUM)} \qquad & \max_{\boldsymbol{x},\boldsymbol{p}} \sum_{i\in\mathcal{L}} U_i x_i \\ & \text{s.t.} \\ & \Gamma_i(\boldsymbol{p}) \geq \gamma_i x_i \ \ \forall i \\ & \boldsymbol{p} \in \mathcal{P}; \ \ \boldsymbol{x} \in \{0,1\}^L \end{aligned} \tag{6.34}$$

for arbitrary, fixed values of U_i is NP-complete.

Proof. The MI-NUM can be reduced to the RMP by choosing $U_i = 1 \ \forall i$. That is, for any instance of the RMP, a corresponding instance of MI-NUM can be created in polynomial time which, if solved, induces the solution of the RMP. An algorithm to solve the MI-NUM efficiently would thus directly solve the RMP efficiently as well. □

Proposition 6.5. The general, interference aware NUM-problem of the form

$$\begin{aligned} \text{(IA-NUM)} \quad & \max_{\boldsymbol{\gamma},\boldsymbol{p}} \sum_{i\in\mathcal{L}} U_i(\gamma_i) \\ & \text{s.t.} \\ & \Gamma_i(\boldsymbol{p}) \geq \gamma_i \ \ \forall i \\ & \boldsymbol{p} \in \mathcal{P}; \ \ \boldsymbol{\gamma} \in \mathbb{R}_+^L \end{aligned} \tag{6.35}$$

with arbitrary functions $U_i(\gamma_i)$ is NP-complete.

Proof. The IA-NUM can be reduced to the MI-NUM by choosing a utility of the form

$$U_i(\gamma_i) = \begin{cases} U_i, & \gamma_i \geq \gamma_i' \\ 0, & \gamma_i < \gamma_i' \end{cases}$$

where U_i is the fixed-value parameter of MI-NUM, whereas $U_i(\gamma_i)$ denotes the function of the IA-NUM. □

It must be stressed that NP-completeness here does not induce all NUM problems to be NP-complete. Instead, the completeness refers to that the problem statements in their most general form. This does not constrain that problems with special form can be efficiently solvable. In fact, such special forms are known, e.g., when using log-concave utility functions [55], [57], or their combinatorial counter-parts, sub-modular utility values.

Finally, the complexity statements relate to the D2D-NUM problem defined in this thesis:

Corollary 6.1. The D2D-NUM problem defined in equations (2.66)-(2.74) is NP-complete.

Proof. By allowing only a single PRB and MCS, i.e., setting $K = 1$ and $C_{\mathrm{UL}} = 1$, the D2D-NUM turns into the MI-NUM. Thus, it contains the MI-NUM as special case and can be reduced to it in polynomial time. □

6.3 Set-Based Solution Approach

The main driver of complexity has been motivated in Section 6.2.4 to be that the closest attainable bounds for $\mathcal{F}_x$ are most probably trivial. The only remaining optimization structure that can be leveraged is that $\mathcal{F}_x$ forms an independence set: Let $\mathcal{F}_\mathcal{L} = \{\mathcal{X} \subseteq \mathcal{L} : \boldsymbol{x} \in \mathcal{F}_x\}$ be the set of feasible link sets, where $\boldsymbol{x}$ is an activation vector such that each element is one if and only if the corresponding link is in $\mathcal{X}$. Then, for any $\mathcal{A}, \mathcal{A}' \subseteq \mathcal{L}$ with $\mathcal{A}' \subseteq \mathcal{A}$:

$$\mathcal{A} \in \mathcal{F}_\mathcal{L} \Rightarrow \mathcal{A}' \in \mathcal{F}_\mathcal{L} \quad \mathcal{A}' \notin \mathcal{F}_\mathcal{L} \Rightarrow \mathcal{A} \notin \mathcal{F}_\mathcal{L}. \tag{6.36}$$

As the independence set is a set theoretic property, it might provide insights to investigate the RMP from a set theoretic point of view, which is done in this section. The produced approach is similar to those presented for CAC in Section 6.2.2.

In this context, the interference limited case is assumed, such that SINRs become SIRs. Let $\mathcal{A} = \{i : x_i = 1\} \subseteq \mathcal{L}$ be the set of active links and let $\|\mathcal{A}\| = M \leq N$. Then consider the matrix

$$\boldsymbol{F}_\mathcal{A} = \boldsymbol{X}(\boldsymbol{x})\boldsymbol{F}\boldsymbol{X}(\boldsymbol{x}), \tag{6.37}$$

which is the relative gain matrix of all active links. Recall that the elements $f_{ij} = \gamma_i h_{ij}/h_{ii}$ can be seen as indicators of how severe the interference from link j to link i is when both are active, considering the desired SIR, interference path gain and signal path gain. Hence, the row sum $\sum_{j=1}^{M} x_i f_{ij} x_j$ is an indicator for the severity of the overall interference that link i is exposed to. The column sum $\sum_{i=1}^{M} x_i f_{ij} x_j$ indicates, how severe the interference is that link i produces.

Assume a matrix $\boldsymbol{F}_\mathcal{L}$, which is the relative gain matrix when all links are activated, i.e., when $\mathcal{A} = \mathcal{L}$. Then, any matrix $\boldsymbol{F}_\mathcal{A}$ is a sub-matrix of $\boldsymbol{F}_\mathcal{L}$ that is by deleting the rows and columns of all inactive links from $\boldsymbol{F}_\mathcal{L}$. Whenever an inactive link is activated, both a row and a column of entries is added to $\boldsymbol{F}_\mathcal{A}$. When a link is deactivated, its row and column are deleted from $\boldsymbol{F}_\mathcal{A}$. For the corresponding graph $\mathcal{G}_{\boldsymbol{F}_\mathcal{A}}$, this means that with activation and deactivation a node and all adjacent links are added or removed. From this perspective, the RMP can be formulated as:

$$\max_{\boldsymbol{x}} \|\mathcal{A}\| \quad s.t. \quad \rho(\boldsymbol{F}_\mathcal{A}) \leq 1. \tag{6.38}$$

6.3.1 Proposed Criteria

In general, the structure of an independence set is a rather weak property for algorithmic assessment. Define a maximal feasible link set $\hat{\mathcal{A}} \in \mathcal{F}_\mathcal{L}$ to be a link set such that no further link can be added without rendering the situation infeasible. This corresponds to a local optimum of the RMP. Because the SINR targets can be chosen arbitrarily, it is possible to create instances for any combinations of sets to become maximal. That is, the number of local optima can be made grow with link numbers at factorial rate. Due to this, an optimization algorithm cannot check the maximal sets but should incorporate criteria that indicate a links' impact on feasibility before activation. Proposals for such are presented in this section.

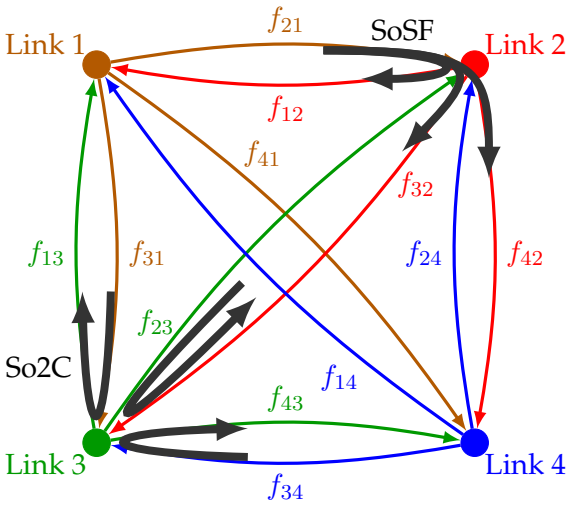

Figure 6.5: Graph showing the interference coupling for $N = 4$ Links. Added in black are the intuitions behind the derived criteria SoSF and So2C. While the So2C sums the amplifications over all mutual link couplings, the SoSF sums the amplifications of all paths through a link.

Criteria Derivation

By leveraging the power control perspective introduced in 2.1.2, from the power iteration (2.13) the following corollary can be derived:

Corollary 6.2 (Diminishing Power Values)**.** Consider two reuse link sets, $\mathcal{A}$ and $\mathcal{A}'$. Then, using the power method, there exists a $K > 0$ such that:

$$\boldsymbol{p}[k] = \boldsymbol{F}_{\mathcal{A}}^k \boldsymbol{p}[0] < \boldsymbol{F}_{\mathcal{A}'}^k \boldsymbol{p}[0] = \boldsymbol{p}'[k] \quad \forall k \geq K \tag{6.39}$$

if, and only if, $\rho(\boldsymbol{F}_{\mathcal{A}}) < \rho(\boldsymbol{F}_{\mathcal{A}'})$.

Proof. Assume that $\rho(\boldsymbol{F}_{\mathcal{A}}) \leq \rho(\boldsymbol{F}_{\mathcal{A}'})$. Let $\boldsymbol{v}_\rho$ be the dominant eigenvector of $\boldsymbol{F}_{\mathcal{A}}$ and $\boldsymbol{v}'_\rho$ be the one of $\boldsymbol{F}_{\mathcal{A}'}$. As all eigenvectors are determined up to constants c, c', according to (2.13) it holds that:

$$\lim_{k\to\infty} \boldsymbol{p}[k] = \rho(\boldsymbol{F}_{\mathcal{A}})^k \boldsymbol{v}_\rho c; \qquad \lim_{k\to\infty} \boldsymbol{p}'[k] = \rho(\boldsymbol{F}_{\mathcal{A}'})^k \boldsymbol{v}'_\rho c' \tag{6.40}$$

Using this, the statement $\exists K > 0 : \boldsymbol{p}[k] \leq \boldsymbol{p}'[k]\ \forall k \geq K$ can be transformed into

$$\exists K > 0 : \qquad \rho(\boldsymbol{F}_{\mathcal{A}}) \leq \rho(\boldsymbol{F}_{\mathcal{A}'}) \sqrt[k]{\min_i \{\boldsymbol{v}'_{\rho,i} c' / \boldsymbol{v}_{\rho,i} c\}} \quad \forall k \geq K, \tag{6.41}$$

which must true because $\lim_{k\to\infty} \sqrt[k]{(\cdot)}$ monotonically converges to one. Equality holds if, and only if, $\rho(\boldsymbol{F}_{\mathcal{A}}) = \rho(\boldsymbol{F}_{\mathcal{A}'})$, so $\rho(\boldsymbol{F}_{\mathcal{A}}) < \rho(\boldsymbol{F}_{\mathcal{A}'})$ is a sufficient condition for (6.39). On the other hand, if $\rho(\boldsymbol{F}_{\mathcal{A}}) \not< \rho(\boldsymbol{F}_{\mathcal{A}'})$, then $\rho(\boldsymbol{F}_{\mathcal{A}}) \geq \rho(\boldsymbol{F}_{\mathcal{A}'})$, which is sufficient for falsifying the statement. Hence, $\rho(\boldsymbol{F}_{\mathcal{A}}) < \rho(\boldsymbol{F}_{\mathcal{A}'})$ is also necessary. □

Note that, as all inequalities on vectors are taken element-wise, if Corollary 6.2 is true, then also

$$\sum_{i=1}^{M} p_i[k] < \sum_{i=1}^{M} p'_i[k] \quad \forall k \geq K \Leftrightarrow \rho(\boldsymbol{F}_{\mathcal{A}}) < \rho(\boldsymbol{F}_{\mathcal{A}'}). \tag{6.42}$$

Assuming that $\boldsymbol{p}[0] = \mathbf{1}$ is chosen, where $\mathbf{1}$ is a vector containing only ones, by writing out the matrix-vector product, (6.42) corresponds to:

$$\begin{aligned}\sum_{s_0=1}^{M} p_{s_0}[k] &= \sum_{s_0=1}^{M}\sum_{s_1=1}^{M} x_{s_0} f_{s_0 s_1} x_{s_1} p_{s_1}[k-1] \\ &= \sum_{s_0=1}^{M}\cdots\sum_{s_k=1}^{M}\prod_{l=1}^{k} x_{s_{l-1}} f_{s_{l-1}s_l} x_{s_l} p_{s_l}[0] \\ &= \sum_{s_0=1}^{M}\cdots\sum_{s_k=1}^{M}\prod_{l=1}^{k} x_{s_{l-1}} f_{s_{l-1}s_l} x_{s_l}. \end{aligned} \tag{6.43}$$

Each summand of (6.43) is in fact a product of elements from $\boldsymbol{F}_{\mathcal{A}}$, which are chosen such that the sequence $\{x_{s_0}, ..., x_{s_l}\}$ is a path in $\mathcal{G}_{\boldsymbol{F}_{\mathcal{A}}}$. So (6.43) sums up the weights of all paths with length k in $\mathcal{G}_{\boldsymbol{F}_{\mathcal{A}}}$.

This interpretation gives an interesting insight into the coupling of interference, which is illustrated in Figure 6.5 for better clarification. The graph can be interpreted as a "signal flow" that represents the evolution of the power method. Any input signal $p_i[k]$ is forwarded via all outgoing edges and amplified by $x_i f_{ij} x_j$. The sum of all incoming, weighted signals of vertex i form the input $p_i[k+1]$ for the next iteration. When $\rho(\boldsymbol{F}_{\mathcal{A}}) > 1$, i.e., reuse is infeasible, then the amplification will be unstable and tend to infinity for any arbitrary small input. In the other case, it will be stable and tend to zero for any arbitrary large input.

Assume that the interference situation is infeasible and that a link needs to be removed. Then it should be the link that reduces $\rho(\boldsymbol{F}_{\mathcal{A}})$ most, because the aim is to come as close to feasibility as possible. When adding a link to a feasible set, on the other hand, the added link should be the one that increases $\rho(\boldsymbol{F}_{\mathcal{A}})$ least. From Corollary 6.2 and equation (6.42), the link that reduces $\rho(\boldsymbol{F}_{\mathcal{A}})$ most, or increases it least, is also the one that reduces (6.43) most or increases it least, respectively. This is the one whose impact on the overall amplification is largest/smallest. Evaluating the full impact of a link removal or addition to $\mathcal{A}$ is clearly very hard because (6.43) contains an exponentially increasing number of summands, of which not all are influenced when adding/removing a single link.

The approaches presented in Section 6.2.2 focus on norms of $\boldsymbol{F}_{\mathcal{A}}$. From graph perspective in (6.43), the weights themselves only capture part of the interference situation. The full severity of interference is captured by all combinations that the weights can form, which are the paths on the graph $\mathcal{G}_{\boldsymbol{F}_{\mathcal{A}}}$. With this perspective, it makes sense to propose the following two criteria in addition to the existing ones:

Criterion 6.1 (Sum of 2 Circles (So2C))**.** Add/Remove the link i for which

$$\sum_{j=1}^{L} f_{ij} x_j f_{ji}$$

is minimal/maximal.

Algorithm 5: Link Activation Algorithm

Set $\mathcal{A}$ to contain only C-UE
Choose $\mathcal{M} \in \{\text{So2C}, \text{SoSF}, ...\}$
Create $\mathcal{F}_\mathcal{A}$.
while $\rho(\mathcal{F}_\mathcal{A}) \leq 1$ **do**
    Find $l = \arg\min_{k \in (\mathcal{L} \setminus \mathcal{A})} \mathcal{M}(l, \mathcal{A} \cup l)$.
    $\mathcal{A} := \mathcal{A} \cup l$
    Create $\mathcal{F}_\mathcal{A}$, Calculate $\rho(\mathcal{F}_\mathcal{A})$.
end while
Output $(\mathcal{A} \setminus l)$

Algorithm 6: Link Removal Algorithm

Set $\mathcal{A} = \mathcal{L}$
Choose $\mathcal{R} \in \{\text{So2C}, \text{SoSF}, ...\}$
Create $\mathcal{F}_\mathcal{A}$.
while $\rho(\mathcal{F}_\mathcal{A}) > 1$ **do**
    Find $l = \arg\max_{k \in \mathcal{A}} \mathcal{R}(l, \mathcal{A})$.
    $\mathcal{A} := \mathcal{A} \setminus l$
    Create $\mathcal{F}_\mathcal{A}$, Calculate $\rho(\mathcal{F}_\mathcal{A})$.
end while
Output $\mathcal{A}$

Criterion 6.2 (Sum of Signal Flows (SoSF))**.** Add/Remove the link i for which

$$\sum_{m=1}^{L} \left(x_m f_{mi} \sum_{j=1}^{M} f_{ij} x_j \right) = \left(\sum_{m=1}^{M} x_m f_{mi} \right) \left(\sum_{j=1}^{M} f_{ij} x_j \right)$$

is minimal/maximal.

As indicated by the subtitles of the criteria, Criterion 6.1 removes the link i for which the sum of all amplifications over circles with size 2 through i is largest. This captures the mutual interference amplification among all link pairs but neglects amplifications of longer paths. Criterion 6.2 removes the link for which the sum of amplifications over all possible paths through i is largest. The intuition of both criteria is shown in Figure 6.5. It must be stressed that these criteria are not optimal. For example, it might happen that $f_{mi} f_{ij}$ is very large but all f_{lm} are so small that $f_{lm} f_{mi} f_{ij}$ is very small $\forall l$. Then, link i will probably be chosen for removal by both criteria but the influence on $\rho(\boldsymbol{F}_\mathcal{A})$ might be small. However, it will be shown that these criteria capture the influence of links better than the state-of-the-art.

Criteria Implementations

The proposed criteria induce both an algorithm for link activation and link removal. The algorithms are summarized as Algorithms 5 and 6. In the activation case there is an active link set $\mathcal{A}$, and any link that is not in $\mathcal{A}$ will evaluate the selected criterion with respect to all active links. The link with the lowest value is added to $\mathcal{A}$. In the removal case, all links in $\mathcal{A}$ evaluate the considered criterion and the one with the largest value is removed from $\mathcal{A}$.

6.3.2 Simulation

The quality of the proposed criteria are now evaluated and compared with the state-of-the-art. In particular two aspects are of interest: (1) What is the largest average reuse set found by the criteria and (2) is there a performance gap between link activation and link removal? The proposed criteria So2C and SoSF are compared with *SMART* [156] and *2-Norm* [158] from literature.

Table 6.2: Simulation Parameters and Values

Parameter	Value
Maximal Transmission Power	26 dBm
Cell Radius	550 m
D2D Distance Range	$0 - 50$ m
Target SINR	5 dB
Expected Number of Links (Mean)	10, 20,..., 60
Number of Simulations per Round	200
Confidence Level	0.9

Simulation Setup

The simulation is implemented using SimuLTE [97], which is based on OMNeT++ [98]. SimuLTE uses a realistic channel model based on ITU-R M.2135-1 that includes shadowing and fading. A circular cell, with a radius chosen such that the coverage area is 10^6 m^2, is used. The eNodeB is located in the center of the cell and the only cellular UE is placed randomly within the cell. The number of active D2D links and their locations inside the cell follow a poisson point process with density λ. The eNodeB gathers the exact channel information between all links in a centralized fashion, creates $F_{\mathcal{L}}$ and then determines the maximal set of feasible D2D links, according to the Algorithms 5 and 6. Table 6.2 shows chosen parameter settings of the simulation.

Simulation Results

First, the performance difference of removing and merging links is compared. For each criterion, the density of D2D-links λ is varied and the mean number of active links evaluated after simulation for both removal and activation. The mean difference of feasible links is established by subtracting the results of link activation from those of link removal.

Figure 6.6a shows the performance differences of removal and activation for the selected criteria. There is only a small performance difference between link removal and link activation for the *SMART* and So2C criteria. However, for the SoSF criterion, with increasing link density, link activation on average outputs slightly more feasible links than link removal. This effect becomes a little more dominant with increasing link density. On the other hand, for the 2-Norm criterion, link removal always achieves a larger number of feasible links than link activation. Also, the performance gap becomes larger when the total link density increases. However, compared to the total link densities, the performance differences are not dominant. The conclusion is that in most cases, the performance gap between link removal and link activation is on the edge of being negligible. This has an impact on the chosen implementation for the semi-distributed case: In general, when the algorithm becomes distributed, the active link set slowly increases or decreases. Then, link activation is preferable

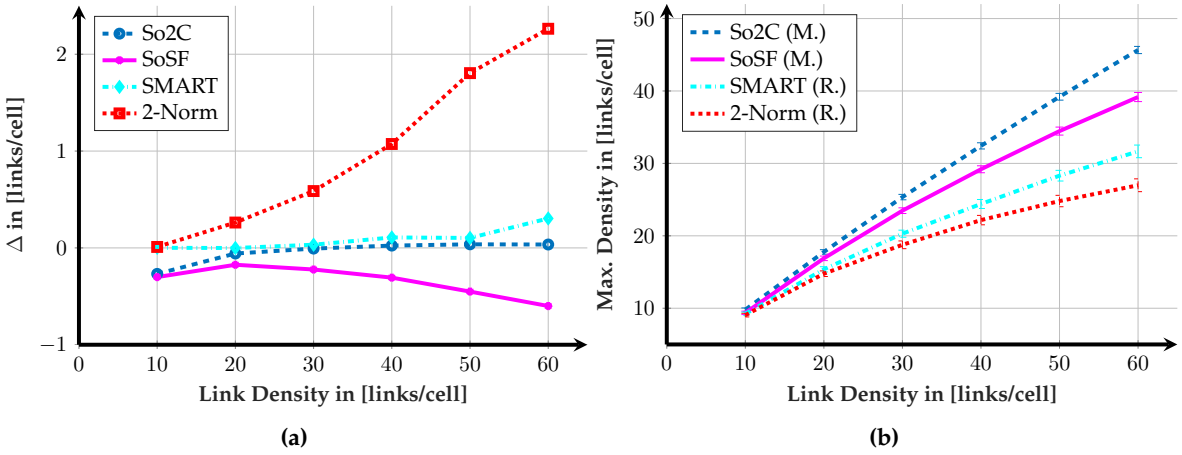

Figure 6.6: Simulation results of the proposed and compared criteria. 6.6a shows the difference of mean feasible link density between link removal and link activation comparing each criterion. The mean of link activation is subtracted from that of link removal.6.6b shows the mean feasible link density for each simulated criterion.

over link removal because smaller, suboptimal feasible combinations will be found earlier. In the process of accepting more D2D links into the feasible set, the whole system will also remain feasible with high probability, so data or control packets can be sent already by all active links while the link selection is still in progress.

Now take the absolute performance of each criterion into consideration, which is shown in Figure 6.6b. For each criterion, the variant among removal or mergence is chosen that yields the better results. The confidence intervals of a 99% confidence level are also shown for each curve. For lower total link density, from 10 to 20, the difference between So2C and SoSF and the difference between *SMART* and *2-Norm* are both very small, considering the overlapping of confidence intervals. However as the density increases, even though all curves encounter difficulty of keeping a linear rate of growth, the performance difference among them becomes obvious. So2C remains the best, while *2-Norm* performs worst. When the total active link density reaches 60, So2C produces 20 more feasible links than *2-Norm*. This is a performance increase of nearly 70 %! The SoSF-criterion also produces more feasible links than the two from literature, with performance gains from 20 % to 50 %. For all criteria, larger link densities lead to larger confidence intervals.

6.4 GBD based Solution Approach

Apart from set theory, the RMP can be approached with tools from mixed-integer, nonlinear programming [160]. In particular, the Generalized Benders Decomposition (GBD) provides an implementable structure, which can further be extended to similar problems such as the D2D-NUM. A formal introduction of GBD is given in Appendix B. The application of GBD to the RMP, and the resulting communication structure, is presented and investigated here. As both, the algorithmic structure and implementation pose challenges, they are tackled in independent steps: First, only algorithmic aspects are considered by solving the interference-

limited case and assuming full access to the relative gain matrix. In Section 6.4.3, the results are adapted into an implementable algorithm.

Problem Adaptation for GBD

For the RMP, the activation variables $\boldsymbol{x}$ are interpreted as complicating variables. A prerequisite to apply the GBD is that with fixed complicating variables, the remaining problem is convex. The only known way to achieve this is logarithmic transformation, which has issues around $x_i = 0$, as discussed in Section 6.2.4. To circumvent these, the problem structure is adapted as follows: Instead of choosing binary x_i, which cannot be entirely mapped to logarithmic domain, choose $x_i^\varepsilon \in \{\varepsilon, 1\}$ for some positive $\varepsilon \ll 1$. The technical interpretation of this is that are not fully shut down but instead use an *SINR target backoff*. That is, links that should be deactivated choose an SINR constraint of $\varepsilon\gamma_i$, while those that are activated use their full γ_i. By choosing ε sufficiently small, the link shut-down can be achieved in the limit.

The logarithmic transformation [57], [73] of the form $\tilde{x}_i^\varepsilon = \log(x_i^\varepsilon)$, $\tilde{p}_i = \log(p_i)$ is used and auxiliary variables w_i are introduced in logarithmic domain with $\tilde{x}_i^\varepsilon \leq w_i$. The aim of the auxiliary variables is to decouple the primal problem from the relaxed master problem. ε can be transformed into logarithmic domain by considering it as $\varepsilon = \exp(-\tilde{\varepsilon})$. Correspondingly, in logarithmic domain $\tilde{x}_i^\varepsilon \in \{-\tilde{\varepsilon}, 0\}$. Now re-write:

$$\tilde{x}_i^\varepsilon \in \{-\tilde{\varepsilon}, 0\} = \tilde{\varepsilon} \cdot \{-1, 0\} \Rightarrow \tilde{x}_i = (x_i - 1)\tilde{\varepsilon}, \tag{6.44}$$

where $x_i \in \{0, 1\}$ is the original activation parameter. The adapted optimization problem then is written as:

$$\begin{aligned}
\text{(GBD-RMP)} \qquad & \max_{\boldsymbol{x}, \tilde{\boldsymbol{p}}, \boldsymbol{w}} \sum_{i \in \mathcal{L}} x_i \\
& \text{s.t.} \\
& (x_i - 1)\tilde{\varepsilon} - w_i \leq 0 && (6.45) \\
& \exp(w_i) \textstyle\sum_{j \neq i} f_{ij} \exp(\tilde{p}_j) - \exp(\tilde{p}_i) \leq 0 \ \ \forall i && (6.46) \\
& \boldsymbol{x} \in \{0, 1\}^L.
\end{aligned}$$

Note that power constraints can be neglected, since $\exp(\tilde{p}_i)$ is restricted to positive values by definition and maximum power constraints can be neglected in the considered noiseless case. Constraint (6.45) is a reformulated version of $\tilde{x}_i^\varepsilon \leq w_i$. The SINR constraint (6.46) creates a convex space, as it can be re-written into $\sum_{j \neq i} f_{ij} \exp(w_i + \tilde{p}_j - \tilde{p}_i) \leq 1$ and hence be interpreted as sub-level set of a convex function. However, it is kept this way it creates optimality conditions that are easier to analyze. Finally, it can be conclude that the GBD-RMP has a convex problem structure.

The Decomposition

Now, the GBD is applied to the formulated optimization problem. The detailed derivation and property analysis of GBDs can be found in [160]. The primal problem is to optimize GBD-RMP for a fixed $\boldsymbol{x}^{(k)}$ and to obtain optimal Lagrange multipliers. If $\boldsymbol{x}^{(k)}$ turns out to

be infeasible, a feasibility problem is solved instead and the related optimal multipliers are obtained. For the investigated case, the primal problem becomes:

$$\begin{aligned} \text{(GBD-P)} \qquad & \min_{\tilde{\boldsymbol{p}},\boldsymbol{w}} \sum_{i\in\mathcal{L}} -x_i^{(k)} \\ & \text{s.t.} \\ & (x_i^{(k)}-1)\tilde{\varepsilon} - w_i \leq 0 \\ & \exp(w_i)\textstyle\sum_{j\neq i} f_{ij}\exp(\tilde{p}_j) - \exp(\tilde{p}_i) \leq 0 \;\; \forall i. \end{aligned}$$

If GBD-P turns out to be infeasible, the SRMP is used as feasibility problem to find $\tilde{\boldsymbol{p}}$ and $\boldsymbol{w}$ as close to feasibility as possible. The relaxed master problem uses the resulting Lagrange functions identified in the primal problem to create an outer approximation for the complicating variables. The master problem, in an abstract form, reads:

$$\begin{aligned} \text{(GBD-M)} \qquad & \min_{\boldsymbol{x}} \max_{k} \zeta^{(k)}(\boldsymbol{x}) \\ & \text{s.t.} \\ & 0 \geq \xi^{(l)}(\boldsymbol{x}) \;\; \forall l \\ & \boldsymbol{x} \in \{0,1\}^L. \end{aligned}$$

$\zeta^{(k)}(\boldsymbol{x}) = L^{(k)}(\boldsymbol{x})$ is the Lagrange function of GBD-P, where all multipliers and variables except $\boldsymbol{x}$ are constant and set to their optimal values of the k'th feasible primal optimization. Similarly, $\xi^{(l)}(\boldsymbol{x})$ is the Lagrange function of the SRMP with all multipliers and variables kept at their optimal values of the l'th infeasible primal optimization. The only free variables in the master problem GBD-M are the elements of $\boldsymbol{x}$. The function $\max_k \zeta^{(k)}(\boldsymbol{x})$ creates an outer approximation of the utility function, whereas all $\xi^{(l)}(\boldsymbol{x})$ approximate the feasible region $\mathcal{F}_x$. The master problem then uses both for optimizing $\boldsymbol{x}$.

Assessing the Primal Problem

Consider the primal problem GBD-P. As all $x_i^{(k)}$ are fixed, so is the utility of GBD-P. The problem thus reduces to finding an arbitrary feasible point in the $\tilde{\boldsymbol{p}}$-$\boldsymbol{w}$ space. If $\boldsymbol{x}_i^{(k)}$ turns out to be infeasible, the target is to find a point as close to feasibility as possible, which can be found by using the SRMP. Both, GBD-P and SRMP can be combined into a single optimization problem of the form:

$$\begin{aligned} \text{(GBD-F)} \qquad & \min_{c,\tilde{\boldsymbol{p}},\boldsymbol{w}} c \\ & \text{s.t.} \\ & 1 - c \leq 0 && (6.47) \\ & (x_i^{(k)}-1)\tilde{\varepsilon} - w_i \leq 0 && (6.48) \\ & e^{w_i}\sum_{j\neq i} f_{ij}e^{\tilde{p}_j} - ce^{\tilde{p}_i} \leq 0 \;\; \forall i. && (6.49) \end{aligned}$$

Constraint (6.47) lower bounds c to one. If the optimal value of c is one, then the GBD-P is feasible and the found solution of GBD-F is also a valid solution to the GBD-P. Otherwise, the problem equals the SRMP and a point as close to feasibility as possible is obtained. Similar

to constraint (6.46) of the GBD-RMP, constraint (6.49) can be interpreted as sub-level set of a convex function and hence creates a convex optimization space. So GBD-F is a convex optimization problem on continuous space. Additionally, as it satisfies Slaters' condition, strong duality holds and any KKT point is a local and global optimum. The Lagrange function associated with GBD-F is

$$L^{(k)} = c + \nu(1-c) + \sum_{i=1}^{L} \tau_i((x_i^{(k)} - 1)\tilde{\varepsilon} - w_i) + \sum_{i=1}^{L} \eta_i(e^{w_i} \sum_{j \neq i} f_{ij} e^{\tilde{p}_j} - ce^{\tilde{p}_i}),$$

where $\nu \geq 0$, $\tau_i \geq 0$, $\eta_i \geq 0$ are Lagrange multipliers. From the complementary slackness conditions, $\tau_i = 0$ as long as condition (6.48) is not active for link i. However, from $\tau_i = 0$ follows $\partial L^{(k)}/\partial w_i \geq 0$, which means that a smaller feasible w_i can be found that can reduce, but never increase, the value of the Lagrange function. That is, without loss of generality, $w_i^* = (x_i^{(k)} - 1)\tilde{\varepsilon} = \tilde{x}_i^{\varepsilon,(k)}$ and $e^{w_i^*} = x_i^{\varepsilon,(k)}$ can be assumed as optimal solution for w_i. If GBD-P is infeasible, i.e., if $\rho(\boldsymbol{X}(\boldsymbol{x}^{\varepsilon})\boldsymbol{F}) > 1$, then $\nu^* = 0$ and the solution corresponds to that of SRMP, given in (6.28)-(6.29), with

$$\tau_i^* = \eta_i^* \left[\boldsymbol{X}(\boldsymbol{x}^{\varepsilon})\boldsymbol{F}\boldsymbol{p}^*\right]_i = s_{\rho,i} \left[\boldsymbol{X}(\boldsymbol{x}^{\varepsilon})\boldsymbol{F}\boldsymbol{p}_\rho\right]_i = x_i^{\varepsilon} m_i = m_i^{\varepsilon}. \tag{6.50}$$

By re-arranging terms and using $\boldsymbol{\eta}^{*T}\boldsymbol{p}^* = \boldsymbol{s}_\rho^T \boldsymbol{p}_\rho = 1$, $\sum_{i=1}^{N} m_i^{\varepsilon,(l)} = \rho(\boldsymbol{x}^{\varepsilon,(l)})\boldsymbol{s}_\rho^T\boldsymbol{p}_\rho = \rho(\boldsymbol{x}^{\varepsilon,(l)})$, $\nu^* = 0$ and (6.50), the resulting Lagrange function for infeasible instances is

$$L^{(l)}(\boldsymbol{x}) = \sum_{i=1}^{L} m_i^{\varepsilon,(l)}(\tilde{x}_i^{\varepsilon} - w_i^*) + \sum_{i=1}^{L} m_i^{\varepsilon,(l)} = \rho(\boldsymbol{x}^{\varepsilon,(l)}) + \sum_{i=1}^{L} m_i^{\varepsilon,(l)} \left(\tilde{x}_i^{\varepsilon} - \tilde{x}_i^{\varepsilon,(l)}\right). \tag{6.51}$$

$\rho(\boldsymbol{x}^{\varepsilon,(l)}) = \rho(\boldsymbol{X}(\boldsymbol{x}^{\varepsilon,(l)})\boldsymbol{F})$ is an estimate of the spectral radius for the k'th choice of $\boldsymbol{x}^{\varepsilon}$. Note that equation (6.51) takes the exact form of (6.33). By using that $\tilde{x}_i^{\varepsilon} \in \{-\tilde{\varepsilon}, 0\}$ and substituting (6.44) the approximation takes the form

$$\xi^{(l)}(\boldsymbol{x}) = \rho(\boldsymbol{x}^{\varepsilon,(l)}) + \tilde{\varepsilon} \sum_{i=1}^{L} m_i^{\varepsilon,(l)} \cdot \left(x_i - x_i^{(l)}\right). \tag{6.52}$$

$\xi^{(l)}(\boldsymbol{x})$ is linear in x_i, however, setting $x_i = 0$ in (6.52) does not correspond to shutting down the link. Instead, it takes account that a link that *should* be shutdown actually backs off the SINR constraint by a factor ε.

If GBD-P is feasible, i.e., $\rho(\boldsymbol{X}(\boldsymbol{x}^{\varepsilon,(k)})\boldsymbol{F}) < 1$, then GBD-F provides a feasible point for GBD-P. Because the complementary slackness conditions hold at an optimal point, without loss of generality all multipliers can be set to zero, achieving the optimal value of $L(\boldsymbol{x})$. The resulting approximation for the master problem then is obtained from the GBD-P as

$$\zeta^{(k)}(\boldsymbol{x}) = -\sum_{i=1}^{L} x_i. \tag{6.53}$$

As all feasible estimates generate the same approximation, it is in fact the optimizing function of the master problem.

Algorithm 7 Worst Pressure Shutdown (WPS)

1: Set $x_i := 1 \; \forall i$
2: Identify $m_i = s_{\rho,i} \cdot l_{\rho,i} \; \forall i$, $\rho(\boldsymbol{x})$.
3: **while** $\rho(\boldsymbol{x}) > 1$ **do**
4: Set $x_i = 0$, where $i = \arg\max_{i \in \mathcal{A}} m_i$.
5: Identify $m_i = s_{\rho,i} \cdot l_{\rho,i} \; \forall i$, $\rho(\boldsymbol{x})$.
6: **end while**
7: **return** $\boldsymbol{x}$.

Assessing the Master Problem

Now combine the created approximations into an explicit form of the GBD-M, which is:

$$\begin{aligned} \text{(GBD-M)} \qquad & \max_{\boldsymbol{x}} \sum_{i=1}^{N} x_i \\ & \text{s.t.} \\ & \sum_{i=1}^{L} m_i^{\varepsilon,(l)} x_i \leq \textstyle\sum_{i=1}^{L} m_i^{\varepsilon,(l)} x_i^{(l)} - \rho(\boldsymbol{x}^{\varepsilon,(l)})/\tilde{\varepsilon} \;\; \forall l \\ & \boldsymbol{x} \in \{0,1\}^L. \end{aligned} \tag{6.54}$$

The constraints (6.54) are a reformulation of (6.52), where the right hand side is constant. GBD-M corresponds to a multi-dimensional Knapsack-Problem, where all profits are set to unity and the weights are the relative interference pressure values. Knapsack problems form a well investigated class of combinatorial optimization [164]. While the Knapsack Problem is NP-hard in the general case, with equal profits it is polynomial-time solvable in its original formulation. However, for the multi-dimensional knapsack problems, even with equal profits there is no known, efficient solution.

6.4.1 Algorithm Design

After presenting the GBD, now algorithms for maximizing the frequency reuse in a D2D enabled cellular network can be proposed. First, a heuristic is developed, afterwards a ε-Approximation based on the GBD is designed. In this section, the focus is on the algorithmic aspects of the problem. The resulting implementation structure is investigated in Section 6.4.3.

The proposed algorithms are based on the relative interference pressure and spectral radius, therefore, their complexities are analyzed by evaluating the number of times that these quantities need to be estimated. The estimation can, in general, be done by using appropriate power control algorithms, e.g. [58], [165]. The exact impact of estimation and the development of efficient ways to do so is out of scope of this work. For simulations, they are evaluated using eigenvalue-decomposition of $\boldsymbol{X}(\boldsymbol{x})\boldsymbol{F}$.

Worst Pressure Shutdown (WPS)

The first algorithm is summarized in Algorithm 7. At start, all links are activated. The load and spillage vectors $\boldsymbol{l}_\rho$ and $\boldsymbol{s}_\rho$ are estimated, as well as the spectral radius $\rho(\boldsymbol{x})$. If the radius

is larger than one, the link with the largest interference pressure $m_i = l_{\rho,i}s_{\rho,i}$ is shut down. This procedure is repeated until $\rho(\boldsymbol{x}) \leq 1$, i.e., until a situation is feasible.

The intuition is that at each iteration, the link with the locally largest impact on the spectral radius, i.e., the largest derivative in form of interference pressure, is shut down. The algorithm is sub-optimal because of the nonlinear nature of $\rho(\boldsymbol{x})$, which allows the interference pressure of a link to increase, or decrease, with its activation level. Nevertheless, the heuristic shows near optimal performance in simulative evaluations with an approximation factor of less than 1.05. In the worst-case, $N-1$ links need to be deactivated, as a single link always has a spectral radius of zero. So the algorithmic worst-case complexity of the WPS-algorithm is $\Omega(\text{WPS}) = \Omega(N)$.

The $\tilde{\varepsilon}$-Pressure Packing ($\tilde{\varepsilon}$-PP) Algorithm

The second algorithm uses the GBD and operates as follows: First, solve the master problem with no constraints and activate all links. Identify the load and spillage vectors $\boldsymbol{l}_\rho$ and $\boldsymbol{s}_\rho$, as well as the spectral radius $\rho(\boldsymbol{x})$. If $\rho(\boldsymbol{x}) \leq 1$, the algorithm ends. Otherwise, add a constraint of form (6.52) to the relaxed master problem. Again solve the master problem and repeat the procedure for the newly identified $\boldsymbol{x}$ until a feasible set is found. The formal algorithmic statement is given in Algorithm 8.

$\tilde{\varepsilon}$-PP combines a Knapsack problem with an outer approximation, where the approximations are created by identifying the interference pressure and spectral radius. This can be interpreted in a way that pressure values are packed subject to maximum pressure constraints, which is why it is called it $\tilde{\varepsilon}$-Pressure Packing.

Note that the GBD introduces a standardized way to deal with MINLPs, which are problems that often become NP-complete or even NP-hard. In general, the only statement that can be made about complexity is that the GBD finds an optimal value in a finite number of steps [160]. As the RMP is NP-complete, it must be concluded that the $\tilde{\varepsilon}$-PP has exponential worst-case complexity if P $\neq$ NP. However, it is analytically ensured that it will solve the GBD-RMP problem optimally for fixed $\tilde{\varepsilon}$. When $\tilde{\varepsilon} \to \infty$, the GBD-RMP converges to the original RMP and still is guaranteed to produce an optimal solution. Hence the $\tilde{\varepsilon}$-PP algorithm is an approximation algorithm capable of solving the RMP optimally, at the cost of potentially exponential complexity.

6.4.2 Simulative Analysis

Now the proposed algorithms are evaluated with simulations. Thereby, the focus is on the algorithmic aspects of the proposed algorithms such as complexity and solution quality rather than their implementation, which will be investigated in Section 6.4.3. It is assumed that possibilities to estimate the current values of load, spillage and spectral radius of a networking set-up exist. The estimation can in general be done by using appropriate power control algorithms, e.g. [58], [165]. The resulting Knapsack problems are solved with a general purpose solver software.

Algorithm 8 $\tilde{\varepsilon}$-Pressure Packing ($\tilde{\varepsilon}$-PP)

1: Choose $\tilde{\varepsilon} \geq 0$.
2: Initialize GBD-M as:
3: $\max_{\boldsymbol{x}} \sum_{i=1}^{N} x_i$ s.t. $x_i \in \{0,1\}$.
4: **repeat**
5: Solve GBD-M, yielding $\boldsymbol{x}^{(k)}$.
6: Let links with $x_i^{(k)} = 0$ reduce SINR target by $\tilde{\varepsilon}$ dB.
7: Identify $\rho(\boldsymbol{x}^{(k)})$, $m_i^{(k)} = s_{\rho,i} \cdot l_{\rho,i}\ \forall i$.
8: Add $\sum_{i=1}^{L} m_i^{\varepsilon,(k)} x_i \leq \sum_{i=1}^{L} m_i^{\varepsilon,(k)} x_i^{(k)} - \rho(\boldsymbol{x}^{\varepsilon,(l)})/\tilde{\varepsilon}$ to GBD-M.
9: **until** $\rho(\boldsymbol{x})^{(k)} \leq 1$
10: **return** $\boldsymbol{x}^{(k)}$.

The algorithms assume a two-tier structure, which is composed of a decentralized power control part and a centralized optimization. The power control part aims at estimating load, spillage and spectral radius, respectively. In the current simulations, they are evaluated using eigenvalue-decomposition of $\boldsymbol{X}(\boldsymbol{x})\boldsymbol{F}$.

Three schemes are considered for comparison: i) The So2C algorithm introduced in Section 6.3 is the closest with respect to the considered set-up and has been shown to outperform the CAC related literature, which is why it is used as benchmark. ii) The D2D related works mostly neglect power control capabilities, which makes it inappropriate to compare against them. To relate this work to them, a brute-force search with fixed powers (BFS-FP) is performed, searching for the maximum size link set that has all SINR constraints satisfied while assuming that all links transmit with maximum power. As this provides an optimal solution for the fixed power case, it upper bounds the impact of D2D related works. iii) Finally, a brute-force search (BFS) including power control capabilities is performed, searching for the maximum amount of reusing links that have a spectral radius smaller than one. This is used to evaluate the degree of optimality that is achieved by all algorithms. By comparing both BFS and BFS-FP, the general impact of power control on reuse maximization can be evaluated.

Simulation Set-Up

Consider the cell of a D2D enabled network in which a cellular uplink shares its resources with a set of D2D side-links. The aim is to maximize the reuse factor among all links. The D2D links are treated equally to the cellular uplink, that is, deactivating the uplink to favor reuse among D2D links is also a valid choice. The considered cell covers a circular area of defined radius, where the base station is positioned at its center. One uplink user and a predefined number of D2D transmitters are placed randomly in the cell with uniformly distributed positions. D2D receivers are placed within a maximum distance from the sender, also following a uniform distribution. At the beginning of the simulation, each link randomly sets an SINR target chosen from a set of allowed values. This allowed set consists of 13 discrete SINR targets, each of which corresponds to a MCS used in LTE networks. The

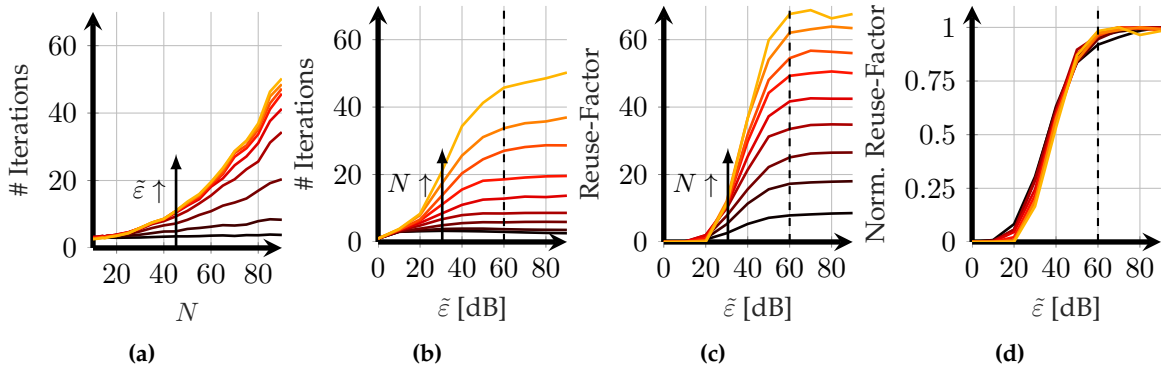

Figure 6.7: Impact of $\tilde{\varepsilon}$ on $\tilde{\varepsilon}$-PP. Each line in a plot corresponds to simulations where either $\tilde{\varepsilon}$ or N is varied and the other is kept fixed. All values are averaged over 300 simulation runs. The parameter range is $\tilde{\varepsilon} \in \{10, 20, ..., 90\}$ and $N \in \{10, 20, ..., 90\}$. 6.7a shows the link number N versus required iterations and indicates exponential increase of $\tilde{\varepsilon}$-PP with N. 6.7b-6.7d show saturation effects with respect to $\tilde{\varepsilon}$. The dashed lines in Figures 6.7b-6.7d indicate, where $\tilde{\varepsilon}$ can be considered sufficiently large.

values are derived from [95]. The attenuation between links follows the WINNER-II channel models for the urban macro scenario with non line-of-sight channels [60]. Fading follows a log-normal distribution with defined variance. The base station is assumed to have a height of 25m, whereas all D2D devices have one of 1.5m.

Impact of $\tilde{\varepsilon}$ on $\tilde{\varepsilon}$-PP

The simulative analysis starts by investigating the influence of the SINR back-off value $\tilde{\varepsilon}$ on the $\tilde{\varepsilon}$-PP algorithm. The intuition is that with increasing $\tilde{\varepsilon}$, the solved GBD-RMP matches closer to the actual RMP, because backed off links are closer to shut-down ones. However, the used approximations become less meaningful and more trivial, due to the issues with logarithmic estimation, which have been discussed in detail already. To evaluate the influence of $\tilde{\varepsilon}$, 300 sample networks are generated according to the described scenario, with a maximum D2D distance of $50m$. In each set-up, the frequency reuse is maximized via $\tilde{\varepsilon}$-PP and $\tilde{\varepsilon}$ is varied from 10dB to 90dB in steps of ten, as well as the size of the link set N from 10 links to 90 links in steps of ten. For each combination of $\tilde{\varepsilon}$ and N, both the achieved reuse factor and the required iterations are averaged over all 300 sample networks. The results are shown in Figure 6.7.

Figure 6.7a shows the influence of link numbers N on the iterations required by the $\tilde{\varepsilon}$-PP algorithm to find a maximal set, for fixed values of the SINR back-off $\tilde{\varepsilon}$. The values of $\tilde{\varepsilon}$ are increasing in the direction indicated by the arrow and the change of color. It can be seen that, for any $\tilde{\varepsilon}$, the number of iterations increases exponentially with N. The magnitude of $\tilde{\varepsilon}$ determines the growth rate of the exponential increase and a larger $\tilde{\varepsilon}$ induces a faster growth. The largest required number of iterations is around 50 and results in a reuse factor of around 68. It is generated by a value of $\tilde{\varepsilon} = 90$dB and $N = 90$. While the exponential increase is a disadvantage, the absolute required iterations are in an acceptable range over the considered link sizes. For comparison, a brute-force search would require up to $\binom{90}{68} \approx$

$5 \cdot 10^{20}$ iterations only to ensure that a feasible combination of 68 links is found! Compared to this, even if the complexity of the $\tilde{\varepsilon}$-PP algorithm increases exponentially, it is still drastically reduced.

Figures 6.7b-6.7c show the impact of the SINR back-off $\tilde{\varepsilon}$ on the number of required iterations and the achieved reuse factor in terms of links per cell. The influence is shown for different fixed values of N, where the direction of increase is again indicated by an arrow and line colors. It can be seen that, for increasing $\tilde{\varepsilon}$, the achievable reuse factor increases and so does the required number of iterations. However, after some sufficiently large $\tilde{\varepsilon}$, the values saturate to an upper bound. The interpretation is that, for increasing $\tilde{\varepsilon}$, the solution to GBD-RMP better approximates that of the RMP. However, at some point this effect diminishes and only small improvement can be gained from further increasing $\tilde{\varepsilon}$.

In Figure 6.7d, the values of 6.7c are normalized for fixed N to the maximum that each line attains on the considered space. As is shown in the figure, all normalized curves fall together into one overall effect. This shows that the saturation point for the achievable reuse factor is at the same back-off value, independent of link size N. It can be concluded that an SINR back-off value of around $\tilde{\varepsilon} = 60$dB is sufficient to achieve almost optimal performance. However, it also induces almost maximal complexity.

Algorithm Comparison

The proposed algorithms are now compared with the state of the art in terms of achieved reuse factors and required number of iterations. For $\tilde{\varepsilon}$-PP, an SINR back-off of $\tilde{\varepsilon} = 90$dB is chosen, to ensure that the algorithm runs at maximal performance. Algorithm performance is assessed in two ways. First, as in the previous section, link numbers N are increased from 10 to 90 with steps of ten. For each fixed N, 1000 network instances are created, on which $\tilde{\varepsilon}$-PP, WPS and So2C are compared. The resulting average iteration numbers and achieved reuse factors are shown in Figure 6.8a-6.8b. For the BFS algorithms, however, scalability issues prevent the evaluation of more than 20 links. To compare against them the link numbers are kept fixed at $N = 10$ and the cell area is decreased. As this increases the link density, the effect is similar to that of increasing the link number, while keeping the complexity at an acceptable level. Then, all algorithms are compared with respect to the maximum achievable link densities. The result is shown in Figure 6.8c.

Figure 6.8a shows the runtime required by the proposed algorithms to maximize the reuse. It can be seen again that the number of iterations for $\tilde{\varepsilon}$-PP increases exponentially. Both the WPS and So2C require iterations proportionally to $N - E\{K\}$, where $E\{K\}$ is the expected, found maximal link set size. This complies with their linear complexity. In Figure 6.8b the achieved reuse factors are shown. The So2C algorithm achieves the smallest and the $\tilde{\varepsilon}$-PP the largest reuse factor over the entire examined domain. However, the absolute difference is small. Finally, Figure 6.8c shows achieved link densities for all algorithms including brute force search, where the link numbers are fixed to $N = 10$ and the cell area is reduced. The $\tilde{\varepsilon}$-PP, WPS and So2C algorithms are all within 95% optimality, whereas the BFS-FP performs significantly worse than the BFS and achieves around 70% optimality. The BFS-FP is well outperformed by the power control enabled algorithms. As the BFS-FP is an

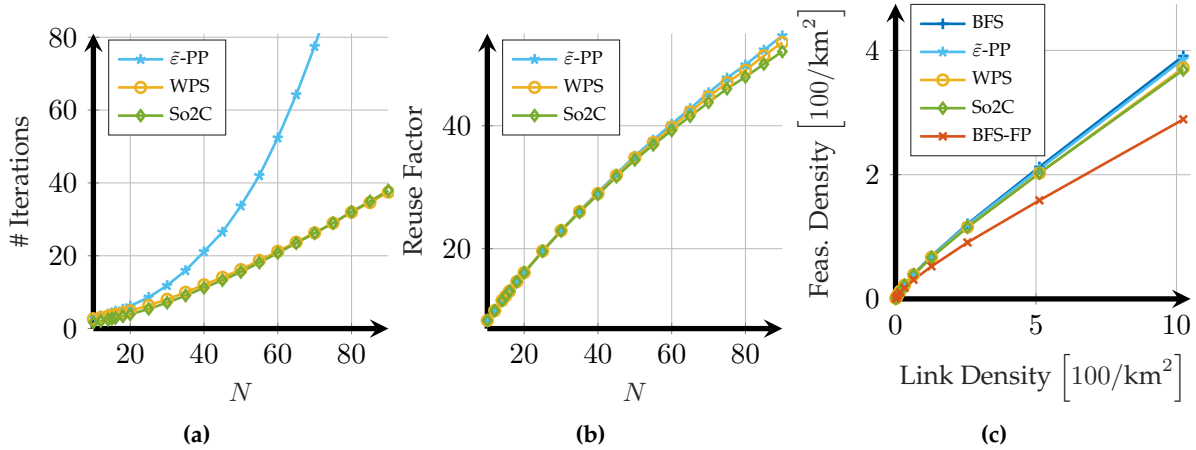

Figure 6.8: Simulative Comparison of the proposed algorithms WPS and $\tilde{\varepsilon}$-PP with brute-force search (BFS), BFS with fixed powers (BFS-FP) and So2C from literature. 6.8a shows the link numbers versus required iterations, whereas 6.8b shows the achieved reuse factors. 6.8c compares the algorithms with respect to the optimal bounds and indicates the impact of power control.

upper bound for the D2D related solutions proposed in [122], [143], [145]–[147], [149], [151], [152], [154], [166], the conclusion is that the proposed schemes must outperform the related works in terms of achievable reuse, too. Both the relative ordering of the algorithms as well as their optimality values of 95% and 70% have been verified in other set-ups as well, where the maximum D2D distances and cell sizes were changed. This motivates them as typically achievable values. The used tool-chain have been made publicly available at [167], for the reader to verify these rules of thumb. It seems that around 70% of achievable reuse can be accessed by using fixed powers. Thus, power control acts as enabler to unlock the remaining 30%. Around 95% optimality can be achieved by So2C and WPS, which have linear complexity. It seems that both algorithms already capture the main aspects of the interference condition but fail to incorporate the effects of non-linearity. For the last 5%, which can be conquered by $\tilde{\varepsilon}$-PP, the price of exponential complexity needs to be payed.

6.4.3 Implementation Aspects

The previous results give an understanding of underlying problem properties and general ways to resolve them. However, the WPS and $\tilde{\varepsilon}$-PP Algorithms cannot directly be implemented due to the inherent assumption that estimates of the spectral radius ρ and the pressure values m_i are available. Further, it assumes the unrealistic noiseless case. These shortcomings will be targeted now by slightly adapting the feasibility problem and re-applying the results. It is assumed in the following that $N_i > 0 \; \forall i$, such that u_i cannot be neglected anymore. Also, the focus is on implementable structures rather than algorithmic properties.

Adaptation of the Feasibility Problem

A standard form for feasibility problems is given in [160], which is applied to the given problem as:

$$\text{(GBD-F)} \qquad \min_{\boldsymbol{c},\tilde{\boldsymbol{p}},\boldsymbol{w}} \|\boldsymbol{c}\| \tag{6.55}$$

s.t.

$$c_i \geq 0 \ \ \forall i \tag{6.56}$$

$$(x_i^{(k)} - 1)\tilde{\varepsilon} - w_i \leq 0 \ \ \forall i \tag{6.57}$$

$$\exp(w_i - \tilde{p}_i)\left(\textstyle\sum_{j\neq i} \gamma_i \frac{h_{ij}}{h_{ii}} \exp(\tilde{p}_j) + u_i\right) - 1 \leq c_i \ \ \forall i. \tag{6.58}$$

$$\exp(\tilde{p}_i) \leq p_{\text{max},i} \tag{6.59}$$

$\|\cdot\|$ is an arbitrary vector norm that can be chosen according to design considerations. Whenever $\|\boldsymbol{c}^*\| = 0$ for the optimal $\boldsymbol{c}^*$, a feasible solution has been found. Otherwise, the solution is as close to feasibility as possible, with respect to the chosen norm. If $\|\cdot\|$ is convex, GBD-F is a convex optimization problem on continuous space and hence efficiently solvable.

The SRMP, which was used as feasibility problem, can be interpreted as minimizing the norm $\|\boldsymbol{c}\|_\infty = \max_i c_i$. The SRMP allows an interpretation as spectral radius minimization and relates to Perron-Frobenius Theory. However, for actual implementation the $\|\cdot\|_\infty$ norm turns out to be not well suitable, as the impact of a link on the norm can only be determined from a global point of view. The norm itself couples all links and the feasibility problem cannot be well solved in a decentralized fashion. By choosing $\|\boldsymbol{c}\|_1 = \sum_i c_i$ as norm to be minimized, decentralization can be achieved. Further, the use of this norm enables the use of well-known PCAs, such as the FM-PCA [54], as will become clear at the end of this section.

Recall the observation that at optimality, $w_i^* = (x_i^{(k)} - 1)\tilde{\varepsilon}$, which is assumed in the following. By defining $c_i' = 1 + c_i$ and $\gamma_{t,i} = e^{w_i^*}\gamma_i$, constraint (6.58) can be re-formulated into:

$$\frac{\gamma_{t,i}}{c_i'}\left(\sum_{j\neq i} \frac{h_{ij}}{h_{ii}} e^{\tilde{p}_j} + \frac{N_i}{h_{ii}}\right) - e^{\tilde{p}_i} \leq 0 \ \ \forall i. \tag{6.60}$$

The term $\gamma_{t,i}$ can be interpreted as current SINR target, which might be reduced by a factor ε with respect to γ_i due to the back-off. In a similar fashion, the expression $\gamma_i' = \gamma_{t,i}/c_i'$ can be interpreted as an achieved SINR, as c_i' is chosen to be the minimum value that does not violate the SINR constraint. Reverting the relationship yields $c_i' = \gamma_{t,i}/\gamma_i'$. By using logarithmically scaled variables $\tilde{\gamma}_i' = \log(\gamma_i')$, $\tilde{\gamma}_{t,i} = \log(\gamma_{t,i})$ [57] and plugging the relations into GBD-F, the problem can be re-phrased into:

$$\min_{\tilde{p}_i,\tilde{\gamma}_i'} \sum_{i\in\mathcal{L}} \left(e^{\tilde{\gamma}_{t,i} - \tilde{\gamma}_i'} - 1\right)$$

s.t.

$$\tilde{\gamma}_i' \leq \tilde{\gamma}_{t,i} \ \ \forall i, \tag{6.61}$$

$$e^{\tilde{\gamma}_i'}\left(\textstyle\sum_{j\neq i} \frac{h_{ij}}{h_{ii}} e^{\tilde{p}_j} + \frac{N_i}{h_{ii}}\right) - e^{\tilde{p}_i} \leq 0 \ \ \forall i, \tag{6.62}$$

$$e^{\tilde{p}_i} \leq p_{\text{max},i} \ \ \forall i. \tag{6.63}$$

In words, the feasibility problem is that of minimizing the sum of factors $\gamma_{t,i}/\gamma'_i$, under the constraints that the variables γ'_i exceed neither the achieved SINR (eq. (6.62)), nor the targets $\gamma_{t,i}$ (eq. (6.61)). The stated problem is convex on continuous problem space and satisfies Slaters' condition. Hence, it has either one unique local optimum that is also globally optimal or several local optima that all are globally optimal. For any local optimum, the KKT conditions are necessary and sufficient, hence they can serve to identify optimal points. The associated Lagrange function is:

$$\begin{aligned} L(\tilde{p}_i, \tilde{\gamma}'_i, \eta_i, \nu_i, \mu_i) &= \sum_{i\in\mathcal{L}} \left(e^{\tilde{\gamma}_{t,i}-\tilde{\gamma}'_i} - 1\right) + \sum_{i\in\mathcal{L}} \eta_i \left[e^{\tilde{\gamma}'_i}\left(\sum_{j\neq i} \frac{h_{ij}}{h_{ii}} e^{\tilde{p}_j} + \frac{N_i}{h_{ii}}\right) - e^{\tilde{p}_i}\right] \\ &\quad \sum_{i\in\mathcal{L}} \mu_i \left[\tilde{\gamma}'_i - \tilde{\gamma}_{t,i}\right] + \sum_{i\in\mathcal{L}} \nu_i \left[e^{\tilde{p}_i} - p_{\max,i}\right], \end{aligned} \tag{6.64}$$

where $\eta_i \geq 0$, $\mu_i \geq 0$, $\nu_i \geq 0$ are multipliers. As the defined problem is convex, the optimal solution can be found by solving $\min\limits_{\tilde{p}_i,\tilde{\gamma}'_i} \max\limits_{\eta_i,\nu_i,\mu_i} L(\tilde{p}_i, \tilde{\gamma}'_i, \eta_i, \nu_i, \mu_i)$. That is, $\tilde{p}_i$ and $\tilde{\gamma}'_i$ should be chosen to minimize L, whereas η_i, ν_i and μ_i should be chosen to maximize it. The necessary and sufficient KKT conditions correspond to $\partial L/\partial\tilde{\gamma}'_i = 0$, $\partial L/\partial\tilde{p}_i = 0$. The derivatives of the Lagrange function L with respect to $\tilde{\gamma}_i$, $\tilde{p}_i$ are:

$$\partial L/\partial\tilde{\gamma}'_i = -e^{\tilde{\gamma}_{t,i}-\tilde{\gamma}'_i} + \eta_i e^{\tilde{\gamma}'_i}\left(\textstyle\sum_{j\neq i} \frac{h_{ij}}{h_{ii}} e^{\tilde{p}_j} + \frac{N_i}{h_{ii}}\right) + \mu_i \ \ \forall i, \tag{6.65}$$

$$\partial L/\partial\tilde{p}_i = \ \ e^{\tilde{p}_i}\left[\textstyle\sum_{j\neq i} e^{\tilde{\gamma}'_j} \frac{h_{ji}}{h_{jj}} \eta_j - \eta_i + \nu_i\right] \forall i. \tag{6.66}$$

The corresponding complementary slackness conditions are:

$$\eta^*_i \left[e^{\tilde{\gamma}'^*_i}\left(\textstyle\sum_{j\neq i} \frac{h_{ij}}{h_{ii}} e^{\tilde{p}^*_j} + \frac{N_i}{h_{ii}}\right) - e^{\tilde{p}^*_i}\right] = 0 \ \ \forall i, \tag{6.67}$$

$$\mu^*_i \left[\tilde{\gamma}'^*_i - \tilde{\gamma}_{t,i}\right] = 0 \ \ \forall i, \quad \nu^*_i \left[e^{\tilde{p}^*_i} - \tilde{p}_{\max,i}\right] = 0 \ \ \forall i. \tag{6.68}$$

Now some properties of optimal solutions can be observed:

Observation 6.1. At any optimal point, it holds that $\gamma'^*_i = \min\{\Gamma_i(\boldsymbol{p}^*), \gamma_{t,i}\}$.

Proof. Observe that if $\gamma'^*_i = \gamma_{t,i}$, constraint (6.61) is tight and if $\gamma'^*_i = \Gamma_i(\boldsymbol{p}^*)$, constraint (6.62) is. Assume that $\gamma'^*_i < \min\{\Gamma_i(\boldsymbol{p}^*), \gamma_{t,i}\}$, then due to the complementary slackness conditions, $\eta^*_i = \mu^*_i = 0$. Plugging this into (6.65) leads to $\partial L/\partial\tilde{\gamma}'_i < 0$. Thus, by increasing $\tilde{\gamma}'_i$, a lower value of L can be obtained. The result is that for the optimal $\tilde{\gamma}'^*_i$ one of (6.61), (6.62) must be tight, leading to the stated observation. □

Observation 6.2. There is at least one optimal point for which $\gamma'^*_i = \Gamma_i(\boldsymbol{p}^*)\ \forall i$ holds.

Proof. Again observe that $\gamma'^*_i = \Gamma_i(\boldsymbol{p}^*)$ corresponds to constraint (6.62) being tight. Assume that $\gamma'^*_i < \Gamma_i(\boldsymbol{p})$, then due to the complementary slackness conditions, $\eta^*_i = 0$. As all considered variables are non-negative, plugging this into (6.66) leads to $\partial L/\partial\tilde{p}_i \geq 0$, with equality if, and only if $\boldsymbol{\eta}^* = \mathbf{0}$ and $\mu^*_i = 0$. When $\boldsymbol{\eta}^* \neq \mathbf{0}$ or $\mu^*_i \neq 0$, by decreasing $\tilde{p}_i$, the value of L will be decreased and there is a unique, optimal point such that $\eta_i > 0\ \forall i$. If $\boldsymbol{\eta}^* = \mathbf{0}$ and

$\mu_i^* = 0$, decreasing $\tilde{p}_i$ does not change the value of L for any link, so there are many optimal points. Among them are the points at the border of the feasible region, which make (6.62) tight. □

Observation 6.3. For at least one optimal point,

$$p_i^* = \min\left\{\gamma_{t,i}\left(\sum_{j\neq i}\frac{h_{ij}}{h_{ii}}p_j^* + \frac{N_i}{h_{ii}}\right), p_{\max,i}\right\} \quad \forall i \tag{6.69}$$

holds.

Proof. The combination of Observation 6.1 and 6.2 lead to the corollary that there is a point such that $\Gamma_i(\boldsymbol{p}^*) = \gamma_i'^* \leq \gamma_{t,i}\ \forall i$. This can be reformulated into

$$p_i^* \leq \gamma_{t,i}\left(\sum_{j\neq i}\frac{h_{ij}}{h_{ii}}p_j^* + \frac{N_i}{h_{ii}}\right), \tag{6.70}$$

with equality if, and only if, $\gamma_i'^* = \gamma_{t,i}$. Equation (6.69) corresponds to the claim that if $\gamma_i'^* < \gamma_{t,i}$, then $p_i^* = p_{\max,i}$ must hold. To prove this, a perturbation analysis is done: Assume that $\gamma_i'^* = \Gamma_i(\boldsymbol{p}^*) < \gamma_{t,i}$ and $p_i^* < p_{\max,i}$, which induces $\mu_i^* = 0$ and $\nu_i^* = 0$. Then, as both, $\gamma_i'^*$ and p_i^* are in the relative interior of their feasible domains, the value of $\gamma_{t,i}$ can be altered into any value $\gamma_{t,i}'$, $\gamma_i'^* < \gamma_{t,i}' < \gamma_{t,i}$, while keeping $\gamma_{t,j}$ with $j \neq i$ constant. $\mu_i^* = 0$ then still holds due to the complementary slackness conditions. Now the original problem using $\gamma_{t,i}$ can be interpreted as relaxation of the perturbed problem with $\gamma_{t,i}'$. It is known that if the solution of a relaxed problem lies in the non-relaxed optimization domain, it is also optimal for the non-relaxed problem [160]. So as the optimal values of p_i^*, $\gamma_i'^*$ are within the perturbed optimization domain by design, they must remain optimal throughout the perturbation process. However, by demanding $\partial L/\partial\tilde{\gamma}_i' = \partial L/\partial\tilde{p}_i = 0$, reformulating (6.65), (6.66) and combining the results, it can be deduced that at any optimal point,

$$\begin{aligned} \eta_i^* &= \textstyle\sum_{j\neq i}\gamma_j'^*\frac{h_{ji}}{h_{jj}}\eta_j^*; \qquad \eta_i^* = \frac{\gamma_{t,i}'}{(\gamma_i'^*)^2 I_i(\boldsymbol{p}^*)}; \\ \Rightarrow \gamma_{t,i}' &= (\gamma_i'^*)^2 I_i(\boldsymbol{p}^*)\left(\textstyle\sum_{j\neq i}\gamma_j'^*\frac{h_{ji}}{h_{jj}}\frac{\gamma_{t,j}'}{(\gamma_j'^*)^2 I_j(\boldsymbol{p}^*)}\right), \end{aligned} \tag{6.71}$$

where $I_i(\boldsymbol{p}) = \sum_{j\neq i}\frac{h_{ji}}{h_{ii}}p_j + \frac{N_i}{h_{ii}}$. Equation (6.71) depends only on $\gamma_{t,i}'$, p_i^* and $\gamma_i'^*\ \forall i$. Any unilateral change of $\gamma_{t,i}'$ cannot satisfy (6.71), as the right hand side remains constant. That is, optimal points of the original problem cannot remain optimal after perturbation. This forms a contradiction to the assumption that $\gamma_i'^*$, p_i^* are in the relative interior of the optimization domain, for which they would have to remain optimal after perturbation. As conclusion, $\gamma_i'^* < \gamma_{t,i}$ and $p_i^* < p_{\max,i}$ cannot hold at the same time. Taking this result, the conclusion is that if $\gamma_i'^* = \Gamma_i(\boldsymbol{p}^*) < \gamma_{t,i}$, $p_i^* = p_{\max,i}$ must hold and vice versa, leading to equation (6.69). □

The result of Observation 6.3 is important, as it relates the RMP to a set of well-known power control algorithms. The power-constrained FM-PCA [54], [68] iteratively adapts powers exactly according to the rule

$$p_i[k+1] = \min\left\{\gamma_{t,i}\left(\sum_{j\neq i}\frac{h_{ij}}{h_{ii}}p_j[k] + \frac{N_i}{h_{ii}}\right), p_{\max,i}\right\}. \tag{6.72}$$

It is known to always converge to a unique point, at which (6.69) holds. The PCA can be implemented in a distributed fashion, where each transmitter and receiver optimize solely themselves but do not coordinate with other links. Also, it does not require any information on channel gains, because the update rule can be interpreted as:

$$\gamma_{t,i}\left(\frac{\sum_{j\neq i} h_{ij}p_j[k]+N_i}{h_{ii}p_i[k]}\right)p_i[k] = \frac{\gamma_{t,i}}{\Gamma_i(\boldsymbol{p}[k])}p_i[k]. \tag{6.73}$$

The PCA is known to converge towards its solution with at least linear rate. Typically, convergence can be claimed after 6-10 iterations, where one iteration comprises of one transmission and one SINR feedback. The algorithm has been further re-fined for a variety of use-cases, including the use of safety margins on the SINR target [69], asynchronous operation [68] and discrete power levels [72].

The conclusion of Observation 6.3 is that Foschini-Miljanic types of PCAs can be used to determine the optimal solution of the feasibility problem. By letting the algorithm run for a sufficient amount of iterations and then setting $\gamma_i'^* = \Gamma_i(\boldsymbol{p}^*)$, the optimal value of $\gamma_i'^*$ can be found.

Constraints of the Master Problem

After adapting the feasibility problem, the constraints added to the master problem need to be re-established. For these, parameters w_i explicitly need to be included into the formulation. Using the introduced nomenclature, it is transformed into $w_i = \tilde{\gamma}_{t,i} - \tilde{\gamma}_i$. This yields a Lagrange function of the form

$$\begin{aligned} L \;=\; & \sum_{i\in\mathcal{L}}\left(e^{\tilde{\gamma}_{t,i}-\tilde{\gamma}_i'}-1\right)+\sum_{i\in\mathcal{L}}\mu_i\left[\tilde{\gamma}_i'-\tilde{\gamma}_{t,i}\right]+\sum_{i\in\mathcal{L}}\tau_i\left[(x_i-1)\tilde{\varepsilon}+\tilde{\gamma}_i-\tilde{\gamma}_{t,i}\right]+ \\ & \sum_{i\in\mathcal{L}}\eta_i\left[e^{\tilde{\gamma}_i'}\left(\sum_{j\neq i}\frac{h_{ij}}{h_{ii}}e^{\tilde{p}_j}+\frac{N_i}{h_{ii}}\right)-e^{\tilde{p}_i}\right]+\sum_{i\in\mathcal{L}}\nu_i\left[e^{\tilde{p}_i}-p_{\max,i}\right], \end{aligned} \tag{6.74}$$

where $\tau_i \geq 0$ are newly introduced multipliers corresponding to (6.48). Note that L is now also dependent on $\tilde{\gamma}_{t,i}$. Compared to (6.64), the derivatives of (6.74) do not change but are enhanced with

$$\partial L/\partial\tilde{\gamma}_{t,i} = e^{\tilde{\gamma}_{t,i}-\tilde{\gamma}_i'} - \mu_i - \tau_i \;\; \forall i. \tag{6.75}$$

Observation 6.4. At optimality, $\tilde{\gamma}_{t,i}^* = (x_i^{(k)}-1)\tilde{\varepsilon}+\tilde{\gamma}_i$ holds.

Proof. By an argumentation similar to that of Observation 6.1, if $\tilde{\gamma}_{t,i}^* > \max\{\tilde{\gamma}_i'^*, (x_i^{(k)}-1)\tilde{\varepsilon}+\tilde{\gamma}_i\}$, then $\mu_i^*=0$ and $\tau_i^*=0$. In this case, $\partial L/\partial\tilde{\gamma}_{t,i} > 0$ and by decreasing $\tilde{\gamma}_{t,i}$, the value of L can be decreased, hence $\tilde{\gamma}_{t,i}^* = \max\{\tilde{\gamma}_i'^*, (x_i^{(k)}-1)\tilde{\varepsilon}+\tilde{\gamma}_i\}$ must hold. Further, when $\gamma_{t,i}^* = \tilde{\gamma}_i'^* > (x_i^{(k)}-1)\tilde{\varepsilon}+\tilde{\gamma}_i$, it follows that $\tau_i^*=0$ and $\mu_i^* = e^{\tilde{\gamma}_{t,i}^*-\tilde{\gamma}_i'^*}$, which renders $\partial L/\partial\tilde{\gamma}_i' > 0$. This enables further minimization of L by decreasing $\tilde{\gamma}_i'$ and thus, $\tilde{\gamma}_{t,i}^* = (x_i^{(k)}-1)\tilde{\varepsilon}+\tilde{\gamma}_i$ must hold at optimality. □

As the optimal value of $\tilde{\gamma}^*_{t,i}$ can directly be computed as $\tilde{\gamma}^*_{t,i} = (x_i^{(k)}-1)\tilde{\varepsilon}+\tilde{\gamma}_i$, the constraint $\tilde{\gamma}'_i \leq \tilde{\gamma}_{t,i}$ can in fact be dropped from GBD-F and replaced by restricting the optimization domain of $\tilde{\gamma}_i$ to $\tilde{\gamma}_i \in [0, (x_i^{(k)} - 1)\tilde{\varepsilon} + \tilde{\gamma}_i]$. The resulting Lagrange function equals (6.74) with $\mu_i = 0$. By considering (6.75) and including that by Observation 6.2 $\gamma'^*_i = \Gamma_i(\boldsymbol{p}^*)$ holds, this leads to an optimal value of

$$\tau_i^* = \frac{\gamma^*_{t,i}}{\Gamma_i(\boldsymbol{p}^*)}. \tag{6.76}$$

Finally, the Lagrange function (6.75) can be used to derive a constraint for the master problem, by plugging in the optimal values for all variables and assuming them fixed, while x_i are assumed variable. After considering that several terms cancel each other out, this leads to a constraint function of the form:

$$\begin{aligned} \xi^{(l)}(\boldsymbol{x}) &= \sum_{i\in\mathcal{L}} \left(\frac{\gamma^{(l)}_{t,i}}{\Gamma_i(\boldsymbol{p}^{(l)})} - 1 \right) + \tilde{\varepsilon} \sum_{i=1}^{L} \frac{\gamma^{(l)}_{t,i}}{\Gamma_i(\boldsymbol{p}^{(l)})} \cdot \left(x_i - x_i^{(l)} \right), \\ &= \rho^{(l)} + \tilde{\varepsilon} \sum_{i=1}^{L} m_i^{(l)} \left(x_i - x_i^{(l)} \right), \qquad (6.77) \\ \text{where} \qquad & m_i^{(l)} = \frac{\gamma^{(l)}_{t,i}}{\Gamma_i(\boldsymbol{p}^{(l)})}; \quad \rho^{(l)} = \sum_{i\in\mathcal{L}} \left(m_i^{(l)} - 1 \right). \end{aligned}$$

In this case, $m_i^{(l)}$ corresponds to the interference pressure generated by link i, assuming an activation vector of $\boldsymbol{x}^{(l)}$. $\xi^{(l)}(\boldsymbol{x})$ induces an outer approximation $\hat{\mathcal{F}}_x^{(l)}$ of the feasible activation region, which is defined as $\hat{\mathcal{F}}_x^{(l)} = \{\boldsymbol{x} : \xi^{(l)}(\boldsymbol{x}) \leq 0\}$. The pressure values m_i are the derivatives of $\xi^{(l)}(\boldsymbol{x})$ with respect to x_i, indicating the local influence of x_i on feasibility.

Final Adjustment

Finally, two adjustments are made which improve the speed of the subsequently proposed algorithms. A result from initial evaluations is that links with sufficiently bad channel can severely degrade the performance of the GBD in terms of run-time. In particular, this is the case for links which could not even achieve their full SINR targets without interference. Such links clearly must be turned off in the optimal solution, yet increase the search space for the algorithm. Improvement can be achieved by de-activating such links in first place:

Lemma 6.1. Let $\boldsymbol{x}^*$ be the optimal solution to the RMP. Then $x_i^* = 0$ if $p_{\text{max},i} h_{ii}/N_i < \gamma_i$.

Proof. Consider the SINR constraint (6.15) of the RMP, which can be re-formulated into:

$$p_i \geq x_i \gamma_i \left(\sum_{j\neq i} \frac{h_{ij}}{h_{ii}} p_j + \frac{N_i}{h_{ii}} \right). \tag{6.78}$$

From the fact that $0 \leq p_i \leq p_{\text{max},i}$ follows that if $p_{\text{max},i} h_{ii}/N_i < \gamma_i$, then

$$p_i^* \leq p_{\text{max},i} \;<\; \gamma_i N_i/h_{ii} \leq \gamma_i \left(\sum_{j\neq i} \frac{h_{ij}}{h_{ii}} p_j^* + \frac{N_i}{h_{ii}} \right). \tag{6.79}$$

As conclusion, link i's SINR constraint can only be satisfied for $x_i^* = 0$. □

Algorithm 9 Implementation of WPS

Set $\mathcal{A} = \{i \in \mathcal{L} : p_{\max,i} h_{ii}/N_i \geq \gamma_i\}$.
Set $K \geq 1$, $\rho := \infty$, $x_i = \mathbb{1}_{\{i \in \mathcal{A}\}}$.
while $\rho > 0$ **do**
  All Tx set $p_i[1] := x_i p_{\max,i}$.
  for $k := 1$ to K **do**
    Active Tx transmit with power $p_i[k]$.
    Rx report SINR $\Gamma_i(\boldsymbol{p}[k])$ to Tx.
    Active Tx set $p_i[k+1] := \min\{x_i \gamma_i / \Gamma_i(\boldsymbol{p}[k]), p_{\max,i}\}$.
  end for
  Active Tx report $m_i = \gamma_i / \Gamma_i(\boldsymbol{p}[k])$ to CC.
  CC sets $\rho := \sum_{i \in \mathcal{A}} (m_i - 1)$.
  if $\rho > 0$ **then**
    CC identifies $l = \arg\max_i m_i$.
    CC sets $\mathcal{A} := \mathcal{A} \setminus l$, $x_l := 0$.
    CC shuts down link l.
  end if
end while

Lemma 6.1 allows to fully shut links down, instead of backing their SINR off. A second adjustment identifies links that must definitely be part of the solution, to further reduce the search space. Consider the master problem, which starts with no constraints and hence activates all links by default. Any link that achieves its SINR target in this instance must be part of the optimal solution:

Lemma 6.2. Let $\boldsymbol{x}^*$ be the optimal solution of the RMP and let $\hat{\boldsymbol{x}} \in \{0,1\}$ be a vector such that $x_i^* = 1 \Rightarrow \hat{x}_i = 1$ and $\sum_i \hat{x}_i \geq \sum_i x_i^*$. Further, let $\Gamma_i(\hat{\boldsymbol{p}})$ be the SINR value achieved at the optimal solution of the feasibility problem using $\hat{\boldsymbol{x}}$. Then $\Gamma_i(\hat{\boldsymbol{p}}) \geq \gamma_i \Rightarrow x_i^* = 1$.

Proof. It holds that

$$\gamma_i \leq \Gamma_i(\hat{\boldsymbol{p}}) \leq \frac{h_{ii}\hat{p}_i}{\sum_{j \neq i} h_{ij}\hat{p}_j\hat{x}_j + N_i} \leq \frac{h_{ii}\hat{p}_i}{\sum_{j \neq i} h_{ij}\hat{p}_j x_j^* + N_i}. \tag{6.80}$$

The first inequality is due to the fact that instead of shutting down, inactive links actually back-off their SINR and still produce interference. By completely shutting them down, interference is reduced. The second inequality is due to $\sum_i \hat{x}_i \geq \sum_i x_i^*$. That is, by simply deactivating all links that do not belong to the optimal solution and keeping the power $\hat{p}_i$ for the remaining links, the SINR is increased. Links that already achieve their SINR targets thus must also achieve them in the optimal solution. Hence, they are part of the optimal solution. □

Algorithm Re-Design

After all adjustments have been made, the resulting algorithmic structures are adapted and given in Algorithms 9 and 10. The intuition behind the algorithms remains the same and has

Algorithm 10 Implementation of $\tilde{\varepsilon}$-PP

Set $\mathcal{A} = \{i \in \mathcal{L} : p_{\max,i} h_{ii}/N_i \geq \gamma_i\}$.
Set $K \geq 1$, $\tilde{\varepsilon} \geq 0$, $l := 0$, $x_i = \mathbb{1}_{\{i \in \mathcal{A}\}}$.
Initialize GBD-M at CC as:
$$\max_{\boldsymbol{x}} \sum_{i \in \mathcal{A}} x_i \text{ s.t. } x_i \in \{0, 1\}.$$
repeat
  $l := l + 1$.
  Solve GBD-M at CC, yielding $\boldsymbol{x}^{(l)}$.
  Links set their SINR targets as $\gamma_{t,i} := \varepsilon^{1-x_i^{(l)}} \gamma_i$.
  All Tx in $\mathcal{A}$ set $p_i[1] := p_{\max,i}$.
  for $k := 1$ to K **do**
    Tx in $\mathcal{A}$ transmit with power $p_i[k]$.
    Rx in $\mathcal{A}$ report SINR $\Gamma_i(\boldsymbol{p}[k])$ to Tx.
    Tx in $\mathcal{A}$ set $p_i[k+1] := \min\{\gamma_i/\Gamma_i(\boldsymbol{p}[k]), p_{\max,i}\}$.
  end for
  Tx in $\mathcal{A}$ report $m_i^{(l)} := \gamma_{t,i}/\Gamma_i(\boldsymbol{p}[k])$ to CC.
  CC calculates $\rho^{(l)} := \sum_{i \in \mathcal{A}} (m_i^{(l)} - 1)$.
  CC adds $\rho^{(l)} + \tilde{\varepsilon} \sum_{i \in \mathcal{A}} m_i^{(l)} \left(x_i - x_i^{(l)}\right) \leq 0$ to GBD-M.
until $\rho^{(l)} = 0$

been extensively explained in Section 6.4.1, so they are not re-explained here. The implementation assumes the existence of a general CC, that is in charge of deciding the next link to be shut down. The CC can be located at the BS, which would be a natural choice. However, it might just as well be implemented as function in an edge-cloud, which is targeted to be part of future cellular networks. A CC that resides in the core network could even coordinate interference across cell borders, as the problem structure does not change when different cells are considered. In contrast to Lemma 6.1, Lemma 6.2 is a "trick" that can be used to reduce the search space at each instance of the master problem and it is thus not explicitly included in the formulation of the master problem.

Analysis of PCA Delay

After adaptation, the main properties of the proposed algorithms remains the same. However, the feasibility estimation introduces a delay vs. accuracy trade-off that will now be investigated with simulations. The simulation set-up and parameters are the same of those used in Section 6.4.2. Assume that the FM-PCA is operated in a synchronous fashion, such that all transmitters transmit a probing signal of fixed length, the receivers measure the achieved SINR and report it back to their transmitters. This may take an arbitrary, fixed delay of D, which typically will comprise of a transmission delay and feedback delay. After K iterations of the PCA have been performed, the resulting SINRs are reported to the CC, which does some calculations and notifies the links whether they should shut down or back off their SINR during the next PCA run. This is assumed to take a delay of Δ, which will differ for WPS and $\tilde{\varepsilon}$-PP. The main difference originates from processing at the CC, which

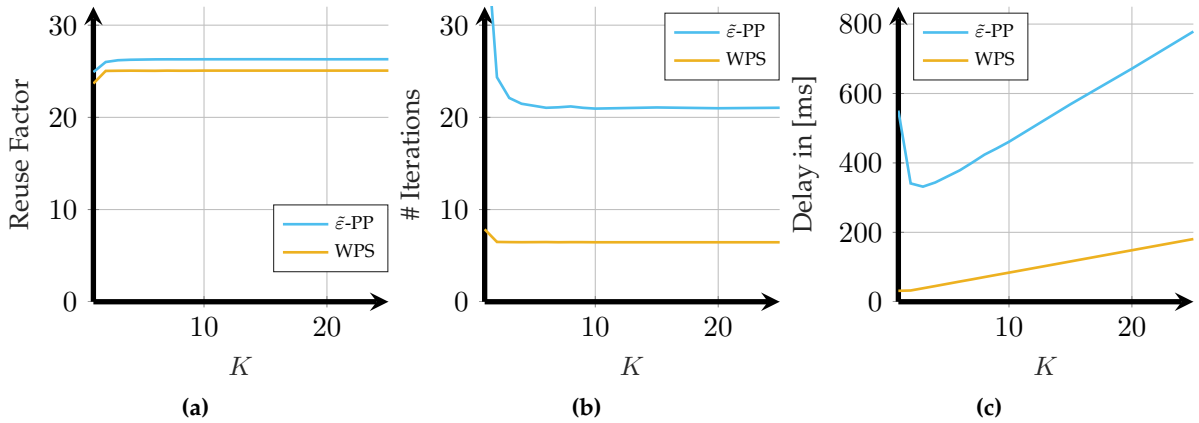

Figure 6.9: Impact of K on the optimality and delay of the proposed algorithms WPS and $\tilde{\varepsilon}$-PP. 6.9a shows impact on reuse factor, 6.9b on required iterations and 6.9c on the generated delay. It is assumed that $D = 1$ ms, $\Delta = 3$ ms for the WPS and $\Delta = 12$ ms for the $\tilde{\varepsilon}$-PP algorithm.

contains a single maximum and a sum operation for the WPS, whereas it requires the solution of a Knapsack problem for the $\tilde{\varepsilon}$-PP.

Figure 6.9 shows the achieved reuse factor, required iterations and introduced delay for WPS and C with $N = 40$ links, while the number of PCA iterations K is varied. For the simulations, it is assumed that $D = 1$ ms and that $\Delta = 3$ ms for the WPS, which comprises of one millisecond each for reporting, processing and notification. For the $\tilde{\varepsilon}$-PP algorithm, the assumption is that the processing takes 10 ms, which induces $\Delta = 12$ ms. While this is a magnitude increase compared to the WPS, it is in fact a very optimistic approximation.

It can be seen from Figure 6.9a that only few PCA iterations are required to achieve maximum algorithm performance, as near maximal reuse is already achieved for $K = 2$. While further increase does not significantly affect the achieved reuse, it does reduce the required iterations for the $\tilde{\varepsilon}$-PP, as can be seen from Figure 6.9b. The reason for the reduced number of iterations is that for larger K, the generated bounds become tighter, hence the feasible activation space is better approximated. Both, K and the number of iterations have opposite effects on the delay, which increases with K but decreases with the better bound accuracy. Figure 6.9c depicts the impact of K on the delay. Clearly, the $\tilde{\varepsilon}$-PP has the larger delay and also achieves a minimum delay value at $K = 3$. At this optimal K, the $\tilde{\varepsilon}$-PP requires ca. 330 ms to find the optimal solution, whereas the WPS requires only 40 ms.

6.5 Connection to NUM problems

It was stated already that the RMP is tightly related to network utility maximization problems. In this section, the resulting management structure will thus be generalized to arbitrary NUM problems with interference coupling. As many special cases of NUM problems are hard to solve in general, they remain hard after applying the developed solution approach. However, the implementation structure enables to decouple the interference management and channel specific aspects from the remaining utility maximization, effectively reducing

the latter to be a purely mathematical problem without need for further adaptation of signaling structures. The application of generated results thus is complete in the sense that it can serve to optimize for an arbitrary utility, as long as the corresponding algorithmic problem can be efficiently solved.

6.5.1 The General D2D-NUM Problem Re-Visited

To tighten the notion of the considered problems, the D2D-NUM problem formulated in Section 2.2 is considered. The formulation is slightly varied to incorporate the logarithmic transformation, which yields:

$$\text{(D2D-NUM)} \qquad \max_{\boldsymbol{R},\boldsymbol{x}_i^{(k)},\boldsymbol{p},\boldsymbol{\gamma}_i^{(k)}} \sum_{i\in\mathcal{L}} U_i(R_i) \tag{6.81}$$

$$\text{s.t.}$$

$$0 \leq R_i \leq \sum_{k\in\mathcal{R}} R_i^{(k)} \tag{6.82}$$

$$- - - - - - - - - - - - - - - - - - - -$$

$$R_i^{(k)} \leq \boldsymbol{r}_t^T \boldsymbol{x}_i^{(k)} \qquad \forall i,k \tag{6.83}$$

$$\sum_{q=1}^{C_{\text{UL}}} x_{qi}^{(k)} \leq \mathbb{1}_{\{k\in\mathcal{U}\}} \qquad \forall k \tag{6.84}$$

$$\sum_{k\in\mathcal{T}_t} \sum_{q=1}^{C_{\text{UL}}} x_{qi}^{(k)} \leq 1 \qquad \forall i,\mathcal{T}_t \tag{6.85}$$

$$x_{qi}^{(k)} \in \{0,1\} \qquad \forall i,q,k \tag{6.86}$$

$$- - - - - - - - - - - - - - - - - - - -$$

$$\tilde{\boldsymbol{\gamma}}_t^T \boldsymbol{x}_i^{(k)} \leq \tilde{\gamma}_i^{(k)} \qquad \forall i,k \tag{6.87}$$

$$e^{\tilde{\gamma}_i^{(k)}} \left(\textstyle\sum_{j\neq i} \frac{h_{ij}}{h_{ii}} e^{\tilde{p}_j^{(k)}} + \frac{N_i}{h_{ii}} \right) \leq e^{\tilde{p}_i^{(k)}} \qquad \forall i,k \tag{6.88}$$

$$[p_i^1,...,p_i^K]^T \in \mathcal{P}_i \qquad \forall i \tag{6.89}$$

The intuition of this optimization problem has been discussed in detail in Section 2.2 already. The D2D-NUM problem is a full MAC-layer formulation for the operation of a D2D network.

6.5.2 Transfer from RMP to D2D-NUM

Although the problem significantly differs from the studied RMP, the core approach of using an outer approximation for interference management can be applied. This leads to a similar communication structure as that developed in Section 6.4.

Similar to the RMP, constraints (6.88)-(6.89) could in principle be dropped and replaced with a constraint that demands

$$\tilde{\boldsymbol{\gamma}}^{(k)} = \left[\tilde{\gamma}_1^{(k)},...,\tilde{\gamma}_{|\mathcal{L}|}^{(k)}\right]^T \in \mathcal{F}_{\tilde{\gamma}}^{(w)}; \;\; w \text{ s.t. } k \in \mathcal{B}_w. \tag{6.90}$$

Therein, w is the frequency channel on which the physical resource block k resides and $\mathcal{F}_{\tilde{\gamma}}^{(w)}$ is the set of feasible SINR targets on w, in logarithmic domain. Choosing such a formulation would be equivalent to (6.88)-(6.89) because there exist transmission powers to realize $\tilde{\boldsymbol{\gamma}}^{(k)}$ if, and only if, it is in $\mathcal{F}_{\tilde{\gamma}}^{(w)}$. The remaining task then would be to realize the SINR targets with an appropriate power control, e.g., the Foschini-Miljanic PCA. By using such an approach, the entire utility maximization problem could be solved purely algorithmically, without employing any intermediate signaling, because all channel specific aspects of utility maximization are captured in $\mathcal{F}_{\tilde{\gamma}}^{(w)}$. The solution thus could be run somewhere in an edge-cloud or at a remote, powerful machine and the schedule determined as solution could afterwards be distributed to the UEs. However, the problem with realizing such an approach is that $\mathcal{F}_{\tilde{\gamma}}^{(w)}$ must be assumed unknown. By applying the GBD, an outer approximation scheme can be generated that approximates $\mathcal{F}_{\tilde{\gamma}}^{(w)}$ over time and yields an optimal solution after sufficient iterations have been run.

To apply the GBD, it must be noted again that in logarithmic domain, $\mathcal{F}_{\tilde{\gamma}}^{(w)}$ is known to be convex and thus can be approximated arbitrarily close with linear hyperplanes. By choosing $\boldsymbol{R}$ and $\boldsymbol{x}_i^{(k)}$ as complicating variables, the primal problem assumes exactly the same structure as that of the RMP, namely:

$$\text{(D2D-NUM-P)} \qquad \max_{\tilde{\boldsymbol{p}},\tilde{\gamma}_i^{(k)}} \sum_{i\in\mathcal{L}} U_i(R_i) \tag{6.91}$$

$$\text{s.t.}$$

$$\tilde{\boldsymbol{\gamma}}_t^T \boldsymbol{x}_i^{(k)} \leq \tilde{\gamma}_i^{(k)} \qquad \forall i,k \tag{6.92}$$

$$e^{\tilde{\gamma}_i^{(k)}} \left(\sum_{j\neq i} \frac{h_{ij}}{h_{ii}} e^{\tilde{p}_j^{(k)}} + \frac{N_i}{h_{ii}} \right) \leq e^{\tilde{p}_i^{(k)}} \qquad \forall i,k \tag{6.93}$$

$$[p_i^1, ..., p_i^K]^T \in \mathcal{P}_i \qquad \forall i \tag{6.94}$$

Constraints (6.82)-(6.86) must be satisfied by default, as they also depend only on complicating variables, and thus could be dropped here. Same as for the RMP, this primal problem has a constant utility, which depends only on complicating variables, and thus is a feasibility problem in itself. Note that here, the variables $\tilde{\gamma}_i^{(k)}$ play the role of the w_i in the GBD-RMP. Applying the concept of GBD and the properties derived in the previous sections for the RMP, a general feasibility problem of the form GBD-F (6.55)-(6.59) in Section 6.4.3 can be generated, by minimizing the sum-norm $\|\boldsymbol{c}\|_1$ of a non-negative vector $\boldsymbol{c}$. By the same arguments of Section 6.4.3, the feasibility problem is optimally solved by the FM-PCA and yields constraint functions of the form:

$$\begin{aligned} \xi_w^{(l)}(\boldsymbol{x}_i) &= \sum_{i\in\mathcal{L}} \left(\frac{\gamma_{t,i}^{(l)}}{\Gamma_i(\boldsymbol{p}^{(l)})} - 1 \right) + \sum_{i=1}^{L} \frac{\gamma_{t,i}^{(l)}}{\Gamma_i(\boldsymbol{p}^{(l)})} \cdot \tilde{\boldsymbol{\gamma}}_t^T \left(\boldsymbol{x}_i - \boldsymbol{x}_i^{(l)} \right), \\ &= \rho^{(l)} + \sum_{i=1}^{L} m_i^{(l)} \cdot \tilde{\boldsymbol{\gamma}}_t^T \left(\boldsymbol{x}_i - \boldsymbol{x}_i^{(l)} \right), \\ \text{where} \qquad & m_i^{(l)} = \frac{\gamma_{t,i}^{(l)}}{\Gamma_i(\boldsymbol{p}^{(l)})}; \qquad \rho^{(l)} = \sum_{i\in\mathcal{L}} \left(m_i^{(l)} - 1 \right). \end{aligned}$$

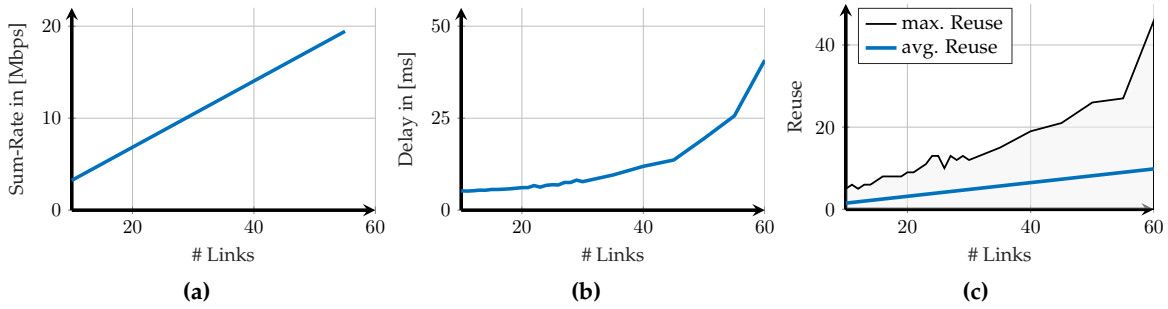

Figure 6.10: Simulation Results for a sum-rate maximization problem with SC-FDMA links and arbitrary interference constellations.

Note that the constraint function does not depend on the used PRB itself but rather on the channel that the PRB resides on. Due to this, all PRBs on the same channel generate constraints to approximate the same feasible SINR-region, $\mathcal{F}_{\tilde{\gamma}}^{(w)}$.

The application of GBD infers the same communication structure as the one developed for the RMP: A central coordinator (CC) solves instances of the master problem, which is the general utility maximization problem D2D-NUM without constraints (6.88)-(6.89), and decides the next schedule, which consists of MCS assigned on each PRB to each link with possible, mutual interference. For each decided schedule, the links identify the related SINR targets and run FM-PCAs independently on every PRB. Here, one iteration of the PCA can take one LTE frame or one TTI. After K iterations, the resulting SINRs on all PRBs are reported to the CC, which adds one constraint of the form $\xi_w^{(l)}(\boldsymbol{x}_i^{(k)}) \leq 0$ per time slot to the master problem. This algorithmic structure in fact corresponds to the $\tilde{\varepsilon}$-PP algorithm from Section 6.4 applied to the D2D-NUM.

Simulation Results

To prove the validity of the proposed structure, the simulation results of the RMP are extended to the D2D-NUM problem for a sum-rate utility. It can be shown that for this utility, the optimal solution for an LTE frame is that of a single time-slot, repeated in all slots. It thus makes sense to create the corresponding solutions in a TTI basis of a single slot with 1 ms duration, rather than per frame of 10 ms duration.

For simulation, six frequency channels of 180 kHz width were considered that were placed with center frequencies of 2 GHz and larger, and a slot-length of 1 ms. A fixed number of links are distributed on a spatial area of $500\text{m} \times 500\text{m}$, with the BS at the center and a maximum D2D distance of 25 m. For each channel, an independent realization according to the channel model was generated, i.e., without correlation among channels for the fading parameters. On each channel, SINR targets and their achievable rates per slot were modeled, which were derived according to [95], corresponding to Figure 2.15. The maximum transmission powers were assumed as 26 dBm. The BS was assumed to solve the master problem. Between two schedules, the FM-PCA was run for 5 iterations, generating a new constraint. Each data point was averaged over 1000 different, random samples of device distributions

and channels.

The results are shown in Figure 6.10. While the delay analysis shows again the exponential increase in delay, and thus directly reflects the exponential worst-case complexity of the underlying algorithms, it is in an acceptable delay range for the considered numbers of links. It can be seen that the achievable system sum-rate increases with the number of links. Further, the average reuse over all six channels, shown in 6.10c, indicates that channels are on average reused up to 10 times, which indeed is an order of magnitude larger than the often targeted one- or two-fold reuse. Considering the maximum reuse over all 1000 system realizations, which is shown in black, the magnitude increases even beyond 40-fold frequency reuse within a cell.

Note that typically, increase in reuse seems to be linear at first but then saturates for larger device densities. As this saturation is not observed in the figures yet, it must be assumed that even larger reuse numbers would be possible. However, the master problem does not scale well with link numbers in the used, general purpose solver, which is the reason that not more links were included. In general, more effort is required to provide scalable, yet well-performing algorithms to solve the master problem.

6.6 Lessons Learned

The results of the chapter can be captured in a few lessons learned. Interference management in D2D systems encounters the same, fundamental challenges as in any other, wireless system, which is the complex, non-linear coupling of different links. Further, the structure of D2D communication demands for a distributed, or at least semi-distributed solution.

As first task, the feasibility of reuse with given SINR targets was investigated. In contrast to existing works, which mainly focused on decentralized estimation, some parts of feasibility estimation could be offloaded to the base station, which greatly increased convergence time and accuracy of produced results.

For general interference management, the RMP was investigated as exemplary, core problem set-up. A semi-distributed communication structure was derived, which resulted from an application of the Generalized Benders Decomposition. Due to the generalizability of the RMP, it can be considered as prototypical structure for arbitrary semi-distributed interference management. In this structure, SINR targets are assigned as result of an optimization which is performed on a powerful machine in the fixed network. Using these targets, all devices adapt their powers according to the FM-PCA. The outcome can then be used to approximate the feasible SINR-region, in logarithmic domain. The information on the feasible SINR region can be used to derive new targets, according to an arbitrary utility metric, which in turn are used to further approximate the SINR region. The optimization structure faces the fundamental limit that apparently, the effect of entirely shutting down a link on the spectral radius of the relative gain matrix can only be bounded with trivial bounds. To circumvent this, it was proposed to perform an SINR-back-off instead. This back-off realizes an algorithmic approximation that can, in principle, become arbitrarily accurate. However, with increased accuracy it also induces exponential worst-case complexity.

Chapter 7

Conclusion and Outlook

In this thesis, the impact of introducing Device-to-Device communication in cellular networks was investigated and ways to correctly manage D2D links were explored.

The potential spatial densities of D2D links were investigated and scaling laws were derived. It could be shown that in general, the spatial density of direct links depends on the considered application types, which were grouped into the four service classes one-to-one, one-serves-all, all-serve-one and full-mesh. It was shown that the potential densities of direct links are largest for full-mesh type services, which can scale quadratic with device densities, followed by one-serves-all and all-serve-one, which have linear increase. The exact scaling parameters depend on the service penetration among UEs, i.e., their probability to offer or demand a D2D service, and the interplay of device pairing and mode selection. For the latter, the gained intuition is that for each mode selection scheme, a D2D service area around each device can be imagined, containing all spatial points where another device needs to be located to have a non-zero offloading probability. The number of direct links scale stronger with increased ability of the pairing step to identify devices within their mutual service area. Two simple pairing strategies were identified to provide strong scaling for large device densities, the random pairing and the nearest pairing strategy.

Potentials of D2D communication to create an overall, "better" network state were evaluated. It was argued that there exists a mismatch among the commonly employed network management for utility maximization and the concurrently claimed D2D-gains of proximity-gain, hop- and reuse-gain. Further, it was shown that the D2D-gains can consistently be captured with a throughput-resource efficiency metric. This efficiency metric was investigated in detail: Fundamental properties were established and a method to schedule links in a resource efficient manner was proposed. It was shown that only when there exist links with elastic traffic demands, the D2D-gains are actually leveraged by utility maximization. As counter-example, for links with constant bit-rate demands, utility maximization might fail to leverage the gains properly.

The insights were used to develop two mode selection schemes. The first is based on resource efficiency and optimizes a lower efficiency bound. The second is based on utility maximization. It can be claimed to be utility-optimal, provided that it is possible to solve the underlying utility maximization problem optimally.

Finally, the operation of D2D links was investigated, with focus on interference management. Two methods to quickly identify the feasibility of frequency reuse for a given link set were proposed. Then, the RMP was investigated in detail, which aims at maximizing the number of active links on a single channel. Two approaches were considered, one based on a combination of set theory and power control theory and the other based on mixed-integer optimization. The set-based approach outperforms the known state of research but requires fully centralized implementation. With the optimization based approach, the number of active links can be increased even further, while enabling a semi-decentralized implementation. The resulting structure consists of a power control step, where all links aim at adapting their powers to SINR targets with known, decentralized power control algorithms, and an optimization step that uses the outcome of the power control algorithms to adapt the SINR targets in a purely combinatorial fashion. A fundamental limit of both approaches seems to be that both, binary activation and deactivation of links creates unpredictable effects on the interference situation, that can only be bounded with trivial bounds and thus keep the search space very large. The results of the optimization based approach were generalized to more general resource allocation for utility maximization. It could be demonstrated that the same communication structure can serve to solve a larger class of network management problems.

7.1 Open Aspects

Several aspects could not be investigated to full satisfaction in this thesis or emerge as interesting follow-up topics, which are briefly discussed here.

The resource efficiency discussion and application to D2D-gain open a new perspective on network operation that goes beyond traditional utility maximization. In particular, it can be argued that for special cases, such as constant bit-rate traffic, utility maximization might not lead to a desirable network state, as it mostly neglects the resource usage required to transport traffic. On the other hand, the resource efficiency metric does capture this aspect. While the fundamental basis of resource efficiency was laid in this thesis, a satisfactory implementation for resource efficient scheduling could not be developed. Such a scheduling type would target the reduction of resource usage under utility constraints.

As for mode selection, while a utility-optimal strategy could be proposed in this thesis, it was not fully tested beyond analytic proof. Convergence properties thus are not yet established. Further, different implementation structures can be imaged, using the same algorithmic structure of optimization decomposition. While the decomposition can be done on rate basis, as was proposed in this thesis, it can just as well be an approximation that lower bounds the achieved utility itself at each link. This slightly changes the implementation, because not rate targets are set at the Central Coordinator but rather utility targets, while the exact realization of these targets need to be established by the links in a decentralized manner. Benefits and drawbacks of this alternative approach is an open research aspect. Also, decentralization of the master problem and the impact of dynamic change of channels was not investigated.

Further, an optimal mode selection allows the establishment of fundamental properties

for D2D links, which were out of scope of this thesis. One such property is the limited spatial range of direct links. While this property is commonly assumed to hold, investigations performed in context of this thesis indicate the achievable distance to be generally underestimated. With a utility-optimal mode selection, the typical communication range under which direct links are beneficial can be assessed by simply observing the outcome over different scenarios. Further, in literature there is an indirect assumption that D2D networks consist of one-hop links only. However, this property has not been questioned to the best of the authors' knowledge. If multi-hop D2D would prove to be beneficial, the aspect of routing in D2D networks needed to be evaluated, which is almost completely neglected in literature. In fact, first investigations performed in a masters thesis indicate the single-hop property to be true for the resource efficiency metric, except for the special case of range extension. By employing an optimal mode selection scheme, these results can be further extended.

Finally, the introduced, basic interference management structure can be extended to a variety of use-cases, including D2D-multicast and OFDM-based D2D. For many of the possible use-cases, the master problem must be expected to be hard to solve. Then fast, well-defined approximations become necessary but are yet unknown. Further, some fundamental aspects of real-world implementations have been abstracted away in this thesis for better tractability. First, the channels are assumed to be constant during the convergence time of the interference management. In reality, at some point in time the channels will change, rendering some created bounds outdated. The exact assessment on how to deal with channel variations in approximating the SINR-region is open. Second, the presented approach encounters scalability issues for large numbers of links, due to the NP-completeness of the underlying problem structure. In future cellular networks, device densities are assumed to create interference couplings that might span several cells, creating problems with very large optimization space. For these, good ways for decomposing the SINR-region approximations need to be found, which also is an open topic.

Appendix A

Mathematical Notations

In this thesis, the mathematical notations use the following nomenclature:

An upper case, calligraphic letter $\mathcal{A}$ denotes a set, which is explicitly enumerated within braces of the form $\mathcal{A} = \{...\}$. Exceptions are sets of matrices, which are written upper case and bold $\boldsymbol{S}$, and mathematical number sets such as the set of real numbers $\mathbb{R}$ or integer numbers $\mathbb{N}$. Restrictions of number sets to their non-negative orthant are expressed with a subscript plus, i.e., the set $\mathbb{R}_+$ is the set of non-negative, real numbers. The convex hull of a set is given by $\text{Conv}\{\mathcal{A}\}$ and the projection onto $\mathcal{A}$ with respect ot the euclidean norm by $[\cdot]^{\mathcal{A}}$. Consequently, the projection onto positive number space is given by $[\cdot]^+ = \max\{\cdot, 0\}$.

Column vectors are written as lower-case and bold letters $\boldsymbol{v}$, whereas matrices are upper case and bold $\boldsymbol{V}$. Elements of vectors and matrices are indexed with subscripts of the form v_i or $[v]_i$ and $\boldsymbol{V}_{ij}$ or $[\boldsymbol{V}]_{ij}$, respectively. Transposition is indicated with a superscript $(\cdot)^T$. Any function and relational statement on vectors, such as $e^{\boldsymbol{v}}$, $\max\{\boldsymbol{v}_1, \boldsymbol{v}_2\}$, $\boldsymbol{v}_1 \leq \boldsymbol{v}_2$ is to be interpreted element-wise. Same holds for relational statements on matrices.

Norms are written as $|\cdot|$ for scalars, as $\|\cdot\|$ for vectors to denote an arbitrary norm, or with a subscript that specifies the norm more clearly. Examples of specific norms are the euclidean norm $\|\cdot\|_2$, the sum-norm $\|\cdot\|_1$ or the maximum norm $\|\cdot\|_\infty$. For sets, a norm $\|\mathcal{A}\|$ denotes a mathematical, locally finite and non-null measure that is explained in the context, e.g., the cardinality for discrete set, its area or volume for continuous sets.

Probabilities for events are written as $P\{\cdot\}$, whereas expectations are given as $E\{\cdot\}$. A subscript $E_{\boldsymbol{c}}\{\cdot\}$ denotes the variable with respect to which the expectation is used.

Indicator functions are denoted with $\delta\{\cdot\}$ or $\mathbb{1}\{\cdot\}$, where the part within the curly braces describes the statement that is indicated. The indicator function is one if the statement is true and zero if it is false.

Logical statements are negated with $\neg$ and combined with $\vee$ and $\wedge$, where $\vee$ is the "or" operation and $\wedge$ the "and" operation.

As for control variables, a variable t describes a continuous variable, whereas τ, k or l denotes an integer one. Integer variables are further enclosed by rectangular brackets $[\cdot]$, while continuous variables are enclosed with normal brackets, $(\cdot)$.

Appendix B

The Generalized Benders Decomposition

Here, the basic algorithmic statement of the GBD will be introduced in short. The GBD is a decomposition approach that has initially been developed by J.F. Benders [168] to solve problems with "complicating variables" that, if kept fixed, allowed an easy problem solution. It was extended by A.M. Geoffrion [169] for MINLPs. The introduction here follows the one presented in [160, Chap. 6].

A core idea of the Generalized Benders Decomposition is the notion of *complicating variables*. These are variables which, if fixed, render the remaining problem "easy" by allowing the application of known solutions or standard techniques. By leveraging this, complex problem structures can be decomposed into easier to solve sub-problems. In mixed-integer problems, the integer variables are typically considered as complicating and the decomposition produces an integer problem and a continuous one.

GBD based algorithms use an outer and inner optimization loop. The inner optimization, called *primal problem*, solves the problem with fixed complicating variables, or a feasibility problem if the fixed complicating variables render the problem infeasible. In the outer optimization, called *relaxed master problem*, an approximation of the outer target function and its solution space is generated, based on the solution of the primal problem. The complicating variables are then optimized with respect to this outer optimization.

Both, inner and outer optimization are run alternately with the variables of the other optimization kept fixed. Each solution of the primal problem creates a constraint for the relaxed master problem, thus further re-fining it.

Problem Statement

Consider an optimization problem stated as [160]:

$$\begin{aligned} \min_{\boldsymbol{x},\boldsymbol{y}} \quad & f(\boldsymbol{x},\boldsymbol{y}) \\ \text{s.t.} \quad & \boldsymbol{h}(\boldsymbol{x},\boldsymbol{y}) = \boldsymbol{0}, \\ & \boldsymbol{g}(\boldsymbol{x},\boldsymbol{y}) \leq \boldsymbol{0}, \\ & \boldsymbol{x} \in \mathcal{X} \subseteq \mathbb{R}^n, \\ & \boldsymbol{y} \in \mathcal{Y} \subseteq \{0,1\}^q, \end{aligned} \tag{B.1}$$

where $\boldsymbol{h}(\boldsymbol{x},\boldsymbol{y})$ is an m-dimensional and $\boldsymbol{g}(\boldsymbol{x},\boldsymbol{y})$ a p-dimensional function vector. Assume that the following conditions hold [160]:

C1: $\mathcal{X}$ is a nonempty, convex set and the functions

$$f : \mathbb{R}^n \times \mathbb{R}^q \mapsto \mathbb{R}, \;\; g : \mathbb{R}^n \times \mathbb{R}^q \mapsto \mathbb{R}^p$$

are convex for each fixed $\boldsymbol{y} \in \mathcal{Y}$, while the functions $h : \mathbb{R}^n \times \mathbb{R}^p \mapsto \mathbb{R}^m$ are linear for each fixed $\boldsymbol{y} \in \mathcal{Y}$.

C2: The set $\mathcal{Z}_{\boldsymbol{y}} = \{\boldsymbol{z} \in \mathbb{R}^p : \boldsymbol{h}(\boldsymbol{x},\boldsymbol{y}) = \boldsymbol{0}, \boldsymbol{g}(\boldsymbol{x},\boldsymbol{y}) \leq \boldsymbol{z} \text{ for some } \boldsymbol{x} \in \mathcal{X}\}$ is closed for each fixed $\boldsymbol{z}$.

C3: For each fixed $\boldsymbol{y} \in \mathcal{Y} \cap \mathcal{V}$, where

$$\mathcal{V} = \{\boldsymbol{y} : \boldsymbol{h}(\boldsymbol{x},\boldsymbol{y}) = \boldsymbol{0}, \boldsymbol{g}(\boldsymbol{x},\boldsymbol{y}) \leq \boldsymbol{0} \text{ for some } \boldsymbol{x} \in \mathcal{X}\},$$

one of the two conditions holds:

(i) the resulting problem has a finite solution and has an optimal multiplier vector for the equalities and inequalities

(ii) the resulting problem is unbounded, that is, its objective function value goes to $-\infty$.

Note that $\mathcal{V}$ is the set of $\boldsymbol{y}$ variables for which, if fixed, the remaining problem in $\boldsymbol{x}$ is feasible. It is stressed in [160] that the conditions C1-C3 are not fully stringent for optimality of the GBD, however, they are sufficient.

Projection onto the y-Space

Problem B.1 can be re-written into the form [160]

$$\begin{aligned} \min_{\boldsymbol{y}} \inf_{\boldsymbol{x}} \quad & f(\boldsymbol{x},\boldsymbol{y}) \\ \text{s.t.} \quad & \boldsymbol{h}(\boldsymbol{x},\boldsymbol{y}) = \boldsymbol{0}, \\ & \boldsymbol{g}(\boldsymbol{x},\boldsymbol{y}) \leq \boldsymbol{0}, \\ & \boldsymbol{x} \in \mathcal{X}, \;\; \boldsymbol{y} \in \mathcal{Y}. \end{aligned}$$

Further, define $v(\boldsymbol{y})$ to be

$$\begin{aligned} v(\boldsymbol{y}) \quad &= \quad \inf_{\boldsymbol{x}} f(\boldsymbol{x}, \boldsymbol{y}), \\ \text{s.t.} \quad &\quad \boldsymbol{h}(\boldsymbol{x}, \boldsymbol{y}) = \boldsymbol{0}, \\ &\quad \boldsymbol{g}(\boldsymbol{x}, \boldsymbol{y}) \leq \boldsymbol{0}, \\ &\quad \boldsymbol{x} \in \mathcal{X}. \end{aligned}$$

Then, B.1 corresponds to the problem [160]

$$\min_{\boldsymbol{y}} v(\boldsymbol{y}) \text{ s.t. } \boldsymbol{y} \in \mathcal{Y} \cap \mathcal{V}. \tag{B.2}$$

Problem B.2 is the projection of B.1 onto the $\boldsymbol{y}$-space.

Dual Representation

Due to conditions C1-C3, strong duality holds in $\boldsymbol{x}$ for fixed $\boldsymbol{y}$. This can be leveraged to refine $v(\boldsymbol{y})$ as [160]:

$$\begin{aligned} v(\boldsymbol{y}) \quad &= \quad \inf_{\boldsymbol{x} \in \mathcal{X}} \sup_{\boldsymbol{\lambda} \geq 0, \boldsymbol{\mu} \geq 0} L(\boldsymbol{x}, \boldsymbol{y}, \boldsymbol{\lambda}, \boldsymbol{\mu}) \ \ \forall \boldsymbol{y} \in \mathcal{Y} \cap \mathcal{V} \\ &= \quad \sup_{\boldsymbol{\lambda} \geq 0, \boldsymbol{\mu} \geq 0} \inf_{\boldsymbol{x} \in \mathcal{X}} L(\boldsymbol{x}, \boldsymbol{y}, \boldsymbol{\lambda}, \boldsymbol{\mu}) \ \ \forall \boldsymbol{y} \in \mathcal{Y} \cap \mathcal{V}, \\ \text{where } L(\boldsymbol{x}, \boldsymbol{y}, \boldsymbol{\lambda}, \boldsymbol{\mu}) \quad &= \quad f(\boldsymbol{x}, \boldsymbol{y}) + \boldsymbol{\lambda}^T \boldsymbol{h}(\boldsymbol{x}, \boldsymbol{y}) + \boldsymbol{\mu}^T \boldsymbol{g}(\boldsymbol{x}, \boldsymbol{y}). \end{aligned} \tag{B.3}$$

Note that $L(\boldsymbol{x}, \boldsymbol{y}, \boldsymbol{\lambda}, \boldsymbol{\mu})$ is a Lagrange-function and $\boldsymbol{\lambda}$, $\boldsymbol{\mu}$ are the corresponding multipliers.

In a similar fashion, the set $\mathcal{V}$ can be re-fined. For this, consider a feasibility problem [160]:

$$\begin{aligned} \min_{\boldsymbol{x}, \boldsymbol{c}} \quad &\|\boldsymbol{c}\|, \\ \text{s.t.} \quad &\boldsymbol{h}(\boldsymbol{x}, \boldsymbol{y}) = \boldsymbol{0}, \\ &\boldsymbol{g}(\boldsymbol{x}, \boldsymbol{y}) \leq \boldsymbol{c}, \\ &\boldsymbol{c} \geq 0, \ \ \boldsymbol{x} \in \mathcal{X} \end{aligned} \tag{B.4}$$

for an arbitrary norm $\|\cdot\|$ that can be chosen to be suitable. If the optimal solution to B.4 is the all-zero vector, a feasible solution to B.1 in $\boldsymbol{x}$ has been found for given $\boldsymbol{y}$. If not, it can be concluded that there is no feasible solution and further, the resulting point is closest to feasibility with respect to the chosen norm. Define $\overline{L}(\boldsymbol{x}, \boldsymbol{y}, \boldsymbol{c}, \overline{\boldsymbol{\lambda}}, \overline{\boldsymbol{\mu}})$ to be the Lagrange-function associated with B.4, where $\overline{\boldsymbol{\lambda}}$, $\overline{\boldsymbol{\mu}}$ are the corresponding multipliers. Now, it can be shown [169] that, assuming conditions C1 and C2, a point $\boldsymbol{y} \in \mathcal{Y}$ belongs to the set $\mathcal{V}$ if and only if it satisfies the system:

$$\begin{aligned} &0 \geq \inf_{\boldsymbol{x} \in \mathcal{X}} \overline{L}(\boldsymbol{x}, \boldsymbol{y}, \boldsymbol{0}, \overline{\boldsymbol{\lambda}}, \overline{\boldsymbol{\mu}}), \ \ \forall \overline{\boldsymbol{\lambda}}, \overline{\boldsymbol{\mu}} \in \Lambda, \\ \text{where} \quad &\Lambda = \left\{ \overline{\boldsymbol{\lambda}} \in \mathbb{R}^m, \overline{\boldsymbol{\mu}} \in \mathbb{R}^p : \overline{\boldsymbol{\mu}} \geq \boldsymbol{0}, \sum_{i=1}^{p} \overline{\mu}_i = 1 \right\}. \end{aligned} \tag{B.5}$$

Geometric Interpretation

The preceding formulation has an insightful geometric interpretation. Consider the functions:

$$\begin{aligned}\zeta(\boldsymbol{y}, \boldsymbol{\lambda}, \boldsymbol{\mu}) &= \inf_{\boldsymbol{x}\in\mathcal{X}} L(\boldsymbol{x}, \boldsymbol{y}, \boldsymbol{\lambda}, \boldsymbol{\mu}),\\ \xi(\boldsymbol{y}, \overline{\boldsymbol{\lambda}}, \overline{\boldsymbol{\mu}}) &= \inf_{\boldsymbol{x}\in\mathcal{X}} \overline{L}(\boldsymbol{x}, \boldsymbol{y}, \boldsymbol{0}, \overline{\boldsymbol{\lambda}}, \overline{\boldsymbol{\mu}}).\end{aligned}$$

From B.3 and B.5 it becomes clear that, for any fixed $\boldsymbol{\lambda}^k$, $\boldsymbol{\mu}^k$, $\overline{\boldsymbol{\lambda}}^k$, $\overline{\boldsymbol{\mu}}^k$ [160]:

$$\begin{aligned}v(\boldsymbol{y}) = \sup_{\boldsymbol{\lambda},\boldsymbol{\mu}} \zeta(\boldsymbol{y}, \boldsymbol{\lambda}, \boldsymbol{\mu}) &\geq \zeta(\boldsymbol{y}, \boldsymbol{\lambda}^k, \boldsymbol{\mu}^k) \text{ and}\\ \mathcal{V} &\subseteq \{\boldsymbol{y} : \xi(\boldsymbol{y}, \overline{\boldsymbol{\lambda}}^k, \overline{\boldsymbol{\mu}}^k) \leq 0\}.\end{aligned}$$

That is, the functions $\zeta(\boldsymbol{y}, \boldsymbol{\lambda}, \boldsymbol{\mu})$ with fixed $\boldsymbol{\lambda}$, $\boldsymbol{\mu}$ are support functions of $v(\boldsymbol{y})$, whereas the sub-level sets of the functions $\xi(\boldsymbol{y}, \overline{\boldsymbol{\lambda}}, \overline{\boldsymbol{\mu}})$ with fixed $\overline{\boldsymbol{\lambda}}$, $\overline{\boldsymbol{\mu}}$ form outer approximations of $\mathcal{V}$, respectively.

Algorithmic Statement

The intuition behind a GBD is to leverage this interpretation by running an outer approximation algorithm, using $\zeta(\boldsymbol{y}, \boldsymbol{\lambda}, \boldsymbol{\mu})$ and $\xi(\boldsymbol{y}, \overline{\boldsymbol{\lambda}}, \overline{\boldsymbol{\mu}})$. For each approximation, the complicating variables $\boldsymbol{y}$ are kept fixed and an optimization over $\boldsymbol{x}$ is performed, yielding optimal multipliers $\boldsymbol{\lambda}$, $\boldsymbol{\mu}$. If the optimization in $\boldsymbol{x}$ turns out to be infeasible a feasibility problem is solved, yielding $\overline{\boldsymbol{\lambda}}$, $\overline{\boldsymbol{\mu}}$, respectively. Using these multipliers, an optimization over $\boldsymbol{y}$ is performed. Formally, define the primal problem for fixed $\hat{\boldsymbol{y}}$ as [160]

$$\begin{aligned}(\mathrm{P}(\hat{\boldsymbol{y}}))\quad \min_{\boldsymbol{x}} \quad & f(\boldsymbol{x}, \hat{\boldsymbol{y}})\\ \text{s.t.} \quad & \boldsymbol{h}(\boldsymbol{x}, \hat{\boldsymbol{y}}) = \boldsymbol{0},\\ & \boldsymbol{g}(\boldsymbol{x}, \hat{\boldsymbol{y}}) \leq \boldsymbol{0},\\ & \boldsymbol{x} \in \mathcal{X},\end{aligned} \tag{B.6}$$

and the feasibility problem as B.4 for fixed $\boldsymbol{y} = \hat{\boldsymbol{y}}$. Let $k \in \mathbb{N}$, $k \geq 1$ be an index counting $\boldsymbol{y}$ set to a feasible value and $l \in \mathbb{N}$, $l \geq 1$ be an index counting the infeasible values of $\boldsymbol{y}$. Then the master problem is [160]:

$$\begin{aligned}(\mathrm{M})\quad \min_{\mu_B, \boldsymbol{y}\in\mathcal{Y}} \quad & \mu_B\\ \text{s.t.} \quad & \mu_B \geq \zeta(\boldsymbol{y}, \boldsymbol{\lambda}^k, \boldsymbol{\mu}^k)\ \ \forall k,\\ & 0 \geq \xi(\boldsymbol{y}, \overline{\boldsymbol{\lambda}}^l, \overline{\boldsymbol{\mu}}^l)\ \ \forall l.\end{aligned} \tag{B.7}$$

The algorithmic statement of the GBD, as given in [160], is as follows:

Step 1: Let an initial point $\hat{\boldsymbol{y}} \in \mathcal{Y} \cap \mathcal{V}$ (i.e., by fixing $\boldsymbol{y} = \hat{\boldsymbol{y}}$ the primal problem is feasible). Solve the resulting primal problem P($\hat{\boldsymbol{y}}$) and obtain an optimal solution $\hat{\boldsymbol{x}}$ and optimal multipliers $\hat{\boldsymbol{\lambda}}$, $\hat{\boldsymbol{\mu}}$. Add constraint $\mu_B \geq \zeta(\boldsymbol{y}, \hat{\boldsymbol{\lambda}}, \hat{\boldsymbol{\mu}})$ to the master problem. Initialize an upper bound as $U = v(\hat{\boldsymbol{y}})$, a lower bound as $L = -\infty$ and fix an accuracy parameter $\varepsilon \geq 0$.

Step 2: Solve the master problem (M), yielding $(\hat{\boldsymbol{y}}, \hat{\mu}_B)$. Obtain a lower bound $L = \max\{L, \hat{\mu}_B\}$. If $U - L \leq \varepsilon$, terminate.

Step 3: Solve the primal problem for $\hat{\boldsymbol{y}}$, i.e., P($\hat{\boldsymbol{y}}$).

Step 3a - Feasible Primal: If the primal has $v(\hat{\boldsymbol{y}})$ finite with optimal solution $\hat{\boldsymbol{x}}$ and optimal multipliers $\hat{\boldsymbol{\lambda}}$, $\hat{\boldsymbol{\mu}}$, update upper bound $U := \min\{U, v(\hat{\boldsymbol{y}})\}$ and add a constraint $\mu_B \geq \zeta(\boldsymbol{y}, \hat{\boldsymbol{\lambda}}, \hat{\boldsymbol{\mu}})$ to the master problem.

Step 3b - Infeasible Primal: The primal does not have a feasible solution for $\boldsymbol{y} = \hat{\boldsymbol{y}}$. Solve a feasibility problem to determine optimal multipliers $\overline{\boldsymbol{\lambda}}$, $\overline{\boldsymbol{\mu}}$. Add a constraint of the form $0 \geq \xi(\boldsymbol{y}, \overline{\boldsymbol{\lambda}}, \overline{\boldsymbol{\mu}})$ to the master problem.

Goto Step 2

The convergence of this algorithm is given as follows [160], [169]:

Theorem B.1. If C1, C2, C3 hold and $\mathcal{Y}$ is a discrete set, then the GBD algorithm terminates in a finite number of iterations for any given $\varepsilon > 0$ and even for $\varepsilon = 0$.

Appendix C

Simulation Results for Chapter 5

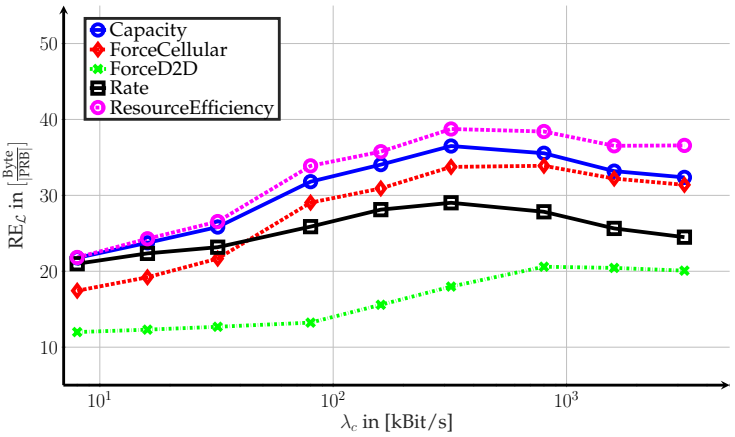

Figure C.1: Input rates versus achieved resource efficiency (Transported Byte per PRB and Cell) for different mode selection schemes, using the Maximum C/I scheduler.

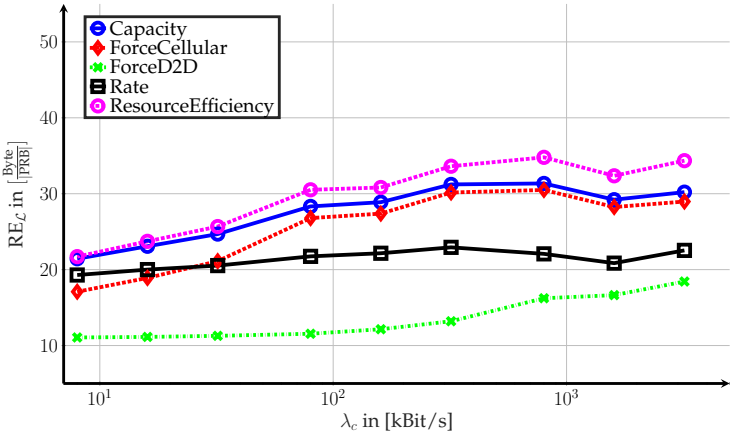

Figure C.2: Input rates versus achieved resource efficiency (Transported Byte per PRB and Cell) for different mode selection schemes, using the Proportional Fair scheduler.

Glossary

AM Acknowledged Mode.
AP Access Point.

BFS brute-force search.
BLER Block Error Rate.
BP Backpressure.
BS Base Station.
BSR Buffer Status Report.

CAC Call Admission Control.
CC Central Coordinator.
CE Control Element.
CM Cellular Mode.
CP Control-Plane.
CQI Channel Quality Indicator.

D2D Device-to-Device.
DCPC Distributed Constrained Power Control.
DFT Discrete Fourier Transformation.
DiffServ differentiated services.
DL Downlink.
DM Direct Mode.
DMT Direct Measurement Test.
DP Data-Plane.

$\tilde{\varepsilon}$-PP $\tilde{\varepsilon}$-Pressure Packing.

FDD Frequency Division Duplex.
FM-PCA Foschini-Miljanic PCA.

GBD Generalized Benders Decomposition.
GSM Global System for Mobile Communications.

HARQ Hybrid Automatic Repeat Request.

IntServ integrated services.
IP Internet Protocol.

KKT Karush-Kuhn-Tucker.

LAN Local Area Network.
LQ Link Quality.
LTE Long Term Evolution.
LTE-U LTE Unlicensed.
LTE-A LTE Advanced.

MAC Medium Access Control.
MCS Modulation and Coding Scheme.
MINLP Mixed-Integer Nonlinear Problem.
MNO Mobile Network Operator.
MS Mobile Station.
MTC Machine-Type Communication.

NLP Nonlinear Problem.
NP Non-Deterministic, Polynomial Time.
NUM Network Utility Maximization.

OFDM Orthogonal Frequency Division Multiplex.
OFDMA Orthogonal Frequency Division Multiple Access.

p.p.p. Poisson Point Process.

PC Power Control.
PCA Power Control Algorithm.
PDCP Packet Data Convergence Protocol.
PDU Packet Data Unit.
PF Proportional Fair.
PHY Physical.
PRB Physical Resource Block.

QAM Quadrature Amplitude Modulation.
QoS Quality of Service.
QPSK Quadrature Phase Shift Keying.

R-RMP Relaxed RMP.
RAP Random Access Procedure.
RLC Radio Link Control.
RM Reuse Mode.
RMP Reuse Maximization Problem.
RQT Rayleigh-Quotient Test.

SBT SI(N)R-Bound Test.
SC-FDMA Single-Channel Frequency Division Multiple Access.
SC-FDM Single-Channel Frequency Division Multiplex.
SINR Signal to Interference and Noise Ratio.
SIR Signal to Interference Ratio.
SL Sidelink.
SMS Short Message Service.
SNR Signal to Noise Ratio.
So2C Sum of 2 Circles.
SoSF Sum of Signal Flows.
SRA Stepwise Removal Algorithm.
SRMP Spectral Radius Minimization Problem.

TBS Transport Block Sizie.
TCP Transmission Control Protocol.
TDD Time Division Duplex.
TDMA Time Division Multiple Access.
TM Transparent Mode.
TTI Transmission Time Interval.

UDP User Datagram Protocol.
UE User Equipment.
UL Uplink.
UM Unacknowledged Mode.
UMTS Universal Mobile Telecommunications System.

WCDMA Wideband Code Division Multiple Access.
WLAN Wireless-LAN.
WPS Worst Pressure Shutdown.

Bibliography

Publications by the author

Journal publications

[1] M. Klügel and W. Kellerer, "Dominant factors for device-to-device occurrence probabilities in cellular networks," *Wireless Networks*, 2017, ISSN: 1572-8196. DOI: 10.1007/s11276-017-1503-4. [Online]. Available: https://doi.org/10.1007/s11276-017-1503-4.

[2] M. Klügel and W. Kellerer, "The device-to-device reuse maximization problem with power control," *IEEE Transactions on Wireless Communications*, 2017. DOI: 10.1109/TWC.2017.2785818.

[3] T. Şahin, M. Klügel, C. Zhou, and W. Kellerer, "Virtual cells for 5g v2x communications," *IEEE Communication Standards Magazine*, 2018.

Conference publications

[4] M. Klügel and W. Kellerer, "Introduction of an efficiency metric for device-to-device communication in cellular networks," in *Vehicular Technology Conference (VTC Fall) 2014*, 2014, pp. 1–6. DOI: 10.1109/VTCFall.2014.6966021.

[5] M. Klugel and W. Kellerer, "Leveraging the d2d-gain: Resource efficiency based mode selection for device-to-device communication," in *2016 IEEE Global Communications Conference (GLOBECOM)*, 2016, pp. 1–7. DOI: 10.1109/GLOCOM.2016.7841953.

[6] M. Klügel and W. Kellerer, "Determining frequency reuse feasibility in device-to-device cellular networks," in *2015 IEEE 26th Annual International Symposium on Personal, Indoor, and Mobile Radio Communications (PIMRC)*, 2015, pp. 1503–1508. DOI: 10.1109/PIMRC.2015.7343536.

[7] M. Klügel, M. He, and W. Kellerer, "Investigation of decision metrics for reuse link selection in device-to-device communication," in *2016 IEEE 27th Annual International Symposium on Personal, Indoor, and Mobile Radio Communications (PIMRC)*, 2016, pp. 1–6. DOI: 10.1109/PIMRC.2016.7794861.

[8] M. Klügel and W. Kellerer, "Poster abstract: Semi-decentralized interference management in d2d-enabled cellular networks," pp. 1–2, 2018. DOI: 10.1109/INFCOMW.2018.8406902.

[9] M. Klügel and W. Kellerer, "On the feasibility of frequency reuse and spatial occupation in wireless device-to-device networks," in *2014 IEEE International Black Sea Conference on Communications and Networking (BlackSeaCom)*, 2014, pp. 154–159. DOI: 10.1109/BlackSeaCom.2014.6849029.

[10] M. Botsov, M. Klügel, W. Kellerer, and P. Fertl, "Location dependent resource allocation for mobile device-to-device communications," in *2014 IEEE Wireless Communications and Networking Conference (WCNC)*, 2014, pp. 1679–1684. DOI: 10.1109/WCNC.2014.6952482.

[11] M. Botsov, M. Klügel, W. Kellerer, and P. Fertl, "Location-based resource allocation for mobile d2d communications in multicell deployments," in *2015 IEEE International Conference on Communication Workshop (ICCW)*, 2015, pp. 2444–2450. DOI: 10.1109/ICCW.2015.7247545.

[12] M. Klügel, M. Newinger, W. Utschick, and W. Kellerer, "The relaxed power control algorithm," in *2017 European Conference on Networks and Communications (EuCNC)*, 2017, pp. 1–6. DOI: 10.1109/EuCNC.2017.7980715.

[13] T. Şahin, M. Klügel, C. Zhou, and W. Kellerer, "Multi-user-centric virtual cell operation for v2x communications in 5g networks," in *2017 IEEE Conference on Standards for Communications and Networking (CSCN)*, 2017, pp. 84–90. DOI: 10.1109/CSCN.2017.8088603.

General publications

[14] *3rd generation partnership project (3GPP) - release 15*, http://www.3gpp.org/release-15, Accessed: Dec. 2017.

[15] *3rd generation partnership project (3GPP) - release 16*, http://www.3gpp.org/release-16, Accessed: Dec. 2017.

[16] *Mobile and wireless communications enablers for twenty-twenty (2020) information society (METIS)*, https://www.metis2020.com/, Accessed: Dec. 2017.

[17] *The 5g infrastructure public private partnership (5G-PPP)*, https://5g-ppp.eu, Accessed: Dec. 2017.

[18] *5g americas*, http://www.5gamericas.org, Accessed: Dec. 2017.

[19] *The fifth generation mobile communications promotion forum (5G-MF)*, http://5gmf.jp, Accessed: Dec. 2017.

[20] *Imt-2020 (5g) promotion group*, http://www.imt-2020.cn, Accessed: Dec. 2017.

[21] ERICSSON, "What is a 5g system," Accessed: Dec. 2017, 2015, [Online]. Available: https://www.ericsson.com/assets/local/news/2015/1/what-is-a-5g-system.pdf.

[22] ERICSSON, "5g systems – enabling the transformation of industry and society," Accessed: Dec. 2017, 2017, [Online]. Available: https://www.ericsson.com/en/publications/white-papers/5g-systems--enabling-the-transformation-of-industry-and-society.

[23] ERICSSON, "5g radio access – capabilities and technologies," Accessed: Dec. 2017, 2016, [Online]. Available: https://www.ericsson.com/en/publications/white-papers/5g-radio-access--capabilities-and-technologies.

[24] Huawei, "5g: A technology vision," Accessed: Dec. 2017, 2013, [Online]. Available: www.huawei.com/ilink/en/download/HW_314849.

[25] Huawei, "5g: New air interface and radio access virtualization," Accessed: Dec. 2017, 2015, [Online]. Available: http://www.huawei.com/minisite/has2015/img/5g_radio_whitepaper.pdf.

[26] Qualcomm, "5g: Vision for the next generation of connectivity," Accessed: Dec. 2017, 2015, [Online]. Available: https://www.qualcomm.com/documents/whitepaper-5g-vision-next-generation-connectivity.

[27] NTT Docomo, "5g radio access: Requirements, concept and technologies," Accessed: Dec. 2017, 2014, [Online]. Available: https://www.nttdocomo.co.jp/english/binary/pdf/corporate/technology/whitepaper_5g/DOCOMO_5G_White_Paper.pdf.

[28] Nokia, "5g masterplan – five keys to create the new communications era," Accessed: Dec. 2017, 2016, [Online]. Available: https://onestore.nokia.com/asset/200316/Nokia_5G_Masterplan_White_Paper_EN.pdf.

[29] K. Doppler, M. Rinne, C. Wijting, C. Ribeiro, and K. Hugl, "Device-to-device communication as an underlay to lte-advanced networks," *IEEE Communications Magazine*, vol. 47, no. 12, pp. 42–49, 2009, ISSN: 0163-6804. DOI: 10.1109/MCOM.2009.5350367.

[30] G. Fodor, E. Dahlman, G. Mildh, S. Parkvall, N. Reider, G. Miklos, and Z. Turanyi, "Design aspects of network assisted device-to-device communications," *IEEE Communications Magazine*, vol. 50, no. 3, pp. 170–177, 2012, ISSN: 0163-6804. DOI: 10.1109/MCOM.2012.6163598.

[31] 3rd Generation Partnership Project (3GPP), "Tr 36.843 - study on lte device to device proximity services; radio aspects," Tech. Rep., 2014.

[32] Y. Shinpei, H. Harada, S. Nagata, and Q. Zhao, "D2d communications in lte-advanced release 12," *NTT Docomo Technical Journal*, vol. 17, no. 2, pp. 1–9, 2015. [Online]. Available: https://www.nttdocomo.co.jp/english/binary/pdf/corporate/technology/rd/technical_journal/bn/vol17_2/vol17_2_009en.pdf.

[33] Qualcomm and Signals Research Group, "Expanding your horizons with lte direct enabling the next generation of," 2015, [Online]. Available: https://www.qualcomm.com/documents/srg-whitepaper-expanding-your-horizons-lte-direct.

[34] J. Schlienz and A. Roessler, "Device to device communication in lte whitepaper," 2016, [Online]. Available: https://www.rohde-schwarz.com/us/applications/device-to-device-communication-in-lte-application-note_56280-142855.html.

[35] 3rd Generation Partnership Project (3GPP), "Ts 23.303 - proximity-based services (prose); stage 2," 2017, [Online]. Available: https://portal.3gpp.org/desktopmodules/Specifications/SpecificationDetails.aspx?specificationId=840.

[36] *Wi-fi alliance*, https://www.wi-fi.org/, Accessed: Dec. 2017.

[37] *IEEE 802.11 Wireless Local Area Network*, http://www.ieee802.org/11/, Accessed: Dec. 2017.

[38] *Bluetooth*, https://www.bluetooth.com/, Accessed: Dec. 2017.

[39] *IEEE 802.15 Wireless Personal Area Network*, http://www.ieee802.org/15/pub/TG1.html, Accessed: Dec. 2017.

[40] *Wi-Fi Direct*, https://www.wi-fi.org/discover-wi-fi/wi-fi-directl, Accessed: Dec. 2017.

[41] H. Ishii, Y. Kishiyama, and H. Takahashi, "A novel architecture for lte-b: C-plane/u-plane split and phantom cell concept," in *2012 IEEE GLOBECOM Workshops (GC Wkshps)*, 2012, pp. 624–630. DOI: 10.1109/GLOCOMW.2012.6477646.

[42] V. Chandrasekhar, J. G. Andrews, and A. Gatherer, "Femtocell networks: A survey," *IEEE Communications Magazine*, vol. 46, no. 9, pp. 59–67, 2008, ISSN: 0163-6804. DOI: 10.1109/MCOM.2008.4623708.

[43] X. Lin, J. G. Andrews, A. Ghosh, and R. Ratasuk, "An overview of 3gpp device-to-device proximity services," *IEEE Communications Magazine*, vol. 52, no. 4, pp. 40–48, 2014, ISSN: 0163-6804. DOI: 10.1109/MCOM.2014.6807945.

[44] A. Asadi, Q. Wang, and V. Mancuso, "A survey on device-to-device communication in cellular networks," *IEEE Communications Surveys Tutorials*, vol. 16, no. 4, pp. 1801–1819, 2014, ISSN: 1553-877X. DOI: 10.1109/COMST.2014.2319555.

[45] T. Adachi and M. Nakagawa, "Battery consumption and handoff examination of a cellular ad-hoc united communication system for operational mobile robots," in *1998. The Ninth IEEE International Symposium on Personal, Indoor and Mobile Radio Communication*, vol. 3, 1998, 1193–1197 vol.3. DOI: 10.1109/PIMRC.1998.731367.

[46] Y.-D. Lin and Y.-C. Hsu, "Multihop cellular: A new architecture for wireless communications," in *Proceedings IEEE INFOCOM 2000. Conference on Computer Communications. Nineteenth Annual Joint Conference of the IEEE Computer and Communications Societies (Cat. No.00CH37064)*, vol. 3, 2000, 1273–1282 vol.3. DOI: 10.1109/INFCOM.2000.832516.

[47] O. Dousse, P. Thiran, and M. Hasler, "Connectivity in ad-hoc and hybrid networks," in *IEEE INFOCOM 2002. Proceedings.*, vol. 2, 2002, 1079–1088 vol.2. DOI: 10.1109/INFCOM.2002.1019356.

[48] H. Luo, R. Ramjee, P. Sinha, L. E. Li, and S. Lu, "Ucan: A unified cellular and ad-hoc network architecture," in *Proceedings of the 9th Annual International Conference on Mobile Computing and Networking*, ser. MobiCom '03, San Diego, CA, USA: ACM, 2003, pp. 353–367, ISBN: 1-58113-753-2. DOI: 10.1145/938985.939021. [Online]. Available: http://doi.acm.org/10.1145/938985.939021.

[49] P. Mach, Z. Becvar, and T. Vanek, "In-band device-to-device communication in ofdma cellular networks: A survey and challenges," *IEEE Communications Surveys Tutorials*, vol. 17, no. 4, pp. 1885–1922, 2015, ISSN: 1553-877X. DOI: 10.1109/COMST.2015.2447036.

[50] F. Baccelli and B. Błaszczyszyn, "Stochastic geometry and wireless networks: Volume i theory," *Foundations and Trends® in Networking*, vol. 3, no. 3–4, pp. 249–449, 2008, ISSN: 1554-057X. DOI: 10.1561/1300000006. [Online]. Available: http://dx.doi.org/10.1561/1300000006.

[51] W. Lu and M. Di Renzo, "Stochastic geometry modeling of cellular networks: Analysis, simulation and experimental validation," in *Proceedings of the 18th ACM International Conference on Modeling, Analysis and Simulation of Wireless and Mobile Systems*, ser. MSWiM '15, Cancun, Mexico: ACM, 2015, pp. 179–188, ISBN: 978-1-4503-3762-5. DOI: 10.1145/2811587.2811597. [Online]. Available: http://doi.acm.org/10.1145/2811587.2811597.

[52] J. G. Andrews, F. Baccelli, and R. K. Ganti, "A tractable approach to coverage and rate in cellular networks," *IEEE Transactions on Communications*, vol. 59, no. 11, pp. 3122–3134, 2011, ISSN: 0090-6778. DOI: 10.1109/TCOMM.2011.100411.100541.

[53] J. Zander, "Performance of optimum transmitter power control in cellular radio systems," *IEEE Transactions on Vehicular Technology*, vol. 41, no. 1, pp. 57–62, 1992, ISSN: 0018-9545. DOI: 10.1109/25.120145.

[54] G. Foschini and Z. Miljanic, "A simple distributed autonomous power control algorithm and its convergence," *IEEE Transactions on Vehicular Technology*, vol. 42, no. 4, pp. 641–646, 1993, ISSN: 0018-9545. DOI: 10.1109/25.260747.

[55] T. L. Mung Chiang Prashanth Hande and C. W. Tan, "Power control in wireless cellular networks," *Foundations and Trends® in Networking*, vol. 2, no. 4, pp. 381–533, 2007.

[56] P. Hande, S. Rangan, M. Chiang, and X. Wu, "Distributed uplink power control for optimal sir assignment in cellular data networks," *IEEE/ACM Transactions on Networking*, vol. 16, no. 6, pp. 1420–1433, 2008, ISSN: 1063-6692. DOI: 10.1109/TNET.2008.918070.

[57] S. Stanczak, M. Wiczanowski, and H. Boche, *Fundamentals of Resource Allocation in Wireless Networks: Theory and Algorithms*, 2nd. Springer Publishing Company, Incorporated, 2009, ISBN: 3540793852, 9783540793854.

[58] E. Karamad, R. S. Adve, and J. Chow, "Scalable and efficient power control algorithms for wireless networks," *IEEE Transactions on Signal Processing*, vol. 62, no. 8, pp. 2028–2041, 2014, ISSN: 1053-587X. DOI: 10.1109/TSP.2014.2305643.

[59] S. Sesia, I. Toufik, and M. Baker, *LTE, The UMTS Long Term Evolution: From Theory to Practice*. Wiley Publishing, 2009, ISBN: 0470697164, 9780470697160.

[60] P. Kyösti, J. Meinilä, L. Hentilä, *et al.*, "WINNER II Channel Models," WINNER IST, TR IST-4-027756 WINNER II D1.1.2 V1.1, Sep. 2007. [Online]. Available: https://cept.org/files/8339/winner2-finalreport.pdf.

[61] "Guidelines for evaluation of radio interface technologies for IMT-Advanced," ITU, Report ITU-R M.2135-1, Dec. 2009. [Online]. Available: https://www.itu.int/dms_pub/itu-r/opb/rep/R-REP-M.2135-1-2009-PDF-E.pdf.

[62] A. Osseiran, F. Boccardi, V. Braun, K. Kusume, P. Marsch, M. Maternia, O. Queseth, M. Schellmann, H. D. Schotten, T. Hidekazu, H. M. Tullberg, M. A. Uusitalo, B. Timus, and M. Fallgren, "Scenarios for 5g mobile and wireless communications: The vision of the METIS project," *IEEE Communications Magazine*, vol. 52, no. 5, pp. 26–35, 2014. DOI: 10.1109/MCOM.2014.6815890. [Online]. Available: http://dx.doi.org/10.1109/MCOM.2014.6815890.

[63] "METIS Channel Models," METIS, Report ICT-317669-METIS/D1.4, Sep. 2015. [Online]. Available: https://www.metis2020.com/wp-content/uploads/METIS_D1.4_v3.pdf.

[64] C. E. Shannon, "Communication in the presence of noise," *Proc. Institute of Radio Engineers*, vol. 37, no. 1, pp. 10–21, 1949.

[65] Q. Wu, "Optimum transmitter power control in cellular systems with heterogeneous SIR thresholds," *IEEE Transactions on Vehicular Technology*, vol. 49, no. 4, pp. 1424–1429, 2000, ISSN: 00189545. DOI: 10.1109/25.875275. [Online]. Available: http://ieeexplore.ieee.org/lpdocs/epic03/wrapper.htm?arnumber=875275.

[66] Y. Cui and S. V. Hanly, "Distributed optimal power and rate control in single-hop wireless interference networks," *Conference Record - Asilomar Conference on Signals, Systems and Computers*, pp. 1407–1411, 2012, ISSN: 10586393. DOI: 10.1109/ACSSC.2012.6489257.

[67] S. A. Grandhi and J. Zander, "Constrained power control in cellular radio systems," in *Vehicular Technology Conference, 1994 IEEE 44th*, 1994, 824–828 vol.2. DOI: 10.1109/VETEC.1994.345205.

[68] R. D. Yates, "A framework for uplink power control in cellular radio systems," *IEEE Journal on Selected Areas in Communications*, vol. 13, no. 7, pp. 1341–1347, 1995, ISSN: 0733-8716. DOI: 10.1109/49.414651.

[69] N. Bambos, S. Chen, and G. Pottie, "Channel access algorithms with active link protection for wireless communication networks with power control," *IEEE/ACM Transactions on Networking*, vol. 8, no. 5, pp. 583–597, 2000, ISSN: 1063-6692. DOI: 10.1109/90.879345.

[70] J. D. Herdtner and E. K. P. Chong, "Analysis of a class of distributed asynchronous power control algorithms for cellular wireless systems," *IEEE JSAC*, vol. 18, no. 3, pp. 436–446, 2000, ISSN: 0733-8716. DOI: 10.1109/49.840202.

[71] Q. Wu, "Optimum transmitter power control in cellular systems with heterogeneous sir thresholds," *IEEE Transactions on Vehicular Technology*, vol. 49, no. 4, pp. 1424–1429, 2000, ISSN: 0018-9545. DOI: 10.1109/25.875275.

[72] D. Kim, "On the convergence of fixed-step power control algorithms with binary feedback for mobile communication systems," *IEEE Transactions on Communications*, vol. 49, no. 2, pp. 249–252, 2001, ISSN: 0090-6778. DOI: 10.1109/26.905878.

[73] C. W. Sung, "Log-convexity property of the feasible sir region in power-controlled cellular systems," *IEEE Communications Letters*, vol. 6, no. 6, pp. 248–249, 2002, ISSN: 1089-7798. DOI: 10.1109/LCOMM.2002.1010870.

[74] A. Feiten and R. Mathar, "Optimal power control for multiuser cdma channels," in *International Symposium on Information Theory*, 2005, pp. 1903–1907. DOI: 10.1109/ISIT.2005.1523676.

[75] C. W. Tan, D. P. Palomar, and M. Chiang, "Exploiting hidden convexity for flexible and robust resource allocation in cellular networks," in *Proceedings IEEE INFOCOM 2007 - 26th IEEE International Conference on Computer Communications*, 2007, pp. 964–972. DOI: 10.1109/INFCOM.2007.117.

[76] R. D. Yates and C.-Y. Huang, "Integrated power control and base station assignment," *IEEE Trans. Veh. Technol.*, vol. 44, no. 3, pp. 638–644, 1995, ISSN: 0018-9545. DOI: 10.1109/25.406632.

[77] A. Berman and R. Plemmons, *Nonnegative Matrices in the Mathematical Sciences*. Society for Industrial and Applied Mathematics, 1994.

[78] N. Bambos, S. Chen, and D. Mitra, "Channel probing for distributed access control in wireless communication networks," in *1995 IEEE Global Communications Conference (GLOBECOM)*, vol. 1, 1995, 322–326 vol.1. DOI: 10.1109/GLOCOM.1995.500374.

[79] J. Gentle, *Matrix Algebra: Theory, Computations, and Applications in Statistics*, ser. Springer Texts in Statistics. Springer, 2007, ISBN: 9780387708720. [Online]. Available: https://books.google.de/books?id=Pbz3D7Tg5eoC.

[80] F. Rashid-Farrokhi, K. Liu, and L. Tassiulas, "Downlink power control and base station assignment," *IEEE Communications Letters*, vol. 1, no. 4, pp. 102–104, 1997, ISSN: 1089-7798. DOI: 10.1109/4234.602597. [Online]. Available: http://ieeexplore.ieee.org/lpdocs/epic03/wrapper.htm?arnumber=602597.

[81] T. Holliday, A. Goldsmith, P. Glynn, and N. Bambos, "Distributed power and admission control for time varying wireless networks," in *IEEE Global Telecommunications Conference, 2004. GLOBECOM '04.*, vol. 2, IEEE, 2004, pp. 768–774, ISBN: 0-7803-8794-5. DOI: 10.1109/GLOCOM.2004.1378064. [Online]. Available: http://ieeexplore.ieee.org/document/1378064/.

[82] S. Stanczak and H. Boche, "The infeasible sir region is not a convex set," *IEEE Transactions on Communications*, vol. 54, no. 11, pp. 1905–1907, 2006, ISSN: 0090-6778. DOI: 10.1109/TCOMM.2006.884808. [Online]. Available: http://ieeexplore.ieee.org/lpdocs/epic03/wrapper.htm?arnumber=4012511.

[83] L. Georgiadis, M. J. Neely, and L. Tassiulas, "Resource allocation and cross-layer control in wireless networks," *Foundations and Trends® in Networking*, vol. 1, no. 1, pp. 1–144, 2006, ISSN: 1554-057X. DOI: 10.1561/1300000001. [Online]. Available: http://dx.doi.org/10.1561/1300000001.

[84] G. Scutari, D. P. Palomar, and S. Barbarossa, "Optimal Linear Precoding Strategies for Wideband Non-Cooperative Systems Based on Game Theory – Part II: Algorithms," *IEEE Transactions on Signal Processing*, vol. 56, no. 3, pp. 1250–1267, 2008, ISSN: 1053-587X. DOI: 10.1109/TSP.2007.907808.

[85] X. Lin, N. B. Shroff, and R. Srikant, "A tutorial on cross-layer optimization in wireless networks," *IEEE Journal on Selected Areas in Communications*, vol. 24, no. 8, pp. 1452–1463, 2006, ISSN: 0733-8716. DOI: 10.1109/JSAC.2006.879351.

[86] P. Gupta and P. Kumar, "The capacity of wireless networks," *IEEE Transactions on Information Theory*, vol. 46, no. 2, pp. 388–404, 2000, ISSN: 0018-9448. DOI: 10.1109/18.825799.

[87] A. Jalali, R. Padovani, and R. Pankaj, "Data throughput of cdma-hdr a high efficiency-high data rate personal communication wireless system," in *IEEE Vehicular Technology Conference (VTC Spring) 2000*, vol. 3, 2000, 1854–1858 vol.3. DOI: 10.1109/VETECS.2000.851593.

[88] R. Knopp and P. A. Humblet, "Information capacity and power control in single-cell multiuser communications," in *1995 IEEE International Conference on Communications (ICC)*, vol. 1, 1995, 331–335 vol.1. DOI: 10.1109/ICC.1995.525188.

[89] U. Küchler, *Maßtheorie für Statistiker*. Berlin, Heidelberg: Springer Berlin Heidelberg, 2016, ISBN: 978-3-662-46374-1. DOI: 10.1007/978-3-662-46375-8. [Online]. Available: http://link.springer.com/10.1007/978-3-662-46375-8.

[90] A. Moraleda-Soler, B. Coll-Perales, and J. Gozalvez, "Link-aware opportunistic d2d communications: Open source test-bed and experimental insights into their energy, capacity and qos benefits," in *2014 11th International Symposium on Wireless Communications Systems (ISWCS)*, 2014, pp. 606–610. DOI: 10.1109/ISWCS.2014.6933425.

[91] V. K. Singh, H. Chawla, and V. A. Bohara, "A proof-of-concept device-to-device communication testbed," *CoRR*, vol. abs/1601.01398, 2016. arXiv: 1601.01398. [Online]. Available: http://arxiv.org/abs/1601.01398.

[92] 3rd Generation Partnership Project (3GPP), "Tr 23.803 - feasibility study for proximity services (prose)," 2013, [Online]. Available: https://portal.3gpp.org/desktopmodules/Specifications/SpecificationDetails.aspx?specificationId=653.

[93] *3rd generation partnership project (3GPP) - release 14*, http://www.3gpp.org/release-14, Accessed: Dec. 2017.

[94] 3rd Generation Partnership Project (3GPP), "Evolved Universal Terrestrial Radio Access (E-UTRA); Physical layer procedures," ETSI, TR 136.213, May 2016. [Online]. Available: http://www.etsi.org/deliver/etsi_ts/136200_136299/136213/13.00.00_60/ts_136213v130000p.pdf.

[95] 3rd Generation Partnership Project (3GPP), "Evolved universal terrestrial radio access (e-utra); radio frequency (rf) system scenarios," 3rd Generation Partnership Project (3GPP), TR 36.942, 2012. [Online]. Available: https://portal.3gpp.org/desktopmodules/Specifications/SpecificationDetails.aspx?specificationId=2592.

[96] *Matrix laboratory (matlab)*, https://mathworks.com/products/matlab.html, Accessed: Dec. 2017.

[97] A. Virdis, G. Stea, and G. Nardini, "Simulte - a modular system-level simulator for lte/lte-a networks based on omnet++," pp. 59–70, 2014. DOI: 10.5220/0005040000590070.

[98] A. Varga and R. Hornig, "An overview of the omnet++ simulation environment," in *Proceedings of the 1st international conference on Simulation tools and techniques for communications, networks and systems & workshops*, ICST (Institute for Computer Sciences, Social-Informatics and Telecommunications Engineering), 2008, p. 60.

[99] 3rd Generation Partnership Project (3GPP), "TS 136.322; LTE E-UTRA: Radio Link Control (RLC) protocol specification," 2015, [Online]. Available: https://portal.3gpp.org/desktopmodules/Specifications/SpecificationDetails.aspx?specificationId=2438.

[100] 3rd Generation Partnership Project (3GPP), "TS 136.321; LTE E-UTRA: Medium Access Control (MAC) protocol specification," 2012, [Online]. Available: https://portal.3gpp.org/desktopmodules/Specifications/SpecificationDetails.aspx?specificationId=2437.

[101] 3rd Generation Partnership Project (3GPP), "TS 136.213; LTE E-UTRA: Physical layer procedures," 2016, [Online]. Available: https://portal.3gpp.org/desktopmodules/Specifications/SpecificationDetails.aspx?specificationId=2427.

[102] H. Zhang, Y. Li, D. Jin, M. M. Hassan, A. AlElaiwi, and S. Chen, "Buffer-aided device-to-device communication: Opportunities and challenges," *IEEE Communications Magazine*, vol. 53, no. 12, pp. 67–74, 2015, ISSN: 0163-6804. DOI: 10.1109/MCOM.2015.7355587.

[103] J. Jiang, S. Zhang, B. Li, and B. Li, "Maximized cellular traffic offloading via device-to-device content sharing," *IEEE Journal on Selected Areas in Communications*, vol. 34, no. 1, pp. 82–91, 2016, ISSN: 0733-8716. DOI: 10.1109/JSAC.2015.2452493.

[104] N. Golrezaei, A. Dimakis, and A. Molisch, "Device-to-device collaboration through distributed storage," in *2012 IEEE Global Communications Conference (GLOBECOM)*, 2012, pp. 2397–2402. DOI: 10.1109/GLOCOM.2012.6503475.

[105] H. J. Kang and C. G. Kang, "Mobile device-to-device (d2d) content delivery networking: A design and optimization framework," *Journal of Communications and Networks*, vol. 16, no. 5, pp. 568–577, 2014, ISSN: 1229-2370. DOI: 10.1109/JCN.2014.000095.

[106] Q. Wang, W. Wang, S. Jin, H. Zhu, and N. T. Zhang, "Quality-optimized joint source selection and power control for wireless multimedia d2d communication using stackelberg game," *IEEE Transactions on Vehicular Technology*, vol. 64, no. 8, pp. 3755–3769, 2015, ISSN: 0018-9545. DOI: 10.1109/TVT.2014.2355594.

[107] F. Baccelli, N. Khude, R. Laroia, J. Li, T. Richardson, S. Shakkottai, S. Tavildar, and X. Wu, "On the design of device-to-device autonomous discovery," in *Communication Systems and Networks (COMSNETS), 2012 Fourth International Conference on*, 2012, pp. 1–9. DOI: 10.1109/COMSNETS.2012.6151335.

[108] A. Thanos, S. Shalmashi, and G. Miao, "Network-assisted discovery for device-to-device communications," in *2013 IEEE Globecom Workshops (GC Wkshps)*, 2013, pp. 660–664. DOI: 10.1109/GLOCOMW.2013.6825063.

[109] Z.-J. Yang, J.-C. Huang, C.-T. Chou, H.-Y. Hsieh, C.-W. Hsu, P.-C. Yeh, and C. C. A. Hsu, "Peer discovery for device-to-device (d2d) communication in lte-a networks," in *Globecom Workshops (GC Wkshps), 2013 IEEE*, 2013, pp. 665–670. DOI: 10.1109/GLOCOMW.2013.6825064.

[110] L. Hu, "Resource allocation for network-assisted device-to-device discovery," in *Wireless Communications, Vehicular Technology, Information Theory and Aerospace Electronic Systems (VITAE), 2014 4th International Conference on*, 2014, pp. 1–5. DOI: 10.1109/VITAE.2014.6934508.

[111] K. W. Choi and Z. Han, "Device-to-device discovery for proximity-based service in lte-advanced system," *IEEE Journal on Selected Areas in Communications*, vol. 33, no. 1, pp. 55–66, 2015, ISSN: 0733-8716. DOI: 10.1109/JSAC.2014.2369591.

[112] L. Breslau, P. Cao, L. Fan, G. Phillips, and S. Shenker, "Web caching and Zipf-like distributions: evidence and implications," *Ieee Infocom*, vol. 1, pp. 126–134, 1999, ISSN: 0743-166X. DOI: 10.1109/INFCOM.1999.749260.

[113] C. Williamson and N. Carlsson, "On Zipf Models for Probabilistic Piece Selection in P2P Stored Media Streaming," *2013 IEEE 21st International Symposium on Modelling, Analysis and Simulation of Computer and Telecommunication Systems*, pp. 161–171, 2013. DOI: 10.1109/MASCOTS.2013.24. [Online]. Available: http://ieeexplore.ieee.org/lpdocs/epic03/wrapper.htm?arnumber=6730759.

[114] K. Doppler, C. H. Yu, C. B. Ribeiro, and P. Janis, "Mode selection for device-to-device communication underlaying an lte-advanced network," in *2010 IEEE Wireless Communication and Networking Conference*, 2010, pp. 1–6. DOI: 10.1109/WCNC.2010.5506248.

[115] S. Hakola, T. Chen, J. Lehtomaki, and T. Koskela, "Device-to-device (d2d) communication in cellular network - performance analysis of optimum and practical communication mode selection," in *Wireless Communications and Networking Conference (WCNC), 2010 IEEE*, 2010, pp. 1–6. DOI: 10.1109/WCNC.2010.5506133.

[116] T. Koskela, S. Hakola, T. Chen, and J. Lehtomaki, "Clustering concept using device-to-device communication in cellular system," in *Wireless Communications and Networking Conference (WCNC), 2010 IEEE*, 2010, pp. 1–6. DOI: 10.1109/WCNC.2010.5506183.

[117] M. Jung, K. Hwang, and S. Choi, "Joint mode selection and power allocation scheme for power-efficient device-to-device (d2d) communication," in *Vehicular Technology Conference (VTC Spring), 2012 IEEE 75th*, 2012, pp. 1–5. DOI: 10.1109/VETECS.2012.6240196.

[118] S. Wen, X. Zhu, X. Zhang, and D. Yang, "Qos-aware mode selection and resource allocation scheme for device-to-device (d2d) communication in cellular networks," in *Communications Workshops (ICC), 2013 IEEE International Conference on*, 2013, pp. 101–105. DOI: 10.1109/ICCW.2013.6649209.

[119] J. M. B. da Silva, T. F. Maciel, R. L. Batista, C. F. M. e Silva, and F. R. P. Cavalcanti, "Ue grouping and mode selection for d2d communications underlaying a multicellular wireless system," in *2014 IEEE Wireless Communication and Networking Conference Workshops*, 2014, pp. 230–235. DOI: 10.1109/WCNCW.2014.6934891.

[120] C. P. Chien, Y. C. Chen, and H. Y. Hsieh, "Exploiting spatial reuse gain through joint mode selection and resource allocation for underlay device-to-device communications," in *The 15th International Symposium on Wireless Personal Multimedia Communications*, 2012, pp. 80–84.

[121] T. Han, R. Yin, Y. Xu, and G. Yu, "Uplink channel reusing selection ooptimization for device-to-device communication underlaying cellular networks," in *IEEE 23rd Annual Symposium on Personal, Indoor and Mobile Radio Communications, 2012*, 2012, pp. 559–564. DOI: 10.1109/PIMRC.2012.6362848.

[122] M. Zulhasnine, C. Huang, and A. Srinivasan, "Efficient resource allocation for device-to-device communication underlaying lte network," in *2010 IEEE 6th International Conference on WiMob*, 2010, pp. 368–375. DOI: 10.1109/WIMOB.2010.5645039.

[123] M. Belleschi, G. Fodor, and A. Abrardo, "Performance analysis of a distributed resource allocation scheme for d2d communications," in *2011 IEEE GLOBECOM Workshops (GC Wkshps)*, 2011, pp. 358–362. DOI: 10.1109/GLOCOMW.2011.6162471.

[124] P. Janis, V. Koivunen, C. Ribeiro, J. Korhonen, K. Doppler, and K. Hugl, "Interference-aware resource allocation for device-to-device radio underlaying cellular networks," in *IEEE 69th Vehicular Technology Conference (VTC Spring) 2009.*, 2009, pp. 1–5. DOI: 10.1109/VETECS.2009.5073611.

[125] H. Wang and X. Chu, "Distance-constrained resource-sharing criteria for device-to-device communications underlaying cellular networks," English, *Electronics Letters*, vol. 48, 528–530(2), 9 2012, ISSN: 0013-5194. [Online]. Available: http://digital-library.theiet.org/content/journals/10.1049/el.2012.0451.

[126] M.-H. Han, B.-G. Kim, and J.-W. Lee, "Subchannel and transmission mode scheduling for d2d communication in ofdma networks," in *Vehicular Technology Conference (VTC Fall), 2012 IEEE*, 2012, pp. 1–5. DOI: 10.1109/VTCFall.2012.6399205.

[127] L. Lei, X. Shen, M. Dohler, C. Lin, and Z. Zhong, "Queuing models with applications to mode selection in device-to-device communications underlaying cellular networks," *IEEE Transactions on Wireless Communications*, vol. 13, no. 12, pp. 6697–6715, 2014, ISSN: 1536-1276. DOI: 10.1109/TWC.2014.2335734.

[128] H. Xing and S. Hakola, "The investigation of power control schemes for a device-to-device communication integrated into ofdma cellular system," in *2010 IEEE 21st Annual International Symposium on Personal, Indoor and Mobile Radio Communications*, 2010, pp. 1775–1780. DOI: 10.1109/PIMRC.2010.5671643.

[129] X. Lin, J. G. Andrews, and A. Ghosh, "Spectrum sharing for device-to-device communication in cellular networks," *IEEE Transactions on Wireless Communications*, vol. 13, no. 12, pp. 6727–6740, 2014, ISSN: 1536-1276. DOI: 10.1109/TWC.2014.2360202.

[130] H. ElSawy, E. Hossain, and M. S. Alouini, "Analytical modeling of mode selection and power control for underlay d2d communication in cellular networks," *IEEE Transactions on Communications*, vol. 62, no. 11, pp. 4147–4161, 2014, ISSN: 0090-6778. DOI: 10.1109/TCOMM.2014.2363849.

[131] P. Janis, C.-H. YU, K. DOPPLER, C. RIBEIRO, C. WIJTING, K. HUGL, O. TIRKKONEN, and V. KOIVUNEN, "Device-to-device communication underlaying cellular communications systems," *Int'l J. of Communications, Network and System Sciences*, pp. 169–178, 2009, ISSN: 1913-3715. DOI: 10.4236/ijcns.2009.23019. [Online]. Available: http://www.scirp.org/Journal/PaperDownload.aspx?paperID=466&FileName=IJCNS20090300001_51873990.pdf.

[132] C. H. Yu, O. Tirkkonen, K. Doppler, and C. Ribeiro, "Power optimization of device-to-device communication underlaying cellular communication," in *2009 IEEE International Conference on Communications*, 2009, pp. 1–5. DOI: 10.1109/ICC.2009.5199353.

[133] C. H. Yu, K. Doppler, C. B. Ribeiro, and O. Tirkkonen, "Resource sharing optimization for device-to-device communication underlaying cellular networks," *IEEE Trans. Wireless Commun.*, vol. 10, no. 8, pp. 2752–2763, 2011, ISSN: 1536-1276. DOI: 10.1109/TWC.2011.060811.102120.

[134] B. Wang, L. Chen, X. Chen, X. Zhang, and D. Yang, "Resource allocation optimization for device-to-device communication underlaying cellular networks," in *2011 IEEE 73rd Vehicular Technology Conference (VTC Spring)*, 2011, pp. 1–6. DOI: 10.1109/VETECS.2011.5956157.

[135] C. Gao, X. Sheng, J. Tang, W. Zhang, S. Zou, and M. Guizani, "Joint mode selection, channel allocation and power assignment for green device-to-device communications," in *2014 IEEE International Conference on Communications (ICC)*, 2014, pp. 178–183. DOI: 10.1109/ICC.2014.6883315.

[136] D. Marshall, S. Durrani, J. Guo, and N. Yang, "Performance comparison of device-to-device mode selection schemes," in *2015 IEEE 26th Annual International Symposium on Personal, Indoor, and Mobile Radio Communications (PIMRC)*, 2015, pp. 1536–1541. DOI: 10.1109/PIMRC.2015.7343542.

[137] M. Xiao, N. Shroff, and E. Chong, "Distributed admission control for power-controlled cellular wireless systems," *IEEE/ACM Transactions on Networking*, vol. 9, no. 6, pp. 790–800, 2001, ISSN: 1063-6692. DOI: 10.1109/90.974532.

[138] C. Zhu and M. S. Corson, "A distributed channel probing scheme for wireless networks," in *Proceedings IEEE INFOCOM 2001. Conference on Computer Communications. Twentieth Annual Joint Conference of the IEEE Computer and Communications Society (Cat. No.01CH37213)*, vol. 1, 2001, 403–411 vol.1. DOI: 10.1109/INFCOM.2001.916723.

[139] S. Kučera, L. Kučera, and B. Zhang, "Efficient distributed algorithms for dynamic access to shared multiuser channels in sinr-constrained wireless networks," *IEEE Transactions on Mobile Computing*, vol. 11, no. 12, pp. 2087–2097, 2012, ISSN: 1536-1233. DOI: 10.1109/TMC.2011.236.

[140] P.-C. Lin, "Feasibility problem of channel spatial reuse in power-controlled wireless communication networks," in *2013 IEEE Wireless Communication and Networking Conference*, 2013, pp. 591–596. DOI: 10.1109/WCNC.2013.6554630.

[141] A. Quarteroni, R. Sacco, and F. Saleri, *Numerical Mathematics*, ser. Texts in Applied Mathematics. Springer Berlin Heidelberg, 2007, ISBN: 978-3-540-49809-4.

[142] P. Liu, C. Hu, T. Peng, R. Qian, and W. Wang, "Admission and power control for device-to-device links with quality of service protection in spectrum sharing hybrid network," in *2012 IEEE 23rd International Symposium on Personal, Indoor and Mobile Radio Communications - (PIMRC)*, 2012, pp. 1192–1197. DOI: 10.1109/PIMRC.2012.6362527.

[143] H. Sun, M. Sheng, X. Wang, Y. Zhang, J. Liu, and K. Wang, "Resource allocation for maximizing the device-to-device communications underlaying lte-advanced networks," in *2013 IEEE/CIC International Conference on Communications in China - Workshops (CIC/ICCC)*, 2013, pp. 60–64. DOI: 10.1109/ICCChinaW.2013.6670568.

[144] D. H. Lee, K. W. Choi, W. S. Jeon, and D. G. Jeong, "Two-stage semi-distributed resource management for device-to-device communication in cellular networks," *IEEE Trans. Wireless Commun.*, vol. 13, no. 4, pp. 1908–1920, 2014, ISSN: 1536-1276. DOI: 10.1109/TWC.2014.022014.130480.

[145] A. Kuhnle, X. Li, and M. T. Thai, "Online algorithms for optimal resource management in dynamic d2d communications," in *2014 10th International Conference on Mobile Ad-hoc and Sensor Networks*, 2014, pp. 130–137. DOI: 10.1109/MSN.2014.24.

[146] G. Elhami, M. Zehni, and M. R. Pakravan, "Maximum clique-based resource allocation in device-to-device communications," in *2015 IEEE 26th Annual International Symposium on Personal, Indoor, and Mobile Radio Communications (PIMRC)*, 2015, pp. 1195–1200. DOI: 10.1109/PIMRC.2015.7343480.

[147] H. H. Esmat, M. M. Elmesalawy, and I. I. Ibrahim, "Adaptive resource sharing algorithm for device-to-device communications underlaying cellular networks," *IEEE Communications Letters*, vol. 20, no. 3, pp. 530–533, 2016, ISSN: 1089-7798. DOI: 10.1109/LCOMM.2016.2517012.

[148] D. Feng, L. Lu, Y. Yuan-Wu, G. Y. Li, G. Feng, and S. Li, "Device-to-device communications underlaying cellular networks," *IEEE Transactions on Communications*, vol. 61, no. 8, pp. 3541–3551, 2013, ISSN: 0090-6778. DOI: 10.1109/TCOMM.2013.071013.120787.

[149] B. Peng, C. Hu, T. Peng, Y. Yang, and W. Wang, "A resource allocation scheme for d2d multicast with qos protection in ofdma-based systems," in *2013 IEEE 24th Annual International Symposium on Personal, Indoor, and Mobile Radio Communications (PIMRC)*, 2013, pp. 12 383–2387. DOI: 10.1109/PIMRC.2013.6666544.

[150] D. Zhu, J. Wang, A. L. Swindlehurst, and C. Zhao, "Downlink resource reuse for device-to-device communications underlaying cellular networks," *IEEE Signal Process. Lett.*, vol. 21, no. 5, pp. 531–534, 2014, ISSN: 1070-9908. DOI: 10.1109/LSP.2014.2309143.

[151] S. A. Ciou, J. C. Kao, C. Y. Lee, and K. Y. Chen, "Multi-sharing resource allocation for device-to-device communication underlaying 5g mobile networks," in *2015 IEEE 26th Annual International Symposium on Personal, Indoor, and Mobile Radio Communications (PIMRC)*, 2015, pp. 1509–1514. DOI: 10.1109/PIMRC.2015.7343537.

[152] X. Cai, J. Zheng, and Y. Zhang, "A graph-coloring based resource allocation algorithm for d2d communication in cellular networks," in *2015 IEEE International Conference on Communications (ICC)*, 2015, pp. 5429–5434. DOI: 10.1109/ICC.2015.7249187.

[153] W. Zhao and S. Wang, "Resource sharing scheme for device-to-device communication underlaying cellular networks," *IEEE Trans. Commun.*, vol. 63, no. 12, pp. 4838–4848, 2015, ISSN: 0090-6778. DOI: 10.1109/TCOMM.2015.2495217.

[154] M. T. Islam, A. E. M. Taha, S. Akl, and M. Abu-Elkheir, "A stable matching algorithm for resource allocation for underlaying device-to-device communications," in *2016 IEEE International Conference on Communications (ICC)*, 2016, pp. 1–6. DOI: 10.1109/ICC.2016.7511459.

[155] Y. Li, T. Jiang, M. Sheng, and Y. Zhu, "Qos-aware admission control and resource allocation in underlay device-to-device spectrum-sharing networks," *IEEE J. Sel. Areas Commun.*, vol. 34, no. 11, pp. 2874–2886, 2016, ISSN: 0733-8716. DOI: 10.1109/JSAC.2016.2614942.

[156] M. Andersin, Z. Rosberg, and J. Zander, "Gradual removals in cellular pcs with constrained power control and noise," in *2013 IEEE Sixth Annual International Symposium on Personal, Indoor, and Mobile Radio Communications (PIMRC)*, vol. 1, 1995, 56–60 vol.1. DOI: 10.1109/PIMRC.1995.476403.

[157] C. C. Chen and D. S. Lee, "A distributed subset selection algorithm for a set of mobile links with power control," *IEEE Transactions on Wireless Communications*, vol. 7, no. 6, pp. 2221–2230, 2008, ISSN: 1536-1276. DOI: 10.1109/TWC.2008.060966.

[158] N. Lee, X. Lin, J. G. Andrews, and R. W. Heath, "Power control for d2d underlaid cellular networks: Modeling, algorithms, and analysis," *IEEE Journal on Selected Areas in Communications*, vol. 33, no. 1, pp. 1–13, 2015, ISSN: 0733-8716. DOI: 10.1109/JSAC.2014.2369612.

[159] P. Van Mieghem, D. Stevanovic, F. Kuipers, C. Li, R. van de Bovenkamp, D. Liu, and H. Wang, "Decreasing the spectral radius of a graph by link removals," *Phys. Rev. E*, vol. 84, p. 016 101, 1 2011. DOI: 10.1103/PhysRevE.84.016101. [Online]. Available: https://link.aps.org/doi/10.1103/PhysRevE.84.016101.

[160] C. Floudas, *Nonlinear and Mixed-Integer Optimization: Fundamentals and Applications*, ser. Topics in Chemical Engineering. Oxford University Press, 1995, ISBN: 9780195356557. [Online]. Available: https://books.google.de/books?id=OhTfOjSkq18C.

[161] C. W. Sung, "Log-convexity property of the feasible sir region in power-controlled cellular systems," *IEEE Commun. Lett.*, vol. 6, no. 6, pp. 248–249, 2002, ISSN: 1089-7798. DOI: 10.1109/LCOMM.2002.1010870.

[162] M. Andersin, Z. Rosberg, and J. Zander, "Gradual removals in cellular pcs with constrained power control and noise," in *Personal, Indoor and Mobile Radio Communications, 1995. PIMRC'95. Wireless: Merging onto the Information Superhighway., Sixth IEEE International Symposium on*, vol. 1, 1995, 56–60 vol.1. DOI: 10.1109/PIMRC.1995.476403.

[163] J. M. Lewis and M. Yannakakis, "The node-deletion problem for hereditary properties is np-complete," *Journal of Computer and System Sciences*, vol. 20, no. 2, pp. 219–230, 1980, ISSN: 0022-0000. DOI: http://dx.doi.org/10.1016/0022-0000(80)90060-4. [Online]. Available: http://www.sciencedirect.com/science/article/pii/0022000080900604.

[164] H. Kellerer, U. Pferschy, and D. Pisinger, *Knapsack Problems*. Springer Berlin Heidelberg, 2004, ISBN: 9783540402862. DOI: 10.1007/978-3-540-24777-7. [Online]. Available: www.springer.com/de/book/9783540402862.

[165] S. Stanczak, M. Kaliszan, N. Bambos, and M. Wiczanowski, "A characterization of max-min sir-balanced power allocation with applications," in *2009 IEEE International Symposium on Information Theory*, 2009, pp. 2747–2751. DOI: 10.1109/ISIT.2009.5205835.

[166] D. H. Lee, K. W. Choi, W. S. Jeon, and D. G. Jeong, "Resource allocation scheme for device-to-device communication for maximizing spatial reuse," in *2013 IEEE Wireless Communications and Networking Conference (WCNC)*, 2013, pp. 112–117. DOI: 10.1109/WCNC.2013.6554548.

[167] *Result data and tool-chain of the device-to-device reuse maximization problem with power control*, Accessed: 2017-10-04. DOI: 10.14459/2017mp1394930. [Online]. Available: https://mediatum.ub.tum.de/1394930.

[168] J. F. Benders, "Partitioning procedures for solving mixed-variables programming problems," *Numerische mathematik*, vol. 4, no. 1, pp. 238–252, 1962.

[169] A. M. Geoffrion, "Generalized benders decomposition," *Journal of Optimization Theory and Applications*, vol. 10, no. 4, pp. 237–260, 1972, ISSN: 1573-2878. DOI: 10.1007/BF00934810. [Online]. Available: https://doi.org/10.1007/BF00934810.